



This is to certify that the

dissertation entitled

Relaxation Model for Homogeneous Turbulent Flows

presented by

Steven M. Parks

has been accepted towards fulfillment of the requirements for

Ph.D. degree in Chemical Engineering

Major professor

Date August 21,1997

MSU is an Affirmative Action/Equal Opportunity Institution

0-12771

LIBRARY
Michigan State
University

# PLACE IN RETURN BOX to remove this checkout from your record. TO AVOID FINES return on or before date due.

DATE DUE	DATE DUE	DATE DUE
SEP <sub>1</sub> 2, 3 20060		
NOW 2021 7007		
3 2 2 8 2 3 m		
AUS 2 2011 06 1 8 1 2	<del></del>	
LANGUS 2 202012		

1/98 c:/CIRC/DateDue.p65-p.14

## RELAXATION MODEL FOR HOMOGENEOUS TURBULENT FLOWS

by

Steven M. Parks

## **A DISSERTATION**

Submitted to
Michigan State University
in partial fulfillment of the requirements
for the degree of

**DOCTOR OF PHILOSOPHY** 

Department of Chemical Engineering

#### **ABSTRACT**

#### RELAXATION MODEL FOR HOMOGENEOUS TURBULENT FLOWS

by

#### Steven M. Parks

Turbulent closure for the Reynolds stress is investigated for homogeneous turbulent flows. The basic structure of the transport equations for the turbulent kinetic energy and turbulent dissipation is adopted from the standard k- $\epsilon$  model of turbulence. An integral analysis of the Kármán-Howarth relation for isotropic turbulence yields a prediction for the destruction-of-dissipation coefficient in the  $\epsilon$ -equation. This coefficient is applied to the problem of decaying isotropic turbulence and is shown to be able to quantitatively reproduce several data sets for the flow available in the literature.

A Green's function analysis of the equation for the fluctuating velocity and a subsequent smoothing approximation yields a turbulent pre-closure relating the Reynolds stress to mean field quantities and an unclosed quantity: the turbulent pre-stress, which is related to both pressure fluctuations and the fluctuating Reynolds stress. An isotropic pre-stress closure assumption is introduced and applied to the problem of homogeneous shear. This closure is found to guarantee realizability a priori and yields a non-zero primary normal stress difference. Subsequent extension of the closure to an objective, anisotropic pre-stress accounts for both stress relaxation effects as well as a non-zero second normal stress difference for homogeneous shear flows.

The case of homogeneous shear flow in a rotating frame of reference is examined due to its qualitative similarity to a flow in an inertial frame which also includes swirl and/or streamline curvature. The predominant result is that the combination of shear and rotation qualitatively changes the nature of the flow. For intermediate relative rotation rates, both k and  $\epsilon$  are growing without bound. For large absolute relative rotation rates, turbulent production is cut-off and both k and  $\epsilon$  decay to zero.

to Maya

#### **ACKNOWLEDGEMENTS**

First and foremost, I would like to express my gratitude to Professor Charles Petty for his guidance and continuing support throughout this entire research. Additional thanks are due to Dr. Syed Ali and Professor John Foss for their helpful suggestions during the early period of the research. Finally, heartfelt appreciation is expressed to my graduate student colleagues, Maya Murshak, Klaus Weispfennig, and G. Dale Wesson, for their valuable discussions and constant encouragement.

I would also like to acknowledge my families for their unending support and source of inspiration: Mom, Dad, Violetta, Isaiah, Eric, Mike, Isaak, and May, thanks to you all.

Special thanks are given to F.E.C. Laboratories and Michael Goergen for the unique opportunities offered to me, allowing me to pursue both my professional and academic goals.

I would like to recognize my friends and colleagues at the *Lehrstuhl für Strömungmechanik* in Erlangen, Germany, for making my personal growth there as important as the academic. Great thanks go to Professor Cameron Tropea, Suad Jakirlic, Marco Marengo, and Jochen Volkert.

The author would like to thank the Department of Chemical Engineering and the Hydrocyclone Development Consortium at Michigan State University for financial support during this research. Further thanks are extended to the DuPont corporation, the DeVlieg foundation, and the DAAD (*Deutsche Akademische Austauchdienst*; German Academic Exchange Service) for additional funding.

## TABLE OF CONTENTS

			Page
LIST OF	TABI	LES	vii
LIST OF	FIGU	RES	viii
LIST OF	LIST OF NOTATION		
СНАРТІ	ER		
1.	INT	RODUCTION	1
		Background	1
		Objectives	14
		Methodology	15
2.	ТНІ	E DECAY OF ISOTROPIC TURBULENCE IN	21
		INERTIAL FRAME	
	2.1	Introduction	21
	2.2	Local Analysis of the Kármán-Howarth Equation	29
	2.3		33
	2.4	Approximate Analysis of Dissipation and Production Integrals	35
	2.5	Parameter Estimates	42
	2.6	Transient Isotropic Decay	50
	2.7	Conclusions	61
3.	ALC	GEBRAIC PRE-CLOSURE THEORY FOR THE	64
	REY	YNOLDS STRESS	
	3.1	Introduction	64
	3.2	Pre-Closure Theory	70
	3.3	Isotropic Pre-Stress Theory	76
	3.4	Parameter Estimates	81
	3.5	Results and Discussion	83
	3.6	Conclusions	92
4.	AN	ISOTROPIC PRE-STRESS THEORY FOR	94
	HO	MOGENEOUSLY SHEARED FLOWS	
	4.1	Introduction	94
	4.2	Anisotropic Pre-Stress Theory	97
	4.3	Anisotropic Homogeneous Decay	99
	4.4	Homogeneously Sheared Turbulence	103

	4.5 Asymptotic Homogeneous Shear	106
	4.6 Transition States for Homogeneously Sheared Turbulence	109
	4.7 Conclusions	120
5.	HOMOGENEOUSLY SHEARED TURBULENCE	124
	IN A ROTATING FRAME OF REFERENCE	
	5.1 Introduction	124
	5.2 Pre-Closure Theory	128
	5.3 Coriolis Redistribution of Turbulent Energy for	
	Homogeneous Flows	130
	5.4 Isotropic Pre-Stress Theory for Rotating Homogeneous	
	Shear	132
	5.5 Anisotropic Pre-Stress Theory for Rotating Homogeneous	
	Shear	152
	5.6 Conclusions	161
6.	CONCLUSIONS	163
7.	RECOMMENDATIONS	168
	7.1 Further Study	168
	7.2 Further Application	170
APPENI	DICES	
A.	Navier-Stokes Equation in a Rotating Frame of Reference	175
В.	Reynolds Stress Equation in a Rotating Frame of Reference	177
C.	Turbulent Dissipation Equation in a Rotating Frame of Reference	179
D.	Objectivity of Convected Time Derivatives	181
E.	Tables of Referenced Data	183
F.	Relation of Homogeneous, Isotropic Turbulent Production to the	
	Velocity Derivative Skewness	197
G.	Asymptotic State for Homogeneous Shear	199
H.	Computer Program Listings	201
	H.1 Program TRANS.BAS	201
	H.2 Program IPS_ROT.BAS	206
I.	Properties of the Eigenvalues of the Reynolds Stress	209
LISTOF	REFERENCES	211
		211

## LIST OF TABLES

TAB	LE		
	2.1	Summary of Parameters Used in the Analysis of the IKH-Equation	44
	3.1	Parameter Estimates for the IPS-Theory	84
	3.2	Predictions of Asymptotic Statistical Properties for Homogeneously Sheared Turbulence	85
	4.1	Parameter Estimates for the APS-Theory	110
	E.1	Summary of Isotropic Decay Data; Batchelor and Townsend [1948]; M=0.635cm (grid mesh)	184
	E.2	Summary of Isotropic Decay Data; Comte-Bellot and Corrsin [1971]; $U_o=10m/s$	185
	E.3	Summary of Isotropic Decay Data; Sirivat and Warhaft [1983]; M=2.5cm (grid mesh)	186
	E.4	Summary of Isotropic Decay Data of Speziale <i>et al.</i> [1987]; $Re_o = 35.1$	187
	E.5	Summary of Isotropic Decay Data Bardina et al. [1985]; $Re_o = 45.4$	188
	E.6	Homogeneous Shear Flow Data (Tavoularis and Karnik "A", 1989)	189
	E.7	Homogeneous Shear Flow Data (Tavoularis and Karnik "D", 1989)	190
	E.8	Homogeneous Shear Flow Data (Tavoularis and Karnik "G", 1989)	191
	E.9	Homogeneous Shear Flow Data (Tavoularis and Karnik "TC", 1989)	192
	E.10	Homogeneous Shear Flow Data (Tavoularis and Karnik "L", 1989)	193
	E.11	Return to Isotropy Data: Choi and Lumley [1984] (Plane Distortion)	194
	E.12	Return to Isotropy Data: Choi and Lumley [1984] (Axisymmetric Expansion)	195
	E.13	Return to Isotropy Data: LePenven et al. [1985] (Positive Third Invariant)	196

## **LIST OF FIGURES**

## **FIGURE**

1.1	L-Diagram for Realizable Anisotropic States	6
1.2	Anisotropic States for Homogeneous Shear Flows	11
1.3	Closure Methodology	20
2.1	Relaxation States for Decaying Isotropic Turbulence	24
2.2	Literature Data for the Skewness and Correlations for the Destruction-of-Dissipation Coefficient	28
2.3	Qualitative Behavior of the Integrands $I_1$ , $I_2$ , and $I_3$ ; Estimation of the Cut-off Integration Distance $\xi_c$	37
2.4a.	Prediction of the IKH-Equation for the Skewness Using a Prescribed Function for the Destruction of Dissipation	43
2.4b	Parametric Study for the Effect of $Re^*$ on the Resulting Skewness Prediction	46
2.4c	Parametric Study for the Effect of a on the Resulting Skewness Prediction	47
2.5	Predictions of the IKH-Equation for the Destruction of Dissipation Coefficient	48
2.6	Predictions of the IKH-Equation for the Production of Dissipation Using a Prescribed Function for the Destruction of Dissipation	49
2.7a	Model Computations for the Isotropic Decay Data of Batchelor and Townsend [1948] ( $U = 150 \text{ cm/s}$ , $Re_o = 7.58$ )	51
2.7b	Model Computations for the Isotropic Decay Data of Batchelor and Townsend [1948] $(U = 643 \text{ cm/s}, Re = 42.6)$	52

2.7c	Model Computations for the Isotropic Decay Data of Batchelor and Townsend [1948] ( $U = 1286 \text{ cm/s}, Re_o = 83.7$ )	53
2.7d	Model Computations for the Isotropic Decay Data of Comte-Bellot and Corrsin [1971] ( $U = 10 \text{ m/s}, Re_o = 354$ )	54
2.7e	Model Computations for the Isotropic Decay Data of Comte-Bellot and Corrsin [1971] ( $U = 10 \text{ m/s}$ , $Re_o = 769$ )	55
2.7f	Model Computations for the Isotropic Decay Data of Sirivat and Warhaft [1983] ( $U = 340 \text{ cm/s}, Re_o = 139$ )	56
2.7g	Model Computations for the Isotropic Decay Data of Sirivat and Warhaft [1983] ( $U = 630 \text{ cm/s}, Re_o = 262$ )	57
2.7h	Model Computations for the Isotropic Decay Simulations of Speziale, et al. [1987] $(Re_o = 35.1)$	59
2.7i	Model Computations for the Isotropic Decay Simulations of Bardina, et al. [1985] $(Re_o = 45.4)$	60
2.8	Predicted Transient Decay of the Turbulent Kinetic Energy as a Function of the Initial Turbulent Reynolds Number	62
3.1	Asymptotic State for Homogeneously Sheared Turbulent Flows	65
3.2	Energy Simplex with Transition States for Homogeneously Sheared Turbulence	67
3.3	Anisotropy Invariant Diagram with Transition States for Homogeneously Sheared Turbulence	69
3.4	Anisotropy Invariants Predicted by the IPS-Theory for Homogeneously Sheared Turbulence	80
3.5	Estimation of the Relaxation Group for Asymptotic Homogeneously Sheared Turbulence	82
3.6	The Effect of the Development Time on the Relaxation Group for Homogeneously Sheared Turbulence	86
3.7	The Effect of the Development Time on the Distribution of Kinetic Energy for Homogeneously Sheared Turbulence	87
3.8	The Effect of the Development Time on the Shear Component of the	<b>Q</b> 1

4.1	Relaxation to Isotropic, Homogeneous Decay	102
4.2	The Effect of the Development Time on the Relaxation Group for Homogeneously Sheared Turbulence	112
4.3	Transient Response of Isotropic Turbulence to a Sudden Increase in the Mean Strain Rate ( $N_R^o = 0.7$ ): Components of the Normalized Reynolds Stress	114
4.4	Transient Response of Isotropic Turbulence to a Sudden Increase in the Mean Strain Rate ( $N_R^o = 0.7$ ): Components of the Anisotropic Pre-Stress	115
4.5	Transient Response of Isotropic Turbulence to a Sudden Increase in the Mean Strain Rate ( $N_R^o = 0.7$ ): $dH_{yz}/d\xi$	116
4.6	Transient Response of Isotropic Turbulence to a Sudden Increase in the Mean Strain Rate ( $N_R^o = 0.7$ ): $dH_{zz}/d\xi$	117
4.7	Transient Response of Isotropic Turbulence to a Sudden Increase in the Mean Strain Rate ( $N_R^o = 0.7$ ): Anisotropy Invariants	121
4.8	Transient Response of Isotropic Turbulence to a Sudden Increase in the Mean Strain Rate ( $N_R^o = 0.7$ ): Energy Simplex	122
5.1	Schematic for Homogeneously Sheared Turbulence in a Rotating Frame	125
5.2	Coriolis Redistribution of Turbulent Kinetic Energy for Homogeneous Flows	133
5.3	The Effect of Rotation on the Turbulent Relaxation Time for Asymptotic Homogeneous Shear (IPS-Theory)	137
5.4	The Effect of Rotation on the Components of the Asymptotic Reynolds Stress for Homogeneous Shear (IPS-Theory)	138
5.5	Distribution of the Energy Components for Homogeneously Sheared Turbulence	139
5.6	Transient Response of the Relaxation Group for Homogeneously Sheared Turbulence in a Rotating Frame (IPS-Theory)	141
5.7	Relative Growth Rates of Turbulent Statistics in the Asymptotic Regime (IPS-Theory; $N_R^o = 1.0$ , $\Omega/S = -0.5$ )	143

5.8	Relaxation of the Reynolds Stress Components in the Asymptotic Regime (IPS-Theory; $N_R^o = 1.0$ ; $\Omega/S = -0.5$ ; $R_R^o = R(N_R^o, \Omega/S)$ , cf. Eqs. (5.10)-(5.14))	144
5.9	Relative Growth Rates of Turbulent Statistics in the Decay Regime (IPS-Theory; $N_R^o = 1.0$ ; $\Omega/S = +1.0$ and $+2.0$ )	145
5.10	Relaxation of the Reynolds Stress Components in the Decay Regime (IPS-Theory; $N_R^o = 1.0$ ; $\Omega/S = +1.0$ and $+2.0$ ; $R_R^o = R(N_R^o, \Omega/S)$ , cf. Eqs. (5.10)-(5.14))	146
5.11	Anisotropy Invariants for the Asymptotic States of Homogeneously Sheared Turbulence in a Rotating Frame (IPS-Theory)	149
5.12	Anisotropy Invariants for the Decaying States of Homogeneously Sheared Turbulence in a Rotating Frame (IPS-Theory)	150
5.13	The Effect of Rotation on the Turbulent Relaxation Time $(N_R \equiv \tau_R S)$ for Asymptotic Homogeneous Shear (APS-Theory)	154
5.14	The Effect of Rotation on the Components of the Asymptotic Reynolds Stress for Homogeneous Shear (APS-Theory)	156
5.15	The Effect of Rotation on the Asymptotic Pre-Stress Anisotropy for Homogeneous Shear (APS-Theory)	157
5.16	Distribution of the Energy Components for Homogeneously Sheared Turbulence in a Rotating Frame (APS-Theory)	158
5.17	Asymptotic Anisotropy Invariants for Homogeneously Sheared Turbulence in a Rotating Frame (APS-Theory)	159
5.18	Transient Response of the Relaxation Group for Homogeneously Sheared Turbulence in a Rotating Frame (APS-Theory; $N_R^o = 1.0$ ; $H_R^o = 0$ )	160
7 1	Onalitative Sketch of a Hydrogyclone Centrifugal Separator	171

## LIST OF NOTATION

## English Symbols

II	Second invariant of $\frac{b}{z}$
III	Third invariant of $\underline{\underline{b}}$
a	Parameter in objective time derivative; parameter in theoretical correlation for $C_D(Re)$ ; empirical parameter for the estimation of $d[\ln(I_1)]/d[\ln(Re)]$
<u>A</u>	Matrix relating the Reynolds stress and the pre-stress in the pre-closure
<u>b</u>	Anisotropy dyadic of the normalized Reynolds stress
b	Empirical parameter for the estimation of $I_3/I_1$
$B_{LL}$	Double longitudinal velocity correlation
B <sub>NN</sub>	Double normal velocity correlation
$C^*$	Parameter in theoretical correlation for $C_D(Re)$
$C_D$	Coefficient for turbulent destruction of dissipation
$C_{P}$	Coefficient for turbulent production coefficient of dissipation
$C_{R}$	Coefficient for relaxation time scale of Green's function
$C_{\beta}$	Coefficient for linear strain term in phenomenological model for pre-stress
$C_{\lambda}$	Coefficient for relaxation term in phenomenological model for pre-stress
$C_{\mu}$	Eddy viscosity coefficient
B	Viscous destruction of dissipation
$De_t$	Turbulent Deborah number
$E\left(  ilde{k} ight)$	One-dimensional energy spectrum
<u>f</u> '	Fluctuating force
$\langle f f \rangle$	Turbulent pre-stress
<u>H</u>	Anisotropic portion of pre-stress
I :	Unit dyadic
$I_1$	Integral property of the turbulence; $I_1 = \int_0^2 B_{LL} d\xi$

$I_2$	Integral property of the turbulence; $I_2 = \int_0^\infty \frac{1}{\xi} \frac{\partial}{\partial \xi} (B_{LL}) d\xi$ Integral property of the turbulence; $I_3 = \int_0^\infty \frac{1}{\xi} T_{LLL} d\xi$
$I_3$	Integral property of the turbulence; $I_3 = \int_{E}^{1} T_{LLL} d\xi$
<b>J</b>	Fluctuating Reynolds stress
k	Turbulent kinetic energy
$ ilde{k}$	Energy spectrum wavenumber
$\langle t \rangle$	Linear convective-diffusive operator
m	Memory function for the Green's function
n	Empirical parameter for the prescription of turbulent destruction
$N_R$	Turbulent relaxation group; ratio of relaxation time of the Green's function to characteristic time scale of the mean field
p	Instantaneous pressure; parameter in theoretical correlation for $C_D(Re)$
p'	Fluctuating pressure
$\langle p \rangle$	Mean pressure
P	Turbulent production of dissipation due to vortex stretching
q	Ratio of the relaxation time scale of the pre-stress to the growth rate of the turbulent kinetic energy or homogeneous turbulence
<i>R</i> =	Normalized Reynolds stress
<b>Q</b>	Proper orthogonal, time-dependent frame transformation dyadic
æ	Redistribution of Reynolds stress components due to the isotropic portion of the pre-stress
Re	Turbulent Reynolds number
Re*	Empirical parameter for the prescription of turbulent destruction
$Re_A^{}$ , $Re_P^{}$	Parameter in theoretical correlation for $C_D(Re)$
S	Magnitude of velocity gradient $d\langle u_z\rangle/dy$
⟨₹⟩	Symmetric part of mean velocity gradient
$S_{k}$	Velocity derivative skewness
t	Time

$T_{LLL}$	Triple longitudinal velocity correlation
<u>u</u>	Instantaneous fluid velocity
<u>u</u> '	Fluctuating fluid velocity
$\langle \underline{u} \rangle$	Mean fluid velocity
$\langle \underline{u}'\underline{u}' \rangle$	Reynolds stress
$\langle \underline{W} \rangle$	Antisymmetric part of mean velocity gradient

## Greek Symbols

-	
α	One-half the trace of the pre-stress
β	Linear strain parameter in phenomenological model for the pre-stress
Δ	Minimization parameter
ε	Scalar turbulent dissipation
ε	Permutation triadic
η	Kolmogorov length scale
λ	Taylor microscale; relaxation time scale for the pre-stress
$\lambda_i$	Eigenvalues of the characteristic equation for the transient development of homogeneously sheared turbulence
μ	Molecular viscosity
ν	Kinematic molecular viscosity
$v_t$	Eddy viscosity
ξ	Dimensionless separation distance for turbulent correlations; dimensionless evolution time for homogeneous shear flow
$\xi_c$	Cut-off separation distance for approximation of turbulent integrals
ρ	Density
$\tau_D^{}$	Characteristic timescale for destruction of dissipation
$\tau_{P}$	Characteristic timescale for production of dissipation
$\tau_R^{}$	Relaxation time for the Green's function

 $\langle \tau \rangle$  Mean molecular stress  $\underline{\Omega}$  Frame rotation rate  $\underline{\Omega}$  Frame rotation dyadic

## Subscripts/Superscripts

- a Asymptotic value
- e Experimentally observed value
- o Initial value or limiting value at zero Reynolds number
- ∞ Limiting value at infinite Reynolds number
- ~ Dimensional quantity

#### CHAPTER 1

#### INTRODUCTION

## 1.1 Background

#### Turbulence Closure Problem

The ability to predict the low order statistical properties of turbulent flows is an important area of research. Although the exact equations governing the instantaneous pressure and velocity fields of constant density, constant viscosity, Newtonian fluids are known, the field equation for the mean velocity (i.e. the Reynolds equation) is statistically unclosed. With  $u = \langle u \rangle + u'$  and  $p = \langle p \rangle + p'$ ,

$$\frac{\partial \langle \underline{u} \rangle}{\partial t} + \langle \underline{u} \rangle \cdot \nabla \langle \underline{u} \rangle + 2\underline{\Omega} \wedge \langle \underline{u} \rangle =$$

$$-\nabla \left[ \frac{\langle \underline{p} \rangle}{\rho} - \frac{(\underline{\Omega} \wedge \underline{r}) \cdot (\underline{\Omega} \wedge \underline{r})}{2} \right] + \nu \nabla^2 \langle \underline{u} \rangle - \nabla \cdot \langle \underline{u}' \underline{u}' \rangle. \tag{1.1}$$

The statistical correlation  $\rho(\underline{u}'\underline{u}')$  is the Reynolds stress and accounts for the transport of momentum associated with the fluctuating field. In the above equation, the mean fields and the fluctuating fields are relative to a frame of reference rotating at a constant angular velocity  $\Omega$ .  $\Omega$  is related to the temporal connection between the inertial and non-inertial frames by the following expression

$$\underline{\Omega} = -\underline{Q} \cdot \underline{\dot{Q}}^T = \underline{\varepsilon} \cdot \underline{\Omega}. \tag{1.2}$$

In Eq. (1.2),  $\Omega$  is the rotation dyadic,  $\Sigma$  is the permutation triadic,  $\Omega$  is an orthogonal dyadic operator (i.e.  $\Omega \cdot \Omega^T = I$ ), and  $\Omega$  is the time derivative of  $\Omega$ . The orthogonal operator  $\Omega$  defines an arbitrary, time-dependent coordinate transformation:

$$\underline{Q} = \nabla \underline{x}^*, \tag{1.3}$$

where  $\nabla$  is the gradient operator in the rotating frame of reference and  $\underline{x}^*$  is the position vector in the inertial frame. For constant density fluids, the mean velocity field also satisfies the continuity equation:

$$\nabla \cdot \langle \underline{u} \rangle = 0. \tag{1.4}$$

Eddy viscosity type models for the Reynolds stress presume that the mean velocity field and the second order correlation  $\langle u'u' \rangle$  are related by the following model

$$\langle \underline{u}'\underline{u}'\rangle = \frac{2k}{3}I - 2v_t \langle \underline{S}\rangle, \tag{1.5}$$

where k denotes the kinetic energy per unit mass of the fluctuating field,

$$2k = \langle \underline{u}' \cdot \underline{u}' \rangle, \tag{1.6}$$

and  $v_t$  is a turbulent eddy viscosity coefficient which depends on the local statistical state of the turbulence.  $\langle S \rangle$  is the mean strain rate, which is traceless for constant density fluids. This results in a diffusion-type transport model which permits estimates of the mean field behavior, provided a model for the scalar eddy viscosity can be specified.

Turbulent flows can be computed directly by solving the continuity and the Navier-

Stokes equations. Because turbulent fluctuations are three-dimensional, the spatial grid required for direct numerical simulations is also three-dimensional. The computational grid must be fine enough to resolve all the physically significant scales of motion. Even the "simplest" turbulent flows require a four-dimensional discretization (one in time and three in space) whose resolution is directly dependent upon the Reynolds number. As the Reynolds number increases, the grid must become finer because the size of the small scales decreases. This reduction in the small scales can be seen by comparing the Kolmogorov and integral length scales for isotropic turbulence (Tennekes and Lumley, 1972; Hinze, 1975):

$$\frac{\eta}{l} = \frac{\left(v^3/\varepsilon\right)^{1/4}}{l} \propto Re_l^{-3/4}.$$
 (1.7)

In the above expression, the dissipation  $\varepsilon$  is defined by

$$\varepsilon \equiv \mathbf{v} \langle \nabla \mathbf{u}' \colon (\nabla \mathbf{u}')^T \rangle, \tag{1.8}$$

and the integral length scale is given by the integral of the two-point longitudinal velocity correlation

$$l = \int_{0}^{\infty} \langle u'_{L}(\underline{x}, t) u'_{L}(\underline{x} + \underline{r}, t) \rangle dr.$$
 (1.9)

Although direct numerical simulations (DNS) of turbulence are possible, they have only been performed for simple geometries at relatively low Reynolds numbers. For instance, Kim et al. (1987) have reported DNS results for fully-developed channel flow at Reynolds numbers less than 10,000 based on the channel half-width. Such simulations provide important statistical information which is difficult to observe experimentally. However, the use of direct numerical simulation for practical engineering flows with

complex geometries and/or high Reynolds numbers would require computational power beyond what is presently available. Thus, improved models capable of predicting the low order statistical properties for a wide class of turbulent flows remains an intense area of research.

Turbulence models can yield physical insight into the behavior of the mean field provided the important qualitative properties of the Reynolds stress are retained. Thus, turbulence modeling has several distinct advantages over direct simulation. For instance, because of the intrinsic three dimensional and unsteady nature of turbulent fluctuations, direct simulation *cannot* take advantage of simplifying statistical properties. For example, a flow which is statistically stationary must still be simulated as a transient. Furthermore, if a specific flow geometry possesses symmetry planes and/or axisymmetric features, the flow must still be simulated as fully three dimensional. Thus, a Reynolds stress model which is not overly complex will almost certainly be computationally faster (and thereby less expensive) than a direct simulation of the same flow.

## Realizability

The term *realizable* as applied to Reynolds stress models relates to whether or not the eigenvalues of the statistical correlation  $\langle \underline{u}'\underline{u}' \rangle$  are non-negative. An important aspect of this concept relates to invariant mapping, as discussed by Lumley [1978]. Specifically, the invariants of the anisotropic stress, defined by

$$\underline{b} = \frac{\langle \underline{u}'\underline{u}' \rangle}{2k} - \frac{1}{3}\underline{I},\tag{1.10}$$

are computed and cross plotted to form a *II-III* phase plane of permissible turbulent states. The invariants of b are defined as

$$II \equiv tr\left(\underline{b} \cdot \underline{b}\right) \tag{1.11}$$

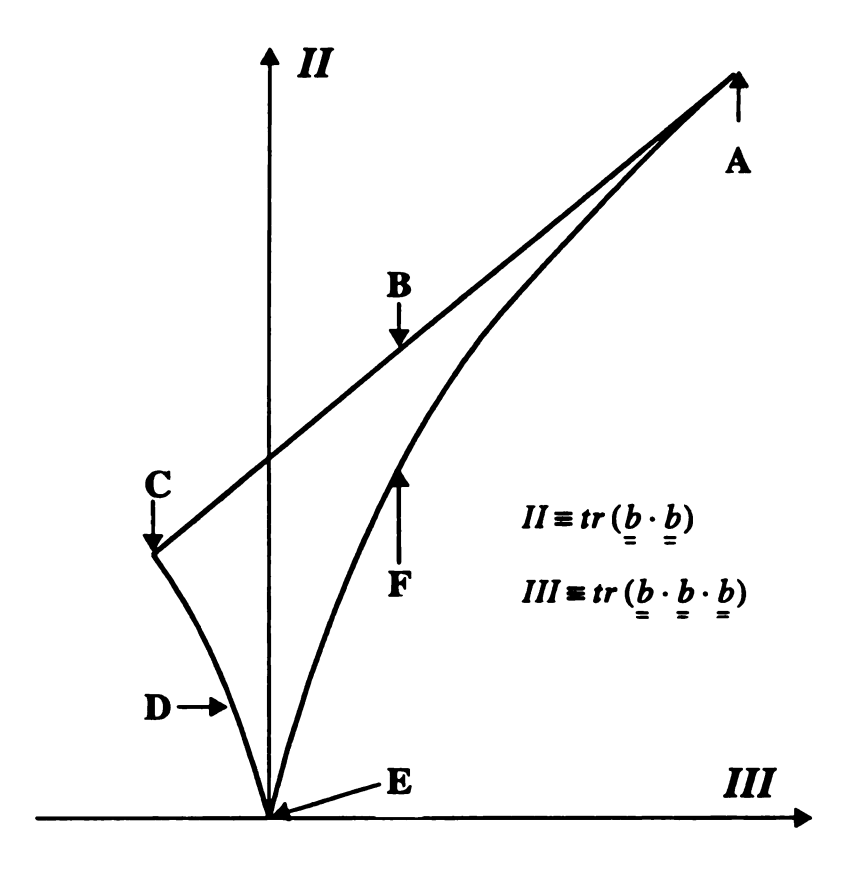
and

$$III \equiv tr \left( b \cdot b \cdot b \right). \tag{1.12}$$

By definition, the first invariant of the isotropic stress is zero (I = tr(b) = 0). Therefore, at least one of the anisotropic eigenvalues associated with b = 1 is negative. Because II is the sum of the squares of the anisotropic eigenvalues, the second invariant is always positive; however, III can be either positive or negative, depending on the local dynamic state of the turbulent field. There are two key mathematical properties of the Reynolds stress which restrict all turbulent states to a subset of the II-III plane. These properties are: (1) the trace of the Reynolds stress is twice the total kinetic energy of the turbulence (see Eq. (1.6)); and, (2) the Reynolds stress dyadic is positive semi-definite, i.e.,

$$z \cdot \langle u'u' \rangle \cdot z \ge 0, \tag{1.13}$$

for any non-zero  $\underline{z}$  in  $E^3$ . These two conditions imply that the anisotropic stress is traceless and its eigenvalues are bounded by 2/3 and -1/3 (see Appendix I). Lumley [1978] showed that all realizable turbulent states map into a quasi-triangular domain in the II-III phase plane, illustrated by Figure 1.1. The portions labeled A, C and E are the vertices of the domain, while B, D and F are the boundaries. Each of the portions are listed in an accompanying table and described mathematically with either the coordinates of the vertices or the equation for the boundaries. If a coordinate pair (II, III) falls on or within the boundaries of the L-diagram (where "L" stands for "Lumley"), then this anisotropic state may be associated with a realizable Reynolds stress. On the other hand, no realizable anisotropic state can fall outside the L-diagram. Non-turbulent, albeit realizable, states



**Description of Points on Anisotropy Simplex** 

Name		Invariants <sup>†</sup>		Eigenvalues of the Reynolds Stress			
		II .	III	R <sub>I</sub>	R <sub>2</sub>	R <sub>3</sub>	Notes
A	1 Component	2/3	2/9	1	0	0	
В	2 Component Anisotropic	II = 2/9 + 2III		1-x	х	0	$0 \le x \le 1/2$
C	2 Component Isotropic	1/6	-1/36	1/2	1/2	0	
D	Oblate Axisymmetric	$III = -6\left(II/6\right)^{3/2}$		x	x	1-2x	$1/3 \le x \le 1/2$
E	3 Component Isotropic	0	0	1/3	1/3	1/3	
F	Prolate Axisymmetric	III = -	6 (II/6) <sup>3/2</sup>	x	x	1-2x	$0 \le x \le 1/3$

Notes: (1) "n-Component" means that the Reynolds stress has "n" non-zero eigenvalues.

Figure 1.1 L-Diagram for Realizable Anisotropic States

<sup>(2) &</sup>quot;Axisymmetric" two of the eigenvalues of the Reynolds stress are equal.

†: Invariants of the anisotropic stress.

may fall within the L-diagram. Further a priori, model-independent restrictions of the anisotropic turbulent states within the L-diagram remains an open question for research. The L-diagram will be employed in this work to represent the local state of turbulence associated with different turbulent models with different experimental data sets.

#### k-& Turbulence Model

The most commonly applied turbulence model is the Boussinesq approximation (defined by Eq. (1.5)). The k- $\epsilon$  theory uses an eddy viscosity related to the kinetic energy and dissipation associated with the fluctuating field:

$$v_t = C_{\mu} k^2 / \varepsilon. \tag{1.14}$$

The universal coefficient  $C_{\mu}$  is estimated from plane jet data to be about 0.09 (Launder and Spalding, 1972). The first models of this type date back to Prandtl (see Speziale, 1991) and use empirical, algebraic models for the specification of the characteristic turbulent scales. Later models have moved away from this and solve differential equations to specify the turbulent scales. These are generally termed two-equation models, as they require two differential equations for the scale-determining parameters. The most prevalent example of this approach to Reynolds stress modeling is the k- $\epsilon$  model of Hanjalic and Launder (1972), hereinafter denoted as the *standard* k- $\epsilon$  model. Transport equations for the turbulent kinetic energy (k) and the turbulent dissipation rate ( $\epsilon$ ) are used to compute turbulent time and length scales at each point in the spatial domain:

$$\frac{Dk}{Dt} = -\langle \underline{u}'\underline{u}' \rangle : \nabla \langle \underline{u} \rangle - \varepsilon + \nabla \cdot \left( \left[ \nabla + \frac{\nabla_t}{\sigma_k} \right] \nabla k \right), \tag{1.15}$$

$$\frac{D\varepsilon}{Dt} = -C_{P} \frac{\varepsilon}{k} \langle \underline{u}' \underline{u}' \rangle : \nabla \langle \underline{u} \rangle - C_{D} \frac{\varepsilon^{2}}{k} + \nabla \cdot \left( \left[ v + \frac{v_{t}}{\sigma_{\varepsilon}} \right] \nabla \varepsilon \right), \tag{1.16}$$

While there are many variants on the two-equation model, the standard k- $\epsilon$  and its low Reynolds number derivatives (see Patel, et al., 1984, for an overview) have become the most widely tested and applied engineering turbulence models. The continuing use of the standard k- $\epsilon$  model is rooted primarily in its relative simplicity combined with its ability to provide some acceptable predictions.

Some of the computational advantages of the k- $\epsilon$  model include the fact that it is simple to implement into existing flow predictor codes and that there is not much additional computational demand inasmuch as only two additional scalar transport equations need be solved simultaneously with the Reynolds equation. Additionally, the k- $\epsilon$  model has been found to be computationally stable and robust, being largely independent of the initial guess for field variables. Because of these advantages and despite its limitations, the k- $\epsilon$  model has become the standard against which other models are judged. The k- $\epsilon$  model is, therefore, well documented in a variety of flows and summarizes a wealth of information. In this respect, any new model ought to be at least comparable to the k- $\epsilon$  model in some basic test flow cases.

One of the many criticisms of the Boussinesq approximation lies in the fact that the eddy viscosity coefficient is a scalar-valued function that only depends on the mean field implicitly through k and  $\epsilon$ . Therefore, at a fixed position in the flow field, Eqs. (1.5) and (1.10) imply that

$$\frac{\mathbf{v}_{t}}{k} = \frac{e_{\alpha} \cdot b \cdot e_{\beta}}{e_{\alpha} \cdot \langle S \rangle \cdot e_{\beta}},\tag{1.17}$$

for all combinations of base vectors  $\underline{e}_{\alpha}$  and  $\underline{e}_{\beta}$ . Eq. (1.17) may fit one of the cross correlations of the anisotropic stress for simple shear flows, but cannot explain the anisotropic distribution of kinetic energy among the components of the fluctuating velocity. Indeed, Kitoh [1991] has shown experimentally that Eq. (1.17) is inconsistent with the observed behavior of the anisotropic stress for the decay of swirling flow in a

pipe and concluded that the Boussinesq model was an inadequate closure for complex flows with strong curvature effects.

#### Simple Shear Flows

While eddy viscosity models typically make good predictions for two dimensional mean shear flows (Hanjalic, 1994), they do have many limitations. For example, the Boussinesq approximation does not predict a normal stress anisotropy for fully developed channel flows or for homogeneous shear flows. A simple shear flow is defined by

$$\nabla \langle \underline{u} \rangle = \frac{d \langle u_z \rangle}{d v} \underbrace{e}_{-y-z} e, \qquad (1.18)$$

where  $S = d\langle u_z \rangle / dy$ . For this flow, the Boussinesq model predicts an equipartition of turbulent kinetic energy among the fluctuating components of the velocity, which is clearly unphysical. Tavoularis and Corrsin [1981], Tavoularis and Karnik [1989], as well as Gibson and Kanellopoulos [1987] have all observed normal stress anisotropies for homogeneously sheared turbulent flows.

Additionally, the Boussinesq model is unable to explain the transient relaxation effects observed in return-to-isotropy experiments or the reorganization of turbulent energy associated with the transient development of homogeneous turbulent shear flows. For simple mean shear flows, the anisotropic stress associated with the Boussinesq model can be written as

$$b = -\left(\frac{C_{\mu}}{2}\right)\left(\frac{Sk}{\varepsilon}\right)\left(\frac{e}{c}\frac{e}{y-z} + \frac{e}{cz-y}\right), \qquad (1.19)$$

The invariants of the anisotropic stress for this situation follow directly from Eq. (1.19), viz.,

$$I = tr(\underline{b}) = 0, \tag{1.20}$$

$$II = tr(\underline{b} \cdot \underline{b}) = (C_{\mu}^2/2) \left(\frac{Sk}{\varepsilon}\right)^2, \tag{1.21}$$

and

$$III = tr(\underline{b} \cdot \underline{b} \cdot \underline{b}) = 0. \tag{1.22}$$

Experimental studies (see, esp., Choi and Lumley, 1984; LePenven, et al., 1985) clearly show that turbulent flows which are initially anisotropic gradually relax towards an isotropic state when the mean strain rate is removed. The Boussinesq model, however, predicts that the Reynolds stress responds instantaneously to a sudden change in  $\langle \underline{S} \rangle$ . Therefore, the intrinsic memory effects observed in low-order statistical properties of turbulent flows cannot be represented by Eqs. (1.5) and (1.19).

Experimental data for homogeneous shear flows (see, esp., Tavoularis and Karnik, 1989) also exhibit a transient relaxation to a strongly anisotropic asymptotic state. Figure 1.2 illustrates the trajectory of the relaxation process on the L-diagram. For simple shear flows, the accessible realizable states permitted by the Boussinesq theory all lie on the line III = 0 and  $0 \le II \le 2/9$ . Clearly the Boussinesq model cannot form the basis of a universal closure theory for the Reynolds equation inasmuch as the Boussinesq states are too restrictive. It is noteworthy that for simple shear flow the Boussinesq model is realizable for III = 0 and

$$0 \le II = (C_{\mu}^2/2) \left(\frac{Sk}{\varepsilon}\right)^2 \le 2/9. \tag{1.23}$$

With  $C_{\mu} = 0.09$ , the above inequality for the Boussinesq model implies that the ratio of turbulent to mean field time scales must be restricted to

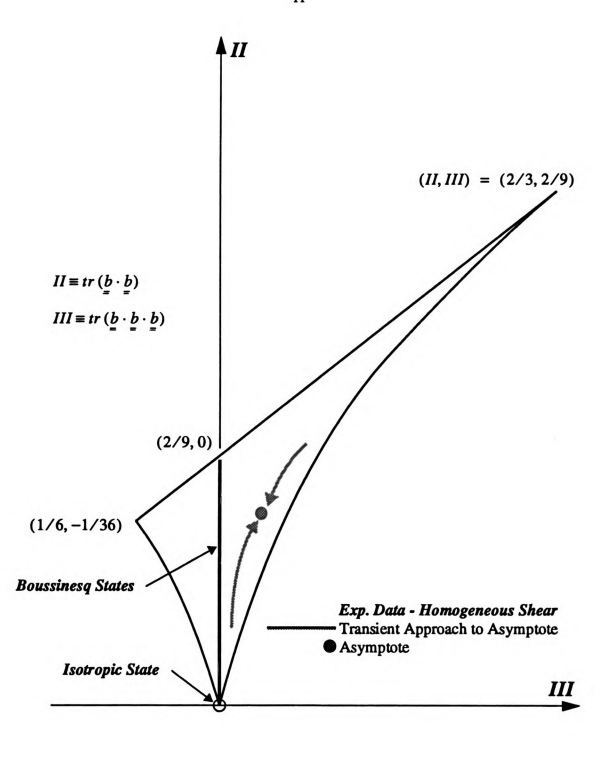


Figure 1.2 Anisotropic States for Homogeneous Shear Flows

$$\left(\frac{Sk}{\varepsilon}\right) < 7.4. \tag{1.24}$$

Thus, application of the Boussinesq model to turbulent flows for which  $k/\epsilon \gg 7/S$  would require  $C_{\mu}$  to be a function of  $Sk/\epsilon$  in order to maintain realizability.

Hanjalic [1994] has also noted the poor performance of eddy viscosity type models in flows with streamline curvature, especially in swirling flows. This is probably related to the misrepresentation of the underlying mechanism which distributes the kinetic energy of the turbulence among the three components of the fluctuating velocity. A primary source of velocity fluctuations in turbulent flows is the convective coupling between the mean field gradient and the fluctuating field, viz,  $\underline{u}' \cdot \nabla \langle \underline{u} \rangle$ . If  $\langle \underline{u} \rangle$  has the following local structure for a fully developed swirling flow

$$\langle \underline{u} \rangle = \langle u_{\theta} \rangle (r) \underline{e}_{\theta}, \tag{1.25}$$

then the local mean field gradient can be written as the sum of the following symmetric and antisymmetric strain rates

$$\nabla \langle \underline{u} \rangle = \frac{1}{2} r \frac{d}{dr} \left( \frac{\langle u_{\theta} \rangle}{r} \right) \left[ \underline{e}_{r-\theta} + \underline{e}_{\theta-r} \right] + \frac{1}{2} \frac{1}{r} \frac{d}{dr} \left( r \langle u_{\theta} \rangle \right) \left[ \underline{e}_{r-\theta} - \underline{e}_{\theta-r} \right]. \tag{1.26}$$

Thus, the convective coupling between  $\nabla \langle \underline{u} \rangle$  and  $\underline{u}$  has two distinct contributions:

$$\underline{u}' \cdot \nabla \langle \underline{u} \rangle = u'_r \left( \frac{d}{dr} \langle u_\theta \rangle \right) \underline{e}_\theta - \frac{u'_\theta \langle u_\theta \rangle}{r} \underline{e}_r. \tag{1.27}$$

The r-component, or cross-stream component, of Eq. (1.27) provides a means to shift the energy into the pressure field, and, thereby, increase the highly anisotropic distribution of turbulent kinetic energy among the three components of the fluctuating velocity.

The coupling between the fluctuating field and the strain associated with streamline

curvature does not arise in simple shear flows in inertial frames inasmuch as

$$\nabla \langle \underline{u} \rangle = \frac{S}{2} \begin{bmatrix} \underline{e} & \underline{e} + \underline{e} & \underline{e} \\ -y - z + \underline{e} & \underline{e} \end{bmatrix} + \frac{S}{2} \begin{bmatrix} \underline{e} & \underline{e} - \underline{e} & \underline{e} \\ -y - z - z - y \end{bmatrix}, \tag{1.28}$$

which yields

$$\underline{u}' \cdot \nabla \langle \underline{u} \rangle = u'_{y} \left( \frac{d}{dy} \langle u_{z} \rangle \right) \underline{e}_{z}. \tag{1.29}$$

Only streamwise fluctuations induced by the mean field occur for simple shear flows. However, as implied by Eq. (1.1), velocity fluctuations in non-inertial frames are produced by convective coupling between the mean field gradient and the rotational strain rate associated with the frame (see Appendix B). Thus, for simple shear flows in a rotating frame of reference, velocity fluctuations occur by streamwise convective coupling and, most significantly, by cross-stream convective coupling with the rotational strain:

$$\underline{u}' \cdot \left[ \nabla \langle \underline{u} \rangle + \underline{\Omega} \right] = \underline{u}'_{y} \left( \frac{d}{dy} \langle u_{z} \rangle + \Omega \right) \underline{e}_{z} - \underline{u}'_{z} \Omega \underline{e}_{y}. \tag{1.30}$$

Eq. (1.30) assumes that the rotation dyadic is constant and given by

$$\underline{\underline{\Omega}} = \underline{\Omega} \left( \underbrace{e}_{-y-z} \underbrace{e}_{-z-y} \right), \tag{1.31}$$

where  $\Omega$  represents the angular velocity of the frame rotation about the x-axis. Thus, as previously noted by Speziale [1991] and others (Speziale, et al., 1990), an analogous streamline curvature coupling between the mean field gradient and the fluctuating field can be achieved by a simple shear flow in a non-inertial frame. This observation provides a means to study the efficacy of phenomenological turbulent models under relatively simple kinematic conditions with an anticipation that a turbulence model which performs

.

adequately for simple shear in a non-inertial frame may provide a reasonable approach to flows with strong streamline curvature in inertial frames. The *ad hoc* basis for this conjecture stems from a comparison between the velocity gradient in an inertial frame (see Eq. (1.28)) and the velocity gradient in a rotating frame, viz.,

$$\nabla \langle \underline{u} \rangle = \frac{S}{2} \begin{bmatrix} e_{-y-z} + e_{-z-y} \\ -y-z \end{bmatrix} + \left( \frac{S}{2} + \Omega \right) \begin{bmatrix} e_{-y-z} - e_{-z-y} \\ -y-z \end{bmatrix}. \tag{1.32}$$

Thus, the mean field gradient associated with streamline curvature in an inertial frame is mathematically analogous to the effective mean field associated with a simple shear flow in a rotating frame provided

$$S \leftrightarrow r \frac{d}{dr} \left( \frac{\langle u_{\theta} \rangle}{r} \right)$$
 and  $\Omega \leftrightarrow \frac{\langle u_{\theta} \rangle}{r}$ .

## 1.2 Objectives

This research examines a new class of phenomenological models for the Reynolds stress. The study supports a long-standing goal of turbulence research to achieve a practical, albeit physical, statistical closure of the Reynolds equation for the mean field (see Eq. (1.1)). The proposed approach addresses some of the limitations of eddy viscosity type models, while maintaining some of their advantages. The following five issues are central elements of this investigation:

- (i) realizability;
- (ii) primary and secondary normal stress differences;
- (iii) spatial and temporal relaxation, or memory, phenomena;
- (iv) frame dependence; and,

## (v) universality.

The Boussinesq model for the Reynolds stress (Eq. (1.5)) which provides closure for the ubiquitous k- $\epsilon$  theory (Hanjalic and Launder, 1972; Speziale, 1991) as well as for the subgrid scale model for large scale eddy simulations (Bardina, et al., 1985), misrepresents some aspects of the above five physical issues. Items (i)-(iv) are fundamental and necessary for any closure hypothesis which aims for some limited form of universality. However, the possibility of a low-order, universal closure theory for turbulent flows remains a speculative, albeit desirable, goal.

This research is limited to the development of a closure for the *normalized* Reynolds stress

$$\underline{R} = \frac{\langle \underline{u}'\underline{u}' \rangle}{2k}.\tag{1.33}$$

Previously published experimental data for homogeneously sheared turbulent flows provides an extensive resource to guide the development (see, esp., Tavoularis and Karnik, 1989; Tavoularis and Corrsin, 1981; Gibson and Kanellopoulos, 1987). In order to develop some understanding of the potential applicability of the proposed approach to flows with streamline curvature, the new theory is used to predict the distribution of asymptotic states for homogeneously sheared turbulence in a rotating frame of reference. This study complements a parallel development of this theory for fully developed channel flows by Weispfennig [1997].

#### 1.3 Methodology

The theoretical approach to closure stems directly from the continuity equation and the

equation of motion for a constant density, constant viscosity, Newtonian fluid. An explicit dependence of the Reynolds stress on the reference frame (i.e. Issue (iv) in Section 1.2) is introduced by a direct analysis of the equation for the fluctuating velocity field relative to a rotating frame of reference (Chapter 3 and Appendix B). The development introduces one level of memory into the closure by using a smoothing approximation related to the relative relaxation of the space-time structure of the turbulence and a convective-diffusive Green's function associated with the non-local transport of momentum fluctuations by the mean field. This strategy, which has been previously employed by Petty [1975] and others (see, esp., Hill and Petty, 1996) for turbulent mass transfer, leads to an algebraic preclosure for the Reynolds stress which relates  $\langle \underline{u}'\underline{u}' \rangle$  to the gradient of the mean field, to a scalar-field relaxation time  $\tau_R$  associated with the temporal structure of the turbulence, and to a statistical correlation hereinafter referred to as the turbulent pre-stress  $(\tau_R \langle \underline{f}, \underline{f$ 

$$\underline{\underline{A}}^T \cdot \langle \underline{\underline{u}}'\underline{\underline{u}}' \rangle \cdot \underline{\underline{A}} = \tau_R \langle \underline{f}'\underline{f}' \rangle, \tag{1.34}$$

where the operator  $\underline{\underline{A}}$  is defined by

$$\underline{A} = I + \tau_R \left( \nabla \left\langle \underline{u} \right\rangle + \underline{\Omega} \right). \tag{1.35}$$

The fluctuating vector  $\underline{f}$  is related to instantaneous fluctuations in the instantaneous Reynolds stress and to pressure fluctuations:

$$\underline{f}' \equiv \nabla \cdot \left[ \frac{p'}{\rho} \underline{I} + \underline{u'}\underline{u'} - \langle \underline{u'}\underline{u'} \rangle \right]. \tag{1.36}$$

An inertial frame pre-closure for  $\langle \underline{u}'\underline{u}' \rangle$  follows directly from Eqs. (1.34) and (1.35) by setting  $\Omega = 0$ .

A phenomenological relaxation model is introduced for the pre-stress and this approach provides an additional means to further address the physical issues associated with Items (i) and (iii) in Section 1.2. The pre-stress is formally decomposed into an isotropic and anisotropic contribution:

$$\tau_{R} \langle \underline{f} \underline{f} \rangle = \frac{2\alpha}{3} \underline{I} + \underline{\tilde{H}}, \tag{1.37}$$

where the anisotropic pre-stress  $\tilde{\underline{H}}$  is both symmetric ( $\tilde{\underline{H}} = \tilde{\underline{H}}^T$ ) and traceless  $(tr(\tilde{\underline{H}}) = 0)$ . This strategy provides an explicit, self-consistent model to relate the isotropic coefficient  $\alpha$  to the mean field properties inasmuch as Eqs. (1.34) and (1.37) imply that

$$2\alpha = tr\left[\underline{\underline{A}}^T \cdot \langle \underline{\underline{u}}'\underline{\underline{u}}' \rangle \cdot \underline{\underline{A}}\right]. \tag{1.38}$$

Thus, no additional closure hypothesis is needed to evaluate the isotropic contribution to the pre-stress. In Chapter 3, the theory is applied to homogeneously sheared turbulence under the assumption that the anisotropic pre-stress is unimportant. This isotropic pre-stress theory (IPS-theory) provides a theoretical limit case to compare with the anisotropic pre-stress theory (APS-theory) developed in Chapter 4 for nontrivial  $\tilde{H}$ . However, the IPS-theory provides a relatively simple extension of the Boussinesq model which incorporates major issues associated with Items (i), (ii), (iv), and (v). The inability of the IPS-theory to account for the well-documented phenomena associated with the return-to-isotropy partly motivates the extension to the APS-theory in Chapter 4.

In Chapter 4, the following property is attached to the anisotropic pre-stress in order to address Item (v) in Section 1.2:

The anisotropic pre-stress is an objective statistical property of a turbulent flow

## and any phenomenological closure model for $\tilde{\underline{H}}$ should be frame invariant.

The above assumption has been applied incorrectly to phenomenological models for  $\langle \underline{u}'\underline{u}'\rangle$ , of which the Boussinesq model is a prime example as well as some algebraic theories proposed by Speziale [1987]. The assumption here is that the operator  $\underline{\underline{A}}$  introduced by the pre-closure provides the necessary frame-dependent effects manifested by the Reynolds stress. The isotropic pre-stress contains a self-consistent frame dependence inasmuch as the anisotropic pre-stress is traceless:

$$tr(\tilde{\underline{H}}) = 0. ag{1.39}$$

Thus, the above closure hypothesis related to the behavior of the anisotropic pre-stress implicitly supports the goal of developing a *universal* closure.

The IPS- and APS-theory are used in Chapter 5 to predict the effect of frame rotation on the asymptotic states of homogeneous shear. The phenomenological coefficients introduced by the model are scaled with the turbulent kinetic energy k and the turbulent dissipation  $\epsilon$ . The large Reynolds number (i.e.  $k^2/v\epsilon \gg 1$ ) scalar transport equations are used to estimate the behavior of k and  $\epsilon$ . However, the coefficients in the k- $\epsilon$  equations are recalibrated using the IPS- and APS- closures for the Reynolds stress. The benchmark flows used to calibrate certain aspects of the theory include:

- homogeneous isotropic decay,
- return-to-isotropy, and
- asymptotic homogeneous shear.

Experimental data for these flows relative to an inertial frame are used to estimate model coefficients.

In Chapter 2, the classical problem of homogeneous isotropic decay is examined to determine the effect of the turbulent Reynolds number  $(k^2/v\epsilon)$  on the decay process. An approximate integral analysis of the Kármán-Howarth equation is employed to relate velocity derivative skewness data to the dissipation coefficient which appears explicitly in the  $\epsilon$ -equation (see the coefficient  $C_D$  in Eq. (1.16)). An extension of the APS-theory developed hereinafter to flows for which  $k^2/v\epsilon \ll 1$  will require a complementary low Reynolds number k- $\epsilon$  theory to calculate the turbulent time scales needed for momentum transport.

Figure 1.3 illustrates the structure of the theory and highlights the specific area of focus. Presently, the development is incomplete and requires further theoretical work. Applications to specific test flows (see the recommendations in Chapter 7) are essential to detect flaws in the proposed closure. However, the methodology developed as part of this research provides a clear and unambiguous framework to introduce further improvements in the proposed low-order closure of the Reynolds stress.

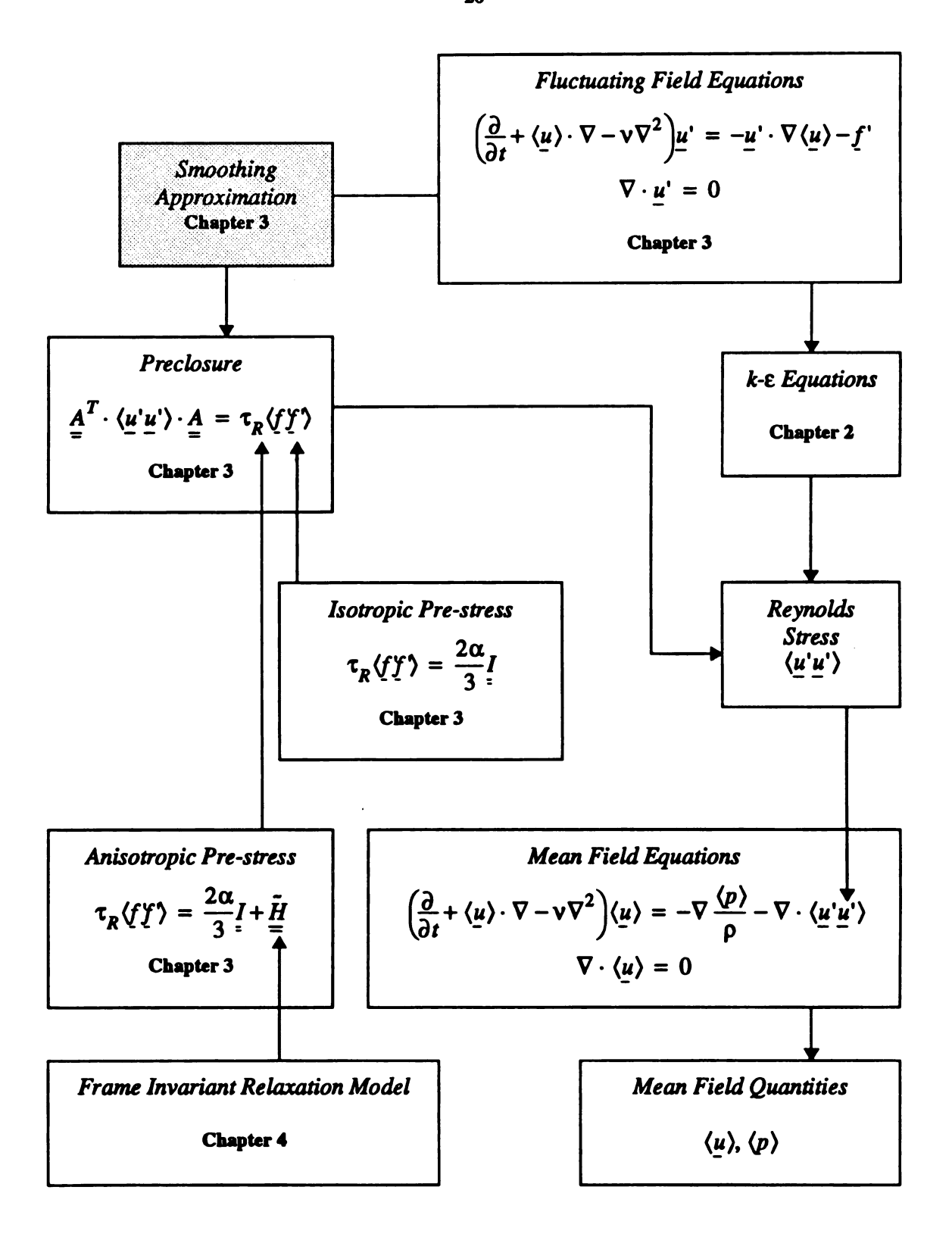


Figure 1.3 Closure Methodology

#### **CHAPTER 2**

### THE DECAY OF ISOTROPIC TURBULENCE IN AN INERTIAL FRAME

## 2.1 Introduction

The problem of decaying isotropic turbulence is a classical benchmark flow in the area of turbulence research. The absence of spatial gradients in any of the mean properties implies that there are no production or diffusive transport effects. Thus, the turbulence decays uniformly with the result that

$$\lim_{t \to \infty} k = 0 \text{ and } \lim_{t \to \infty} \varepsilon = 0. \tag{2.1}$$

Because the flow is isotropic and there exists no means to develop an anisotropic stress, the kinetic energy and the dissipation of turbulence are governed by the following equations (see Appendix A)

$$\frac{dk}{dt} = -\varepsilon \tag{2.2}$$

and

$$\frac{d\varepsilon}{dt} = -2v\langle \left[ \nabla \underline{u}' : (\nabla \underline{u}' \cdot \nabla \underline{u}')^T \right] \rangle - 2v^2\langle \left[ \nabla (\nabla \underline{u}') \right] : \left[ \nabla (\nabla \underline{u}')^T \right] \rangle. \tag{2.3}$$

Although Eqs. (2.2) and (2.3) are formally exact, two unknown statistical correlations

appear in Eq. (2.3). These two terms correspond to the production of dissipation due to vortex stretching and the destruction of dissipation due to viscous effects, respectively. The modeling approach for the dissipation equation introduced by Hanjalic and Launder [1972] assumes that the destruction of turbulent dissipation scales with the local dissipation. Thus, the following statistical *ansatz* is used to represent the underlying physical effect associated with the terms on the right-hand-side of Eq. (2.3):

$$\frac{d\varepsilon}{dt} = -\frac{\varepsilon}{\tau_D},\tag{2.4}$$

where  $\tau_D$  represents a characteristic relaxation time for the dissipation. The conventional  $k-\epsilon$  theory further assumes that  $\tau_D \sim k/\epsilon$  for large turbulent Reynolds numbers. Extension of this closure to low Reynolds numbers involves the introduction of an empirical, albeit universal, destruction of dissipation coefficient  $C_D(Re)$ :

$$\frac{d\varepsilon}{dt} = -C_D(Re)\frac{\varepsilon^2}{k}.$$
 (2.5)

The utility of decaying isotropic turbulence is that Eqs. (2.2) and (2.5) provide a means of determining the closure coefficient  $C_D(Re)$ . Much experimental (Batchelor and Townsend, 1948; Comte-Bellot and Corrsin, 1971; and Sirivat and Warhaft, 1983) and numerical (Bardina *et al.*, 1985; Speziale *et al.*, 1987; and Mansour and Wray, 1994) data are available for the analysis of this model parameter.

Eqs. (2.2) and (2.5) can be combined to yield the following equation for the turbulent time scale  $k/\epsilon$ :

$$\frac{d}{dt}(k/\epsilon) = C_D(Re) - 1. \tag{2.6}$$

Experimental data available for isotropic decay indicate that the time scale  $k/\epsilon$  increases

throughout the decay process, which implies that  $C_D(Re) > 1$ . Analogously, Eqs. (2.2) and (2.5) can be combined to yield an equation for the turbulent Reynolds number Re ( $\equiv k^2/v\epsilon$ ),

$$\frac{d}{dt}(Re) = [C_D(Re) - 2]Re^{\frac{\varepsilon}{k}}.$$
 (2.7)

Eq. (2.7) implies that the decay process can occur at a constant Reynolds number  $Re^*$  defined by  $C_D(Re^*) = 2$ . This critical Reynolds number  $Re^*$  is stable if  $C_D(Re) > 2$  for  $Re < Re^*$  and  $C_D(Re) < 2$  for  $Re > Re^*$ . However, experimental measurements for isotropic decay indicate that Re decreases throughout the decay process. Therefore, the dissipation coefficient  $C_D(Re)$ , introduced by the closure model given by Eq. (2.5), must satisfy the following inequality:

$$1 < C_D(Re) < 2. \tag{2.8}$$

With  $1 < C_D(Re) < 2$ , both k and  $\epsilon$  decay to zero and remain non-negative (i.e. realizable). This follows directly by examining Eqs. (2.2) and (2.5) in the  $k - \epsilon$  plane for which

$$\frac{d\varepsilon}{dk} = C_D(Re)\frac{\varepsilon}{k}.$$
 (2.9)

Figure 2.1 illustrates the set of points consistent with Eq. (2.9) and Ineq. (2.8). The boundaries of the attainable states are constructed by solving Eq. (2.9) with  $C_D = 1$  for the entire decay process (for the upper boundary) and  $C_D = 2$  for the entire decay process (for the lower boundary). If  $1 < C_D(Re) < 2$ , then Eqs. (2.2) and (2.5) predict a realizable relaxation process for k and  $\varepsilon$  consistent with experimental observations, i.e.,

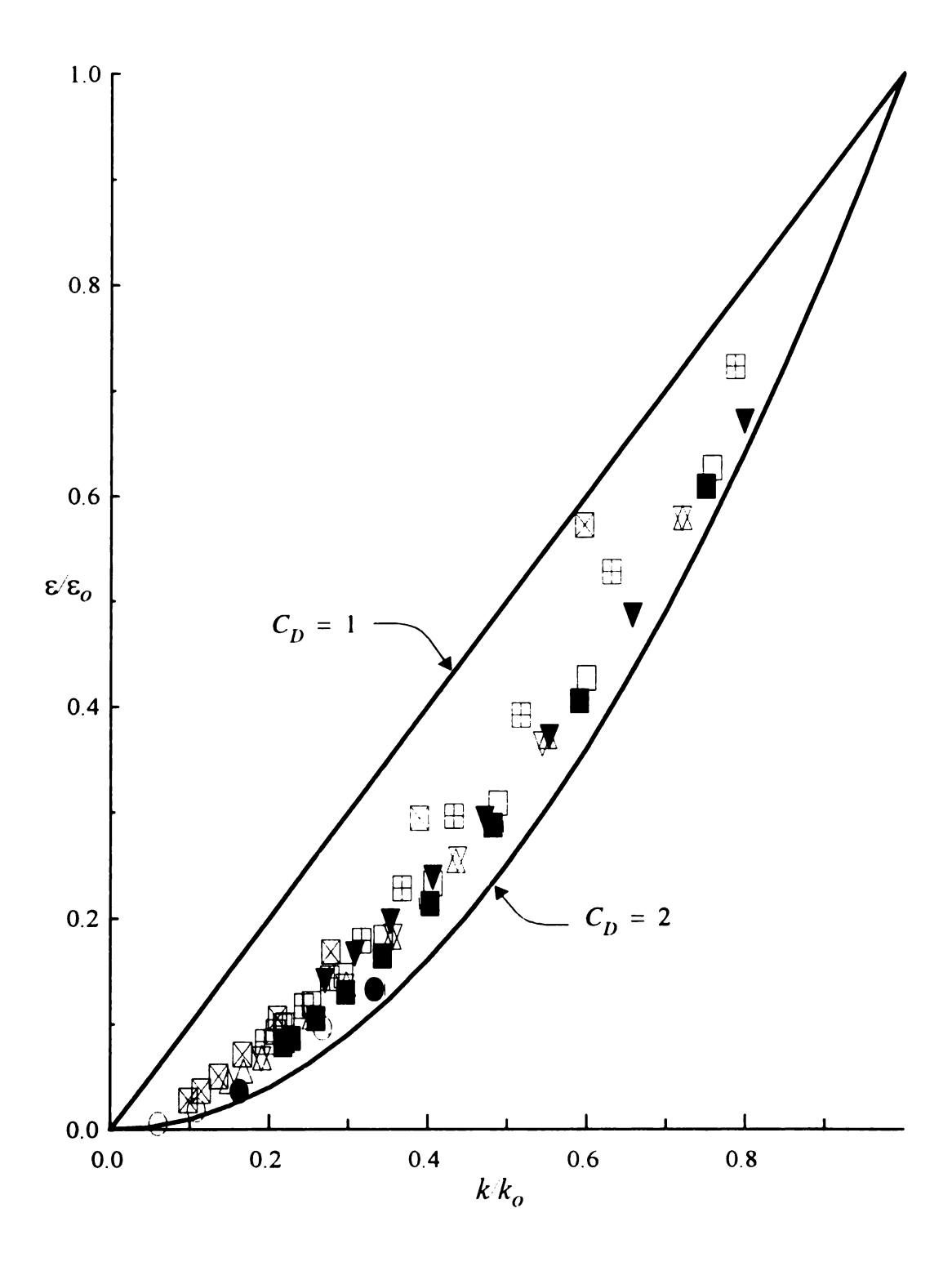


Figure 2.1 Relaxation States for Decaying Isotropic Turbulence (see next page for legend)

# Legend for Figure 2.1

Reo	key	Appendix E Table; Reference
7.58	Δ	Table E.1; Batchelor and Townsend [1948]
42.6	$\nabla$	
83.7	<b>A</b>	
354	0	Table E.2; Comte-Bellot and Corrsin [1971]
769	•	
139		Table E.3; Sirivat and Warhaft [1983]
262		
35.1	Ħ	Table E.4; Speziale, et al. [1987]
45.4	$\boxtimes$	Table E.5; Bardina, et al. [1985]

$$\left(k, \varepsilon, \frac{k}{\varepsilon}, Re\right) \rightarrow (0, 0, \infty, 0)$$
.

Figure 2.1 also shows the relaxation states measured experimentally by Batchelor and Townsend [1948], Comte-Bellot and Corrsin [1971], and Sirivat and Warhaft, [1983]. The DNS results of Bardina et al. [1985] and Speziale et al. [1987] are also indicated. It is noteworthy that the data partly supports the notion that after some initial transient, the destruction of dissipation coefficient approaches a universal function of the Reynolds number.

Using isotropic decay data at high Reynolds numbers (Re > 500, see Comte-Bellot and Corrsin, 1971), Hanjalic and Launder [1972] estimated the decay coefficient to be about two. This value was later refined to 1.92 by Launder and Spalding [1974]. Subsequent investigators introduced empirical functions to account for the effect of the Reynolds number on the coefficient  $C_D$ . For instance, Hanjalic and Launder [1976] proposed the following expression

$$C_D = 1.8 \left[ 1 - \frac{2}{9} exp \left( - \left[ \frac{Re}{6} \right]^2 \right) \right], \tag{2.10}$$

whereas Lumley [1978] suggested

$$C_D = 1.4 + 0.49 exp \left[ -\sqrt{\frac{18}{Re}} \right].$$
 (2.11)

Both of the above empirical expressions for  $C_D$  employ the final decay coefficient estimated by Batchelor and Townsend [1948] (i.e.  $C_D \to 1.4$  as  $Re \to 0$ ). The high Reynolds number asymptote of Comte-Bellot and Corrsin [1971] is used in Eq. (2.10); Eq. (2.11) incorporates the limit  $C_D \to 1.89$  as  $Re \to \infty$ . Both Eqs. (2.10) and (2.11) assume that the destruction of dissipation coefficient increases monotonically as the Reynolds number increases.

Mansour and Wray [1994] studied decaying isotropic turbulence by direct numerical simulation. They computed the skewness of the velocity derivative as well as the destruction-of-dissipation coefficient,  $C_D$ . The velocity derivative skewness is defined by (see p. 58 Monin and Yaglom, 1965):

$$S_{k} = -\langle \left(\frac{\partial u'}{\partial x}\right)^{3} \rangle / \left[\langle \left(\frac{\partial u'}{\partial x}\right)^{2} \rangle\right]^{3/2}, \tag{2.12}$$

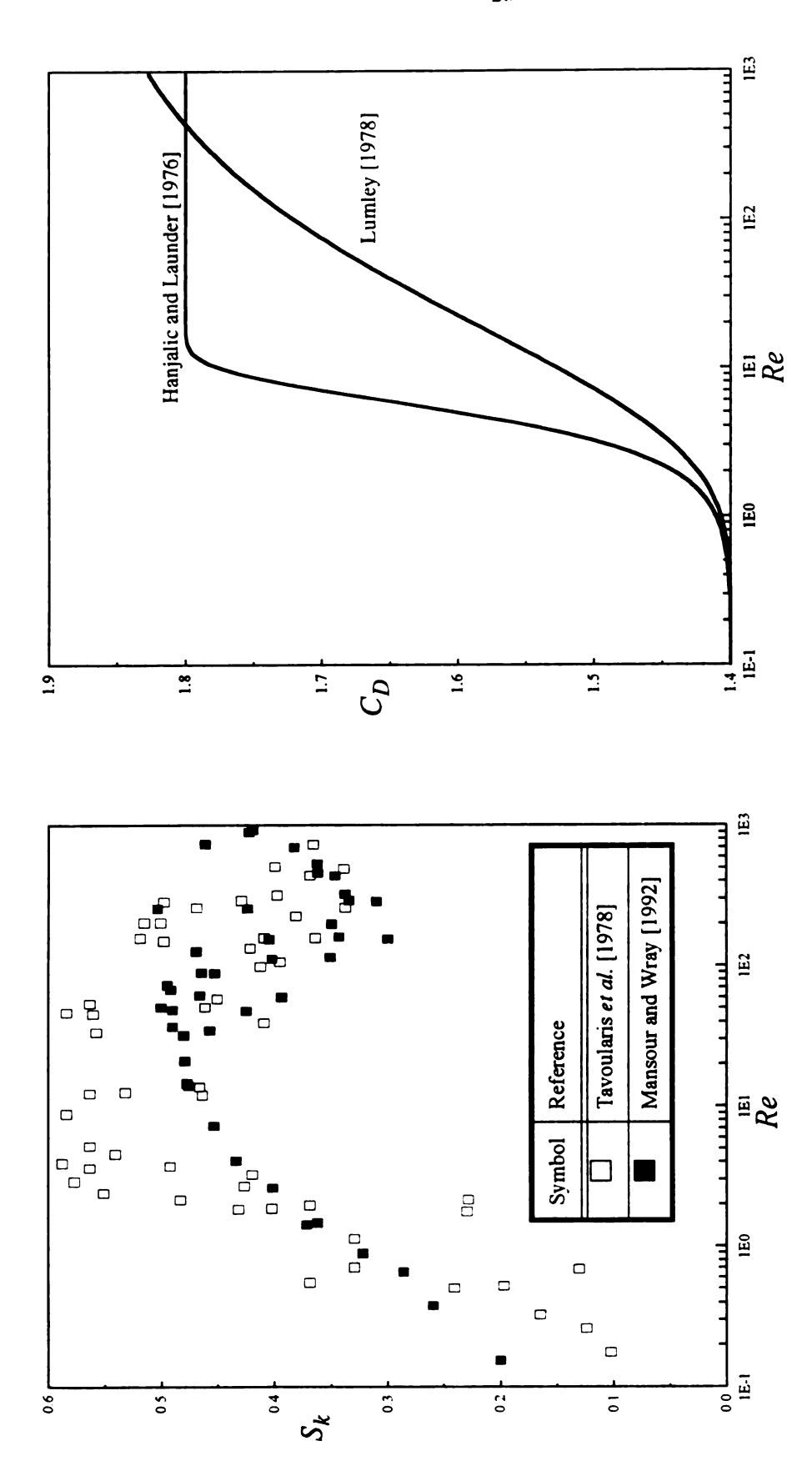
and, as discussed by Tennekes and Lumley [1972], is an important statistical property related to vortex stretching (also see Monin and Yaglom, 1965):

$$-2v\langle \left[\nabla \underline{u}': \left(\nabla \underline{u}' \cdot \nabla \underline{u}'\right)^{T}\right] \rangle \equiv P = \frac{7}{3\sqrt{15}} S_{k} \sqrt{Re}. \tag{2.13}$$

Eq. (2.13) will be derived from the classical Kármán-Howarth equation for isotropic turbulence in Section 2.2. For Re > 100, Mansour and Wray [1994] observed that  $S_k \sim 0.3$  to 0.4. For  $Re \to 0$ ,  $S_k = 0$ . Figure 2.2 shows the effect of Re on the velocity derivative skewness given by Mansour and Wray [1994] and Tavoularis *et al.* [1978]. The empirical representations of  $C_D$  given by Eqs. (2.10) and (2.11) are also shown for comparison.

The goal of this chapter is to develop a relationship between the destruction-of-dissipation coefficient  $C_D$  and the turbulent Reynolds number. In the next section, the rate of change of dissipation will be formally identified as the difference between two statistical properties, viz, the production of dissipation due to vortex stretching and the destruction of dissipation due to viscosity. For decaying isotropic turbulence, the dissipation rate exceeds the production rate, with the net result that the dissipation turnover time (cf. Eqs. (2.4) and (2.5)) is positive:

$$\frac{1}{\tau_D} = (B - P) \frac{\varepsilon}{k} > 0. \tag{2.14}$$



Literature Data for the Skewness and Correlations for the Destruction of Dissipation Coefficient Figure 2.2

The destruction coefficient B and the production coefficient P can be related to specific statistical properties of the flow and possibly provide a means to understand the underlying behavior of the  $k-\varepsilon$  model coefficient  $C_D$ . It follows directly from Eqs. (2.4), (2.5), and (2.14) that

$$C_{D}(Re) = \mathcal{B}(Re) - \mathcal{P}(Re). \tag{2.15}$$

A better understanding of  $C_D(Re)$  is essential for further improvements of the widely used  $k - \varepsilon$  transport equations for turbulent flows.

In Section 2.3, a semi-theoretical approach is used to relate  $C_D$  and Re. Subsequently, an integrated form of the Kármán-Howarth equation (hereinafter referred to as the IKH-equation), which links the double and triple longitudinal velocity correlations, is employed to develop an approximate relationship between  $\mathcal{B}(Re)$  and  $\mathcal{P}(Re)$ . An empirical representation for  $\mathcal{B}(Re)$ , which agrees with experimental results for high and low Reynolds number asymptotes, permits the velocity derivative skewness factor to be predicted from the IKH-equation. The adjustable parameters introduced by the approximation are determined in part from the experimental data summarized by Figure 2.2. In Section 2.6, the non-linear dynamic equations given by Eqs. (2.2) and (2.5) are solved in the time domain for an arbitrary, albeit realizable, initial state  $(k_o, \epsilon_o)$ .

# 2.2 Local Analysis of the Kármán-Howarth Equation

The Kármán-Howarth equation stems directly from the Navier-Stokes equation and provides the following fundamental relationship between the double and triple longitudinal velocity correlations for isotropic turbulence (see Kármán and Howarth, 1938; Hinze, 1975; and, esp., p. 122 Monin and Yaglom, 1965),

$$\frac{\partial}{\partial t}(\tilde{B}_{LL}) = 2\nu \left(\frac{\partial}{\partial r} + \frac{4}{r}\right) \frac{\partial}{\partial r}(\tilde{B}_{LL}) + \left(\frac{\partial}{\partial r} + \frac{4}{r}\right) \tilde{T}_{LLL}. \tag{2.16}$$

In Eq. (2.16),  $\tilde{B}_{LL}(r,t)$  represents the double longitudinal velocity correlation,

$$\tilde{B}_{LL}(r,t) = \langle u'_L(x,t) u'_L(x+r,t) \rangle, \qquad (2.17)$$

and  $\tilde{T}_{LLL}(r, t)$  is the triple longitudinal velocity correlation,

$$\tilde{T}_{LLL}(r,t) = \langle u_L^2(x,t) u_L^i(x+r,t) \rangle. \tag{2.18}$$

 $\tilde{B}_{LL}(r,t)$  is an even function of  $r \in \|r\|$  and  $\tilde{T}_{LLL}(r,t)$  is an odd function of r. Therefore, a Taylor series representation of the two correlations can be written as follows,

$$\tilde{B}_{LL} = \tilde{B}_{LL}(0,t) + \frac{1}{2!} \left( \frac{\partial^2 \tilde{B}_{LL}}{\partial r^2} \right)_{r=0} r^2 + \frac{1}{4!} \left( \frac{\partial^4 \tilde{B}_{LL}}{\partial r^4} \right)_{r=0} r^4 + \dots , \qquad (2.19)$$

and

$$\tilde{T}_{LLL} = \frac{1}{3!} \left( \frac{\partial^3 \tilde{T}_{LLL}}{\partial r^3} \right)_{r=0} r^3 + \dots$$
 (2.20)

An equation for the kinetic energy follows directly from Eq. (2.16) by setting r = 0:

$$\frac{d}{dt}\tilde{B}_{LL}(0,t) = 10v \left(\frac{\partial^2 \tilde{B}_{LL}}{\partial r^2}\right)_{r=0}.$$
 (2.21)

Because  $\tilde{B}_{LL}(0, t) = 2k/3$  for isotropic turbulence, Eqs. (2.21) and (2.2) imply that

$$\varepsilon = -15v \left( \frac{\partial^2 \tilde{B}_{LL}}{\partial r^2} \right)_{r=0}. \tag{2.22}$$

With the Taylor microscale  $\lambda$  defined by the following expression (Tennekes and Lumley, 1972):

$$\left(\frac{\partial^2 \tilde{B}_{LL}}{\partial r^2}\right)_{r=0} = -\frac{\tilde{B}_{LL}(0,t)}{\lambda^2},\tag{2.23}$$

Eq. (2.22) can be rewritten as

$$\varepsilon = 15\nu \frac{\tilde{B}_{LL}(0,t)}{\lambda^2} = \frac{10\nu k}{\lambda^2}.$$
 (2.24)

Eq. (2.21) governs the rate of viscous decrease of the turbulent kinetic energy for an isotropic decay process. The Taylor microscale, or the energy dissipation length scale, is defined by the double longitudinal velocity correlation;  $\lambda$  can also be related to the second moment of the velocity derivative (see p. 143, Monin and Yaglom, 1965).

Eqs. (2.23) and (2.24) suggest that an equation for the energy dissipation also follows from the Kármán-Howarth equation (i.e. Eq. (2.16)) by differentiating twice with respect to r and then setting r = 0. This analysis yields (see p. 144, Monin and Yaglom, 1965)

$$\frac{d}{dt} \left( \frac{\partial^2 \tilde{B}_{LL}}{\partial r^2} \right)_{r=0} = \frac{14}{3} v \left( \frac{\partial^4 \tilde{B}_{LL}}{\partial r^4} \right)_{r=0} + \frac{7}{3} \left( \frac{\partial^3 \tilde{T}_{LLL}}{\partial r^3} \right)_{r=0}. \tag{2.25}$$

Eqs. (2.23) and (2.24) can be used to rewrite Eq. (2.25) as

$$\frac{d\varepsilon}{dt} = -(\vartheta - P)\frac{\varepsilon^2}{k},\tag{2.26}$$

where

$$\vartheta = \frac{7}{15} \frac{\lambda^4}{\tilde{B}_{LL}(0)} \left( \frac{\partial^4 \tilde{B}_{LL}}{\partial r^4} \right)_{r=0}$$
 (2.27)

and

$$\theta = \frac{-7}{3\sqrt{15}} \frac{\lambda^3 \sqrt{Re}}{\left(\tilde{B}_{LL}(0)\right)^{3/2}} \left(\frac{\partial^3 \tilde{T}_{LLL}}{\partial r^3}\right)_{r=0}.$$
(2.28)

The first term on the right-hand side of Eq. (2.26) causes a decrease in energy dissipation due to viscous damping as B is always positive, i.e.,

$$\left(\frac{\partial^4 \tilde{B}_{LL}}{\partial r^4}\right)_{r=0} > 0. \tag{2.29}$$

The second term on the right-hand side of Eq. (2.26) accounts for the "production" of dissipation by vortex stretching (see p.144 Monin and Yaglom, 1965; and, esp., p. 83 Tennekes and Lumley, 1972). For isotropic turbulence, P is generally positive inasmuch as

$$\left(\frac{\partial^3 \tilde{T}_{LLL}}{\partial r^3}\right)_{r=0} < 0. \tag{2.30}$$

The production term can also be written in terms of the velocity derivative using the following result (see Appendix F)

$$\frac{\lambda^{3}}{\left(\tilde{B}_{LL}(0)\right)^{3/2}} \left(\frac{\partial^{3} \tilde{T}_{LLL}}{\partial r^{3}}\right)_{r=0} = \left\langle \left(\frac{\partial u'}{\partial x}\right)^{3} \right\rangle / \left[\left\langle \left(\frac{\partial u'}{\partial x}\right)^{2} \right\rangle\right]^{3/2} \equiv -S_{k}. \tag{2.31}$$

Eq. (2.26) shows that the net destruction of dissipation coefficient  $C_D$  (Re) has two contributions (see Eq. (2.15)). In the next section, an integral analysis of the Kármán-Howarth equation is used to estimate the effect of the Reynolds number on the coefficient  $C_D$  by using velocity derivative skewness data (see Figure 2.2).

## 2.3 Global Analysis of the Kármán-Howarth Equation

Integrating Eq. (2.16) from r = 0 to  $r = \infty$  yields an integrated form of the Kármán-Howarth equation (IKH-equation):

$$\frac{d}{dt}\int_{0}^{\infty} \tilde{B}_{LL}dr = 8v\int_{0}^{\infty} \frac{1}{r}\frac{\partial}{\partial r}(\tilde{B}_{LL})dr + 4\int_{0}^{\infty} \frac{1}{r}\tilde{T}_{LLL}dr . \qquad (2.32)$$

The following conditions on the double and triple longitudinal velocity correlations have been used to obtain Eq. (2.32)

$$\left(\frac{\partial \tilde{B}_{LL}}{\partial r}\right)_{r=0,\infty} = 0 \quad \text{and} \quad \left(\tilde{T}_{LLL}\right)_{r=0,\infty} = 0.$$

With dimensionless velocity correlations defined as

$$B_{LL} = \frac{\tilde{B}_{LL}(r,t)}{\tilde{B}_{LL}(0,t)} \tag{2.33}$$

and

$$T_{LLL} = \frac{\tilde{T}_{LLL}(r,t)}{\tilde{T}_{TLL}(0,t)}, \tag{2.34}$$

Eq. (2.32) can be rewritten as

$$\frac{d}{dt} \left[ \tilde{B}_{LL}(0,t) \lambda I_1 \right] = \frac{8V}{\lambda} \tilde{B}_{LL}(0,t) I_2 + 4 \left( \tilde{B}_{LL}(0,t) \right)^{3/2} I_3. \tag{2.35}$$

The dimensionless integrals in the above equation are defined as follows:

$$I_1 = \int_0^\infty B_{LL} d\xi, \tag{2.36}$$

$$I_2 = \int_0^\infty \frac{1}{\xi} \frac{\partial}{\partial \xi} (B_{LL}) d\xi, \text{ and}$$
 (2.37)

$$I_3 = \int_0^1 \frac{1}{\xi} T_{LLL} d\xi, \tag{2.38}$$

where  $\xi \equiv r/\lambda$ . Because  $k = 3\tilde{B}_{LL}(0, t)/2$ , Eq. (2.35) may also be written as

$$\frac{d}{dt}(k\lambda I_1) = \frac{8vk}{\lambda}I_2 + \sqrt{\frac{32}{3}}k^{3/2}I_3. \tag{2.39}$$

With  $\lambda^2 = 10vk/\varepsilon$ , it follows directly from Eq. (2.6) that temporal changes in the Taylor microscale are governed by

$$\frac{d\lambda}{dt} = (C_D - 1)\sqrt{\frac{10v\varepsilon}{4k}}. (2.40)$$

Therefore, because  $C_D > 1$  for isotropic decay in an inertial frame of reference, Eq. (2.40) implies that the integral microscale increases during the decay process. Note, however, that the rate of change in  $\lambda$  decreases inasmuch as the ratio  $k/\epsilon \to \infty$  as k and  $\epsilon$  decay (see Section 2.1).

Eqs. (2.40), (2.2) and (2.5) can be used to eliminate the Taylor microscale from Eq.(2.39) with the result that

$$(C_D - 3) + 2\frac{k}{\varepsilon} \left[ \frac{d}{dt} \ln (I_1) \right] = \frac{8}{5} \left[ \frac{I_2}{I_1} + \frac{I_3}{I_1} \sqrt{\frac{5Re}{3}} \right]. \tag{2.41}$$

An important assumption regarding the decay process is that the integral  $I_1$  depends only

on the instantaneous Reynolds number  $(k^2/v\varepsilon)$ :

$$I_1 = I_1(Re)$$
. (2.42)

The above *universality* hypothesis uncouples Eq. (2.41) from the initial conditions. Therefore, it follows from Eqs. (2.42) and (2.7) that

$$2\frac{k}{\varepsilon} \left[ \frac{d}{dt} ln(I_1) \right] = 2\frac{k}{\varepsilon} \left[ \frac{dRe}{dt} \frac{dln(I_1)}{dRe} \right] = 2(C_D - 2) \frac{dln(I_1)}{dln(Re)}. \tag{2.43}$$

Eq. (2.41) can now be rewritten as

$$(C_D - 3) + 2(C_D - 2)\frac{dln(I_1)}{dln(Re)} = \frac{8}{5} \left[ \frac{I_2}{I_1} + \frac{I_3}{I_1} \sqrt{\frac{5Re}{3}} \right]. \tag{2.44}$$

The above equation is an integral property of the Kármán-Howarth equation and will be subsequently used to develop some understanding of the possible dependence of the destruction-of-dissipation coefficient  $C_D$  as well as the velocity derivative skewness on the turbulent Reynolds number for  $0 < Re < \infty$ .

# 2.4 Approximate Analysis of the Dissipation and Production Integrals

The previously developed series expansions for the double and triple longitudinal correlations (see Eqs. (2.19) and (2.20)) can be rewritten in terms of  $\xi$ ,  $\vartheta$ , and P by using the definitions given by Eqs. (2.27) and (2.28):

$$B_{LL} = 1 - \frac{1}{2}\xi^2 + \frac{5\theta}{56}\xi^4 + \dots$$
 (2.45)

and

$$T_{LLL} = -\sqrt{\frac{15}{Re}} \frac{\rho}{14} \xi^3 + \dots$$
 (2.46)

Figure 2.3 illustrates the behavior of the three functions which determine the integrals  $I_1$ ,  $I_2$ , and  $I_3$ . As an approximation, the integrals in Eq. (2.44) will be estimated using a finite cut-off separation distance related to the behavior of the dissipation integrand  $I_2$  (see Figure 2.3):

$$I_1 = \int_0^{\xi_c} B_{LL} d\xi = \xi_c - \frac{1}{6} \xi_c^3 + \frac{\vartheta}{56} \xi_c^5 + \dots,$$
 (2.47)

$$I_{2} = \int_{0}^{\xi_{c}} \frac{1}{\xi} \frac{\partial}{\partial \xi} (B_{LL}) d\xi = -\xi_{c} + \frac{20\theta}{168} \xi_{c}^{3} + \dots,$$
 (2.48)

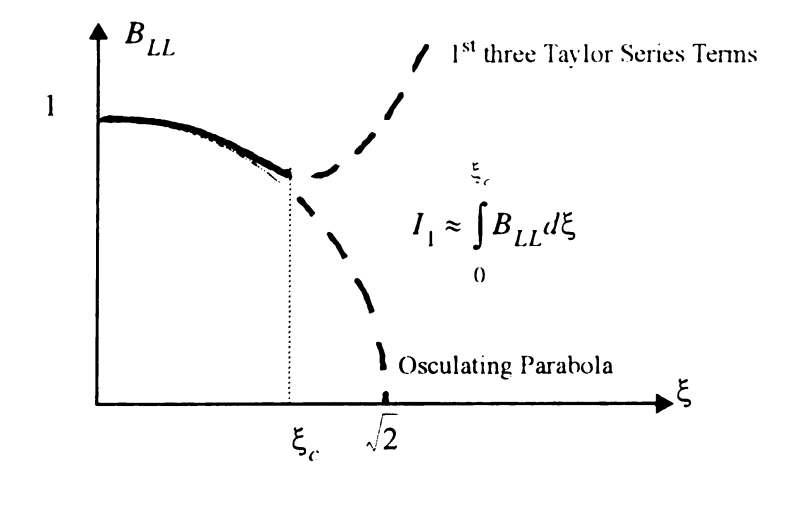
and

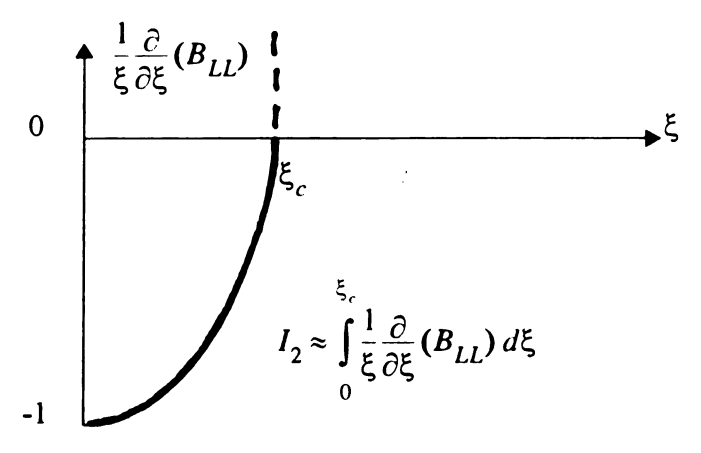
$$I_3 = \int_0^{\xi_c} \frac{1}{\xi} T_{LLL} d\xi = -\sqrt{\frac{15}{Re}} \frac{\rho}{42} \xi_c^3 + \dots,$$
 (2.49)

The cut-off separation distance  $\xi_c$ , defined by Figure 2.3, scales with the Taylor microscale and the dimensionless viscous destruction coefficient,

$$\xi_c = \frac{r_c}{\lambda} = \sqrt{\frac{14}{5\beta}}.\tag{2.50}$$

The experimental results of Tavoularis and Corrsin [1981] and the direct simulation results of Mansour and Wray [1994] show that the velocity derivative skewness  $S_k < \infty$  as  $Re \to \infty$ ; therefore, Eq. (2.13) implies that





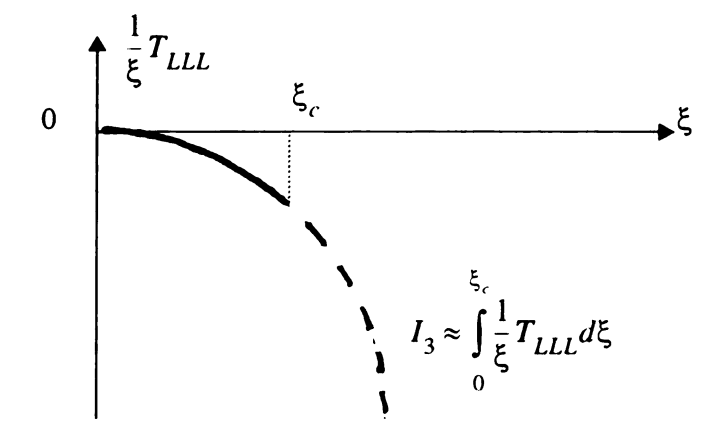


Figure 2.3 Qualitative Behavior of the Integrands of  $I_1$ ,  $I_2$ , and  $I_3$ ; Estimation of the Cut-off Integration Distance  $\xi_c$ .

$$\lim_{Re \to \infty} \rho \sim S_k \sqrt{Re}. \tag{2.51}$$

It follows from Eqs. (2.15) and (2.51) that

$$\lim_{Re \to 0} C_D \equiv C_D^o = \mathcal{S}_o > 1. \tag{2.52}$$

Experimental data of Batchelor and Townsend [1948] at low Reynolds numbers imply that  $C_D^o = 1.4$ ; therefore, it follows from the above limits that  $\theta_o = 1.4$ .

At large Reynolds number, the data of Tavoularis and Corrsin [1981] and the simulations of Mansour and Wray [1994] (see Figure 2.2) indicate that

$$\lim_{R_{\ell} \to \infty} S_k = S_k^{\infty} \approx 0.4. \tag{2.53}$$

Therefore, the production of dissipation coefficient increases with the Reynolds number as follows (see the definition of P given by Eq. (2.13))

$$\lim_{Re \to \infty} \theta = \frac{7}{3\sqrt{15}} S_k^{\infty} \sqrt{Re} . \tag{2.54}$$

Because  $1 < C_D < 2$ , it follows that the asymptotic behavior of  $\mathcal{B}$  at large Reynolds numbers must be as follows

$$\lim_{Re \to \infty} \mathfrak{d} \equiv \mathfrak{d}_{\infty} = C_D^{\infty} + \frac{7}{3\sqrt{15}} S_k^{\infty} \sqrt{Re}, \tag{2.55}$$

where  $C_D^{\infty}$  ~ 1.8 to 1.9 (see Section 2.1; Comte-Bellot and Corrsin, 1971; and Sirivat and Warhaft, 1983).

It follows directly from Eq. (2.50) and the asymptotic behavior of the viscous destruction term that the integral cut-off parameter  $\xi_c$  has the following limits at high and

low Reynolds numbers

$$\lim_{Re \to 0} \xi_c = \sqrt{2} \tag{2.56}$$

and

$$\lim_{Re \to \infty} \xi_c = 0 \tag{2.57}$$

Each of the integral ratios appearing in Eq. (2.44) can be estimated in terms of  $\xi_c$ . For instance, it follows directly from Eqs. (2.47) and (2.48) that

$$\frac{I_2}{I_1} = \frac{-\xi_c + \frac{20\theta}{168} \xi_c^3 + \dots}{\xi_c - \frac{1}{6} \xi_c^3 + \frac{\theta}{56} \xi_c^5 + \dots},$$
(2.58)

As  $Re \to \infty$ , Eq. (2.50) for  $\xi_c$  implies that the ratio  $I_2/I_1$  asymptotically approaches -2/3 inasmuch as

$$\lim_{Re \to \infty} \left[ \frac{I_2}{I_1} \right] = \frac{-\frac{2}{3} + \theta\left(\frac{1}{\beta}\right)}{1 - \frac{45}{150} \frac{1}{\beta} + \theta\left(\frac{1}{\beta^2}\right)} \to -\frac{2}{3}.$$
 (2.59)

For  $Re \rightarrow 0$ , it follows from Eq. (2.38) in the previous section that

$$\lim_{Re \to 0} \left[ \frac{I_2}{I_1} \right] = \frac{5}{8} \left( C_D^o - 3 \right), \tag{2.60}$$

provided  $I_3/I_1 < \infty$  and  $dI_1/dRe < \infty$  for  $Re \to 0$ . Therefore, with  $C_D^o = 1.4$ , Eq.(2.60) implies that

$$\lim_{Re \to 0} \left\lceil \frac{I_2}{I_1} \right\rceil = -1. \tag{2.61}$$

Because  $0 \le \xi_c \le \sqrt{2}$ , a linear interpolation for  $I_2/I_1$  as a function of  $\xi_c$  will be used between the two limits given by Eqs. (2.59) and (2.61). Therefore,

$$\frac{I_2}{I_1} = -\frac{2}{3} - \frac{1}{3} \frac{\xi_c}{\sqrt{2}},\tag{2.62}$$

which can also be written as

$$\frac{I_2}{I_1} = -\frac{2}{3} - \frac{1}{3}\sqrt{\frac{14}{10\vartheta}}. (2.63)$$

It follows from Eqs. (2.47) and (2.50) that  $I_1$  depends on the turbulent Reynolds number implicitly through  $\xi_c$  and, consequently,  $\delta$ . Thus,

$$\frac{Re}{I_1}\frac{dI_1}{dRe} = \left[\frac{Re}{B}\frac{dB}{dRe}\right] \left[\frac{B}{I_1}\frac{dI_1}{dB}\right]. \tag{2.64}$$

It follows from Eqs. (2.47) and (2.50) that

$$\frac{g}{I_1} \frac{dI_1}{d\theta} = -\frac{1}{2} \frac{1 - \theta\left(\frac{1}{g}\right)}{1 - \theta\left(\frac{1}{g}\right)}.$$
 (2.65)

For  $Re \to \infty$ , Eq. (2.55) shows that  $\vartheta \to \infty$ ; therefore,

$$\lim_{Re \to \infty} \left[ \frac{g}{I_1} \frac{dI_1}{dB} \right] = -\frac{1}{2}.$$
 (2.66)

For  $Re \rightarrow 0$ ,

$$\lim_{Re \to 0} \left[ \frac{g}{I_1} \frac{dI_1}{d\theta} \right] = -\frac{1}{2} a. \tag{2.67}$$

The parameter a remains as an adjustable universal parameter. A linear interpolation

similar to Eq. (2.62) is used for intermediate values of the Reynolds number. Therefore,

$$\frac{g}{I_1} \frac{dI_1}{d\theta} = -\frac{1}{2} \left[ 1 + [a-1] \frac{\xi_c}{\sqrt{2}} \right], \tag{2.68}$$

or, in terms of the viscous destruction coefficient,

$$\frac{g}{I_1}\frac{dI_1}{d\theta} = -\frac{1}{2}\left[1 + [a-1]\sqrt{\frac{14}{10\theta}}\right]. \tag{2.69}$$

The estimate of  $I_3/I_1$  follows from the approximations expressed by Eqs. (2.47) and (2.49) along with the integration cut-off distance given by Eq. (2.50):

$$\frac{I_3}{I_1} = \frac{-\frac{1}{\sqrt{15Re}} \frac{\rho}{\delta} \xi_c + \dots}{\xi_c - \frac{7}{60} \xi_c^3 + \dots}.$$
 (2.70)

The limiting behavior of Eq. (2.70) is not apparent, so the lead term in the numerator is factored and the remaining ratio is modeled as a *universal* constant:

$$\frac{I_3}{I_1} = \frac{-1}{\sqrt{15Re}} \frac{\rho}{\delta} b \ . \tag{2.71}$$

The parameter b is a constant to be evaluated at the high Reynolds number asymptote. At infinite Reynolds numbers, Eq. (2.55) implies that

$$\frac{Re}{s}\frac{ds}{dRe} = \frac{1}{2}. \tag{2.72}$$

When combined with Eqs. (2.44), (2.59), (2.66), and (2.71), the above result yields

$$\frac{C_D^{\infty}}{2} - 2 = -\frac{16}{15} - \frac{8}{15}b. \tag{2.73}$$

This gives b = 0.0343 for  $C_D^{\infty} = 1.83$ .

### 2.5 Parameter Estimates

The asymptotic states (i.e.  $Re \to 0$  and  $Re \to \infty$ ) have been used to approximate the integral expressions found in Eq. (2.44). Eq. (2.44) may now be used to predict the intermediate behavior of  $C_D(Re)$ . A parametric study of  $C_D(Re)$  with respect to the empirical parameter in the representation for  $\mathcal{S}(Re)$  will conclude this section. The selection of  $\mathcal{S}(Re)$  may be judged as acceptable based on the resulting prediction of the velocity derivative skewness compared to experimental and simulation data for  $\mathcal{S}_k(Re)$ . The form of  $\mathcal{S}(Re)$  is specified by the following function:

$$\mathcal{B} = \left(C_D^{\infty} + \frac{7}{3\sqrt{15}}S_k^{\infty}\sqrt{Re}\right) - \left(C_D^{\infty} - C_D^{o}\right)exp\left[-\left(Re/Re^{*}\right)^{n}\right],\tag{2.74}$$

where  $S_k^{\infty}$  represents the high Reynolds number asymptote for the skewness.  $Re^*$  and n are empirical parameters which control the transition for the destruction term between its high and low Reynolds number asymptotes.

The parameters a,  $Re^*$  and n are selected to reproduce the trend in  $S_k(Re)$  consistent with Eq. (2.44) and the foregoing approximations to  $I_1$ ,  $I_2$ , and  $I_3$ . The constants, which have been determined as a result of a parametric study, are a=-3.5,  $Re^*=2.2$  and n=1.25. Figure 2.4a shows the behavior of  $S_k(Re)$  predicted by Eq. (2.44). By design, the skewness assumes a value of 0.4 at large Reynolds numbers. Interesting is the prediction that a local maximum of  $S_{k,max}=0.52$  occurs at Re=5, which compares favorably with the data for the skewness:  $S_{k,max}=0.5$  to 0.6 at Re=5 to 10 (Tavoularis et al., 1978; and Mansour and Wray, 1994). All asymptotic and empirical parameters used to support this analysis are summarized in Table 2.1. Of the ten

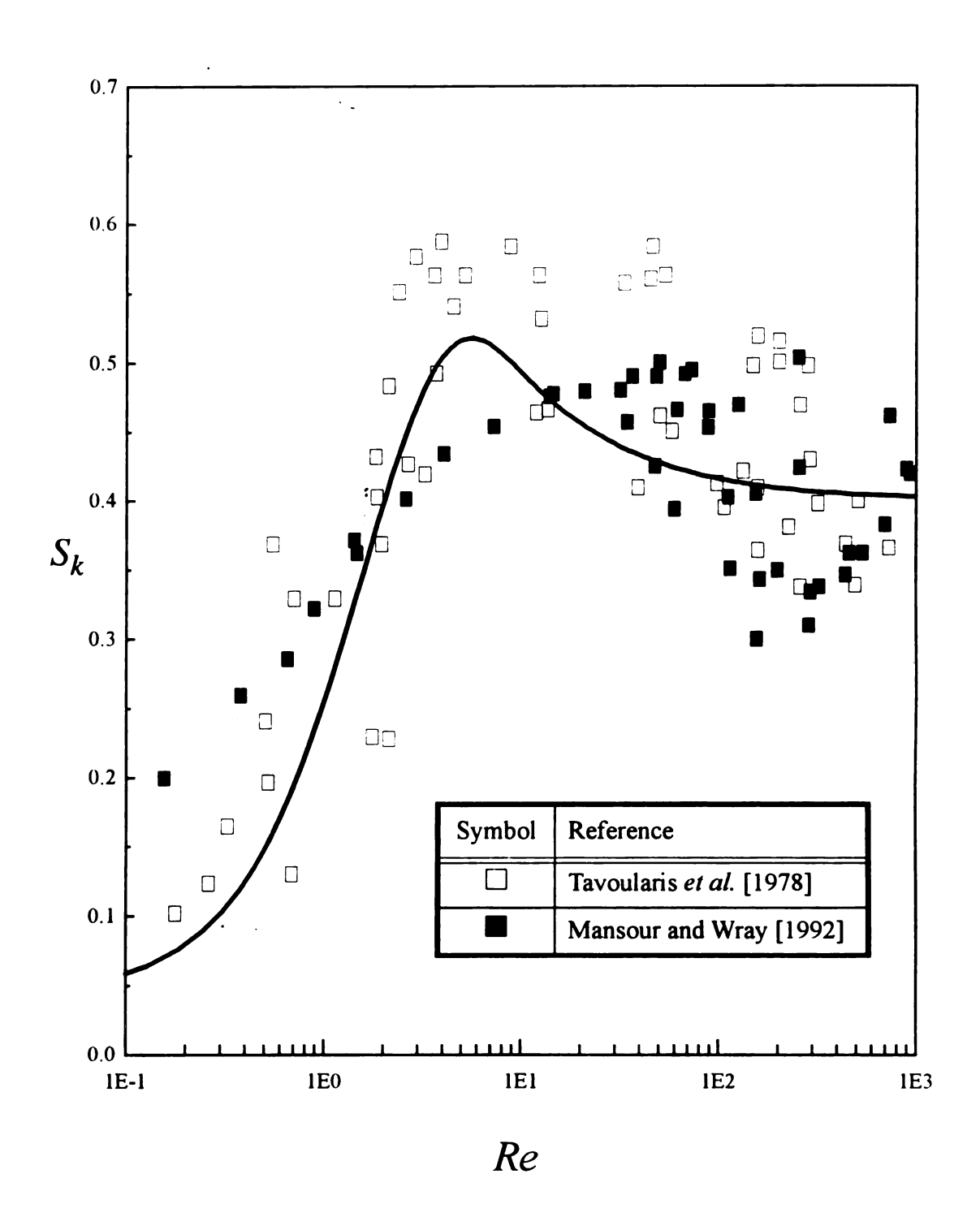


Figure 2.4a Predictions of the IKH-Equation for the Skewness Using a Prescribed Function for the Destruction of Dissipation (a = -3.5,  $Re^{*} = 2.2$  and n = 1.25).

Table 2.1: Summary of Parameters Used in the Analysis of the IKH-Equation

Parameter	Value	Basis
C_D_	1.83	High Re data of Comte-Bellot and Corrsin [1972]; direct simulations of Mansour and Wray [1994]
$C_D^o$	1.4	Final decay period of Batchelor and Townsend [1948]
S <sub>k</sub> <sup>∞</sup>	0.4	Data of Tavoularis et al. [1978]; direct simulations of Mansour and Wray [1994]
$(I_2/I_1)_o$	-1	Consistency with $C_D^o$
(I <sub>2</sub> /I <sub>1</sub> )	-2/3	Asymptotic behavior of series representations for integral quantities
$\left[\frac{g}{I_1}\frac{dI_1}{dB}\right]_{\infty}$	-1/2	Asymptotic behavior of series representations for integral quantities
а	-3.5	Empirical parameter in $(B/I_1)(dI_1/dB)$ selected for consistency with data for skewness
ь	0.0343	Consistency with $C_D^{\infty}$
Re*	2.2	Empirical parameter in $\mathcal{S}(Re)$ selected for consistency with data for skewness
n	1.25	Empirical parameter in $\mathcal{S}(Re)$ selected for consistency with data for skewness

parameters listed in Table 2.1, seven are derived directly from experimental data and/or from consistency conditions with the asymptotic behavior of various quantities. Only three quantities are left as free constants to reproduce the data for the velocity derivative skewness.

The effects of the parameters a and  $Re^*$  on the resulting skewness prediction are shown in Figures 2.4b and 2.4c. In each case, the parameters used in the computations are the same as those listed in Table 2.1, with the exception of the variable shown in the figures. Figure 2.4b indicates that the parameter  $Re^*$  influences both the location (in terms of Re) and the magnitude of the local maximum in the skewness. Figure 2.4c shows that the parameter a also influences the magnitude of the local maximum in the skewness as well as the low Reynolds number behavior of the skewness.

Figure 2.5 illustrates the semi-theoretical prediction of  $C_D$  (Re) and Figure 2.6 shows the individual contributions of  $\mathcal{B}(Re)$  and  $\mathcal{P}(Re)$  to the destruction-of-dissipation coefficient. The curve for  $\mathcal{B}(Re)$  is the empirical prescription described by Eq. (2.74). The curve for  $\mathcal{P}(Re)$  is the resulting prediction of Eq. (2.44). Within the context of the modeled form of the IKH-equation, the local maximum in  $C_D$  (Re) is a direct consequence of the transition of  $\mathcal{B}(Re)$  between high and low Reynolds number behavior. For instance, if  $C_D^{\infty} - C_D^{o} = 0$  (with all other parameters being the same as given above), then  $C_D$  (Re) is constant. As  $C_D^{\infty} - C_D^{o}$  increases, however, the non-monotonic behavior becomes more pronounced. At large Reynolds numbers, the growth of both production and destruction are proportional to  $\sqrt{Re}$ , and  $C_D = \mathcal{B} - \mathcal{P} \to C_D^{\infty} = 1.83$ .

Given that the non-monotonic behavior of  $C_D(Re)$  is supported by: (1) the analysis of the classical Kármán-Howarth Equation; and, (2) the numerical simulations of Mansour and Wray [1994], the following empirical representation of  $C_D(Re)$  is proposed as an improvement on the previous expressions developed in the literature (see Figure 2.2),

$$C_{D} = \frac{C_{D}^{o} + C_{D}^{\infty} (Re/Re_{A})^{s}}{1 + (Re/Re_{A})^{s}} \left[ 1 + C^{*} \left[ exp \left( -p \left\{ ln \left( Re/Re_{P} \right)^{2} \right\} \right) \right] \right]. \tag{2.75}$$

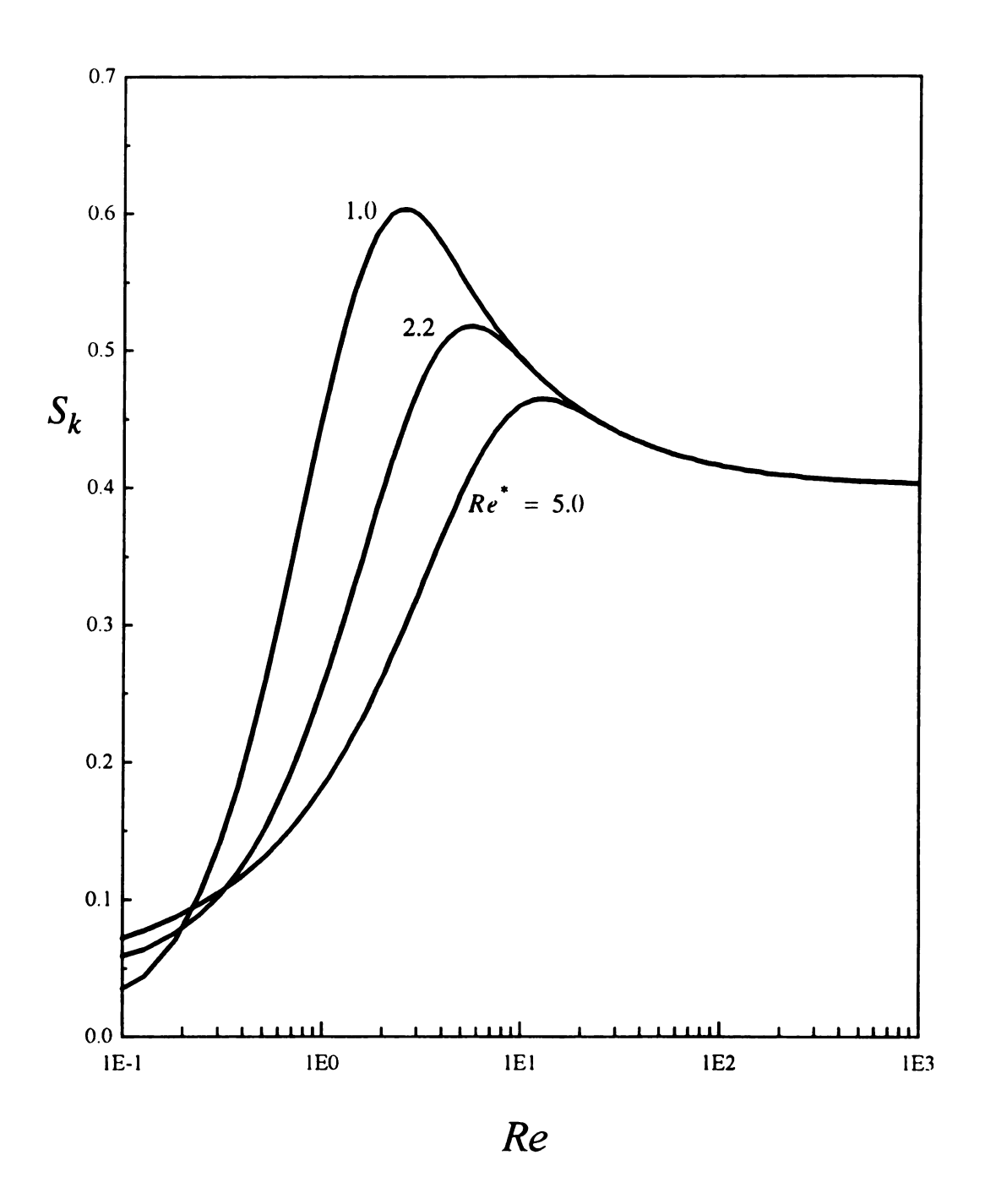


Figure 2.4b The Effect of  $Re^*$  on the Velocity Derivative Skewness (a = -3.5 and n = 1.25).

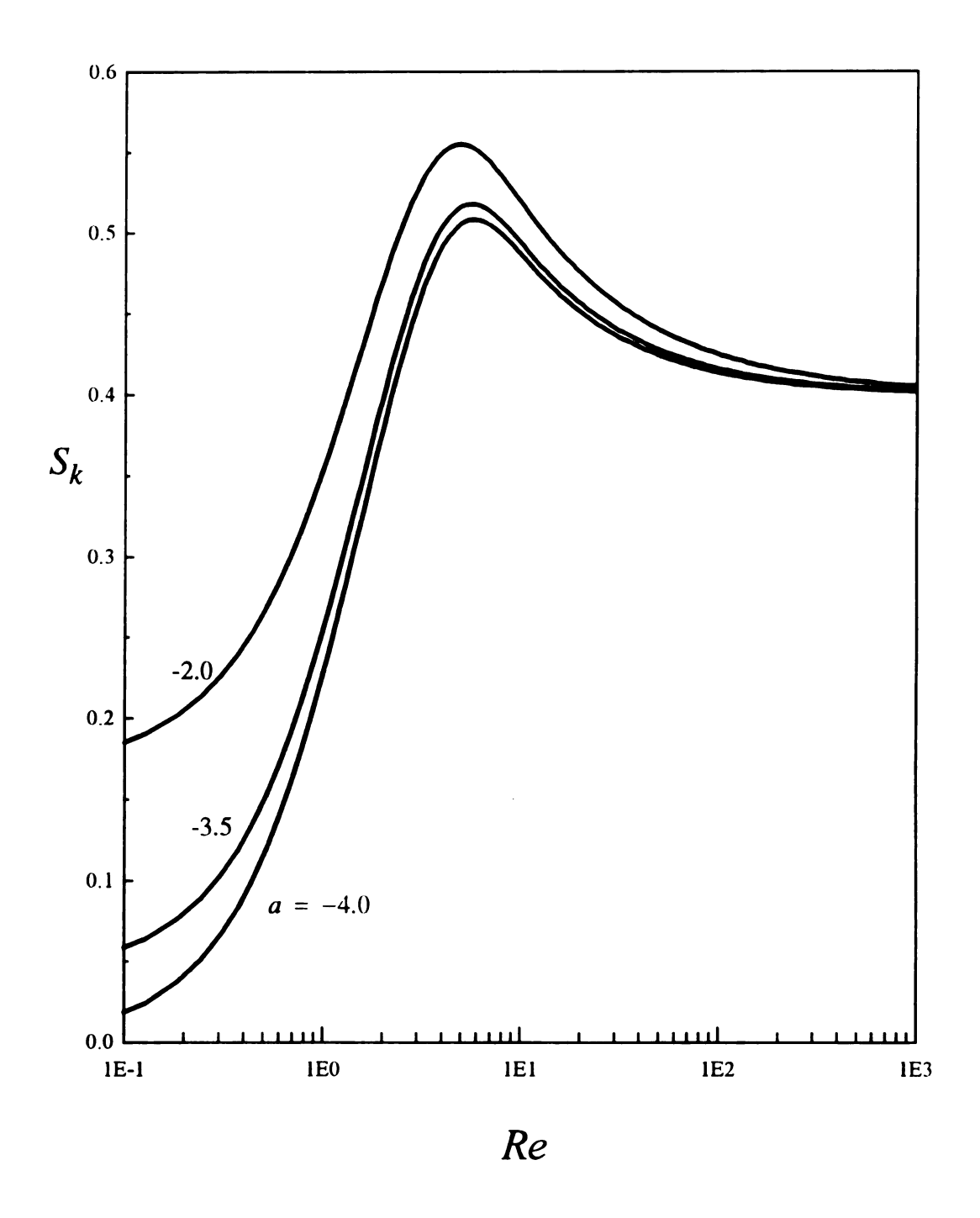


Figure 2.4c The Effect of a on the Velocity Derivative Skewness ( $Re^* = 2.2$  and n = 1.25).

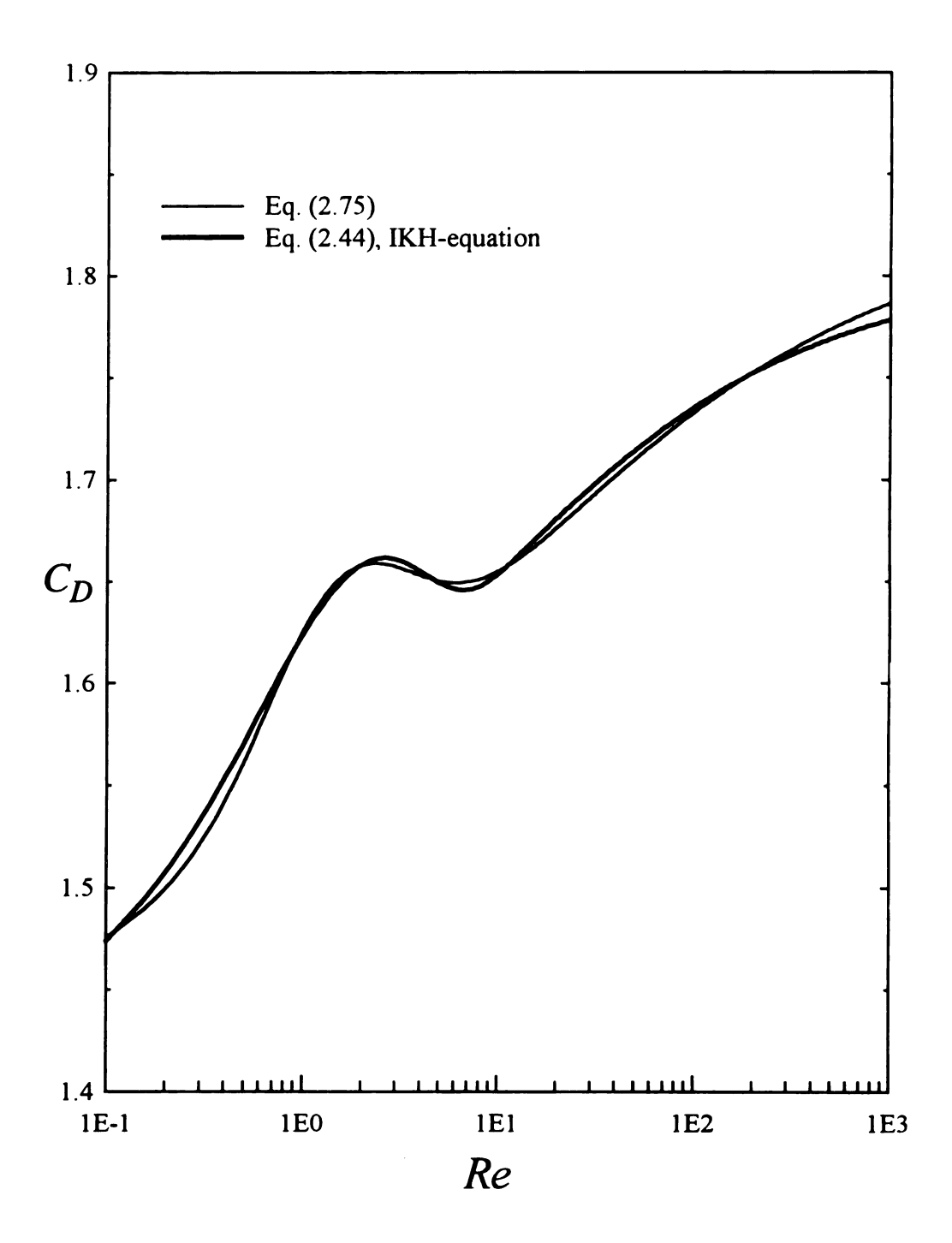


Figure 2.5 Predictions of the IKH-Equation for the Destruction of Dissipation Coefficient

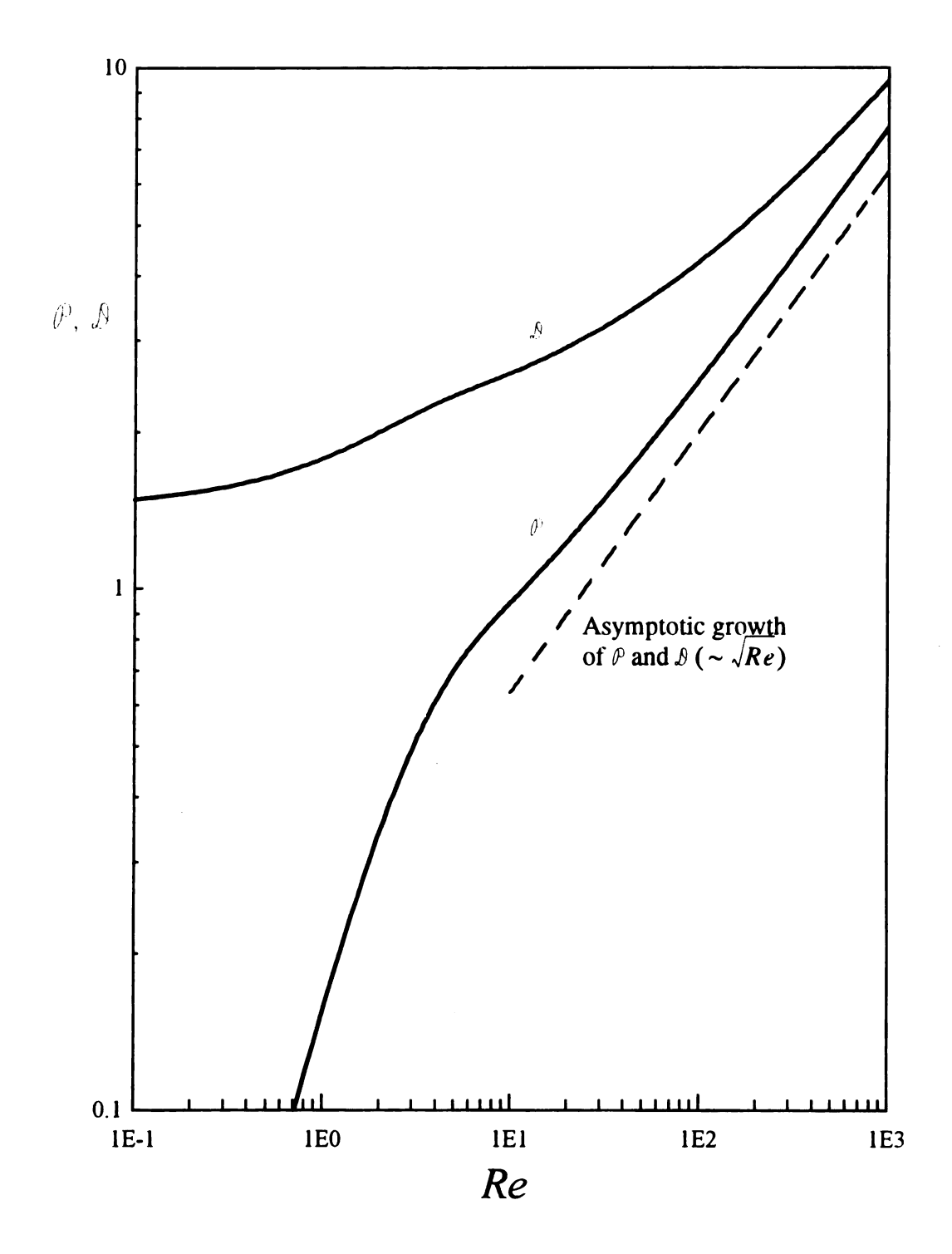


Figure 2.6 Predictions of the IKH-Equation for the Production of Dissipation Using a Prescribed Function for the Destruction of Dissipation.

In Eq. (2.75),  $Re_A$  determines the Reynolds number at which the decay coefficient approaches its high Reynolds number asymptote and s is a sharpness parameter for this approach. Equivalently,  $Re_p$  determines where  $C_D(Re)$  achieves its local peak and p relates to the sharpness of this peak. The quantity  $C^*$  determines the value of  $C_D$  at the local maximum. The following parameters have been selected in order to reproduce the local maximum and minimum in  $C_D(Re)$  illustrated by Figure 2.5:  $Re_A = 5$ , s = 0.4,  $Re_p = 1.5$ , p = 0.65, and  $C^* = 0.054$ .

## 2.6 Transient Isotropic Decay

With  $C_D(Re)$  expressed by Eq. (2.75), Eqs. (2.2) and (2.5) may be employed to compute an isotropic decay process for any arbitrary initial conditions given by  $k_o$ ,  $\varepsilon_o$ , and  $Re_o(k_o^2/v\varepsilon_o)$ . These equations have been integrated using a fourth order Runge-Kutta integration algorithm (Carnahan *et al.*, 1969; see also Appendix H). For an appropriate specification of the initial conditions, this calculation can be used to reproduce the isotropic states which correspond to the experiments of Batchelor and Townsend [1948], Comte-Bellot and Corrsin [1971], and Sirivat and Warhaft [1983] (see Figure 2.1).

Figures 2.7a-2.7g present the results for the seven experimental data sets used in this chapter. The results are given as a crossplot of the turbulent kinetic energy vs. the dissipation. Eqs. (2.2) and (2.5) imply that

$$\frac{dk}{d\varepsilon} = \frac{1}{C_D} \frac{k}{\varepsilon}.$$
 (2.58)

The local slope of the computed line compared to the slope of the data points gives an indication as to the quality of the specification of  $C_D(Re)$ . In general, the reproduction of

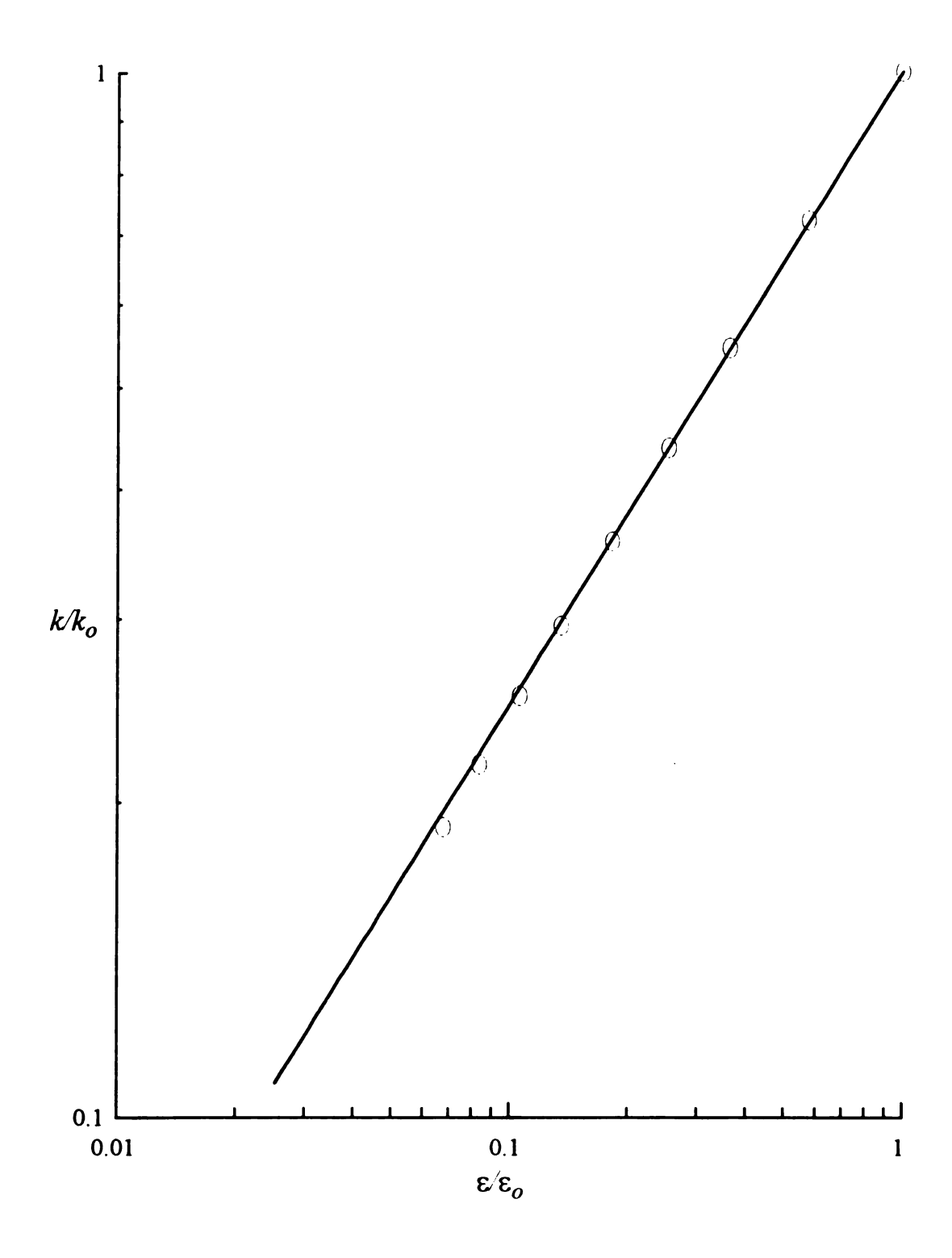


Figure 2.7a Model Computations for the Isotropic Decay Data of Batchelor and Townsend [1948] (U = 150 cm/s,  $Re_o = 7.58$ )

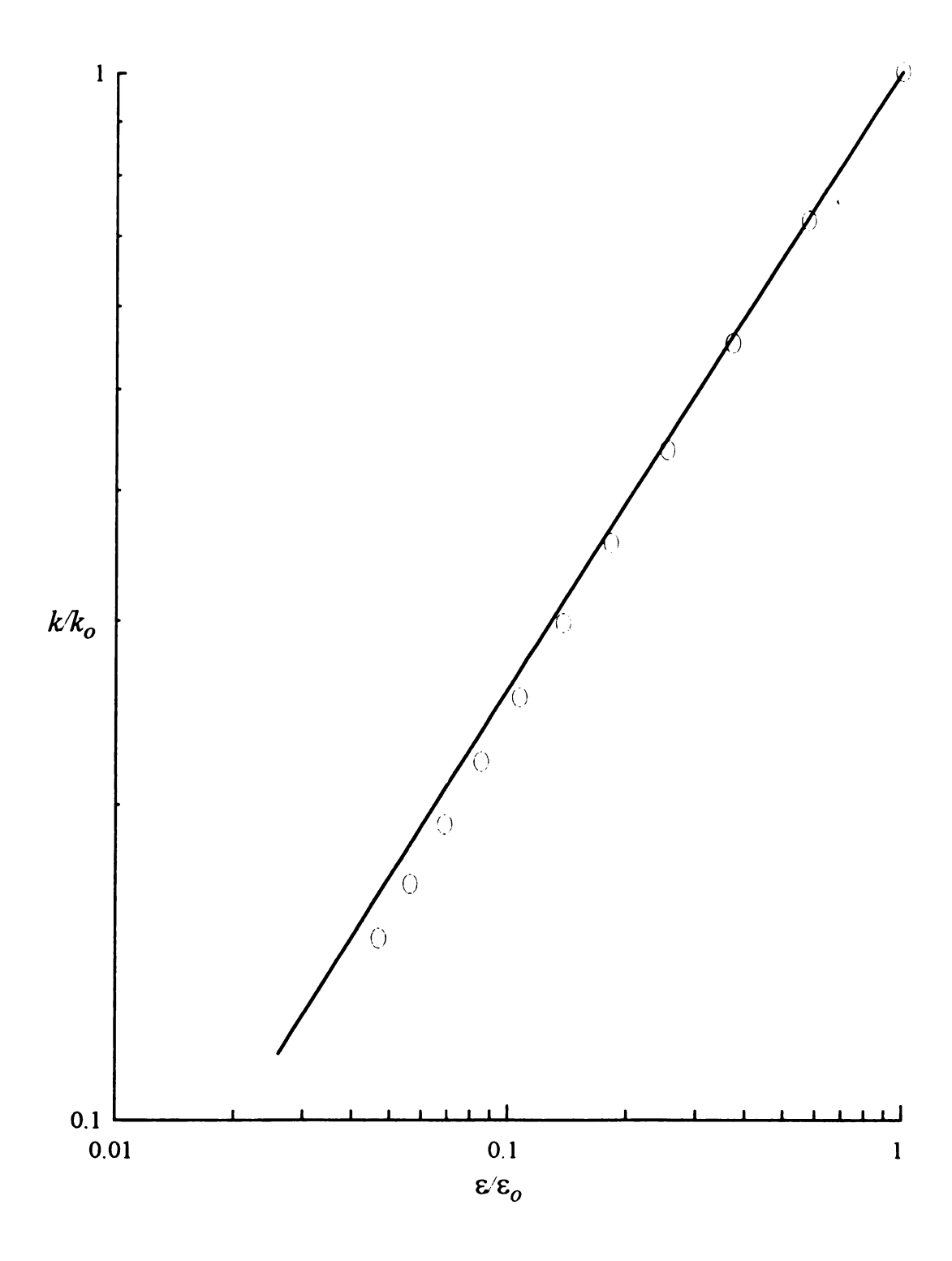


Figure 2.7b Model Computations for the Isotropic Decay Data of Batchelor and Townsend [1948] ( $U = 643 \ cm/s, Re_o = 42.6$ )

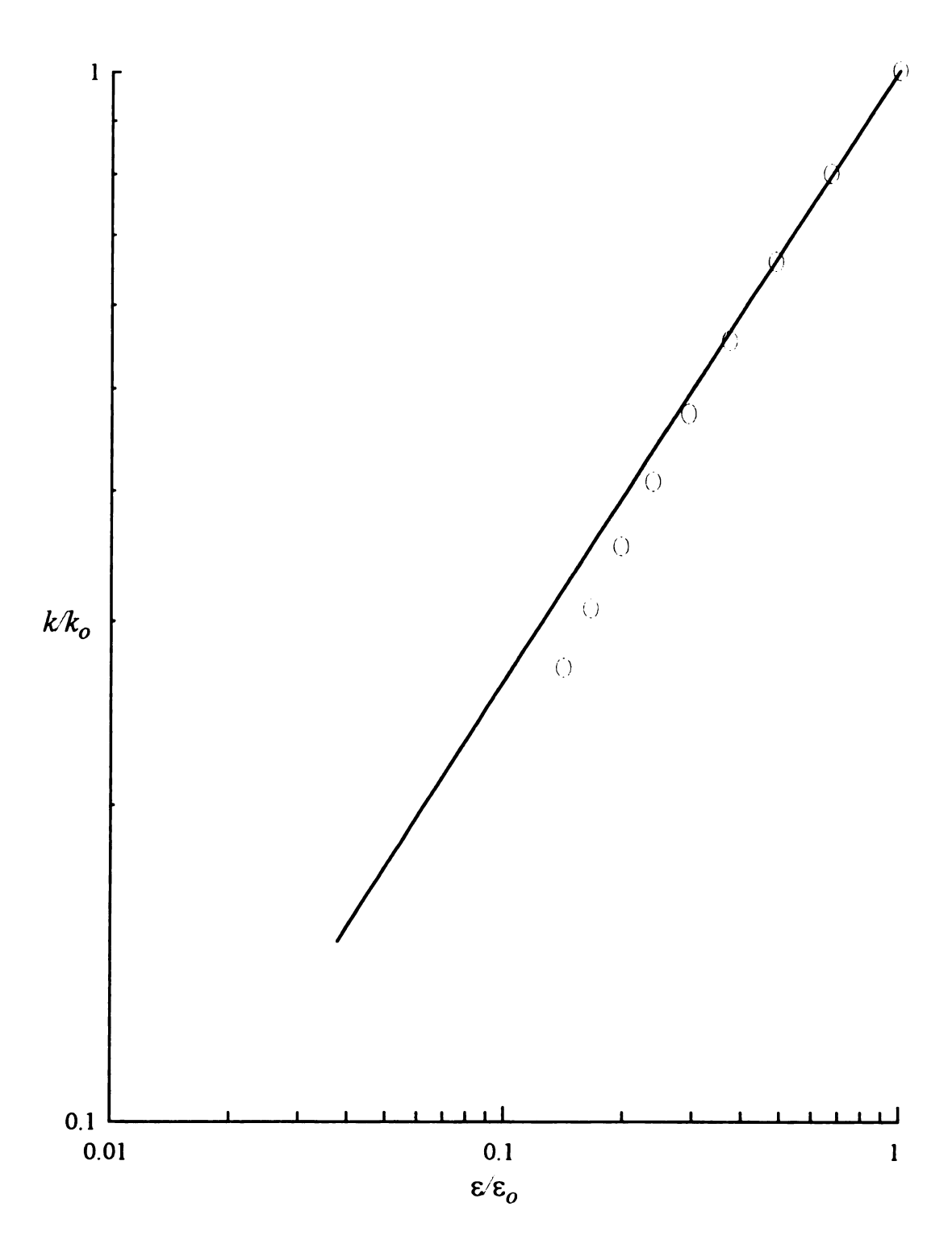


Figure 2.7c Model Computations for the Isotropic Decay Data of Batchelor and Townsend [1948] ( $U = 1286 \text{ cm/s}, Re_o = 83.7$ )

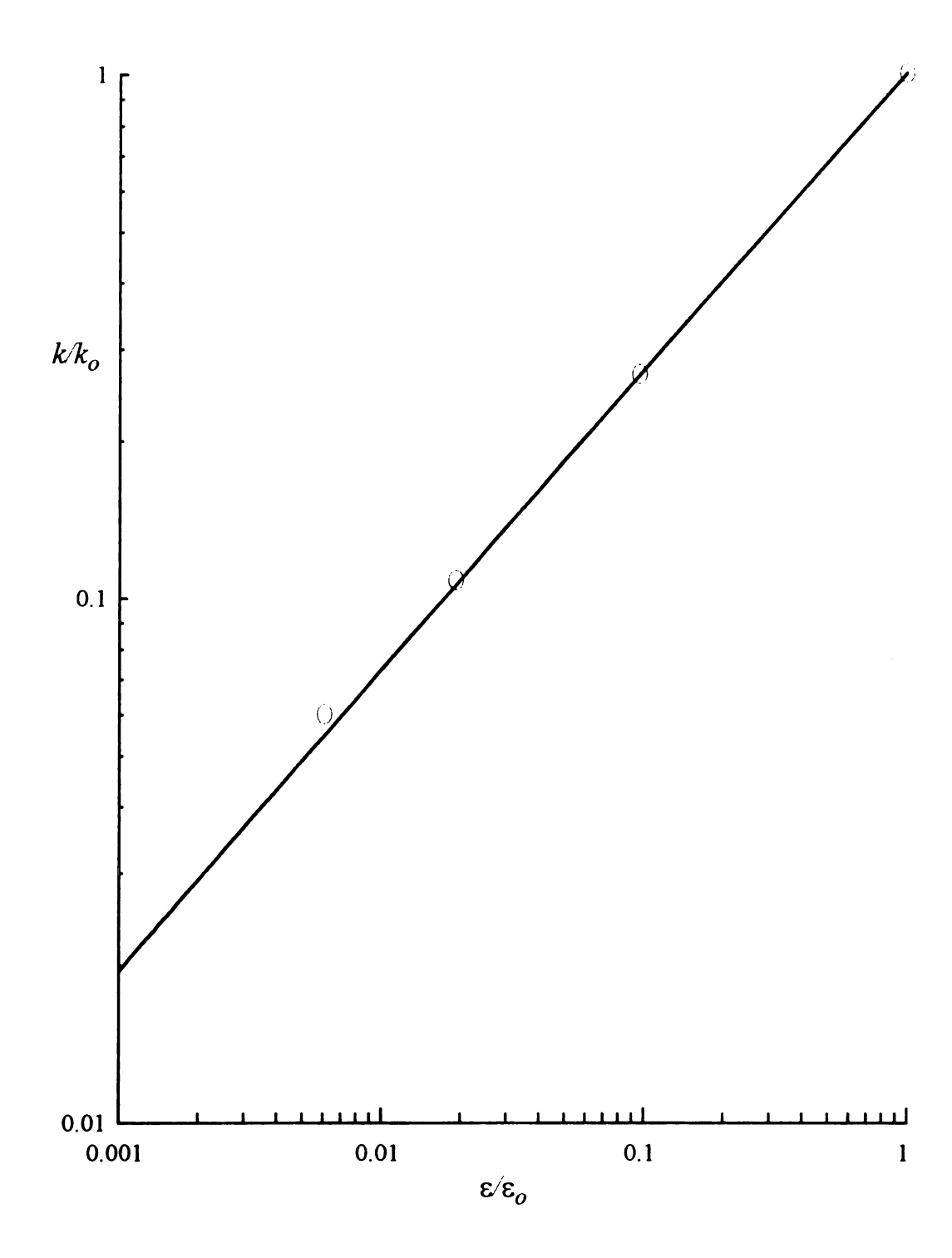


Figure 2.7d Model Computations for the Isotropic Decay Data of Comte-Bellot and Corrsin [1971] (U = 10 m/s,  $Re_o = 354$ )

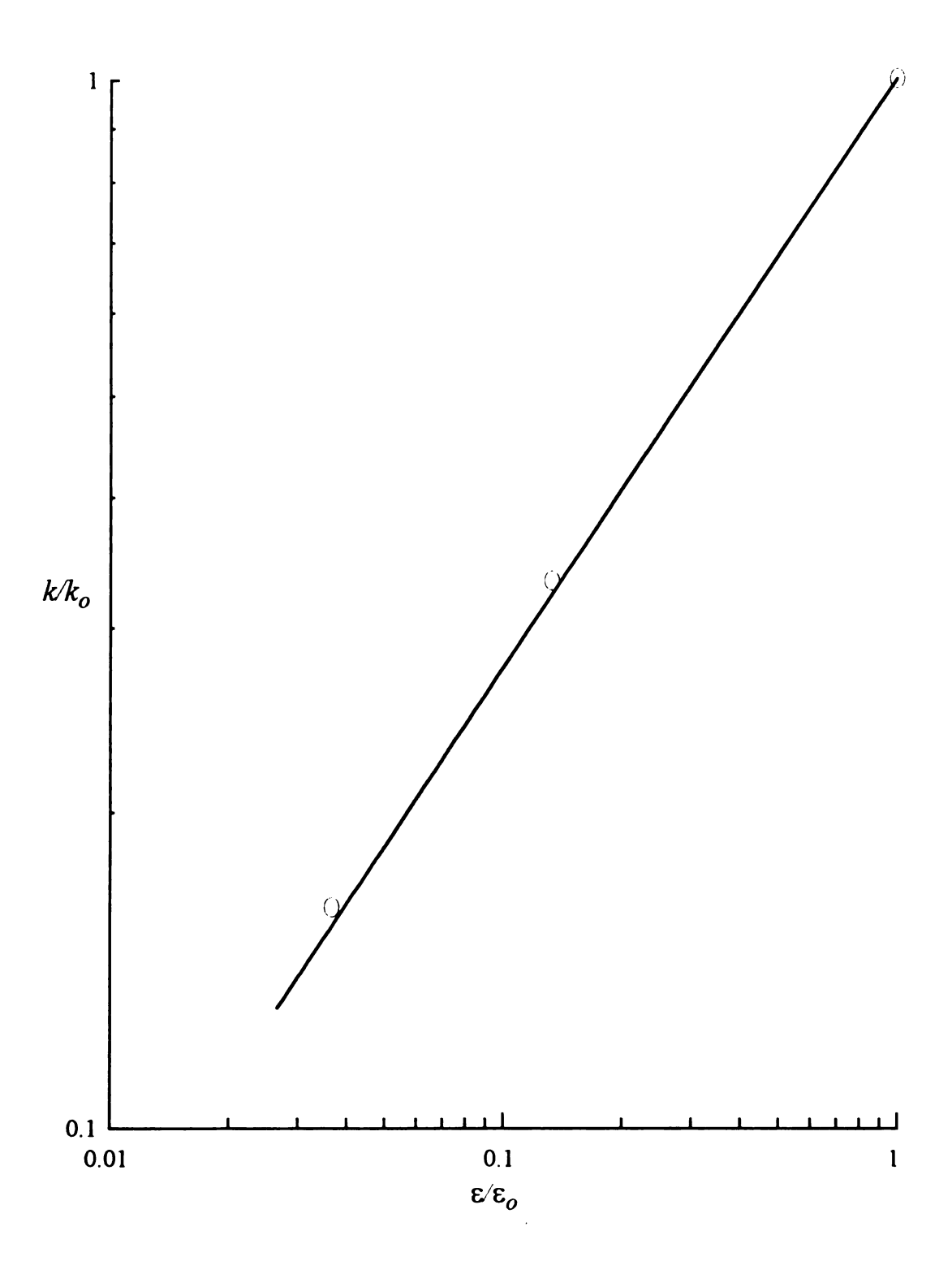


Figure 2.7e Model Computations for the Isotropic Decay Data of Comte-Bellot and Corrsin [1971] (U = 10 m/s,  $Re_o = 769$ )

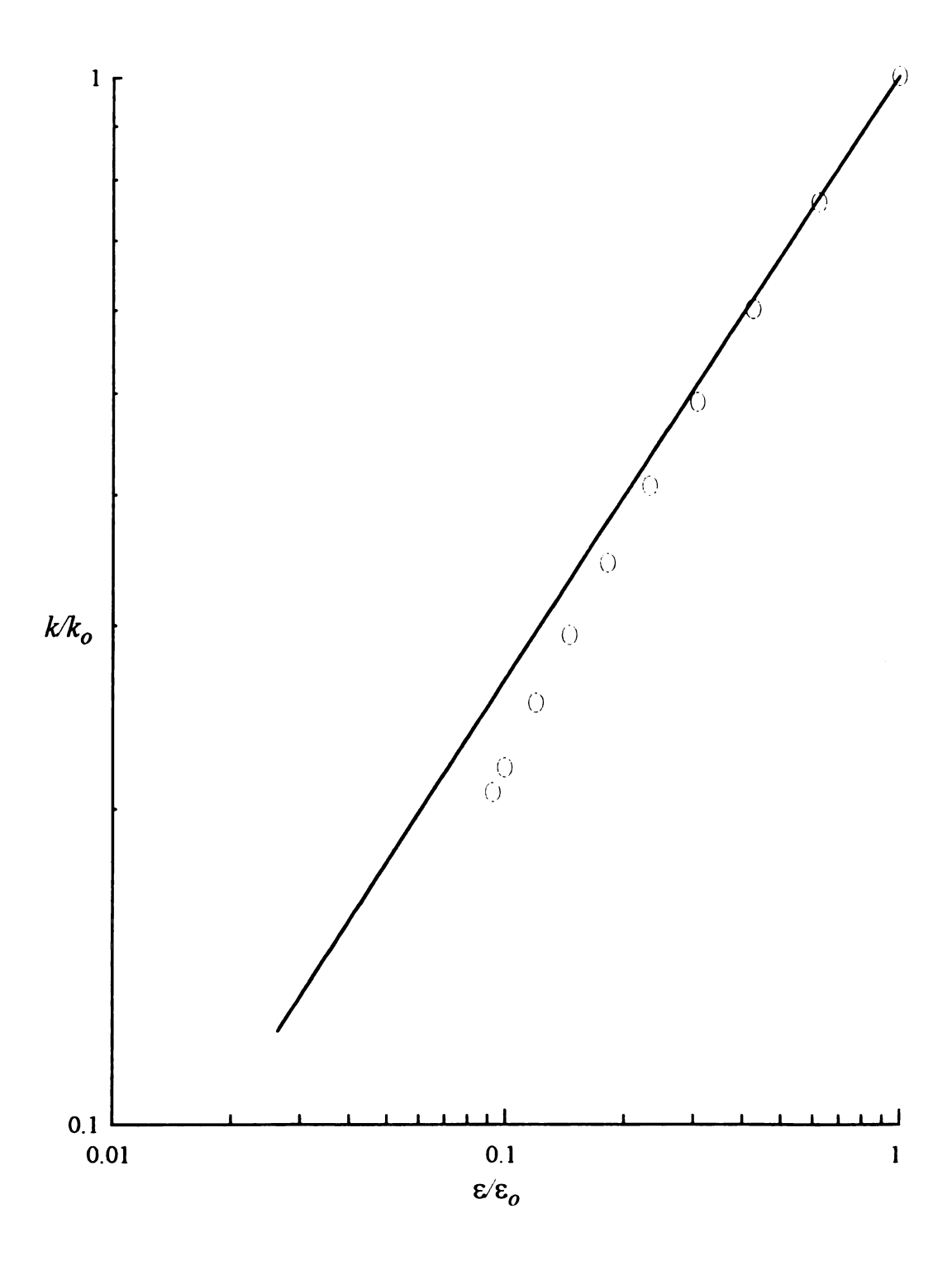


Figure 2.7f Model Computations for the Isotropic Decay Data of Sirivat and Warhaft [1983] ( $U = 340 \text{ cm/s}, Re_o = 139$ )

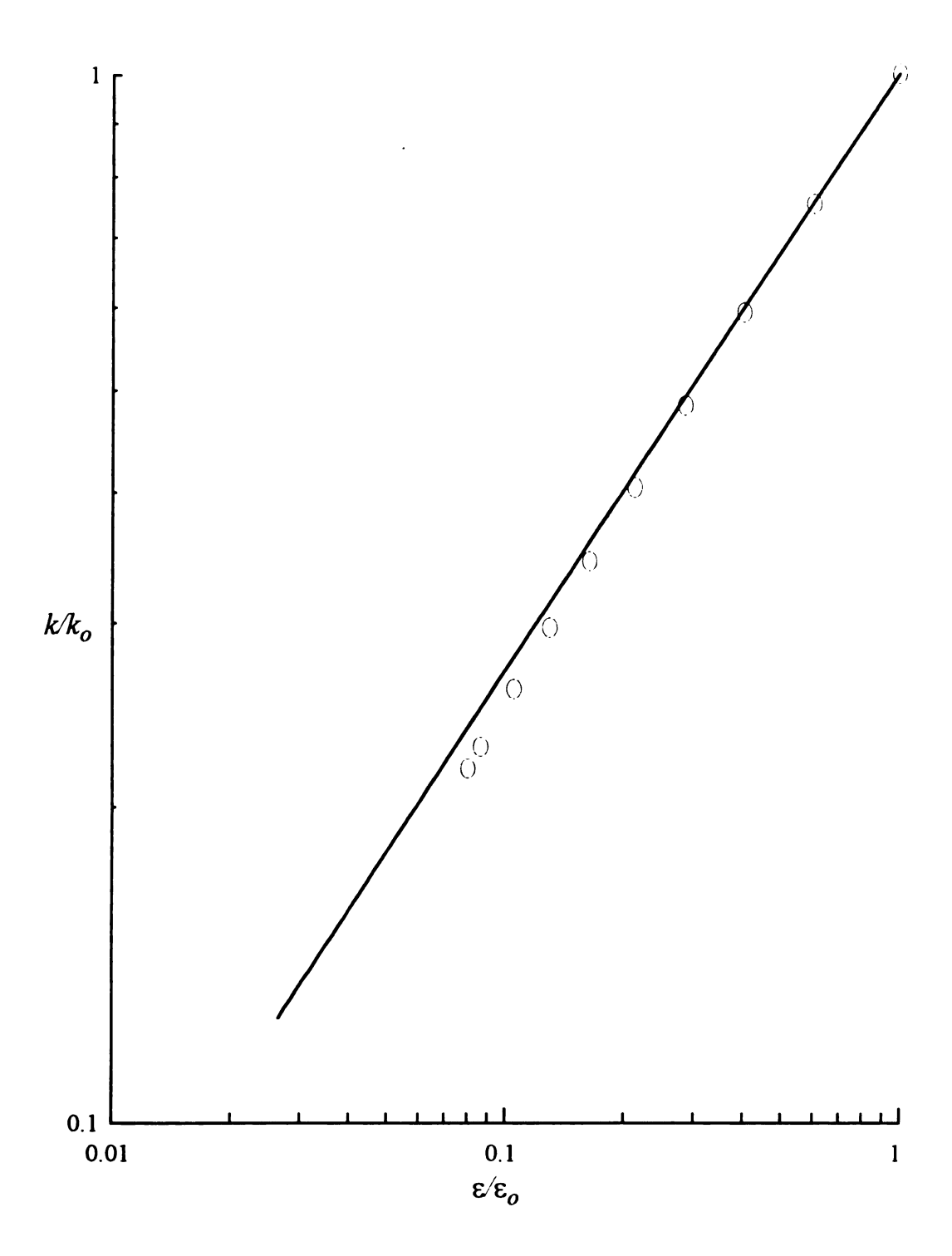


Figure 2.7g Model Computations for the Isotropic Decay Data of Sirivat and Warhaft [1983] (U = 630 cm/s,  $Re_o = 262$ )

the data sets is quite good. Specifically, the initial decay stages of each of the seven data sets is well represented, although some sets show deviation from the computations at points farther along in the decay process. This is not surprising, however, as the degree of homogeneity and isotropy of the flow worsens at larger downstream positions in the wind tunnel (Comte-Bellot and Corrsin, 1971). Of particular note are the two cases which represent the extrema for the experimental Reynolds numbers. Figure 2.7e represents the highest Reynolds number data of Comte-Bellot and Corrsin [1971] ( $Re_o = 769$ ). The slope of the calculation is slightly higher than that of the data, indicating that  $C_D$  is relatively low, and perhaps approaches its asymptote too slowly. Figure 2.7a represents the low Reynolds number data of Batchelor and Townsend [1948] ( $Re_o = 7.58$ ). Here, the representation of the data is excellent throughout the entire decay process. The good agreement of the data sets which span two decades of  $Re_o$  is an indication that Eq. (2.75) is a quantitatively good expression for  $C_D$ .

Figures 2.7h and 2.7i present the results of the same calculations, but compared with the direct simulations of Bardina et al. [1985] and Speziale et al. [1987]. The solid line shows the results of the computations using the data at  $t\varepsilon_o/k_o=0$  as the initial conditions, whereas the dashed line shows the results using the simulation data at  $t\varepsilon_o/k_o=1$  as the initial state for the solution of Eqs. (2.2) and (2.5). What is most noteworthy about these two simulations is the fact that the initial decay period is very poorly characterized, while the final decay is well reproduced. This, however, does not necessarily mean that the model for  $C_D(Re)$  is poor. Rather, the limitations of direct simulations are brought into question. Huang and Leonard [1994] address this problem. They indicate that, during the initial stages of a direct simulation, the maximum resolvable wavenumber  $\tilde{k}_{max}$  of the turbulent energy spectrum  $(E(\tilde{k}))$  is relatively small. Thus, although the larger, energy-containing eddies (i.e. low wavenumber  $\tilde{k}$ ) may be well characterized, the smaller, dissipative eddies (i.e. high wavenumber  $\tilde{k}$ ) are not. Without an accurate characterization of both the energy-containing and dissipative eddies, the decay

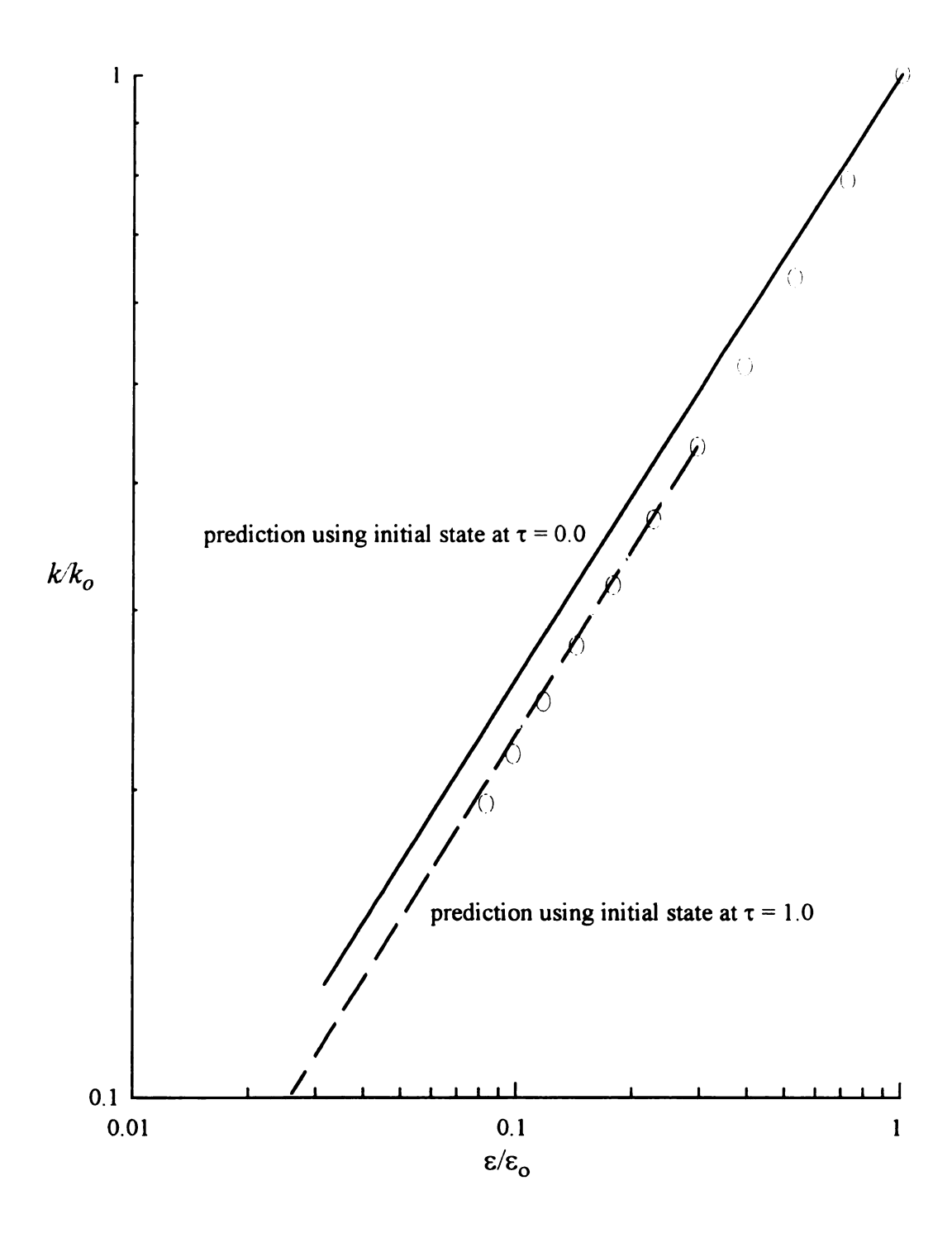


Figure 2.7h Model Computations for the Isotropic Decay Simulations of Speziale, et al. [1987]  $(Re_o = 35.1)$ 

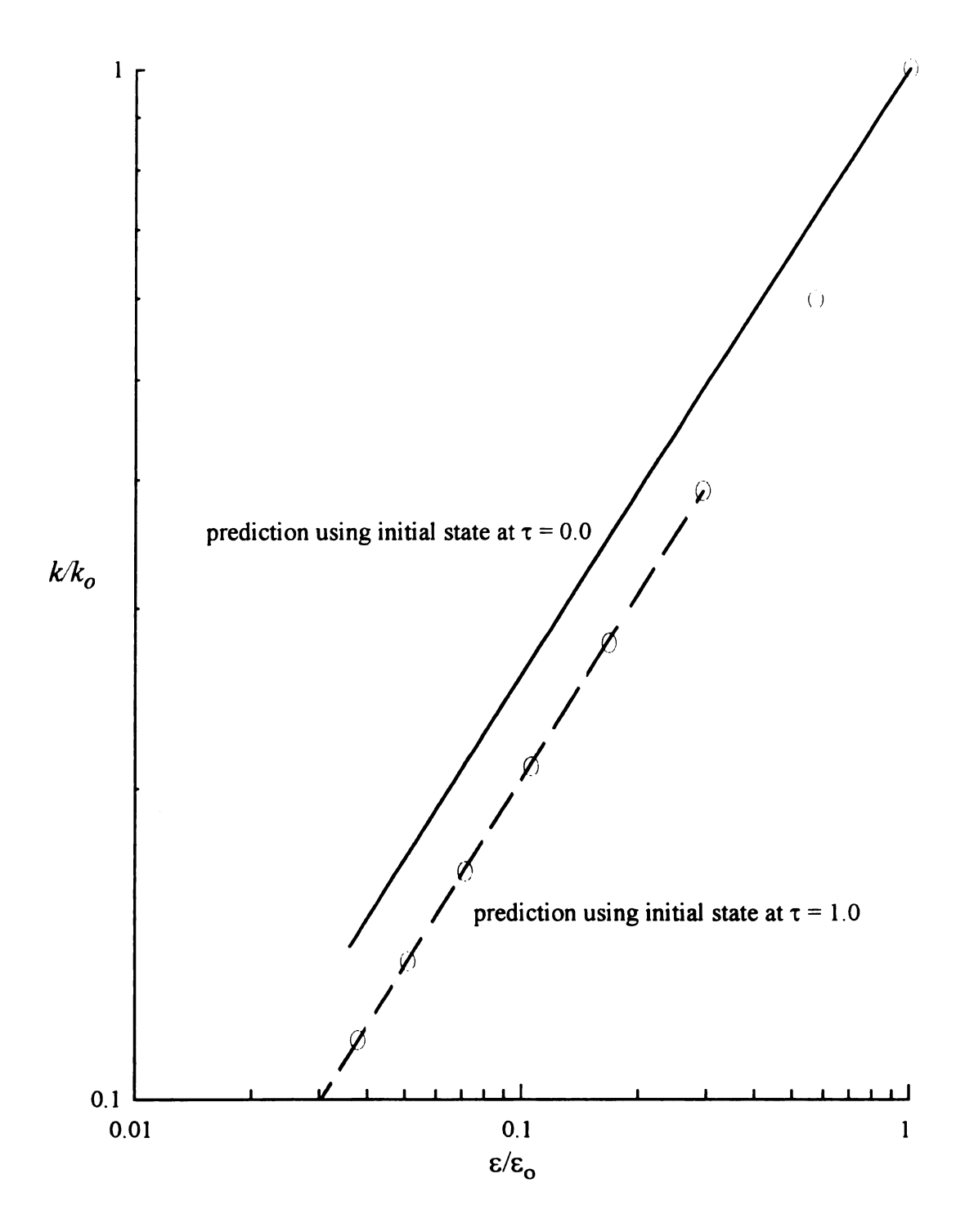


Figure 2.7i Model Computations for the Isotropic Decay Simulations of Bardina, et al. [1985]  $(Re_o = 45.4)$ 

transient is clearly suspect. Huang and Leonard explain, however, that  $\tilde{k}_{max}$  increases during the course of the simulation. Therefore, at longer times, both types of eddies are accurately represented and the quality of the decay transient is much more reliable.

Figure 2.8 presents the decay of the turbulent kinetic energy in the time domain for three different initial Reynolds numbers:  $Re_o = 10, 100, 1000$ . The kinetic energy normalized by its initial value is plotted versus the dimensionless decay time  $(\tau = t\varepsilon_o/k_o)$ . It is noted that the small differences among the three cases are manifested only in the long time behavior. The curves follow the trends expected from the nature of Eqs. (2.2) and (2.5): At higher Reynolds numbers,  $C_D$  is higher and causes the turbulent dissipation to decay more rapidly, causing the turbulent kinetic energy to persist longer.

#### 2.7 Conclusions

The integral form of the Kármán-Howarth equation for isotropic turbulence provides a semi-theoretical prediction for the destruction coefficient  $C_D$  in the equation for the turbulent scalar dissipation. Integral expressions containing the double and triple velocity correlations are estimated using Taylor series representations of the velocity correlations and a characteristic cut-off integration length. A modeling hypothesis is made which assumes that the ratio of the integral quantities is correctly represented, although the absolute magnitudes of the integrals may not be.

Empirical parameters which are chosen to reproduce experimental data for the velocity derivative skewness in decaying isotropic turbulence predict that  $C_D$  spans its upper and lower limits in a non-monotonic fashion. This is unlike previous approaches to this problem, which have simply bridged the two limiting cases with some monotonic, empirical function. The non-monotonic behavior  $C_D(Re)$  is seen in some direct simulations of this flow. The resulting prediction for  $C_D(Re)$  is able to reconstruct the

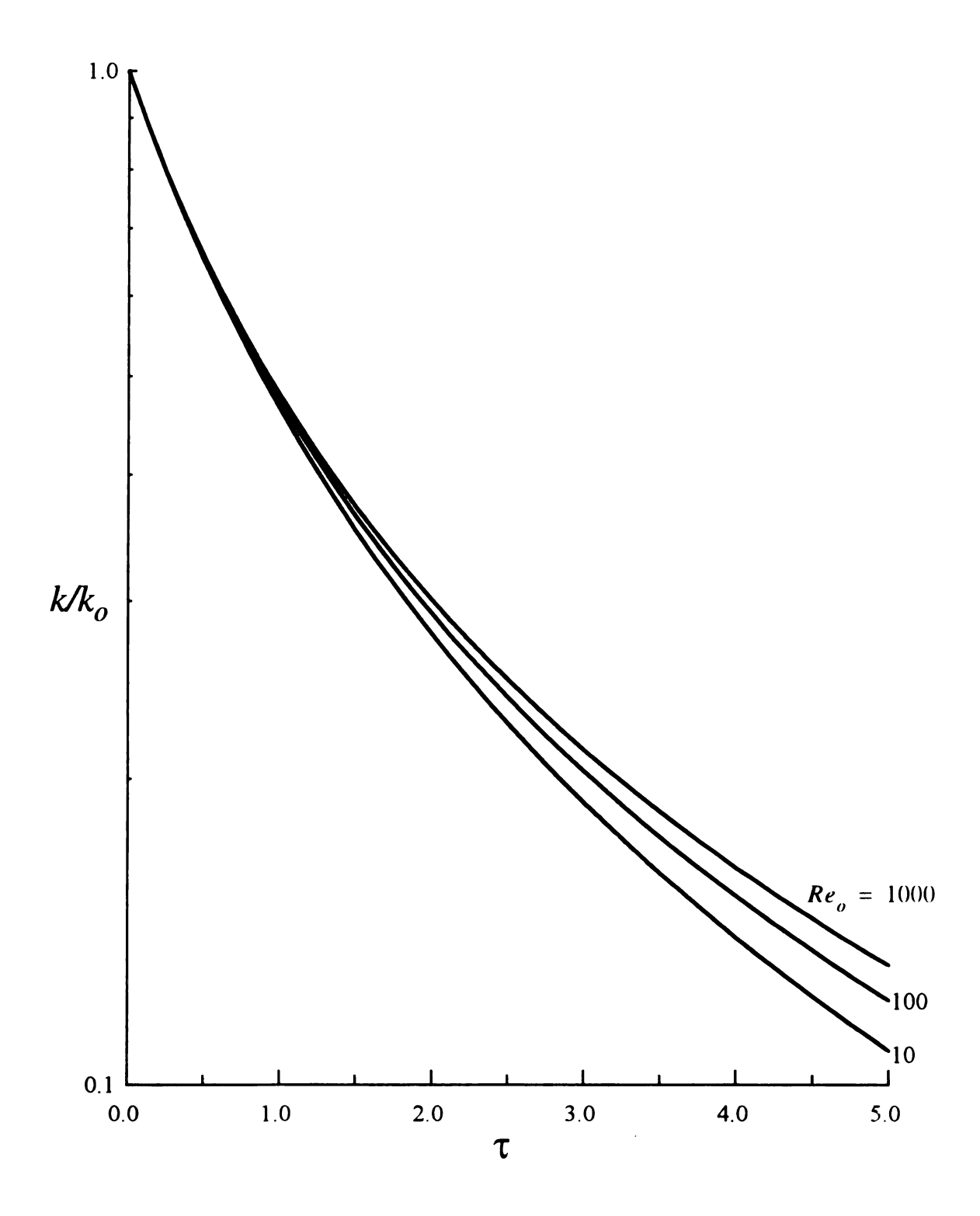


Figure 2.8 Predicted Transient Decay of the Turbulent Kinetic Energy as a Function of Initial Turbulent Reynolds Number

various experimental and direct simulation data available in the literature.

Within the context of the modeled form of the IKH equation, the non-monotonicity of  $C_D(Re)$  is a direct consequence of the fact that  $C_D$  varies between two different upper and lower Reynolds number limits. For  $C_D^{\infty} - C_D^{0} = 0$ ,  $C_D(Re)$  would be a constant function, while the local maximum in  $C_D(Re)$  becomes more pronounced as  $C_D^{\infty} - C_D^{0}$  increases.

The disparity between the calculations and the initial stages of decay in direct simulations illustrates that care must be taken when treating direct simulation data. Only the longer-time simulation data resolve both the large and small turbulent scales and provide meaningful data for comparison.

### **CHAPTER 3**

# ISOTROPIC PRE-STRESS CLOSURE THEORY FOR HOMOGENEOUSLY SHEARED TURBULENCE

## 3.1 Introduction

Homogeneously sheared turbulence has the interesting feature that the turbulent time scale  $k/\epsilon$  approaches a constant finite value as the flow develops (Tavoularis and Corrsin, 1981; Gibson and Kanellopoulos, 1987; Rohr et al., 1988; and, Tavoularis and Karnik, 1989), although the kinetic energy k and the dissipation  $\epsilon$  associated with the velocity fluctuations continuously increase as  $z \to \infty$ . Figure 3.1 summarizes the asymptotic state attained by this flow for which the shear rate S is approximately constant. The existence of this state requires that the transport equations governing the turbulent kinetic energy and the scalar dissipation rate satisfy the following model-independent condition

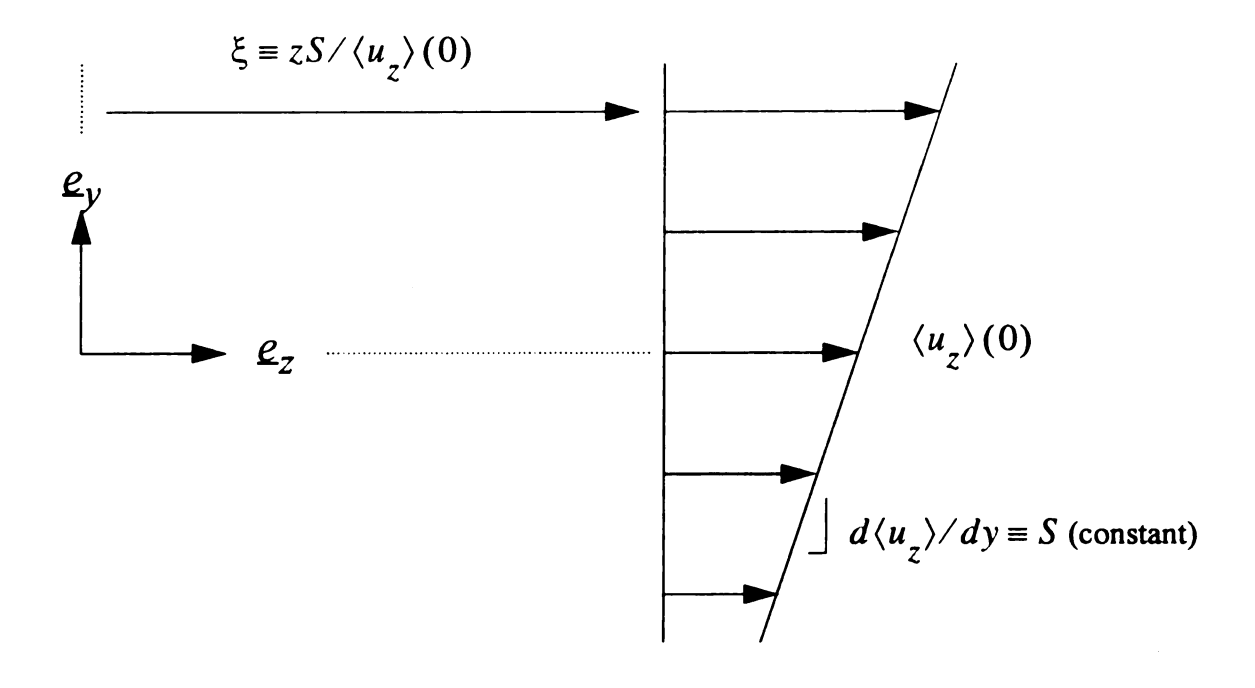
$$\lim_{z \to \infty} \left[ \frac{1}{k} \frac{dk}{dz} \right] = \lim_{z \to \infty} \left[ \frac{1}{\varepsilon} \frac{d\varepsilon}{dz} \right]. \tag{3.1}$$

For homogeneous shear flows at high turbulence Reynolds numbers ( $k^2 \gg v\epsilon$ ), the  $k-\epsilon$  equations (Hanjalic and Launder, 1972) are

$$\langle u_z \rangle(0) \frac{dk}{dz} = -\langle \underline{u}' \underline{u}' \rangle : \nabla \langle \underline{u} \rangle - \varepsilon, \qquad (3.2)$$

$$\langle u_z \rangle (0) \frac{d\varepsilon}{dz} = -C_P \frac{\langle \underline{u}'\underline{u}' \rangle : \nabla \langle \underline{u} \rangle}{\tau_P} - C_D \frac{\varepsilon}{\tau_D}. \tag{3.3}$$

 $\langle u_z \rangle$  (0) is the axial component of the mean velocity along the centerline of the flow field.  $\tau_p$  and  $\tau_D$  represent, respectively, turbulent time scales associated with the production of



Quantity		Asymptotic State <sup>†</sup>	
Turbulent kinetic energy	$k = \langle \underline{u}' \cdot \underline{u}' \rangle / 2$	α	
Turbulent dissipation rate	$\varepsilon = \nu \langle \nabla \underline{u}' : \nabla \underline{u}'^T \rangle$	∞	
Turbulent Reynolds number	$Re_t = k^2/v\varepsilon$	∞	
Time scale ratio	Sk/ε	4.16	
Normalized Reynolds stress	$R = \frac{\langle \underline{u}'\underline{u}' \rangle}{2k}$	$\begin{bmatrix} +0.236 & 0 & 0 \\ 0 & +0.196 & -0.165 \\ 0 & -0.165 & +0.568 \end{bmatrix}$	

†: These numbers represent the average of cases A, B, and C from Tavoularis and Karnik [1989].

Figure 3.1 Asymptotic State for Homogeneously Sheared Turbulent Flows

dissipation and the destruction of dissipation. The standard k- $\epsilon$  theory of turbulence assumes that  $\tau_P = \tau_D = k/\epsilon$  and that  $C_P$  and  $C_D$  are constants independent of the local state of turbulence. According to Eq. (3.1), an asymptotic state of turbulence is predicted by Eqs. (3.2) and (3.3) provided the ratio of production to dissipation satisfies (Speziale, 1991)

$$\lim_{z \to \infty} \left[ \frac{-\langle \underline{u}'\underline{u}' \rangle; \nabla \langle \underline{u} \rangle}{\varepsilon} \right] = \frac{C_D - 1}{C_P - 1}.$$
 (3.4)

Eqs. (3.2) and (3.3) are also consistent with experimental data for homogeneous decay provided  $C_D = 1.83$  (see, esp., Comte-Bellot and Corrsin, 1971; Mansour and Wray, 1994; and Chapter 2 of this dissertation).

The Reynolds stress can be written as the sum of an isotropic and an anisotropic stress (Speziale, 1991)

$$\langle \underline{u}'\underline{u}' \rangle = \frac{2k}{3}I + 2k\underline{b}, \tag{3.5}$$

where  $\underline{b} = \underline{b}^T$  and  $tr(\underline{b}) = 0$ . For a strictly homogeneous flow with S = 0, the anisotropic stress  $\underline{b}$  is zero. Because  $\langle \underline{u}'\underline{u}' \rangle$  is a non-negative operator, the eigenvalues associated with the Reynolds stress are non-negative (Schumann, 1977). Moreover, because

$$tr\langle u'u'\rangle = 2k > 0, \tag{3.6}$$

at least one eigenvalue of  $\langle \underline{u}'\underline{u}'\rangle$  must be non-zero and positive. This means that the normalized components of the turbulent kinetic energy are confined to the energy simplex illustrated by Figure 3.2. The homogeneous shear data (Tavoularis and Karnik, 1989) summarized by Figure 3.2 show that this flow produces a positive primary normal stress difference.



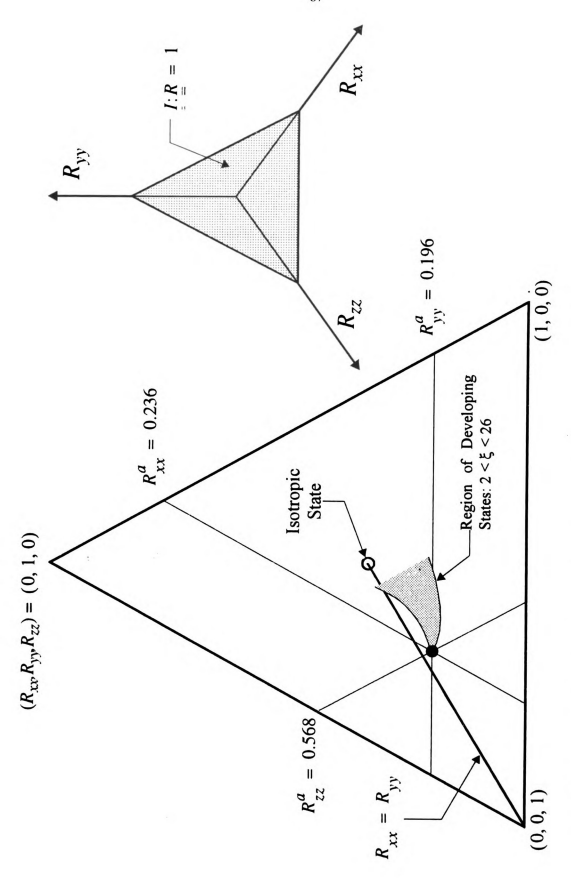


Figure 3.2 Energy Simplex with Transition States for Homogeneously Sheared Turbulence

$$\lim_{z \to \infty} \left[ \frac{\langle u'_z u'_z \rangle - \langle u'_y u'_y \rangle}{2k} \right] \cong 0.377,$$

as well as a negative second normal stress difference,

$$\lim_{z \to \infty} \left[ \frac{\langle u'_y u'_y \rangle - \langle u'_x u'_x \rangle}{2k} \right] \cong -0.040.$$

The anisotropic stress  $\underline{b}$  has two non-trivial invariants:  $II = tr(\underline{b} \cdot \underline{b})$  and  $III = tr(\underline{b} \cdot \underline{b} \cdot \underline{b})$ . Lumley [1978] has shown that all realizable turbulent states (II, III) must fall on or within a two dimensional domain illustrated by Figure 3.3. The experimental data for homogeneous shear approach the asymptotic state given by  $\lim_{z \to \infty} (II, III) \cong (0.138, 0.0174)$ .

For a constant density fluid, the Boussinesq model for the anisotropic stress is (Hinze, 1959 and Brodkey, 1967)

$$2k\underline{b} = -\nu_{e} \left[ \nabla \langle \underline{u} \rangle + \nabla \langle \underline{u} \rangle^{T} \right] = -2\nu_{e} \langle \underline{S} \rangle. \tag{3.7}$$

 $\langle \underline{S} \rangle$  represents the mean strain rate dyadic and  $\mathbf{v}_e$  is a scalar valued *eddy* viscosity. For  $\mathbf{v}_e > 0$ , Eq. (3.7) implies that the kinetic energy is irreversibly transferred from the mean field to the fluctuating field inasmuch as

$$-\langle \underline{u}'\underline{u}'\rangle : \nabla \langle \underline{u}\rangle = 2v_{e}\langle \underline{S}\rangle : \langle \underline{S}\rangle > 0 \tag{3.8}$$

for all turbulent flows. This feature partly justifies the use of Eq. (3.7) as an approximate model for the anisotropic stress. However, for homogeneous shear flows, Eq. (3.7) also predicts an equipartition of kinetic energy among the components of the fluctuating velocity as well as a zero third invariant for  $\frac{b}{z}$  (i.e.,  $III \equiv 0$ ). These results clearly contradict the experimental measurements summarized by Figures 3.2 and 3.3. Thus, as previously noted by Speziale [1991], the Boussinesq model qualitatively misrepresents the underlying mechanism associated with the flux of momentum due to velocity fluctuations.

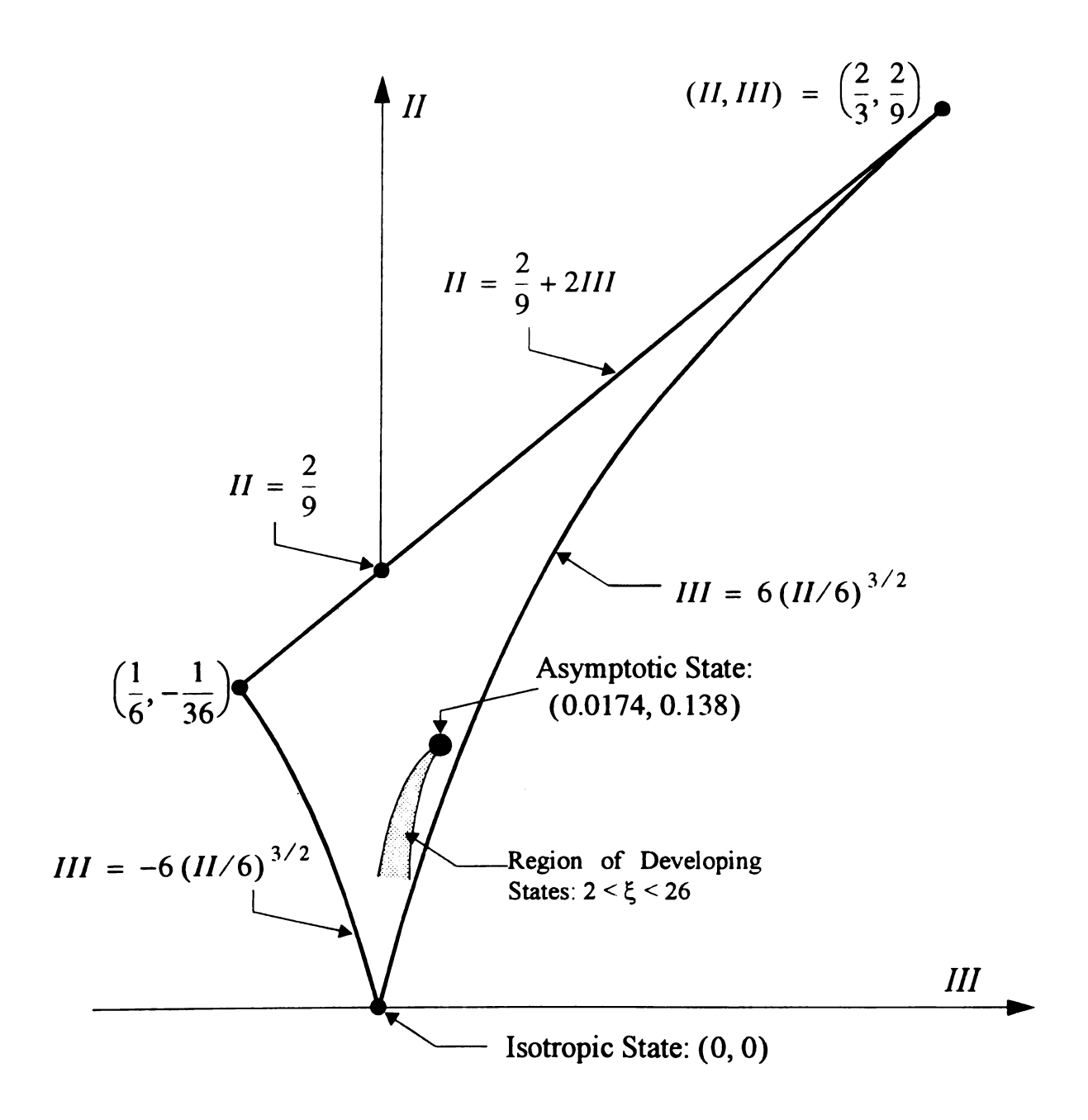


Figure 3.3 Anisotropy Invariant Diagram with Transition States for Homogeneously Sheared Turbulence

The proposed pre-closure representation of the Reynolds stress supports a long-standing goal of turbulence research to achieve a practical statistical closure of the mean field equations and, thereby, complements other algebraic turbulent closure models for the anisotropic stress b (see, esp., Speziale, 1991; Taulbee, 1989; Reynolds 1989; and, Hanjalic, 1994). The development of homogeneously sheared turbulent flows towards an asymptotic state provides a critical experimental test flow to partially guide the evaluation of the proposed theory.

The objective of this chapter is to develop this new pre-closure for the Reynolds stress. In Section 3.2, an analysis of the governing equations for the fluctuating velocity yields a relationship between the Reynolds stress, mean field quantities, and the pre-stress (see Eq. (1.37)). A simplifying assumption is made regarding the isotropic nature of the pre-stress in Section 3.3, which is found to directly impact Issues (i) and (ii) from Section 1.2. The asymptotic state of homogeneously sheared turbulent flows is used to calibrate universal model parameters and the transient approach to this asymptote is examined.

## 3.2 Pre-closure Theory

The fluctuating velocity associated with a constant density, Newtonian fluid satisfies the following equation (Monin and Yaglom, 1965)

$$\langle t \rangle (\underline{u}') = -\underline{h}' , \qquad (3.9)$$

where

$$\underline{h}' = \underline{u}' \cdot \nabla \langle \underline{u} \rangle + \underline{f}', \qquad (3.10)$$

and

$$\underline{f}' \equiv \nabla \cdot \left[ \frac{p'}{\rho} \underline{I} + \underline{u'}\underline{u'} - \langle \underline{u'}\underline{u'} \rangle \right]. \tag{3.11}$$

The convective-diffusive operator  $\langle l \rangle$  depends on the mean velocity field  $\langle \underline{u} \rangle$  and the kinematic viscosity of the fluid,  $\nu$ :

$$\langle L \rangle \equiv \frac{\partial}{\partial t} + \langle \underline{u} \rangle \cdot \nabla - \nu \nabla^2. \tag{3.12}$$

Eq. (3.9) is exact and emphasizes that fluctuations in momentum (i.e.  $\rho \underline{u}'$ ) are produced within the flow domain by (1) a convective coupling between the mean velocity gradient and the fluctuating velocity; (2) pressure fluctuations; and, (3) fluctuations in the instantaneous Reynolds stress,  $\underline{u}'\underline{u}' - \langle \underline{u}'\underline{u}' \rangle$ . Momentum fluctuations are transported by viscous fluctuations in the molecular stress and by mean field convection.

An exact, albeit formal, representation of the fluctuating velocity can be written in terms of a Green's function (Morse and Feshbach, 1953) associated with the linear differential operator  $\langle L \rangle$ . For statistically stationary flows in an unbounded domain,

$$\underline{u}'(\underline{x},t) = -\int_{-\infty}^{t} d\tilde{t} \int d\tilde{V} \langle G \rangle(\underline{x},t \mid \underline{\tilde{x}},\tilde{t}) \underline{h}'(\underline{\tilde{x}},\tilde{t}). \tag{3.13}$$

For  $0 \le t - \tilde{t} < \|x - \tilde{x}\|^2 / v$ , the Greens' function is spatially peaked in a frame of reference moving with the local mean velocity; however, as  $t - \tilde{t} \to \infty$ , viscous momentum transport causes the Green's function to relax to zero over the entire spatial domain. For an unbounded spatial domain, the Green's function satisfies the following integral property

$$\int d\tilde{V} \langle G \rangle \left( \underline{x}, t \mid \underline{\tilde{x}}, \tilde{t} \right) = 1. \tag{3.14}$$

The analog of Eq. (3.13) for a passive scalar field has been previously used by Hill and Petty [1996] and many others.

A formal representation for the Reynolds stress follows by either pre- or post-multiplying Eq. (3.13) by the fluctuating velocity  $\underline{u}'(\underline{x}, t)$  and then forming the ensemble

average to obtain

$$\langle \underline{u}'\underline{u}' \rangle = -\int_{-\infty}^{t} d\tilde{t} \int_{V} d\tilde{V} \langle G \rangle (\underline{x}, t \mid \underline{\tilde{x}}, \tilde{t}) \langle \underline{u}' (\underline{x}, t) \underline{h}' (\underline{\tilde{x}}, \tilde{t}) \rangle =$$

$$-\int_{V}^{t} d\tilde{t} \int_{V} d\tilde{V} \langle G \rangle (\underline{x}, t \mid \underline{\tilde{x}}, \tilde{t}) \langle \underline{h}' (\underline{\tilde{x}}, \tilde{t}) \underline{u}' (\underline{x}, t) \rangle. \quad (3.15)$$

Eq. (3.15) relates the Reynolds stress to the Green's function and to the symmetric spacetime correlation defined by

$$\langle \underline{u}'(\underline{x},t)\underline{h}'(\underline{\tilde{x}},\tilde{t})\rangle \equiv \langle \underline{u}'(\underline{x},t)\underline{u}'(\underline{\tilde{x}},\tilde{t})\rangle \cdot \tilde{\nabla}\langle \underline{\tilde{u}}\rangle + \langle \underline{u}'(\underline{x},t)\underline{f}'(\underline{\tilde{x}},\tilde{t})\rangle =$$

$$\tilde{\nabla}\langle \underline{\tilde{u}}\rangle^T \cdot \langle \underline{u}'(\underline{\tilde{x}},\tilde{t})\underline{u}'(\underline{x},t)\rangle + \langle \underline{f}'(\underline{\tilde{x}},\tilde{t})\underline{u}'(\underline{x},t)\rangle. (3.16)$$

All the components of  $\langle \underline{h}'(\bar{x}, \bar{t}) \underline{u}'(x, t) \rangle$  relax to zero for either  $|t - \bar{t}| \gg \tau_H$  or  $||\underline{x} - \bar{x}|| \gg l_H$ , where  $\tau_H$  ( $\sim k/\epsilon$ ) and  $l_H$  ( $\sim k^{3/2}/\epsilon$ ) represent finite turbulent time and length scales, respectively. The physical hypothesis that  $l_H < \infty$  and  $\tau_H < \infty$  partially motivates the use of a spatial smoothing approximation to simplify the non-local representation of the Reynolds stress given by Eq. (3.15).

A spatial Taylor series expansion of  $\underline{h}'(\tilde{x}, \tilde{t})$  about  $(\underline{x}, \tilde{t})$  gives

$$\underline{h}'(\underline{\tilde{x}}, \tilde{t}) = \underline{h}'(\underline{x}, \tilde{t}) + (\underline{x} - \underline{\tilde{x}}) \cdot \nabla \underline{h}'(\underline{x}, \tilde{t}) 
+ \frac{1}{2} (\underline{x} - \underline{\tilde{x}}) (\underline{x} - \underline{\tilde{x}}) : \nabla \nabla \underline{h}'(\underline{x}, \tilde{t}) + \dots$$
(3.17)

Inserting Eq. (3.17) and Eq. (3.14) into Eq. (3.15) gives the following representation for the Reynolds stress in terms of the spatial moments of the Green's function

$$\langle \underline{u}'\underline{u}' \rangle = -\int_{-\infty}^{t} d\tilde{t} \left[ \langle \underline{h}'(\underline{x}, \tilde{t}) \, \underline{u}'(\underline{x}, t) \rangle + \sum_{i=1}^{\infty} \underline{\underline{A}}^{(i)}(\underline{x}, t - \tilde{t}) \right]$$
(3.18)

where

$$\underline{\underline{A}}^{(1)} = \left[ \int_{V} d\tilde{V}(\underline{x} - \underline{\tilde{x}}) \langle G \rangle (\underline{x}, t | \underline{\tilde{x}}, \tilde{t}) \right] \cdot \langle \nabla \underline{h}'(\underline{x}, \tilde{t}) \underline{u}'(\underline{x}, t) \rangle$$
(3.19)

and

$$\underline{\underline{A}}^{(2)} = \frac{1}{2} \left[ \int_{V} d\tilde{V}(\underline{x} - \underline{\tilde{x}}) (\underline{x} - \underline{\tilde{x}}) \langle G \rangle (\underline{x}, t | \underline{\tilde{x}}, \tilde{t}) \right] : \langle \nabla \nabla \underline{h}'(\underline{x}, \tilde{t}) \underline{u}'(\underline{x}, t) \rangle. \tag{3.20}$$

The temporal correlation  $\underline{A}^{(n)}(\underline{x}, t - \overline{t})$  involves the nth spatial moment of the Green's function contracted with the nth order gradient of the fluctuating field  $\underline{h}$ . For  $t = \overline{t}$ , all of the spatial moments of  $\langle G \rangle(\underline{x}, t \mid \overline{x}, \overline{t})$  are zero; however, these moments become non-zero on a time scale associated with the viscous transport of momentum. The foregoing expansion of Eq. (3.15) exploits the ides that the Green's function  $\langle G \rangle(\underline{x}, t \mid \overline{x}, \overline{t})$  acts like a spatial delta distribution on a time scale for which turbulent correlations become uncorrelated.

For turbulent flows at large Reynolds numbers (i.e.  $\tau_H \ll l_H^2/\nu$ ), the spatial moments of the Green's function are assumed to remain small over the finite time scale for which turbulent fluctuations are temporally correlated. This hypothesis motivates the use of a spatial smoothing approximation which reduces Eq. (3.18) to the following statistically stationary approximation

$$\langle \underline{u}'\underline{u}' \rangle \cong -\int_{0}^{\infty} \langle \underline{h}'(\underline{x}, \tilde{t}) \underline{u}'(\underline{x}, t) \rangle d\tau = -\int_{0}^{\infty} \langle \underline{u}'(\underline{x}, t) \underline{h}'(\underline{x}, \tilde{t}) \rangle d\tau, \tag{3.21}$$

where  $\tau = t - \tilde{t}$ . Eq. (3.21) gives a representation of the Reynolds stress in terms of the temporal history of the turbulence. As previously noted, the autocorrelation  $\langle \underline{h}'(\underline{x}, \tilde{t}) \underline{u}'(\underline{x}, t) \rangle$  must be a symmetric dyadic-valued operator. This follows directly from the fundamental representation of  $\underline{u}'$  in terms of  $\underline{h}'$ , the source of momentum fluctuations.

Eq. (3.21) can be simplified further by assuming that there exists a scalar-valued memory function  $m(x, \tau)$  with a finite cut-off time such that

$$\langle \underline{h}'(\underline{x}, \tilde{t}) \underline{u}'(x, t) \rangle = \langle \underline{h}'(x, t) \underline{u}'(x, t) \rangle m(x, \tau). \tag{3.22}$$

Thus, Eq. (3.21) can be represented by

$$\langle \underline{u}'\underline{u}' \rangle = -\tau_R \langle \underline{h}'\underline{u}' \rangle = -\tau_R \langle \underline{u}'\underline{h}' \rangle, \tag{3.23}$$

where the relaxation time  $\tau_R$  is a phenomenological coefficient dependent on the temporal structure of the turbulence:

$$\tau_R = \int_0^\infty m(\underline{x}, \tau) d\tau . \tag{3.24}$$

For statistically stationary flows, the integral time scale  $\tau_R$  depends on the local statistical properties of the turbulence k and  $\epsilon$ , the mean velocity gradient  $(S \equiv ||\nabla \langle \underline{u} \rangle||)$ , and the viscosity of the fluid. Dimensional reasoning suggests that

$$\tau_R = C_{R_E}^{\frac{k}{\epsilon}}, \qquad (3.25)$$

where  $C_R$  is a dimensionless function of  $kS/\epsilon$  and the turbulent Reynolds number  $k^2/\nu\epsilon$ . It follows from Eq. (3.10) that Eq. (3.23) can be written as

$$\langle \underline{u}'\underline{u}' \rangle = -\tau_R \langle \underline{f}'\underline{u}' \rangle - \tau_R \nabla \langle \underline{u} \rangle^T \cdot \langle \underline{u}'\underline{u}' \rangle = -\tau_R \langle \underline{u}'\underline{f}' \rangle - \tau_R \langle \underline{u}'\underline{u}' \rangle \cdot \nabla \langle \underline{u} \rangle. \tag{3.26}$$

Algebraic equations for the turbulent correlations  $\langle f'\underline{u}' \rangle$  and  $\langle \underline{u}'\underline{f}' \rangle$  follow by pre- and post-multiplying Eq. (3.13) by  $f'(\underline{x}, t)$  and taking the ensemble average. The previously employed spatial smoothing approximation for large turbulent Reynolds numbers and the use of the memory ansatz expressed by Eq. (3.22) yields the following result for the

symmetric correlation  $\langle ff \rangle$ :

$$\tau_{R}\langle \underline{f}\underline{f}\rangle = -\langle \underline{f}\underline{u}'\rangle - \tau_{R}\langle \underline{f}\underline{u}'\rangle \cdot \nabla \langle \underline{u}\rangle = -\langle \underline{u}'\underline{f}\rangle - \tau_{R}\nabla \langle \underline{u}\rangle^{T} \cdot \langle \underline{u}'\underline{f}\rangle. \tag{3.27}$$

In the above expression,  $\tau_R$  is assumed to be the same relaxation time as defined by Eqs. (3.24) and (3.25). The idea that a single scalar relaxation function can be used to characterize the temporal structure of *all* low-order, space-time correlations is a significant unifying step towards a practical closure theory.

Eqs. (3.26) and (3.27) can be combined to yield the following *pre-closure* representation of the Reynolds stress

$$\left[\underline{I} + \tau_R \nabla \langle \underline{u} \rangle\right]^T \cdot \langle \underline{u}' \underline{u}' \rangle \cdot \left[\underline{I} + \tau_R \nabla \langle \underline{u} \rangle\right] = \tau_R^2 \langle \underline{f} \underline{f}' \rangle. \tag{3.28}$$

Eq. (3.28) is called the pre-closure hereinafter because it relates the Reynolds stress to three aspects of the flow field: (1) the spatial gradient of the mean field; (2) the relaxation time  $\tau_R$ ; and, (3) the unclosed turbulent pre-stress,  $\tau_R^2 \langle \underline{f} \underline{f} \rangle$ . For small dimensionless relaxation times:

$$N_{p} = \tau_{p} \|\nabla\langle u\rangle\| \ll 1, \tag{3.29}$$

the pre-stress approaches the Reynolds stress. Like the Reynolds stress, the pre-stress is a non-negative operator, and, thereby, has only non-negative eigenvalues.

Eq. (3.11) could be used to formally relate the turbulent pre-stress to other unknown statistical correlations involving spatial gradients of the fluctuating pressure and the divergence of fluctuations in the *instantaneous* Reynolds stress. Alternatively, a phenomenological theory for the pre-stress could be developed analogous to Eq. (3.5) by first writing  $\tau_R^2 \langle f f \rangle$  as the sum of an *isotropic* pre-stress and an *anisotropic* pre-stress

$$\tau_R^2 \langle f_Z^Y \rangle = \frac{2\alpha}{3} I + 2kH \quad , \tag{3.30}$$

Like the anisotropic stress  $\underline{b}$ , the anisotropic pre-stress  $\underline{H}$  is both symmetric ( $\underline{\underline{H}} = \underline{\underline{H}}^T$ ) and traceless ( $tr(\underline{\underline{H}}) = 0$ ). The isotropic pre-stress coefficient  $\alpha$  must satisfy the following normalization condition

$$\tau_R^2 tr \langle f_T^{\alpha} \rangle = 2\alpha = 2k + 2\tau_R \langle \underline{u}'\underline{u}' \rangle : \nabla \langle \underline{u} \rangle + \tau_R^2 \left[ tr \left( \nabla \langle \underline{u} \rangle^T \cdot \langle \underline{u}'\underline{u}' \rangle \cdot \nabla \langle \underline{u} \rangle \right) \right]. \quad (3.31)$$

As the relaxation group  $N_R$  increases, the isotropic and anisotropic parts of the pre-stress should make significant contributions to the distribution of kinetic energy among the components of the fluctuating velocity as well as to the shear components of the Reynolds stress. Eqs. (3.28), (3.30), and (3.31) provide an alternative closure strategy to previously developed approaches based on the *anisotropic* part of the Reynolds stress.

In this paper, the efficacy of using Eq. (3.28) with

$$\underline{H} = \underline{0} \tag{3.32}$$

will be explored. This assumption provides a closure model for the normalized Reynolds stress

$$R = \frac{\langle \underline{u}'\underline{u}' \rangle}{2k}.$$
 (3.33)

A non-trivial model for H is presented in Chapter 4 of this work. Weispfennig [1997] has also considered non-trivial models for the anisotropic pre-stress.

## 3.3 Isotropic Pre-stress Theory

For homogeneous shear and H = 0, Eqs. (3.28)-(3.30) reduce to the following set of equations for the components of the normalized Reynolds stress

$$R_{xx} = \frac{1}{3 + N_R^2} \,, \tag{3.34}$$

$$R_{yy} = \frac{1}{3 + N_R^2} \,, \tag{3.35}$$

$$R_{zz} = \frac{1 + N_R^2}{3 + N_R^2} \,, \tag{3.36}$$

and

$$R_{yz} = \frac{-N_R}{3 + N_R^2} \ . \tag{3.37}$$

The relaxation group  $N_R$  is defined by  $N_R = \tau_R S$ . The isotropic pre-stress coefficient  $\alpha$  is given by

$$\frac{\alpha}{k} = \frac{3}{3 + N_R^2}.\tag{3.38}$$

The above set of equations, hereinafter termed the isotropic pre-stress (IPS-) theory, approaches the Boussinesq theory (see Eq. (3.7)) for  $N_R \ll 1$  inasmuch as  $R_{xx} = R_{yy} = R_{zz} = \frac{1}{3}$ ,  $R_{yz} = -\frac{1}{3}N_R$ , and  $\alpha = k$ . The *eddy* viscosity coefficient for this limiting case is the same as the standard k- $\epsilon$  theory, viz.

$$\lim_{N_R \to 0} \mathbf{v}_e = \frac{2}{3} C_R \frac{k^2}{\varepsilon}. \tag{3.39}$$

For  $N_R \gg 1$ , the IPS-theory shifts the kinetic energy to the axial component of the fluctuating velocity with the result that  $R_{xx} = R_{yy} = 1/N_R^2$  and  $R_{zz} \to 1$ . Eq. (3.37) predicts that the shear component of the Reynolds stress becomes inversely proportional to the relaxation number,  $R_{yz} = -1/N_R$ , and Eq. (3.38) gives  $\alpha/k = 3/N_R^2$  for  $N_R \gg 1$ .

Eq. (3.37) shows that a maximum in  $-R_{yz}$  (i.e.  $1/\sqrt{12}$ ) occurs at  $N_R = \sqrt{3}$ . Furthermore, Eqs. (3.25) and (3.37) together with  $N_R = \tau_R S$  imply that

$$-\langle u'_{y}u'_{z}\rangle = c_{\mu}\frac{k^{2}}{\varepsilon}\frac{d\langle u_{z}\rangle}{dy}$$
 (3.40)

where

$$c_{\mu} = \frac{2C_R}{3 + N_R^2}. (3.41)$$

Thus, the IPS-theory predicts that the eddy viscosity coefficient  $c_{\mu}$  decreases as the relaxation group increases, provided  $C_R$  is modeled as a universal constant. This non-linear dependence on the mean shear field is fundamentally different than the behavior presumed by the k- $\epsilon$  theory, which employs a constant eddy viscosity coefficient.

The IPS-theory and the Boussinesq theory also predict qualitatively different results for the invariants of the anisotropic stress. For homogeneous shear,

$$II = b_{xx}^2 + b_{yy}^2 + b_{zz}^2 + 2b_{yz}^2 (3.42)$$

and

$$III = b_{xx}^3 + b_{yy}^3 + b_{zz}^3 - 3b_{xx}b_{yz}^2. (3.43)$$

For the Boussinesq theory, Eqs. (3.7) and (3.39) imply that  $b_{xx} = b_{yy} = b_{zz} = 0$ , and

$$b_{yz} = -N_R/3. (3.44)$$

Therefore, for this special case, Eqs. (3.42) and (3.43) yield

$$II_B = \frac{2}{9}N_R^2 \text{ and } III_B = 0.$$
 (3.45)

Because the third invariant is zero, it follows directly from Figure 3.3 and Eq. (3.45) that realizable Boussinesq turbulent states are restricted to  $N_R \in [0, 1]$ .

It follows directly from Eqs. (3.5) and (3.34)-(3.37) that the IPS-theory yields the following results for the components of the anisotropic stress

$$b_{xx} = -\frac{N_R^2}{3(3+N_R^2)},\tag{3.46}$$

$$b_{yy} = -\frac{N_R^2}{3(3+N_R^2)},\tag{3.47}$$

$$b_{zz} = -2b_{yy} \quad , \tag{3.48}$$

and

$$b_{yz} = \frac{-N_R}{3 + N_R^2}. (3.49)$$

The invariants II and III for this theory can be written as

$$II_{IPS} = \frac{2}{3} \left( \frac{N_R^2}{3 + N_R^2} \right) \tag{3.50}$$

and

$$III_{IPS} = \frac{9 + 2N_R^2}{9N_R^2} \left(\frac{N_R^2}{3 + N_R^2}\right)^3. \tag{3.51}$$

As the relaxation number goes to zero, Eqs. (3.50) and (3.51) give the isotropic pair (II, III) = (0,0); as  $N_R \to \infty$ , (II, III) = (2/3, 2/9); and, for  $N_R = 1$ , (II, III) = (1/6, 11/576). Figure 3.4 shows the locus of realizable homogeneous shear states predicted by the IPS-theory for  $0 \le N_R \le \infty$ . The asymptotic state measured by

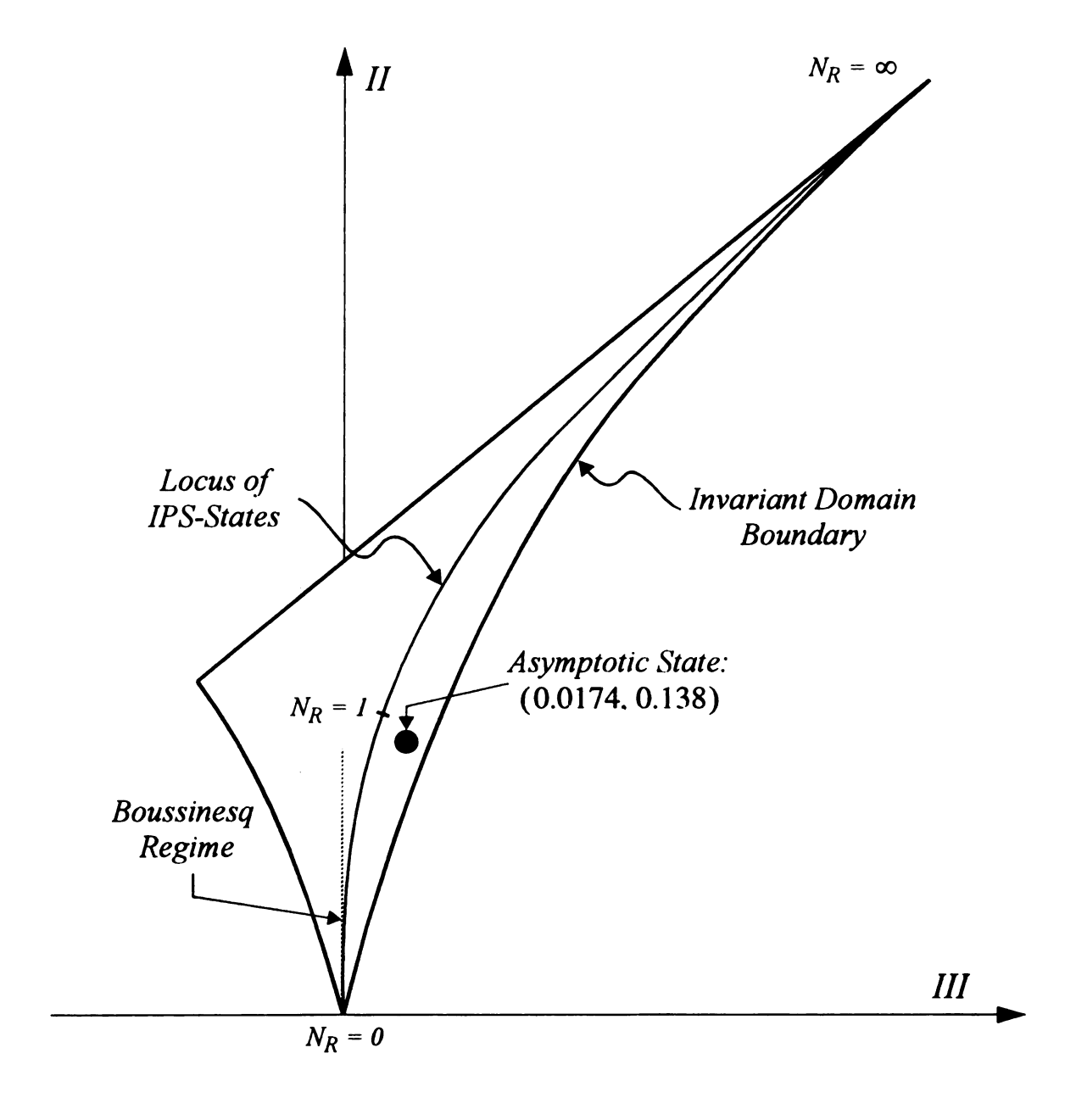


Figure 3.4 Anisotropy Invariants Predicted by the IPS-Theory for Homogeneously Sheared Turbulence

Tavoularis and Karnik [1989] is also shown on Figure 3.4. Clearly, the IPS-theory represents a significant improvement over the classical algebraic Boussinesq theory for which  $III_B = 0$  for all homogeneous shear states (cf. Figure 1.2).

The spatial development in the relaxation group is determined by the transport equations for k and  $\epsilon$ . Eqs. (3.2) and (3.3) can be combined to yield the following non-linear, ordinary differential equation for  $N_R$ 

$$\frac{dN_R}{d\xi} = 2N_R R_{yz} (C_P - 1) + C_R (C_D - 1). \tag{3.52}$$

where the dimensionless development time ξ is defined by

$$\xi = zS/\langle u_z \rangle(0), \qquad (3.53)$$

and  $R_{yz}$  is given by Eq. (37). As  $\xi$  approaches infinity, Eq. (3.52) reduces to the asymptotic condition given by Eq. (3.4).

## 3.4 Parameter Estimates

Although Figure 3.4 shows that the IPS-theory gives an improved prediction of the anisotropic invariants compared to the Boussinesq theory, the experimentally observed asymptotic state is nevertheless unattainable. Figure 3.5 illustrates a selection strategy for the asymptotic value of  $N_R$  which minimizes the relative error between the asymptotic experimental state  $(II_a^e, III_a^e)$  and the locus of attainable states consistent with the IPS-theory. Therefore, with

$$\Delta = \left[ \left\{ \frac{II - II_a^e}{II_a^e} \right\}^2 + \left\{ \frac{III - III_a^e}{III_a^e} \right\}^2 \right]^{1/2}, \tag{3.54}$$

 $N_R^a$  is selected to minimize  $\Delta$  (see Figure 3.5). This procedure yields  $N_R^a = 0.945$ ,

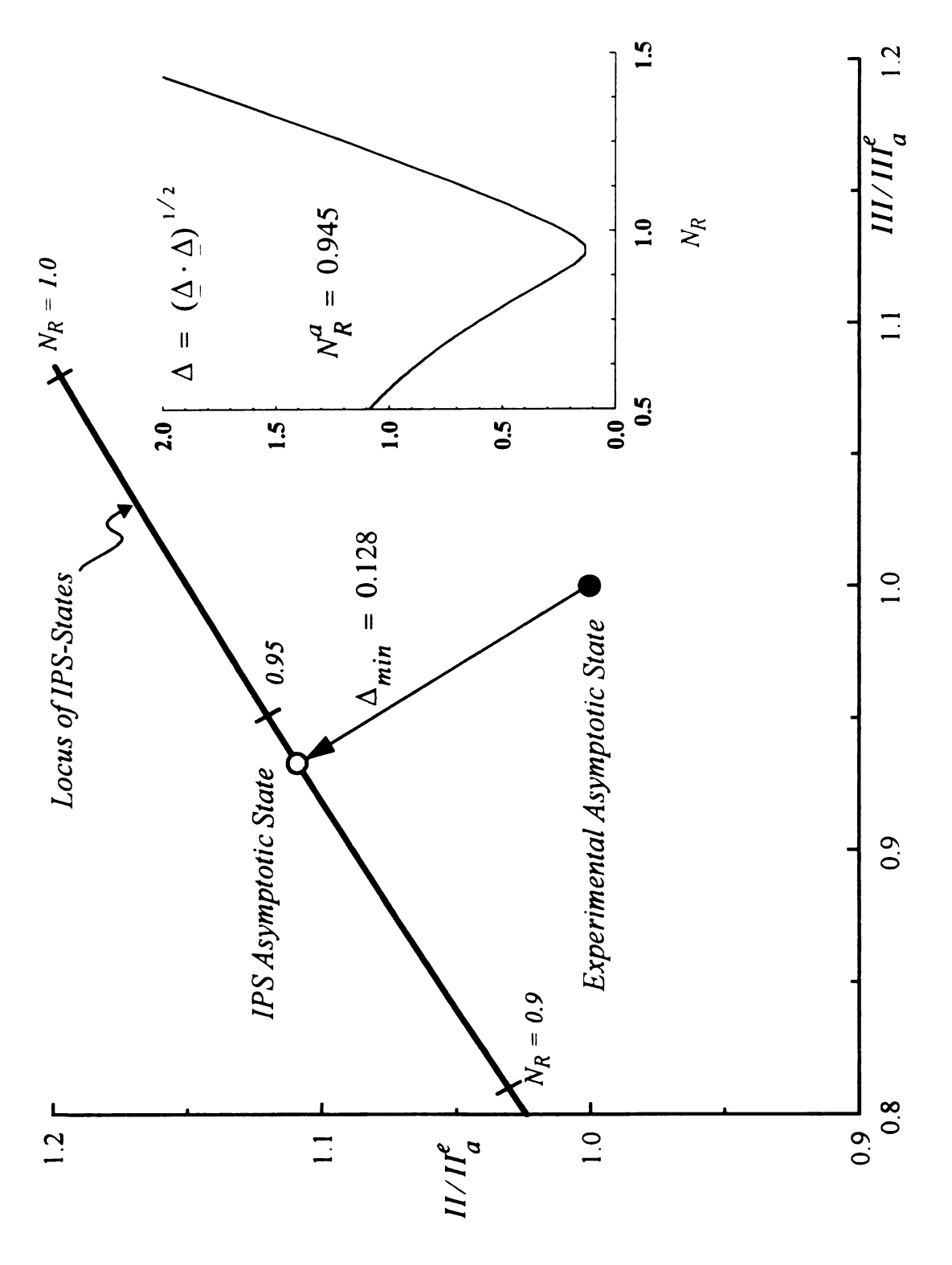


Figure 3.5 Estimation of the Relaxation Group for Asymptotic Homogeneously Sheared Turbulence

 $R_{xx}^a = R_{yy}^a = 0.257$ ,  $R_{zz}^a = 0.486$ , and  $-R_{yz}^a = 0.243$ . With  $N_R^a = C_R (Sk/\epsilon)_a$ , the relaxation coefficient  $C_R = 0.227$  for  $(Sk/\epsilon)_a = 4.16$ , as reported by Tavoularis and Karnik [1989] (see Figure 3.1).

The existence condition for an asymptotic state (see Eqs.(3.4) and (3.52)) provides an additional equation for the model coefficient  $C_p$ :

$$C_{p} = 1 - \frac{C_{R}(C_{D} - 1)}{2N_{R}^{a}R_{vz}^{a}}.$$
(3.55)

Eq. (3.55) implies that  $C_P = 1.41$  for  $C_D = 1.83$  and  $N_R^a R_{yz}^a = -0.229$ . Table 3.1 gives a summary of the model parameters for the IPS-theory. Table 3.2 gives the predicted properties of the asymptotic state for homogeneously sheared flows.

## 3.5 Results and Discussion

Eq. (3.52) with  $R_{yz}$  given by Eq. (3.37) was solved numerically using a fourth order Runge-Kutta algorithm (Carnahan, et al., 1969; see also Appendix H) with a variable time step. The three model parameters  $C_P$ ,  $C_D$ , and  $C_R$  are assumed to be universal constants independent of  $Sk/\varepsilon$ . Figure 3.6 shows that the relaxation group  $N_R$  ( $\equiv \tau_R S$ ) monotonically approaches its asymptotic limit for a wide range of initial states ( $0 \le N_R^o \le 10$ ). The development time for  $N_R \cong N_R^a$  depends on the initial conditions. For an isotropic initial condition (i.e.  $N_R^o = 0$ ), the asymptotic state is approached for developmental times on the order of ten. However, for highly anisotropic initial conditions ( $N_R^o = 10$ ), the approach to the asymptote requires  $\xi = 30$ .

Figure 3.7 shows the response of the normal components of the normalized Reynolds stress subjected to an isotropic initial state (R = I/3 and  $N_R^0 = 0$ ). Like the relaxation group, an asymptotic state is attained for  $\xi = 10$  to 30, depending on the initial turbulent state. This result is comparable to the development times observed experimentally by Tavoularis and Corrsin [1981] and is sensitive to the initial state of turbulence. The

Table 3.1: Parameter Estimates for the IPS-Theory

Parameter	Estimate	Basis
$C_D$	1.83	Isotropic Decay (Comte-Bellot and Corrsin, 1971; Mansour and Wray, 1994; see Chapter 2)
$C_{P}$	1.41	Existence condition for k-E equations
$C_R$	0.227	Optimization of anisotropy invariants

**Table 3.2:** Predictions of Asymptotic Statistical Properties for Homogeneously Sheared Turbulence

Property	IPS-Theory	Experimental
N <sub>R</sub>	0.945	N/A <sup>†</sup>
kS/e	N/A <sup>†</sup>	4.16
R <sub>xx</sub>	0.257	0.236
R <sub>yy</sub>	0.257	0.196
R <sub>zz</sub>	0.486	0.568
-R <sub>yz</sub>	0.243	0.165
II	0.153	0.138
III	0.0162	0.0174

<sup>&</sup>lt;sup>†</sup> Data point not applicable to this entry.

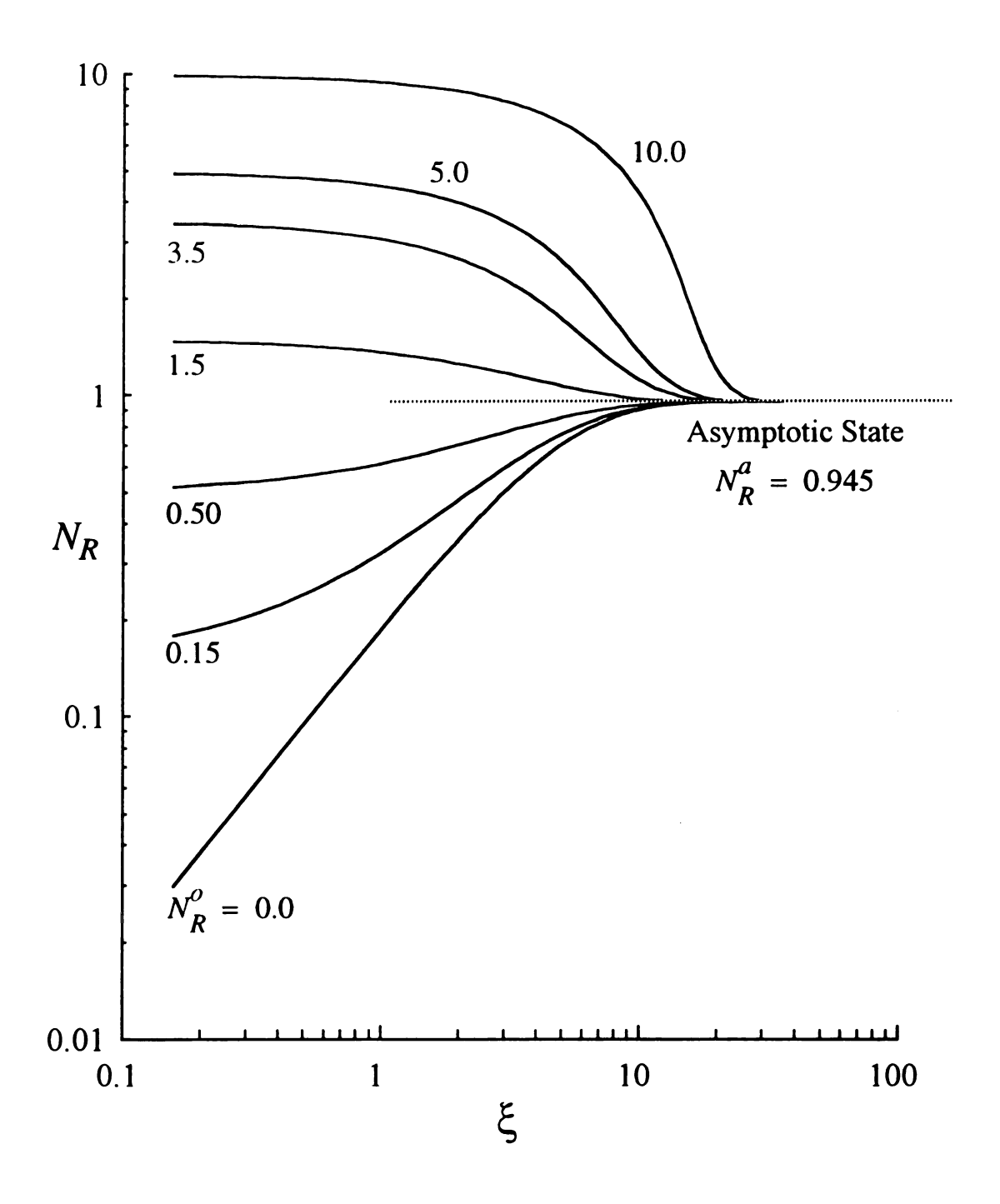


Figure 3.6 The Effect of the Development Time on the Relaxation Group for Homogeneously Sheared Turbulence

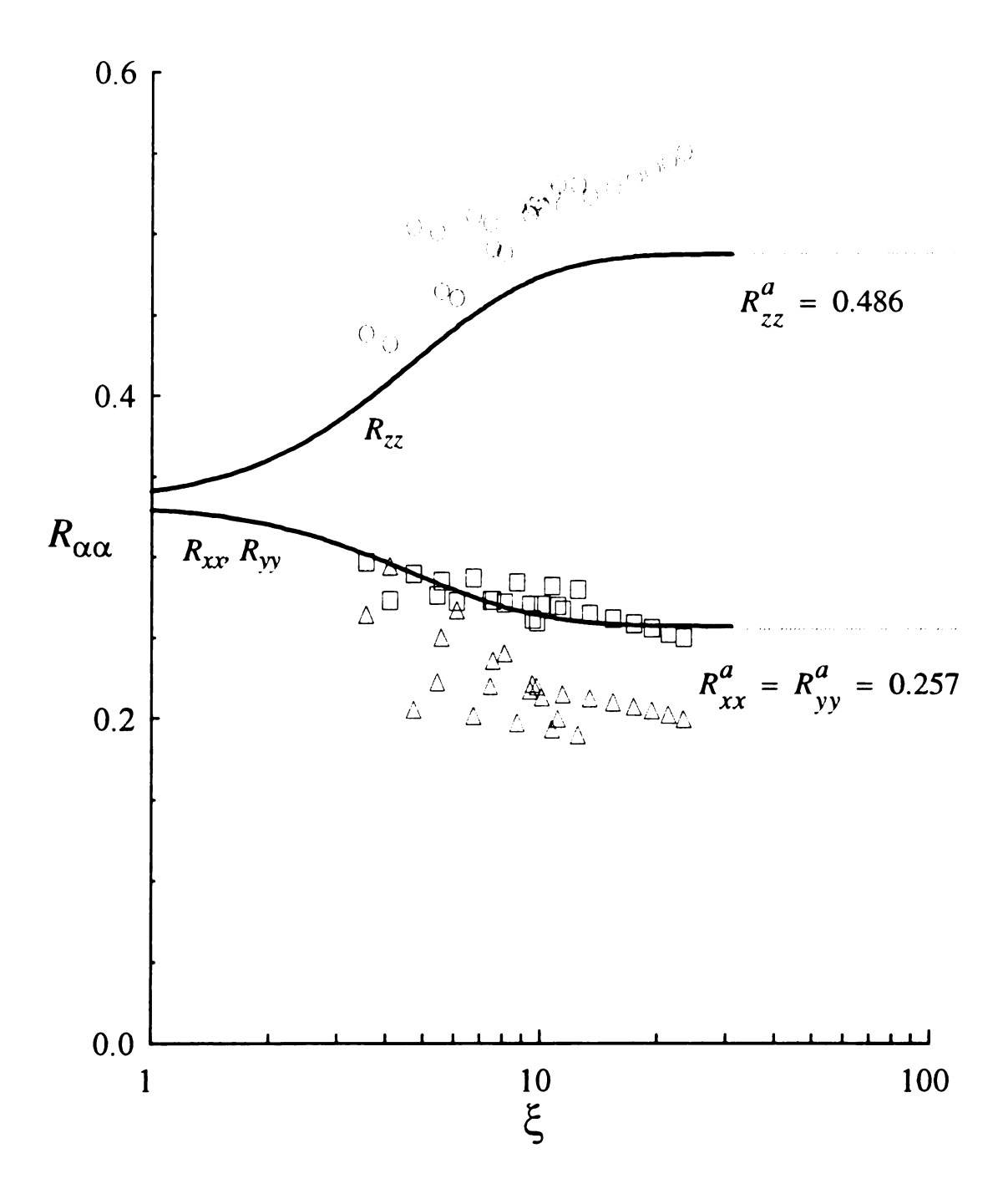


Figure 3.7 The Effect of the Development Time on the Distribution of Kinetic Energy for Homogeneously Sheared Turbulence ( — IPS-theory; experimental data (Tavoularis and Karnik, 1989):  $\square R_{xx}$ ;  $\triangle R_{yy}$ ;  $\bigcirc R_{zz}$ )

asymptotic state for the IPS-theory is as close to the data as allowed by the optimization of the model parameter  $C_R$  (see Figure 3.5). For an anisotropic pre-stress  $(\underline{H} \neq \underline{0})$ , the invariants of the Reynolds stress anisotropy can be reproduced exactly (see Chapter 4).

The IPS-theory clearly does not predict a second normal stress difference, and the predicted primary normal stress difference,  $R_{zz}^a - R_{yy}^a = 0.229$ , is significantly smaller than the experimental estimate of 0.372 (see Figure 3.2). These predictions, however, can easily be improved by using a phenomenological theory with a non-trivial anisotropic prestress. For instance, it follows directly from Eqs. (3.28), (3.29), and (3.30) that

$$R_{xx} = \frac{1}{3} \frac{\alpha}{k} + H_{xx} , \qquad (3.56)$$

$$R_{yy} = \frac{1}{3} \frac{\alpha}{k} + H_{yy} , \qquad (3.57)$$

and

$$R_{zz} = \frac{1}{3} \frac{\alpha}{k} + H_{zz} - 2N_R R_{yz} - N_R^2 R_{yy}. \tag{3.58}$$

Eqs. (3.56) and (3.57) stem directly from the pre-closure and imply that an anisotropic pre-stress is a necessary condition for a non-zero second normal stress difference.

Eqs. (3.57) and (3.58) also show that the primary normal stress difference arises from two distinct physical effects: (1) the primary normal difference  $H_{zz} - H_{yy}$ ; and, (2) the convective coupling between the transverse velocity fluctuations and the mean field gradient,

$$\underline{u}' \cdot \nabla \langle \underline{u} \rangle = u'_y \frac{d\langle u_z \rangle}{dy} e_z. \tag{3.59}$$

This fluctuating field is directly responsible for the two statistical correlations  $\langle u'_z u'_y \rangle S$  and  $\langle u'_y u'_y \rangle S$ , which, as indicated above, make the Reynolds stress anisotropic even if the pre-stress is isotropic.

The normalization of the pre-stress (Eq. (3.31)) gives the following expression for  $\alpha/k$  (see Eq. (3.31))

$$\frac{\alpha}{k} = 1 + 2N_R R_{yz} + N_R^2 R_{yy}. \tag{3.60}$$

For an isotropic pre-stress,  $R_{yz} = -N_R R_{yy}$ , and Eq. (3.60) reduces to

$$\frac{\alpha}{k} = 1 + N_R R_{yz}. \tag{3.61}$$

With this result, Eqs. (3.56)-(3.58) can be re-written in *canonical* form:

$$R_{xx} = \frac{1}{3} (1 - \ell) , \qquad (3.62)$$

$$R_{yy} = \frac{1}{3} (1 - \ell) , \qquad (3.63)$$

and

$$R_{zz} = \frac{1}{3} (1 + 2\ell), \qquad (3.64)$$

where

$$\mathcal{Q} = -N_R R_{yz} = -\tau_R \frac{\langle u'_z u'_y \rangle S}{2k}. \tag{3.65}$$

It follows from Eq. (3.25) that the above expression for & can be rewritten as

$$\mathcal{R} = -\frac{C_R \langle u'_z u'_y \rangle S}{2\varepsilon} . \tag{3.66}$$

Thus, the ratio of production to dissipation of turbulent kinetic energy (see Eq. (3.2)) determines the redistribution of energy among the velocity fluctuations. It follows from

Eq. (3.4) (see also Eq. (3.55) and Table 3.1) that

$$\lim_{z \to \infty} \mathcal{R} = \frac{C_R C_D - 1}{2 C_P - 1} = 0.229. \tag{3.67}$$

Eqs. (3.62)-(3.64) predict a non-zero primary normal stress difference and a zero second normal stress difference:

$$R_{zz} - R_{yy} = \ell \ell$$
 ,  $R_{yy} - R_{xx} = 0$  . (3.68)

For the IPS-theory, Figure 3.7 and Eqs. (3.62)-(3.64) show how  $\ell$  redistributes the energy produced by the coupling between the shear component of the Reynolds stress and the mean gradient. The experimental data of Tavoularis and Karnik [1989] show the same qualitative trend as the theory but, clearly,  $R_{yy} - R_{xx} \neq 0$ .

Figure 3.8 illustrates the possibility that the shear component of the Reynolds stress may not approach its asymptotic state monotonically. The figure also shows that  $-R_{yz}$  has a maximum value at  $N_R = \sqrt{3}$ . Because  $N_R^a = 0.945 < \sqrt{3}$ , the monotonic behavior of the relaxation group towards its asymptote causes the shear stress to relax monotonically for initial states characterized by  $N_R^o < \sqrt{3}$ . On the other hand, for  $N_R^o > \sqrt{3}$ ,  $-R_{yz}$  increases to a local maximum and then decreases to its asymptotic value for development times greater than ten. If  $N_R^o > 2.7$ , the transient shear component of the Reynolds stress overshoots its asymptotic state at some finite time (see Figure 3.8). This complex transient response may have the appearance of a quasi-asymptotic condition, but Figure 3.8 shows that  $R_{yz}$  requires  $\xi > 30$  to attain its ultimate asymptotic state for highly anisotropic initial conditions.

The maximum in  $-R_{yz}$  occurs because of two competing physical processes. For small values of  $N_R$ , the IPS-theory approaches the Boussinesq (or gradient) transport regime for which  $\langle u'_y u'_z \rangle \sim S$ ; for large values of the relaxation group, the shear component of the Reynolds stress approaches the so-called *equilibrium* transport regime:

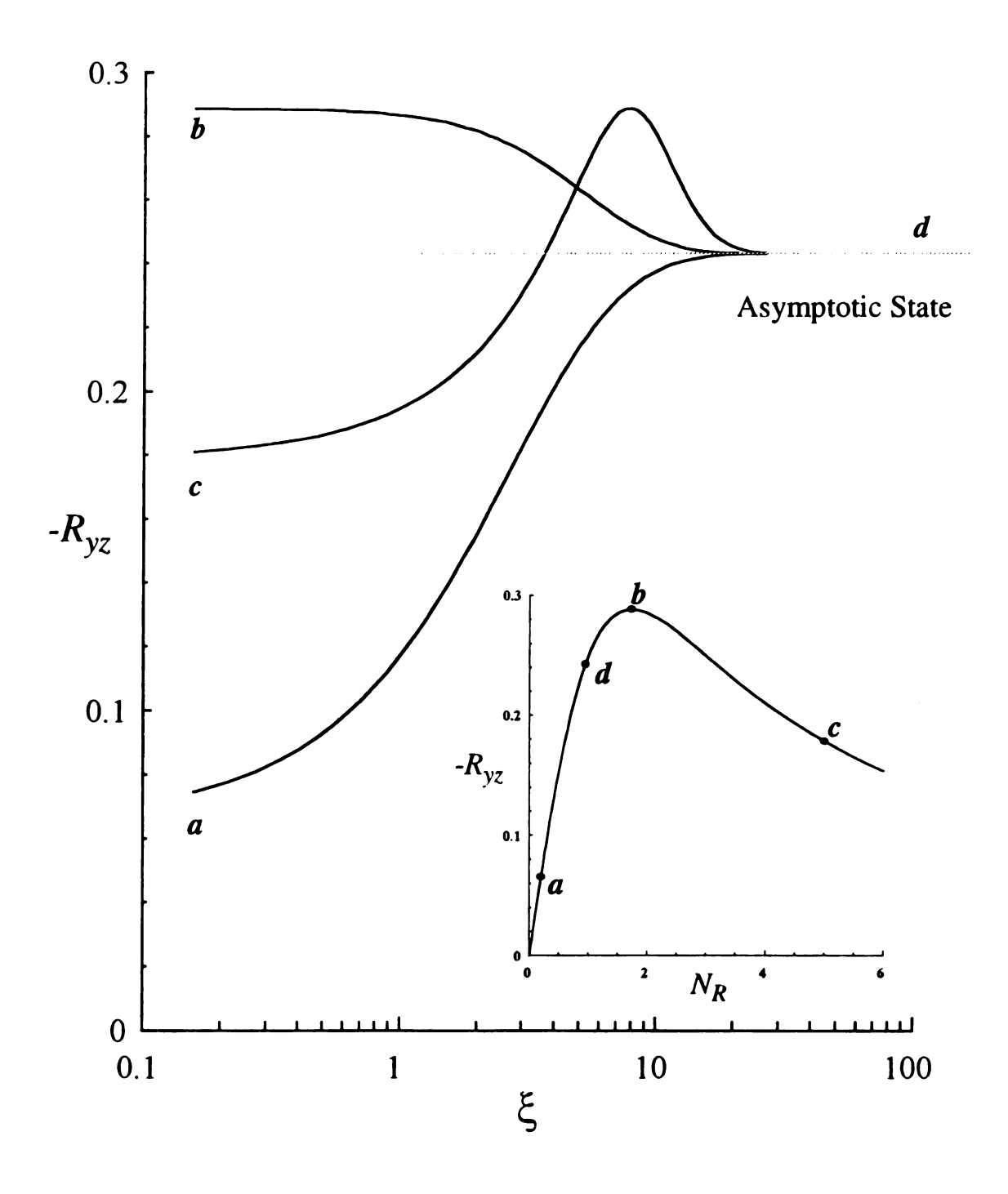


Figure 3.8 The Effect of the Development Time on the Shear Component of the Normalized Reynolds Stress for Homogeneously Sheared Turbulence (a:  $N_R^o = 0.2$ ; b:  $N_R^o = \sqrt{3}$ ; c:  $N_R^o = 5.0$ ; d:  $N_R^a = 0.945$ ,  $-R_{yz}^a = 0.243$ )

$$\lim_{S \to \infty} \langle u'_y u'_z \rangle = -\frac{2k}{N_R} = -\frac{2\varepsilon}{C_R S}.$$
 (3.69)

Eq. (3.69) shows that, in the equilibrium regime, the production of turbulent energy,  $-\langle u'_y u'_z \rangle S$ , is proportional to the dissipation of turbulent energy. This non-linear transport regime arises because the energy in the transverse fluctuations  $\langle u'_y u'_y \rangle$  decreases significantly as  $N_R$  increases due to the redistribution of energy by  $\ell$  (see Eqs. (3.63) and (3.68)). Thus, the IPS-theory for homogeneously sheared turbulent flows yields a shear-thinning eddy viscosity (see Eqs. (3.40) and (3.41)) which bridges the gradient transport regime  $(N_R \to 0)$  with the equilibrium transport regime  $(N_R \to \infty)$ :

$$v_e = \frac{-\langle u'_y u'_z \rangle}{d\langle u_z \rangle / dy} = \tau_R \langle u'_y u'_y \rangle = \frac{2C_R}{3 + N_R^2} \frac{k^2}{\epsilon}.$$
 (3.70)

For some simple shear flows, the relative time scale  $N_R$  may span a wide range of values; Therefore, both transport regimes may occur in the same flow field, albeit at different spatial locations.

## 3.6 Conclusions

As a direct consequence of the pre-closure theory given by Eq. (28), a non-zero primary normal stress difference obtains regardless of the closure hypothesis for the pre-stress; however, a non-zero second normal stress difference requires the existence of a non-trivial anisotropic pre-stress.

For positive k and  $\epsilon$ , the IPS-theory predicts realizable turbulent states for  $0 \le N_R \le \infty$ , whereas realizable states for the Boussinesq theory occur only for  $0 \le N_R \le 1$ . This theoretical result obtains for the IPS-model because the pre-closure relates the Reynolds stress to a pre-stress having only non-negative eigenvalues. For the special case of an isotropic pre-stress, all the eigenvalues of the pre-stress are all equal to  $\alpha/3k$  (>0).

The IPS-theory with  $C_R$  interpreted as a universal constant predicts two distinct

transport regimes bridged by an effective eddy viscosity which depends on  $\tau_R S$ . For  $\tau_R S \ll 1$ , a gradient transport regime occurs (i.e.  $\langle u'_y u'_z \rangle \sim S$ ); whereas, for  $\tau_R S \gg 1$ , an equilibrium transport regime occurs (i.e.  $\langle u'_y u'_z \rangle \sim 1/S$ ).

The time required for the turbulence to achieve an asymptotic state is strongly dependent on initial conditions. The developmental times needed to reach an asymptotic state based on the IPS-theory agree qualitatively with experimental observations.

## **CHAPTER 4**

# ANISOTROPIC PRE-STRESS THEORY FOR HOMOGENEOUSLY SHEARED TURBULENT FLOWS

## 4.1 Introduction

In Chapter 3, an algebraic pre-closure theory for the Reynolds stress from an analysis of the equation of motion for statistically stationary turbulent flows was developed. A spatial smoothing approximation and the use of a memory ansatz for turbulent temporal correlations were key elements in the development of the following pre-closure theory for the Reynolds stress

$$\underline{A}^T \cdot \langle \underline{u}'\underline{u}' \rangle \cdot \underline{A} = \tau_R^2 \langle \underline{f} \underline{f}' \rangle \quad , \tag{4.1}$$

where

$$\underline{\underline{A}} = \left[\underline{I} + \tau_R \nabla \langle \underline{u} \rangle\right] \quad . \tag{4.2}$$

Eq. (4.1) relates the Reynolds stress to the gradient of the mean velocity, the relaxation time  $\tau_R$ , and the turbulent pre-stress. For large turbulent Reynolds numbers (i.e.  $k^2 \gg v\epsilon$ ), the relaxation time is assumed to scale with the characteristic eddy turnover time  $k/\epsilon$ .

$$\tau_R = C_{R_{\varepsilon}}^{k} \quad , \tag{4.3}$$

where k represents the kinetic energy of the turbulent fluctuations  $(2k \equiv \langle \underline{u}' \cdot \underline{u}' \rangle)$  and  $\epsilon$  represents the dissipation of turbulent kinetic energy  $(\epsilon \equiv v \langle \nabla \underline{u}'; (\nabla \underline{u}')^T \rangle)$ . The model

coefficient  $C_R$  is assumed to be independent of turbulent and mean field statistical properties.

The turbulent pre-stress  $\tau_R^2 \langle f \mathcal{I} \rangle$  depends on statistical correlations related to pressure fluctuations and fluctuations in the instantaneous Reynolds stress,

$$\underline{J} = \underline{u}'\underline{u}' - \langle \underline{u}'\underline{u}' \rangle . \tag{4.4}$$

With f' defined by

$$\underline{f}' \equiv \nabla \cdot \left[ \frac{p'}{\rho} \underline{I} + \underline{J}' \right], \tag{4.5}$$

it follows that the correlation  $\langle ff' \rangle$  can be expressed as

$$\langle \underline{f} \underline{f} \rangle = \langle \nabla \left( \frac{\underline{p'}}{\rho} \right) \nabla \left( \frac{\underline{p'}}{\rho} \right) \rangle + \langle \nabla \left( \frac{\underline{p'}}{\rho} \right) (\nabla \cdot \underline{f'}) \rangle + \langle (\nabla \cdot \underline{f'}) (\nabla \cdot \underline{f'}) \rangle + \langle (\nabla \cdot \underline{f'}) (\nabla \cdot \underline{f'}) \rangle. \quad (4.6)$$

Although a closure for the pre-stress could be developed by analyzing the statistical correlations appearing in Eq. (4.6), the approach employed in Chapter 3 was based on an alternative strategy which incorporated a direct decomposition of the pre-stress into isotropic and anisotropic components:

$$\tau_R^2 \langle f_Z^{\nu} \rangle = \frac{2\alpha}{3} I + 2kH \qquad (4.7)$$

The anisotropic pre-stress 2kH is symmetric and traceless. Because  $tr\langle \underline{u}'\underline{u}'\rangle = 2k$ , Eq.(4.1) requires that the isotropic coefficient  $\alpha$  be determined by the following equation

$$2\alpha = \tau_R^2 tr \langle \underline{f} \underline{f} \rangle = 2k + 2\tau_R \langle \underline{u}' \underline{u}' \rangle : \nabla \langle \underline{u} \rangle + \tau_R^2 tr (\nabla \langle \underline{u} \rangle^T \cdot \langle \underline{u}' \underline{u}' \rangle \cdot \nabla \langle \underline{u} \rangle) . \tag{4.8}$$

Eq. (4.8) provides a means to relate the isotropic coefficient  $\alpha$  to the mean field and the specific closure hypothesis for the anisotropic pre-stress H.

In Chapter 3, the implications of an isotropic pre-stress (IPS-) theory, for which  $\underline{\underline{H}} = \underline{0}$ , were examined. Eqs. (4.1) and (4.7) were applied to a homogeneously sheared turbulent flow (i.e.  $S = d\langle u_z \rangle/dy = \text{constant}$ , see Figure 3.1). The evolution of the turbulent time scale  $k/\epsilon$  was computed using the  $k-\epsilon$  theory of turbulence (Hanjalic and Launder, 1972). For homogeneous shear flows at high Reynolds numbers, the equations governing the turbulent kinetic energy and dissipation simplify to

$$\langle u_z \rangle(0) \frac{dk}{dz} = -\langle \underline{u}' \underline{u}' \rangle : \nabla \langle \underline{u} \rangle - \varepsilon \quad , \tag{4.9}$$

$$\langle u_z \rangle (0) \frac{d\varepsilon}{dz} = -C_P \frac{\langle \underline{u}' \underline{u}' \rangle : \nabla \langle \underline{u} \rangle}{\tau_P} - C_D \frac{\varepsilon}{\tau_D} ,$$
 (4.10)

where  $\tau_P = \tau_D = k/\epsilon$ .  $C_P$  and  $C_D$  are constants independent of the local state of turbulence. The IPS-theory predicts a positive first normal stress difference and a shear thinning eddy viscosity coefficient which bridges the more traditional gradient transport regime for which  $\langle u'_y u'_z \rangle \sim S$  with an equilibrium transport regime for which  $\langle u'_y u'_z \rangle \sim 1/S$ . However, the IPS-theory erroneously predicts that the second normal stress difference is zero for homogeneously sheared turbulence. Moreover, the algebraic pre-closure theory with an isotropic pre-stress cannot explain return-to-isotropy experiments for homogeneous turbulent flows (Choi, 1983; Choi and Lumley, 1984; and, LePenven, et al., 1985).

Therefore, the purpose of this chapter is to further demonstrate the utility of Eqs. (4.1) and (4.7) by using an anisotropic pre-stress (APS-) model. In Section 4.2, an APS-model for the pre-stress which incorporates a phenomenological relaxation process consistent with the return-to-isotropy phenomena is introduced in accordance with Issue (iii) of Section 1.2. Return-to-isotropy data are used to determine the phenomenological relaxation parameter. The extension of the closure model to an anisotropic pre-stress also serves to address the limitation of the IPS-theory, which had a zero second normal stress

difference (see (ii) in Section 1.2). The asymptotic state of homogeneous shear is used as in Chapter 3 to determine the APS-model constants. The non-algebraic nature of the APS-theory does not permit an *a priori* evaluation of realizable turbulent states; however, the realizability of the transient computations are verified *a posteriori*.

## 4.2 Anisotropic Pre-stress Theory

Eq. (4.1) can be generalized to a class of non-inertial frames rotating at a constant angular velocity relative to an inertial frame by replacing the frame-dependent  $\nabla \langle \underline{u} \rangle$  operator with  $\nabla^* \langle \underline{u}^* \rangle + \underline{\Omega}$ , where  $\underline{u}^*$  is the instantaneous velocity in the non-inertial frame and  $\underline{\Omega}$  represents the anti-symmetric temporal connection between the inertial and non-inertial frames (Bird *et al.*, 1977):

$$\Omega = -\underline{Q} \cdot \underline{\dot{Q}}^T, \tag{4.11}$$

where  $\underline{Q}$  is an orthogonal dyadic-valued operator (i.e.  $\underline{Q} \cdot \underline{Q}^T = I$ ) and  $\underline{\dot{Q}}$  is the time derivative. Thus, the pre-closure theory for the Reynolds stress contains an explicit dependence on the frame of reference through the operator A defined by Eq. (4.2).

Unlike the Reynolds stress, the theory developed here assumes that the anisotropic pre-stress  $\tilde{H}$  (= 2kH) is an objective property of the motion associated with the mean field and should not depend on the reference frame. Whence, the anisotropic pre-stress in a non-inertial frame can be related to the anisotropic pre-stress in an inertial frame by the following expression (Mase and Mase, 1992)

$$\tilde{\underline{H}}^* = \underline{\underline{Q}} \cdot \tilde{\underline{H}} \cdot \underline{\underline{Q}}^T. \tag{4.12}$$

With this hypothesis, a frame indifferent closure model is proposed for  $\underline{\underline{H}}$ . Thus, an APS-closure theory combines the pre-closure equation for the Reynolds stress (see Eqs. (4.1)

and (4.7)) and the following linear relaxation model for the anisotropic pre-stress

$$\frac{\tilde{H}}{H} + \lambda \left[ \underline{\dot{M}} - \frac{1}{3} \left( \underline{I} : \underline{\dot{M}} \right) \underline{I} \right] = \beta \langle \underline{S} \rangle. \tag{4.13}$$

For large turbulence Reynolds numbers, the phenomenological parameters  $\lambda$  and  $\beta$  are assumed to scale with k and  $\epsilon$ :

$$\lambda = C_{\lambda} \frac{k}{\varepsilon} , \qquad (4.14)$$

and

$$\beta = 2kC_{\beta} \frac{k}{\varepsilon} \quad . \tag{4.15}$$

 $C_{\beta}$  and  $C_{\lambda}$  are universal model coefficients. In the above equation, the mean strain rate dyadic  $\langle \underline{S} \rangle$  is defined by

$$2\langle \underline{S} \rangle = \nabla \langle \underline{u} \rangle + (\nabla \langle \underline{u} \rangle)^T, \tag{4.16}$$

and the mean vorticity dyadic  $\langle w \rangle$  is defined by

$$2\langle W \rangle = \nabla \langle u \rangle - (\nabla \langle u \rangle)^{T}. \tag{4.17}$$

 $\langle \underline{W} \rangle$  can also be written as

$$\langle \underline{W} \rangle = \underline{\varepsilon} \cdot \langle \underline{w} \rangle , \qquad (4.18)$$

where  $\langle \underline{w} \rangle$  is the mean vorticity,  $\langle \underline{w} \rangle = \nabla \times \langle \underline{u} \rangle$ , and  $\underline{\varepsilon}$  is the permutation triadic.

<u>M</u> is an *objective* time derivative defined by (see Joseph, 1990; Denn, 1990; Bird et al., 1977; and Appendix D):

$$\underline{\dot{M}}(\tilde{H}) = \frac{\partial}{\partial t}(\tilde{H}) + \langle \underline{u} \rangle \cdot \nabla \tilde{H} - \langle \underline{W} \rangle^{T} \cdot \tilde{H} - \tilde{H} \cdot \langle \underline{W} \rangle - a \left[ \langle \underline{S} \rangle \cdot \tilde{H} + \tilde{H} \cdot \langle \underline{S} \rangle \right]. \tag{4.19}$$

With a=0, Eq. (4.19) reduces to the corotational Jaumann derivative. For a=1 and a=-1, Eq. (4.19) yields the upper and lower convected derivatives of Oldroyd, respectively. Appendix D demonstrates that the operator  $\dot{\underline{M}}(\tilde{H})$  is objective for  $-\infty < a < +\infty$ . Physically, the Jaumann derivative represents the temporal changes in the pre-stress relative to a frame of reference moving with the local mean velocity and rotating with an angular velocity equal to the mean vorticity. Note that Eqs. (4.13) and (4.19) maintain the symmetry and the contraction properties of the anisotropic pre-stress, i.e.,

$$\tilde{H} = \tilde{H}^{T} \quad \text{and} \quad I: \tilde{H} = 0. \tag{4.20}$$

# 4.3 Anisotropic Homogeneous Decay

For homogeneous turbulence with no mean shear, the anisotropic pre-stress  $\underline{\underline{H}}$  equals the anisotropic stress  $2k\underline{b}$  and Eqs. (4.1), (4.8), and (4.13) imply that

$$\langle \underline{u}'\underline{u}' \rangle = \frac{2k}{3} I + \tilde{H} \tag{4.21}$$

and

$$\frac{\tilde{H}}{L} + C_{\lambda} \frac{k}{\varepsilon} \frac{d}{dt} (\frac{\tilde{H}}{L}) = 0. \tag{4.22}$$

For this flow, the kinetic energy is governed by the following equation (see Eq. (2.2))

$$\frac{1}{k}\frac{dk}{dt} = -\frac{\varepsilon}{k} \ . \tag{4.23}$$

For anisotropic homogeneous decay, the relaxation coefficient  $C_{\lambda}$  associated with the anisotropic pre-stress can be estimated from return-to-isotropy data (Choi, 1983; Choi and Lumley, 1984; and, LePenven, et al., 1985). With  $\frac{\tilde{H}}{L} = 2kH$ , it follows from Eq. (4.22) that

$$\frac{k}{\varepsilon} \frac{d}{dt} \begin{pmatrix} H \end{pmatrix} = -\frac{(1 - C_{\lambda})}{C_{\lambda}} H. \tag{4.24}$$

Eq. (4.24) shows that the pre-stress returns to an isotropic state provided  $C_{\lambda} < 1$ . For homogeneous, shear-free flows, the anisotropic pre-stress  $\underline{H}$  is equivalent to the anisotropic stress  $\underline{b}$ :

$$H = b = \frac{\langle \underline{u}'\underline{u}' \rangle}{2k} - \frac{1}{3!}. \tag{4.25}$$

With the second invariant of the anisotropy tensor defined as

$$II = tr(\underline{b} \cdot \underline{b}), \tag{4.26}$$

it follows directly from Eqs. (4.24) and (4.25) that

$$\frac{k d(II)}{\varepsilon dt} = -\frac{2(1-C_{\lambda})}{C_{\lambda}}II. \tag{4.27}$$

Combining Eqs. (4.23) and (4.27) yields

$$\frac{d(II)}{dk} = \frac{2(1-C_{\lambda})}{C_{\lambda}} \frac{II}{k}.$$
 (4.28)

If  $C_{\lambda}$  is taken to be a constant, it then follows from Eq. (4.28) that

$$II = II_o \left(\frac{k}{k_o}\right)^n,\tag{4.29}$$

where

$$n = \frac{2\left(1 - C_{\lambda}\right)}{C_{\lambda}}.\tag{4.30}$$

Eq. (4.29) provides a convenient means for comparing the above theory with return-to-isotropy data. In Eq. (4.29),  $k_o$  and  $II_o$  are reference values taken as the first data point for which the gradient of the mean field has been effectively removed. Figure 4.1 shows the return-to-isotropy data of Choi and Lumley [1984] and of LePenven et al. [1985], which are summarized in Tables E.11-E13 of Appendix E. In Figure 4.1, only data with a positive third invariant (III > 0) are chosen, as they more closely represent the homogeneous shear flow of interest. In order to model  $C_{\lambda}$  for a wider class of flows (Issue (v) in Section 1.2),  $C_{\lambda}$  could be viewed as a universal function of the invariants II and III (cf. Sarkar and Speziale, 1990 and Lumley, 1978). However, in this work,  $C_{\lambda}$  is assumed to be a constant.

The solid line in Figure 4.1 indicates the trajectory of the linear APS-theory in the II/k phase plane for  $C_{\lambda} = 2/3$  (i.e. n = 1). It is apparent from Figure 4.1 that most of the long time decay data are consistent with a decay exponent of unity. The long time data may deviate from the solid line due to the fact that the initial reference state is not truly homogeneous and/or shear free. The data in Figure 4.1 can also be correlated by using a phenomenological closure model which assumes that the pressure-strain rate correlation in the second-order moment equation for the Reynolds stress is proportional to the anisotropic stress (Launder et al., 1975),

$$\frac{\langle p'\underline{S'}\rangle}{\rho} = -2kC_1 \frac{b}{e} \frac{\varepsilon}{k}. \tag{4.31}$$

The phenomenological coefficient  $C_1$  is often referred to as the Rotta constant. A value of  $C_{\lambda} = 2/3$  in the APS-theory is equivalent to  $C_1 = 3$  (cf. Speziale, 1991).

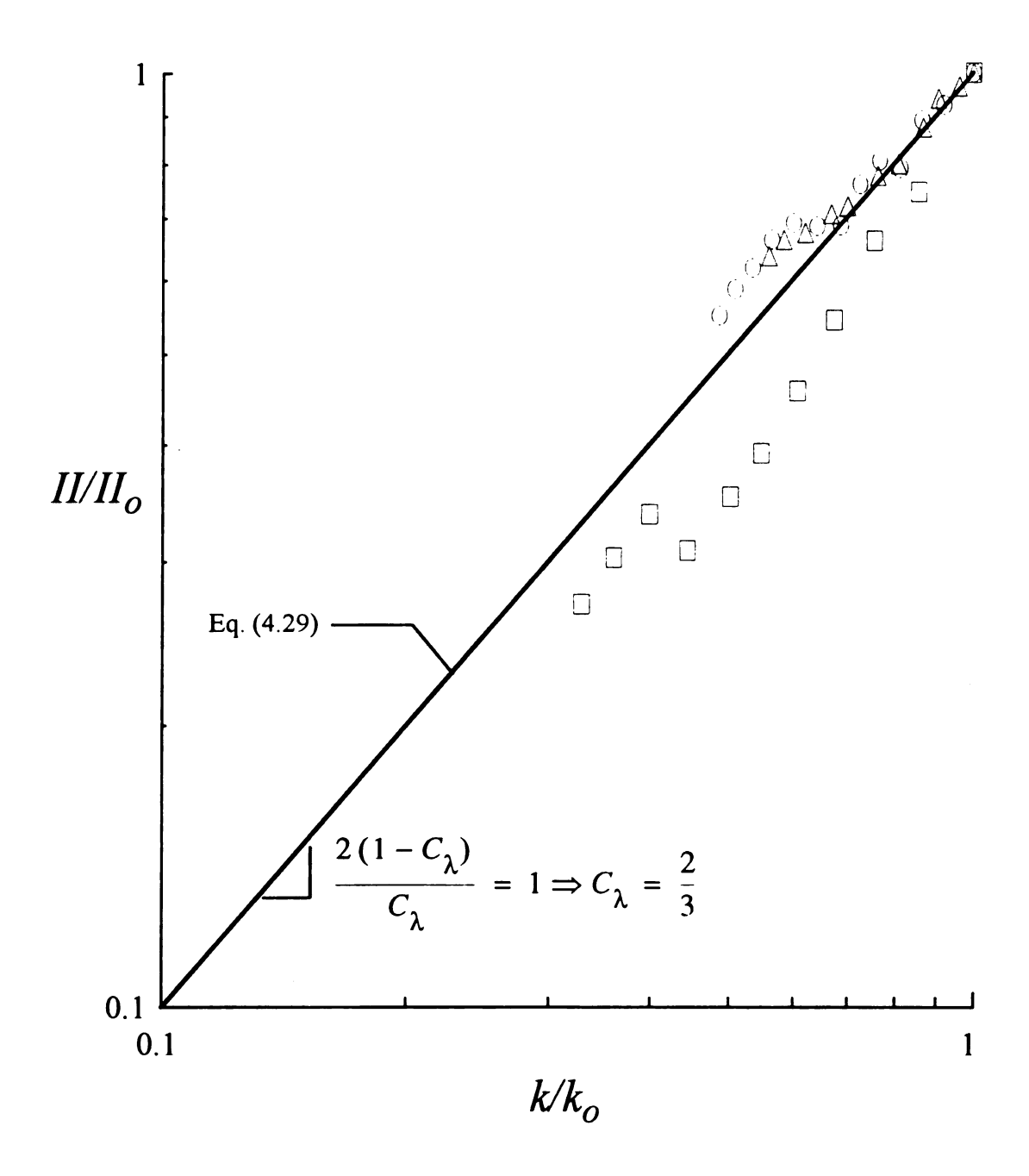


Figure 4.1 Relaxation to Isotropic Homogeneous Decay ( — APS-theory; □ Choi and Lumley, 1984 (plane distortion); O Choi and Lumley, 1984 (axisymmetric expansion); Δ LePenven et al., 1985 (III > 0))

# 4.4 Homogeneously Sheared Turbulence

For homogeneously sheared turbulence,

$$\nabla \langle \underline{u} \rangle = \frac{d\langle u_z \rangle}{dy} \underbrace{e}_{y-z} \underbrace{e}_{y-z}, \tag{4.32}$$

and

$$R = \frac{\langle u'u' \rangle}{2k} = R_{xx-x-x} + R_{yy-y-y} + R_{zz-z-z} + R_{yz-y-z} + R_{zy-z-y}. \tag{4.33}$$

The pre-closure theory (see Eqs. (4.1), (4.2), (4.7), and (4.8)) applied to homogeneous shear yields the following relationships between the components of the Reynolds stress and the components of the pre-stress:

$$R_{xx} = \frac{1}{3} \frac{\alpha}{k} + H_{xx} , \qquad (4.34)$$

$$R_{yy} = \frac{1}{3} \frac{\alpha}{k} + H_{yy} , \qquad (4.35)$$

$$R_{zz} = 1 - \frac{2}{3} \frac{\alpha}{k} + H_{zz}, \tag{4.36}$$

and

$$R_{yz} = -N_R R_{yy} + H_{yz}. (4.37)$$

In Chapter 3, the above set of equations were examined for the special case  $\underline{\underline{H}} = \underline{\underline{0}}$  (IPS-theory). Eqs. (4.35) and (4.36) imply that the first normal stress difference is given by

$$R_{zz} - R_{yy} = 1 - \frac{\alpha}{k} + H_{zz} - H_{yy}. \tag{4.38}$$

The second normal stress difference follows by subtracting Eq. (4.34) from Eq. (4.35):

$$R_{yy} - R_{xx} = H_{yy} - H_{xx} \quad . \tag{4.39}$$

Eq. (4.39) shows that, if  $R_{yy} - R_{xx} \neq 0$ , then the pre-stress must have an anisotropic component which has a second normal pre-stress difference. Eq. (4.38), however, shows that the isotropic portion of the pre-stress causes a primary normal stress difference in the Reynolds stress even if the anisotropic part of the pre-stress is zero. Thus, as previously noted by Parks *et al.* [1997] (also see Chapter 3), the primary role of the isotropic pre-stress is to redistribute the kinetic energy of turbulent fluctuations among the velocity components subject to the normalization requirement that tr(R) = 1. For homogeneous shear, Eq. (4.8) reduces to

$$\frac{\alpha}{k} = 1 + 2N_R R_{yz} + N_R^2 R_{yy} , \qquad (4.40)$$

where

$$N_R \equiv \tau_R S = C_R \frac{Sk}{\varepsilon} . \tag{4.41}$$

The phenomenological role of the isotropic pre-stress is clearly indicated by Eqs. (4.34)-(4.36). On the other hand, the underlying statistical aspects of the flow which cause  $\alpha$  are expressed in Eq. (4.40) and the contraction of Eq. (4.6).

The APS-theory presented here assumes that the anisotropic pre-stress is governed by the phenomenological model given by Eq. (4.13). With  $\frac{\tilde{H}}{\tilde{H}} = 2kH$ , Eq. (4.13) can be written in dimensionless form as

$$(1+q)\underline{H} + \lambda \left[\underline{\dot{M}} - \frac{1}{3}(\underline{I}:\underline{\dot{M}})\underline{I}\right] = \beta \langle \underline{S} \rangle, \tag{4.42}$$

where the temporal operator  $\underline{\underline{M}}$  is defined by Eq. (4.19) with  $\underline{\underline{H}}$  replaced by  $\underline{\underline{H}}$ . In the above equation,

$$q = \lambda \frac{1}{k} \frac{Dk}{Dt} \quad . \tag{4.43}$$

and

$$\frac{Dk}{Dt} = \frac{\partial k}{\partial t} + \langle \underline{u} \rangle \cdot \nabla k . \tag{4.44}$$

For homogeneous shear, the normal components of the anisotropic pre-stress satisfy the following set of ordinary differential equations

$$De_{t}\frac{dH_{xx}}{d\xi} + (1+q)H_{xx} - \frac{2}{3}aDe_{t}H_{yz} = 0, \qquad (4.45)$$

$$De_{t}\frac{dH_{yy}}{d\xi} + (1+q)H_{yy} + \left(\frac{a}{3} + 1\right)De_{t}H_{yz} = 0, \qquad (4.46)$$

and

$$De_{t}\frac{dH_{zz}}{d\xi} + (1+q)H_{zz} + \left(\frac{a}{3} - 1\right)De_{t}H_{yz} = 0.$$
 (4.47)

Note that the sum of Eqs. (4.45)-(4.47) preserves the anisotropy property,  $tr(\underline{H}) = 0$ . In the above equations, the dimensionless development time is defined as

$$\xi = zS/\langle u_z \rangle(0) . \tag{4.48}$$

The turbulent Deborah number  $De_t$  introduced in the dimensionless formulation

compares the phenomenological relaxation time for the anisotropic pre-stress with the characteristic time of the mean field:

$$De_t = \lambda S = C_\lambda \frac{kS}{\varepsilon} . {4.49}$$

The parameter q (see Eq. (4.43)) compares the characteristic relaxation time for the anisotropic pre-stress with the characteristic turnover time of the turbulent kinetic energy.

The off-diagonal components of the anisotropic stress satisfy the following ordinary differential equations

$$De_{t}\frac{dH_{xy}}{d\xi} + (1+q)H_{xy} = 0, (4.50)$$

$$De_{t}\frac{dH_{xz}}{d\xi} + (1+q)H_{xz} = 0, (4.51)$$

and

$$De_{t}\frac{dH_{yz}}{d\xi} + (1+q)H_{yz} + \frac{De_{t}}{2}(H_{zz} - H_{yy}) + \frac{aDe_{t}}{2}(H_{zz} + H_{yy}) = \frac{1}{2}C_{\beta}\frac{kS}{\epsilon}. \quad (4.52)$$

# 4.5 Asymptotic Homogeneous Shear

As the dimensionless development time increases, the above set of equations predict the existence of an asymptotic state provided

$$\lim_{\xi \to \infty} \frac{kS}{\varepsilon} = \left(\frac{kS}{\varepsilon}\right)_a < \infty . \tag{4.53}$$

Thus, with  $q \to q^a < \infty$ ,  $De_t \to De_t^a < \infty$ , and  $(kS/\epsilon)_a < \infty$ , the above set of equations imply that (see Appendix G)  $H_{xy}^a = 0$ ,  $H_{xz}^a = 0$ ,

$$H_{xx}^{a} = \frac{2a}{3} \frac{De_{t}^{a} H_{yz}^{a}}{1 + q^{a}}, \tag{4.54}$$

$$H_{yy}^{a} = -\left(1 + \frac{a}{3}\right) \frac{De_{t}^{a} H_{yz}^{a}}{1 + q^{a}},$$
(4.55)

$$H_{zz}^{a} = \left(1 - \frac{a}{3}\right) \frac{De_{t}^{a} H_{yz}^{a}}{1 + q^{a}},$$
(4.56)

and

$$H_{yz}^{a} = \frac{C_{\beta}}{2C_{\lambda}} \frac{(1+q^{a})De_{t}^{a}}{(1+q^{a})^{2} + (De_{t}^{a})^{2}(1-a^{2}/3)}.$$
 (4.57)

It follows from Eq. (4.43) and (4.9) that

$$q \equiv \lambda \frac{1}{k} \frac{Dk}{Dt} = C_{\lambda} (P - 1), \qquad (4.58)$$

where P represents the ratio of production to dissipation of turbulent kinetic energy:

$$\varrho = \frac{-\langle u'_y u'_z \rangle S}{\varepsilon}.$$
(4.59)

Eqs. (4.9) and (4.10) imply that

$$\lim_{\xi \to \infty} \rho = \rho^a = \frac{C_D - 1}{C_P - 1}.$$
 (4.60)

Thus, the asymptotic value of q can be related to the model parameters in the  $\varepsilon$ -equation and to the relaxation coefficient  $C_{\lambda}$ :

$$\lim_{\xi \to \infty} q = q^a = \frac{C_{\lambda} (C_D - C_P)}{C_P - 1} . \tag{4.61}$$

It follows directly from Eqs. (4.54), (4.55), and (4.57) that a negative second normal stress difference develops for the APS-theory provided  $C_{\beta}C_{\lambda} > 0$  (assuming  $-\sqrt{3} < a < 1$ ) inasmuch as

$$R_{yy}^{a} - R_{xx}^{a} = H_{yy}^{a} - H_{xx}^{a} = -(1-a)\frac{De_{t}^{a}}{1+q^{a}}H_{yz}^{a} = \frac{-(1-a)}{2}\frac{C_{\beta}C_{\lambda}}{(1+q^{a})^{2} + (De_{s}^{a})^{2}(1-a^{2}/3)}\left(\frac{Sk}{\varepsilon}\right)_{a}^{2}. \quad (4.62)$$

The APS-theory at large turbulent Reynolds numbers contains six phenomenological coefficients:  $C_D$ ,  $C_P$ ,  $C_R$ ,  $C_{\beta}$ ,  $C_{\lambda}$ , and a. Isotropic, homogeneous decay requires  $C_D = 1.83$  (see Chapter 2). Anisotropic, homogeneous decay (i.e. return-to-isotropy) requires  $C_{\lambda} = 2/3$  (see Figure 1).

The statistical properties of asymptotic homogeneous shear measured by Tavoularis and Karnik [1989] can be used to estimate  $C_P$ ,  $C_R$ ,  $C_\beta$ , and a. For instance, as  $\xi \to \infty$ ,

$$\left(\frac{kS}{\varepsilon}\right)_a = 4.16,\tag{4.63}$$

and

$$R_{yy}^a - R_{xx}^a = -0.040. (4.64)$$

The invariants II and III associated with the anisotropic stress b = b have also been measured. These parameters are given by (also see Eq.(4.30)):

$$II = tr(\underline{b} \cdot \underline{b}) \tag{4.65}$$

and

$$III = tr(\underline{b} \cdot \underline{b} \cdot \underline{b}). \tag{4.66}$$

For  $\xi \to \infty$ , the data of Tavoularis and Karnik [1989] imply that  $II_a^e = 0.138$  and  $III_a^e = 0.0174$ .

The existence condition for an asymptotic solution (see Eq. (4.60)) can be rewritten as

$$-2R_{yz}^{a}\left(\frac{kS}{\varepsilon}\right)_{a} = \frac{C_{D}-1}{C_{P}-1}.$$
(4.67)

A consistent set of model parameters ( $C_P$ ,  $C_R$ ,  $C_\beta$ , a) can be identified for which Eqs. (4.38), (4.63), (4.64), and (4.67) are satisfied exactly and which also exactly reproduces the experimental values for the asymptotic normalized Reynolds stress components. It is found that  $C_P = 1.60$ ,  $C_R = 0.271$ ,  $C_\beta = 0.174$ , and a = -2/3. Table 4.1 summarizes these parameters

### 4.6 Transition States for Homogeneously Sheared Turbulence

The component equations for the anisotropic pre-stress depend on the development of the time scale  $k/\epsilon$ . Because the mean strain rate is constant (S is a constant) the k- and  $\epsilon$ -equations can be combined into a single equation for the dimensionless relaxation group (see Eq. (3.52)):

$$\frac{dN_R}{d\xi} = 2N_R R_{yz} (C_P - 1) + C_R (C_D - 1), \tag{4.68}$$

where  $N_R = C_R Sk/\epsilon$ . The development of the Reynolds stress towards an asymptotic state can be calculated by solving Eq. (4.68) along with Eqs. (4.45)-(4.47) and (4.50)-(4.52). The transient calculations assume that an initially isotropic, homogeneous

Table 4.1: Parameter Estimates for the APS-Theory

Parameter	Estimate	Basis
$C_D$	1.83	Isotropic Decay (Comte-Bellot and Corrsin, 1971; Mansour and Wray, 1994; see Chapter 2)
$C_P$	1.60	Existence condition for k-\varepsilon equations
$C_R$	0.271	Reproduction of asymptotic state for homogeneous shear (Tavoularis and Karnik, 1989)
C <sub>β</sub>	0.174	
а	-2/3	
$C_{\lambda}$	2/3	Return to isotropy data (III > 0; Choi and Lumley, 1983; LePenven et al., 1985)

turbulence is subjected to an instantaneous increase in the mean shear. Therefore,

$$N_R = \begin{cases} 0 & \text{for } \xi < 0 \\ N_R^o & \text{for } \xi = 0. \end{cases}$$

$$(4.69)$$

Because  $N_R = 0$  for  $\xi < 0$ , the Reynolds stress and the pre-stress are isotropic; however, once  $N_R = N_R^o$ , the Reynolds stress and the *isotropic* part of the pre-stress respond instantaneously and attain a state consistent with the IPS-theory:

$$R = \begin{cases} \frac{1}{3}I & \text{for } \xi < 0\\ R^o & \text{for } \xi = 0, \end{cases}$$

$$(4.70)$$

where  $\underline{R}^o$  is the normalized IPS-Reynolds stress for  $N_R^o > 0$  and  $\underline{H}^o = 0$ . Thus  $\underline{R}^o$  satisfies

$$\underline{A}_{=o}^{T} \cdot \underline{R}^{o} \cdot \underline{A}_{=o} = \frac{1}{3} \frac{\alpha_{o}}{k} \underline{I}.$$
(4.71)

The operator  $A_{R}$  is defined by Eq. (4.2) with  $N_{R} = N_{R}^{o}$ . Thus, Eq. (4.70) defines the initial state of turbulence for which the pre-stress is isotropic and the Reynolds stress has a degree of anisotropy commensurate with the initial relaxation parameter  $N_{R}^{o}$ . Because  $H^{o} = 0$ , it follows from Eqs. (4.50) and (4.51) that  $H_{xy} = 0$ , and  $H_{xz} = 0$  for  $\xi > 0$ . The transient behavior of the components of the anisotropic pre-stress together with the relaxation group  $N_{R}$  were determined by numerical integration using a fourth-order Runge-Kutta integration algorithm (Carnahan, et al., 1969; see also Appendix H).

Figure 4.2 shows the transient response of the relaxation parameter  $N_R$  as a function of its initial value (with  $0 < N_R^o < 10$ ). Unlike the IPS-theory, the approach to the asymptote is not necessarily monotonic; as the turbulence nears the asymptotic state, oscillation in

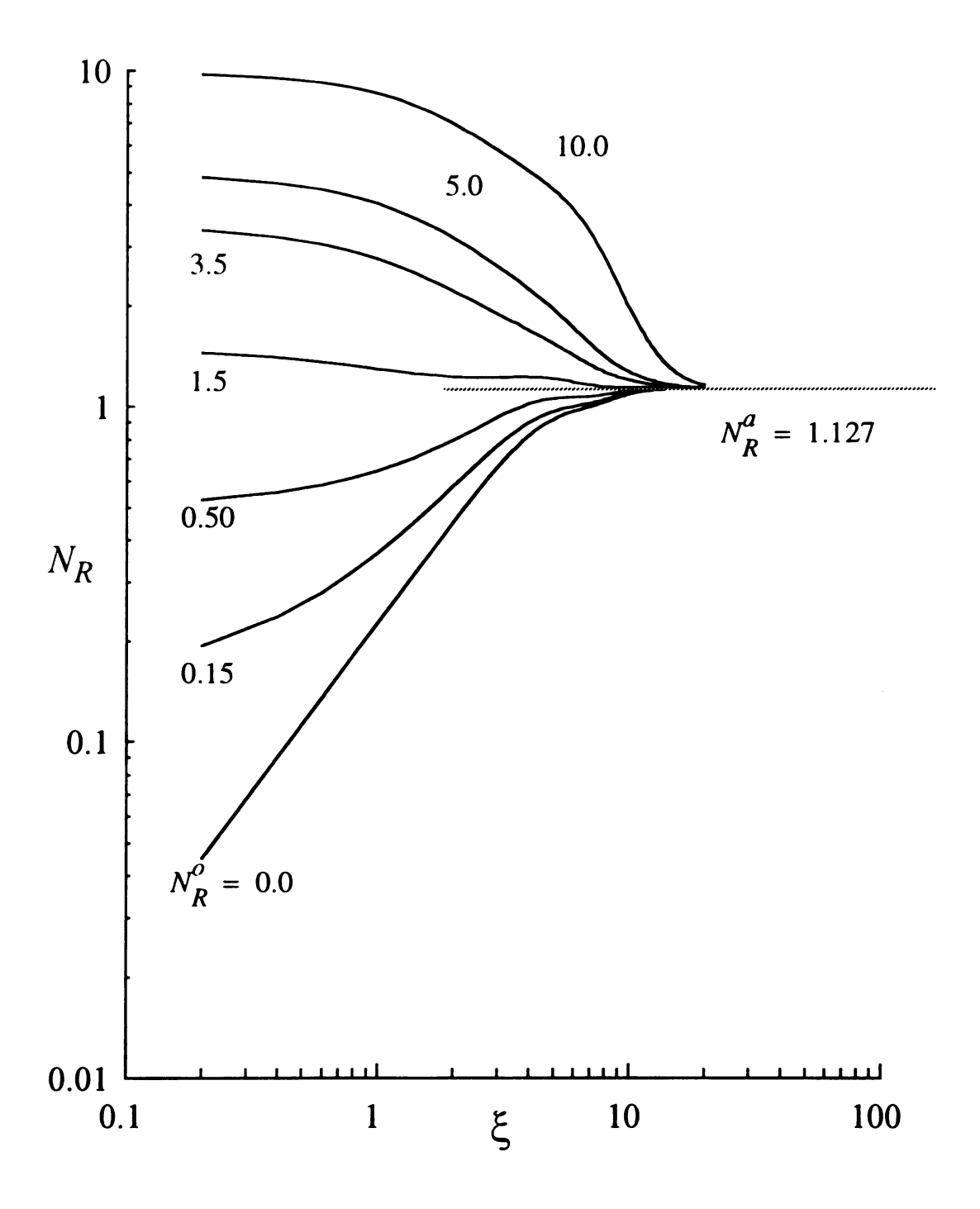


Figure 4.2 The Effect of the Development Time on the Relaxation Group for Homogeneously Sheared Turbulence

the Reynolds stress components (cf. Figures 4.3 and 4.4) can cause the first term on the right-hand-side of Eq. (4.68) to generate oscillations in  $dN_R/d\xi$ . Approximately ten developmental time units are required to reach the asymptote, with more being required for larger values of  $N_R^o$ .

Figures 4.3 and 4.4 present the transient development of the turbulence from an initial state characterized by  $N_R^o = 0.7$ . This initial value of  $N_R$  is selected to closely represent initial states (in terms of the invariant pair (II, III)) from the experimental data. These figures present the individual components of the normalized Reynolds stress and the anisotropic pre-stress, respectively. The development times are on the order of ten to twenty units. Compared to the IPS-theory, the salient difference is an exact representation of the asymptotic values of the Reynolds stress through a non-zero secondary normal stress difference.

From Eqs. (4.34)-(4.37), it is apparent that oscillations in transient development of the Reynolds stress components are directly related to similar oscillations in the components of the pre-stress anisotropy H. As such, it is instructive to investigate the equations governing the transient behavior of the anisotropic pre-stress as well as the individual terms which contribute its transient evolution. Eqs. (4.52) and (4.47) may be recast as the following by dividing each term by  $De_r$ :

$$\frac{dH_{yz}}{d\xi} = \frac{1}{2} \frac{C_{\beta}}{C_{\lambda}} - \frac{(1+q)}{De_t} H_{yz} - \frac{1}{2} (H_{zz} - H_{yy}) - \frac{a}{2} (H_{zz} + H_{yy})$$
(4.72)

and

$$\frac{dH_{zz}}{d\xi} = -\frac{(1+q)}{De_{\star}}H_{zz} - \left(\frac{a}{3} - 1\right)H_{yz}.$$
 (4.73)

Figures 4.5 and 4.6 show the contributions to the development of  $dH_{yz}/d\xi$  and  $dH_{zz}/d\xi$ , respectively, for the simulation shown in Figure 4.4. In Figures 4.5 and 4.6, the solid line represents the net time derivative and the thin lines represent the individual contributions to the net time derivative. From Eq. (4.72), it is evident that an initially

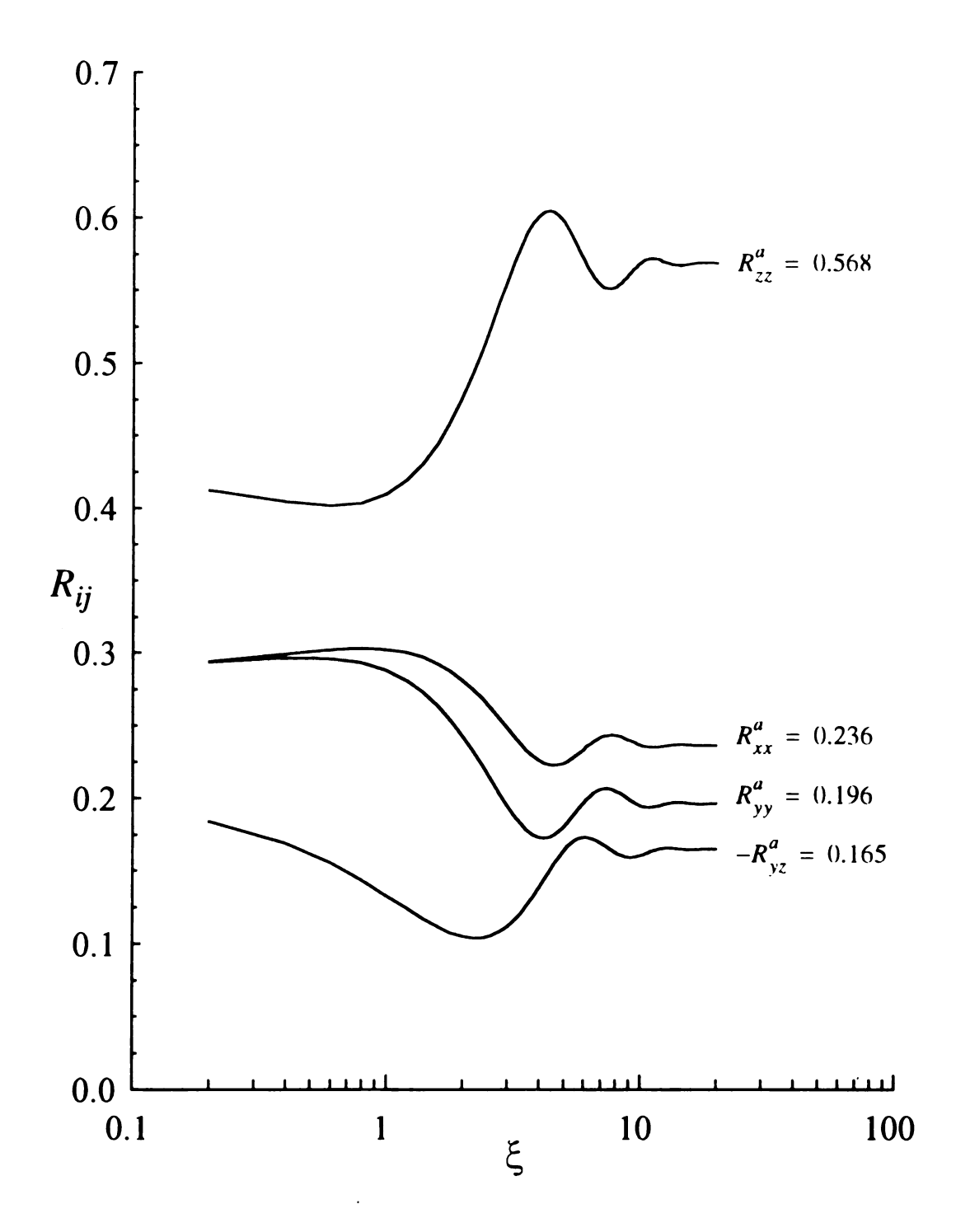


Figure 4.3 Transient Response of Isotropic Turbulence to a Sudden Increase in the Mean Strain Rate ( $N_R^o = 0.7$ ): Components of the Normalized Reynolds Stress

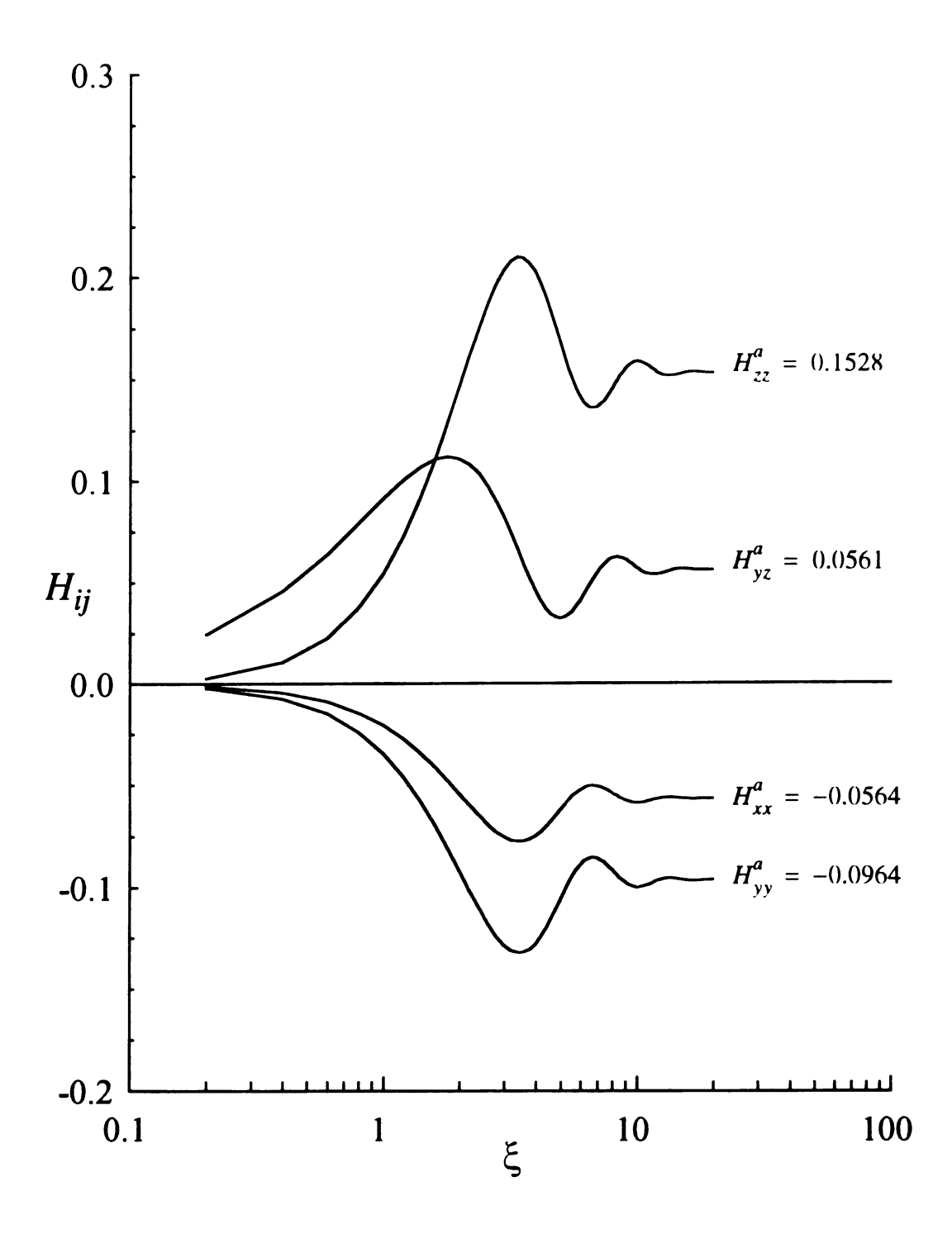


Figure 4.4 Transient Response of Isotropic Turbulence to a Sudden Increase in the Mean Strain Rate ( $N_R^o = 0.7$ ): Components of the Anisotropic Pre-Stress.

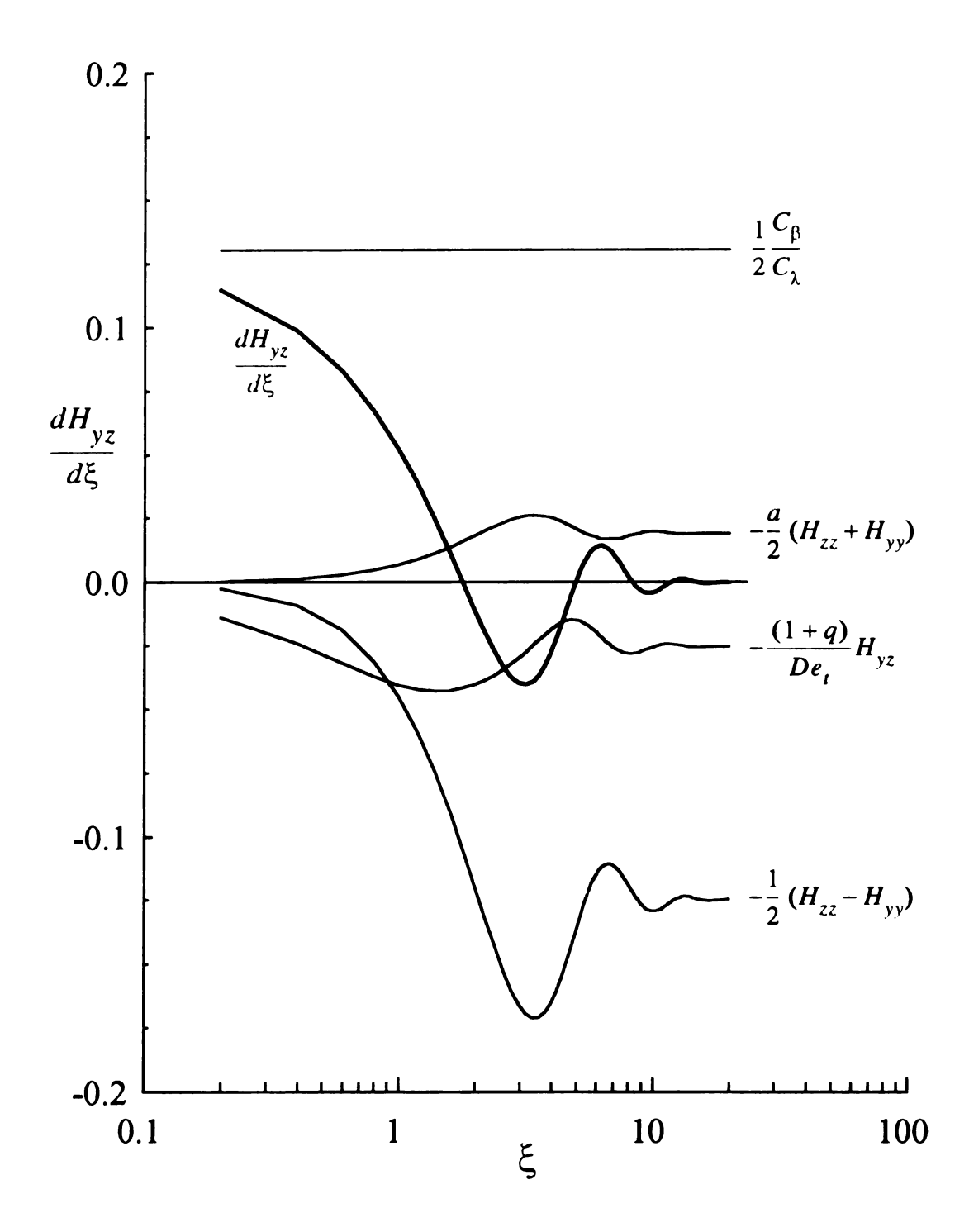


Figure 4.5 Transient Response of Isotropic Turbulence to a Sudden Increase in the Mean Strain Rate  $(N_R^o = 0.7)$ :  $dH_{yz}/d\xi$ .

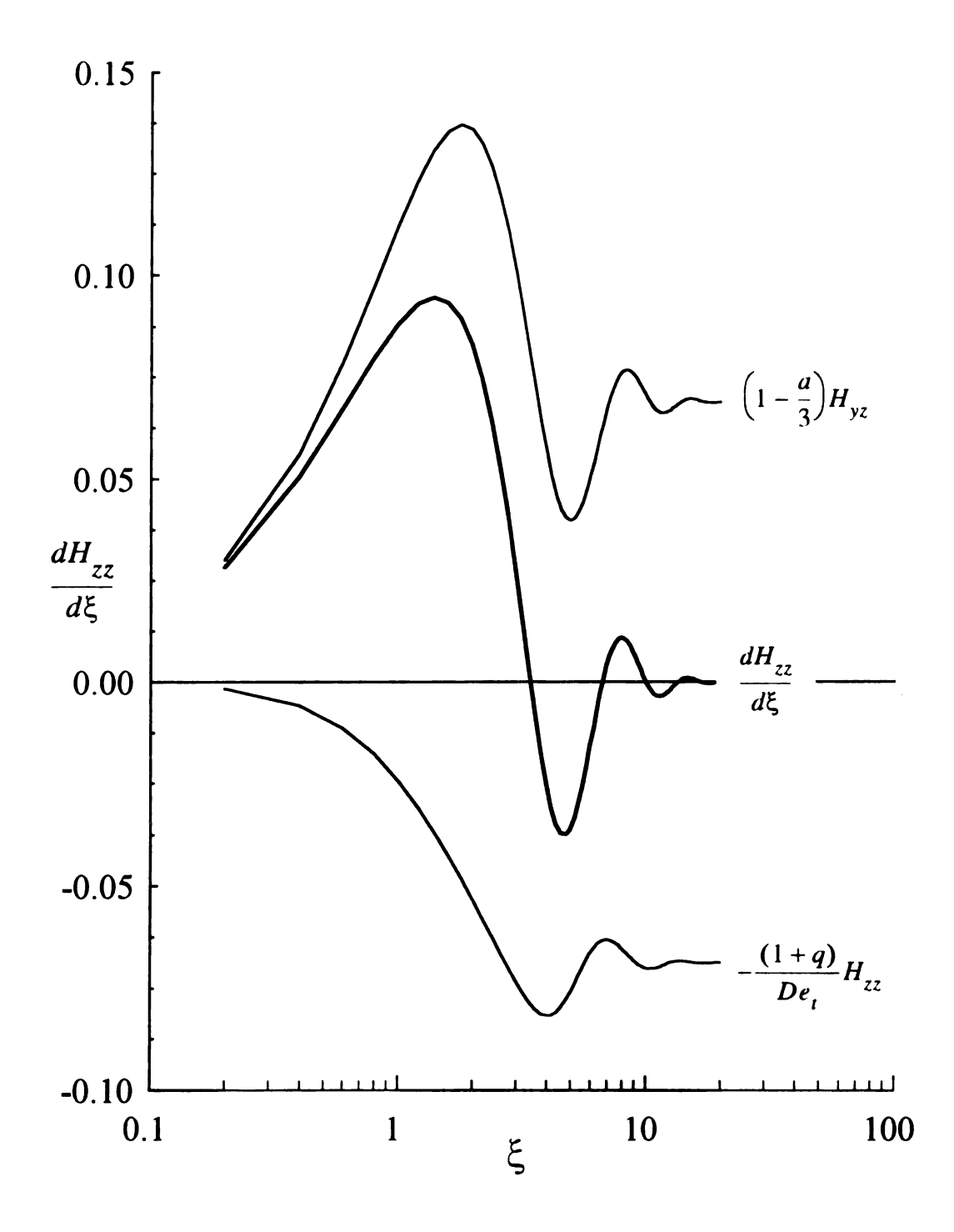


Figure 4.6 Transient Response of Isotropic Turbulence to a Sudden Increase in the Mean Strain Rate  $(N_R^o = 0.7)$ :  $dH_{zz}/d\xi$ .

isotropic turbulence (i.e. H = 0) would remain isotropic in the absence of the linear strain-coupling coefficient ( $C_{\beta}$ ) and the linear relaxation coefficient ( $C_{\lambda}$ ). Since both of these coefficients are modeled as constants, the term  $\frac{1}{2}C_{\beta}/C_{\lambda}$  provides a constant source of anisotropy in the pre-stress, causing the shear component of H to develop more rapidly than the normal components (cf. Figure 4.4). Once a significant component  $H_{yz}$  has developed, it serves as a means to develop normal pre-stress anisotropies (cf. Eqs. (4.45)-(4.47)). From Figure 4.5, it is seen that, once appreciable normal pre-stress anisotropies have been developed, they serve to balance the anisotropy source term  $\frac{1}{2}C_{\beta}/C_{\lambda}$  for the component  $H_{yz}$ . For the normal pre-stress anisotropies, the ultimate asymptotic value obtained represents a balance between a growth term (proportional to  $H_{yz}$ ) and an exponential decay term (proportional to the component itself). Figure 4.6 shows this representative behavior for the component  $H_{zz}$ .

The source of the oscillations may be determined by investigating the governing equations for the anisotropic pre-stress components in the following matrix form:

$$\underline{h}' = \underline{B} \cdot \underline{h} + \underline{b}, \tag{4.74}$$

where the tensors and vectors in Eq. (4.74) are defined as follows:

$$\underline{h}' \equiv \begin{bmatrix} dH_{yy}/d\xi \\ dH_{zz}/d\xi \\ dH_{yz}/d\xi \end{bmatrix}, \tag{4.75}$$

$$\underline{h} \equiv \begin{bmatrix} H_{yy} \\ H_{zz} \\ H_{yz} \end{bmatrix},$$
(4.76)

$$\underline{b} \equiv \begin{bmatrix} 0 \\ 0 \\ \frac{1}{2}C_{\beta}/C_{\lambda} \end{bmatrix}, \tag{4.77}$$

and  $B = \begin{bmatrix}
\alpha & 0 & -\frac{a}{3} - 1 \\
0 & \alpha & -\frac{a}{3} + 1 \\
-\frac{a+1}{2} & -\frac{a-1}{2} & \alpha
\end{bmatrix}.$ (4.78)

In Eq. (4.78), a is the parameter associated with the convected time derivative (see Eq. (4.19)) and  $\alpha$  denotes the term  $-(1+q)/De_t$ . Note that the component  $H_{xx}$  does not appear in the above equations as it is not independent (due to the anisotropic pre-stress being traceless) and has been eliminated from the system of equations.

With the system of equations expressed in the form given by Eq. (4.74), the solution to the characteristic equation for the matrix  $\underline{B}$  yields the eigen values of  $\underline{B}$ . Positive eigenvalues indicate that the asymptotic solution to Eq. (4.74) is not stable, while the reverse is true for negative eigenvalues. In the event of imaginary eigenvalues, the solution exhibits oscillatory behavior (Carnahan *et al.*, 1969). The characteristic equation for the matrix  $\underline{B}$  is:

$$det(\underline{B} - \lambda \underline{I}) = 0. (4.79)$$

Eqs. (4.78) and (4.79) yield the following cubic equation:

$$(\alpha - \lambda) [(\alpha - \lambda)^2 - \phi(a)] = 0, \tag{4.80}$$

where the parameter  $\phi(a)$  denotes the following collection of terms

$$\phi(a) = \left(\frac{a}{3} - 1\right) \left(\frac{a+1}{2}\right) + \left(\frac{a}{3} + 1\right) \left(\frac{a-1}{2}\right). \tag{4.81}$$

By inspection, the roots to Eq. (4.80) are

$$\lambda_1 = \alpha$$

$$\lambda_2 = \alpha - \sqrt{\phi} .$$

$$\lambda_3 = \alpha + \sqrt{\phi}$$
(4.82)

Since  $\alpha < 0$  (i.e. q > -1) for all points during the transient simulation, this represents a contribution to a stable asymptotic state. For  $-\sqrt{3} < a < \sqrt{3}$ ,  $\phi(a) < 0$ , meaning that  $\lambda_2$  and  $\lambda_3$  are a complex conjugate pair, as the value for a selected in these simulations is -2/3. Thus, since the real parts of the eigenvalues are all negative, the asymptotic state is stable. However, since two of the eigenvalues have non-zero imaginary parts, the approach to the asymptote will exhibit oscillations.

The isotropic and anisotropic parts of the pre-stress represent two different responses of the turbulence to an external force. The isotropic portion of the pre-stress causes an instantaneous response to a mean shear, immediately reorganizing the Reynolds stress to an anisotropic state. Subsequently, the components of the anisotropic pre-stress relax towards their asymptotic values as illustrated on the invariant phase plane by Figure 4.7 and on the  $\Delta$ -hyperplane by Figure 4.8. On a very short timescale, the turbulence relaxes towards the isotropic state, but then reverses direction and approaches the asymptote. As it nears the asymptote, the oscillations in the components of the pre-stress (see Figure 4.4) result in the two trajectories in Figures 4.7 and 4.8 approaching the asymptote in a contracting orbit.

## 4.7 Conclusions

The presented anisotropic closure for the pre-stress extends the predictive capabilities of the IPS-theory for the case of homogeneous shear due to the interaction of a linear dependence on the mean strain rate and a frame invariant relaxation effect. Both effects are required to generate a non-zero second normal stress difference as well as an improved primary normal stress difference. The fact that experimentally observed values of the

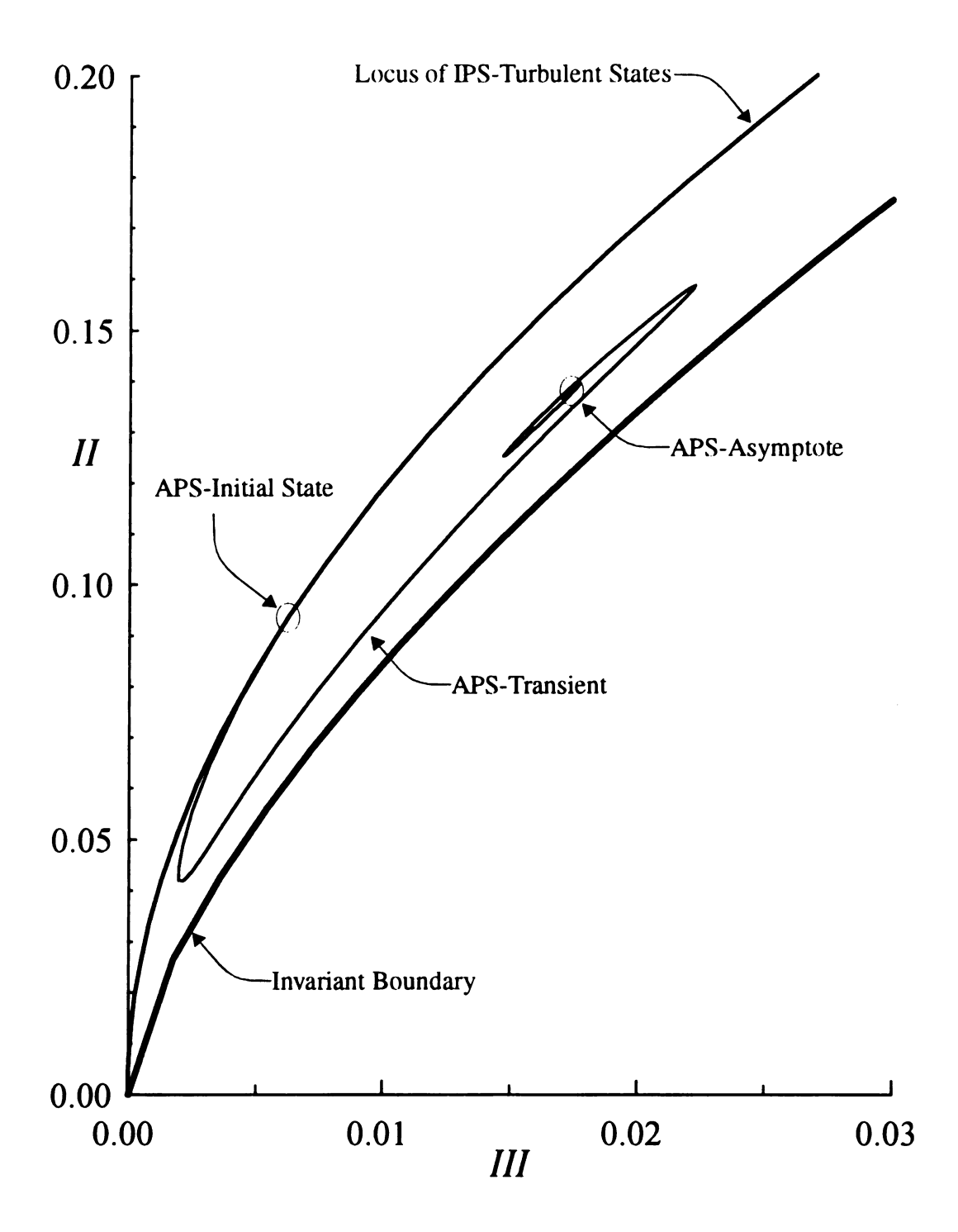


Figure 4.7 Transient response of Isotropic Turbulence to a Sudden Increase in the Mean Strain Rate ( $N_R^o = 0.7$ ): Anisotropy Invariants

Transient response of Isotropic Turbulence to a Sudden Increase in the Mean Strain Rate ( $N_R^o = 0.7$ ): Energy Simplex Figure 4.8

second normal stress difference are negative requires that the phenomenological parameter  $C_{\beta} > 0$ . The choice of a convected time derivative in the phenomenological model for the anisotropic pre-stress is required in order to have a non-trivial second normal stress difference in the absence of non-linear terms in the mean strain rate. Moreover, an interpolated convective derivative (with  $a \cong -2/3$ ) is specifically chosen to represent the finite memory associated with the anisotropic pre-stress (Issue (iii), Section 1.2), inasmuch as it is able to exactly reproduce the experimentally observed asymptotic Reynolds stress components.

The turbulent pre-stress exhibits two qualitatively different means of reacting to an external driving force, such as mean shear. The isotropic portion of the pre-stress causes an instantaneous reorganization of the turbulence in response to the imposition of the mean shear. This state is equivalent to the state predicted by the IPS-theory at a given value of the relaxation parameter. Note that this rapid effect results in a non-zero primary normal stress difference, although the second normal stress difference remains zero. Conversely, the anisotropic portion of the pre-stress reacts slowly to an imposed mean shear. The time scale for this reaction is related by the turbulent Deborah number,  $De_t$ . The anisotropic pre-stress causes the second normal stress difference and partly influences the primary normal stress difference.

As the IPS-theory is realizable for all  $N_R$  given a positive turbulent kinetic energy and dissipation, the initial state of these transient calculations is always realizable. The turbulence predicted by the APS-theory remains realizable during the entire transient approach to the asymptotic state. Similar to the IPS-theory, the developmental times for the turbulent statistics to reach their asymptotic values depend on the initial conditions and are comparable to those seen experimentally

#### CHAPTER 5

## HOMOGENEOUSLY SHEARED TURBULENCE IN A ROTATING FRAME OF REFERENCE

## 5.1 Introduction

Homogeneously sheared turbulence relative to a rotating frame of reference provides a critical test for Reynolds stress closure theories. Figure 5.1 shows a schematic of this flow. The mean velocity gradient is constant within the non-inertial frame:

$$\nabla \langle \underline{u} \rangle = S \underbrace{e}_{\underline{\gamma} - \underline{z}}, \tag{5.1}$$

where S is a constant and both  $\underline{e}_y$  and  $\underline{e}_z$  represent mutually perpendicular unit vectors in the non-inertial frame. For this problem, turbulent fluctuations couple with the mean velocity gradient and the rotational tensor, defined by

$$\underline{\underline{\Omega}} = \underbrace{\varepsilon} \cdot \underline{\omega} = \underline{\Omega} \left( \underbrace{e}_{-y-z} \underbrace{e}_{-z-y} \right), \tag{5.2}$$

where  $\underline{\omega}$  ( $\equiv \Omega_{-x}^e$ ) is the rotation vector,  $\underline{\varepsilon}$  is the permutation triadic, and  $\Omega$  is the scalar rotation rate. The impetus for investigating flows within a rotating frame of reference stems from the following observations drawn in Section 1.1:

the superposition of a frame rotation upon a simple mean shear generates a crossstream turbulent production term analogous to the cross-stream turbulent production which arises in inertial frame flows with streamline curvature.

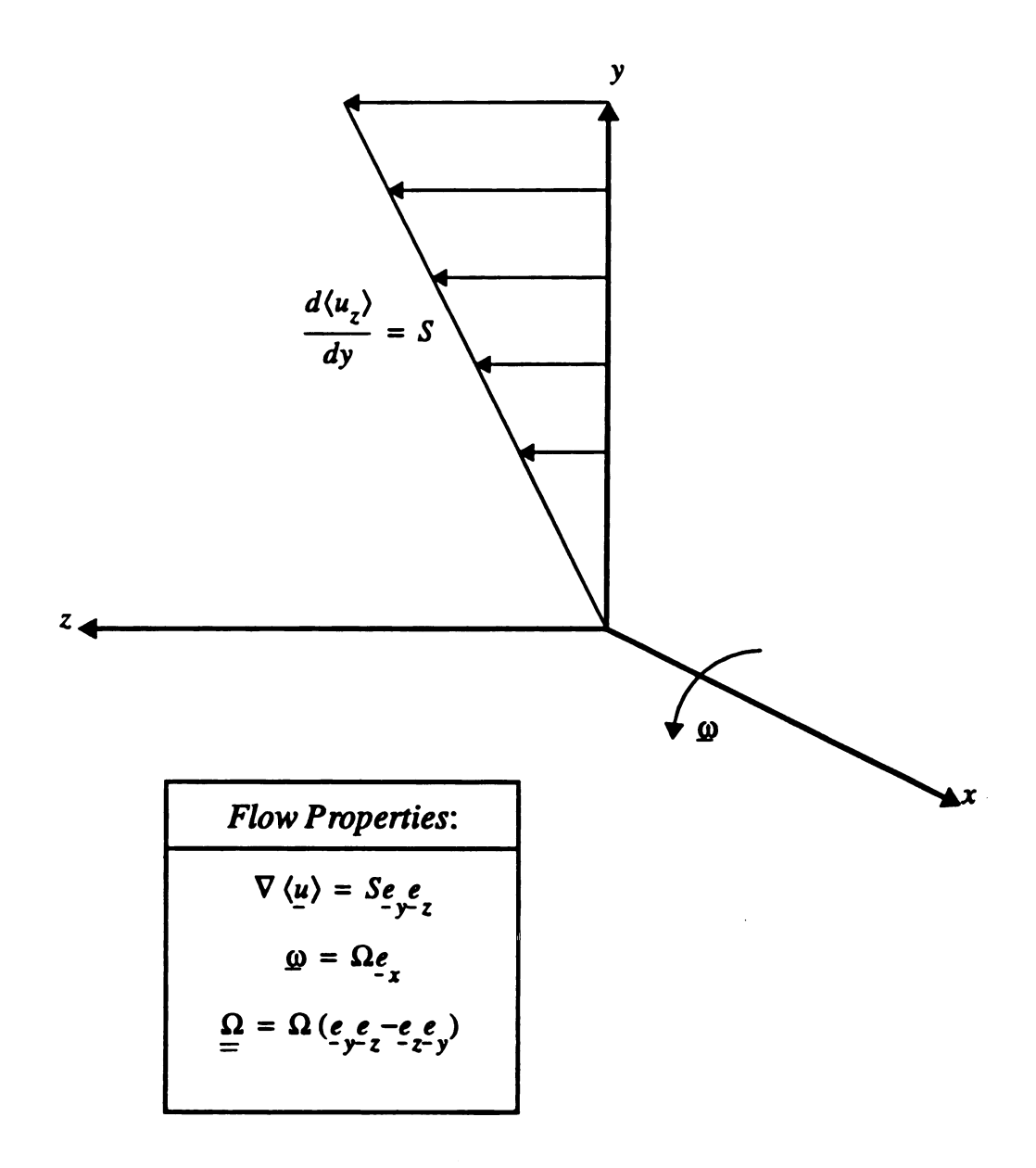


Figure 5.1 Schematic for Homogeneously Sheared Turbulence in a Rotating Frame.

Previous authors (Speziale and Mhuiris, 1989; Speziale, et al., 1990) have investigated rotating homogeneous shear flows using two-equation models and second order closures. They report that asymptotic homogeneous shear states exist for a finite range of the relative rotation rate ( $\Omega/S$ ),

$$-\infty < (\Omega/S)_{min} < \Omega/S < (\Omega/S)_{max} < \infty. \tag{5.3}$$

The asymptotic states are attained for large development times ( $t = z/\langle u_z \rangle(0)$ ) and have the following limiting behavior

$$\lim_{t \to \infty} \left( k, \, \varepsilon, \, \frac{k}{\varepsilon} \right) \to (\infty, \, \infty, \, \text{constant}) \,. \tag{5.4}$$

For  $(\Omega/S) < (\Omega/S)_{min}$  and  $(\Omega/S) > (\Omega/S)_{max}$ , the flow changes qualitatively inasmuch as the turbulent kinetic energy k and the dissipation  $\varepsilon$  decay rather than grow, i.e.,

$$\lim_{t \to \infty} \left( k, \varepsilon, \frac{k}{\varepsilon} \right) \to (0, 0, \infty) \,. \tag{5.5}$$

The standard k- $\epsilon$  model of turbulence is frame indifferent due to the fact that no explicit frame-dependent terms appear in the k- and  $\epsilon$ -transport equations (see Appendix B and C) and the fact that the basic Boussinesq approximation for the Reynolds stress is frame-indifferent. Therefore, the k- $\epsilon$  model incorrectly predicts no influence of  $\Omega$  on the low-order statistical properties of homogeneous shear. However, the k- $\epsilon$  theory does predict a mean field dependence on the rotation because of the Coriolis terms in the Reynolds equation (see Eq. (1.1)). Moreover, second-order closure models for the Reynolds stress (see Appendix B) also include explicit Coriolis effects and, thereby, account for the influence of  $\Omega$  on low-order flow statistics. However, closure models for

the statistical correlations which appear in the second-moment equation for  $\langle \underline{u}'\underline{u}'\rangle$  are often assumed to be frame indifferent. For example, the LRR-model of Launder *et al.* [1975] relative to a rotating frame of reference reduces to the following equation for statistically stationary rotating homogeneous shear flows:

$$\langle u_{z}\rangle(0)\frac{d\langle \underline{u}'\underline{u}'\rangle}{dz} + \langle \underline{u}'\underline{u}'\rangle \cdot \left[\nabla \langle \underline{u}\rangle + 2\underline{\Omega}\right] + \left[\nabla \langle \underline{u}\rangle + 2\underline{\Omega}\right]^{T} \cdot \langle \underline{u}'\underline{u}'\rangle =$$

$$-\frac{2}{3}\varepsilon\underline{I} - C_{1}\frac{\varepsilon}{k}\underline{b}$$

$$+C_{2}\left(\langle \underline{u}'\underline{u}'\rangle \cdot \left[\nabla \langle \underline{u}\rangle + \underline{\Omega}\right] + \left[\nabla \langle \underline{u}\rangle + \underline{\Omega}\right]^{T} \cdot \langle \underline{u}'\underline{u}'\rangle - \frac{2}{3}\langle \underline{u}'\underline{u}'\rangle : \nabla \langle \underline{u}\rangle\underline{I}\right) \quad (5.6)$$

The convective coupling of the Reynolds stress with the mean velocity gradient and the rotation dyadic on the left-hand-side of Eq. (5.6) arises naturally with a change of frame. The terms on the right-hand-side account for two distinct physical processes: (1) an isotropic destruction of the Reynolds stress due to turbulent dissipation of energy; and, (2) a redistribution of energy among the components of the fluctuating velocity. Because  $\langle \underline{u}'\underline{u}'\rangle$ :  $\underline{\Omega} \equiv 0$  and  $tr(\underline{b}) \equiv 0$ , a contraction of the two redistribution terms is identically zero. Thus, these terms do not explicitly influence the energy balance (cf. Eq. (1.15)) which follows directly from the trace of Eq. (5.6):

$$\langle u_{z}\rangle(0)\frac{d}{dz}\langle \underline{u}'\cdot\underline{u}'\rangle = -2\langle \underline{u}'\underline{u}'\rangle:\nabla\langle\underline{u}\rangle - 2\varepsilon. \tag{5.7}$$

Eq. (5.7) has the same form and physical interpretations as its inertial frame counterpart. Clearly, changes in the kinetic energy of the fluctuating field for homogeneous shear occur because of turbulent production and turbulent dissipation. The last two terms on the right-hand-side of Eq. (5.6) account for the *slow* and the *fast* redistribution of energy due to the pressure-strain rate correlation.

Application of the LRR-model to return-to-isotropy experiments in an inertial frame (see Section 4.3) reduces to the same dynamic model as the APS-theory. With a Rotta coefficient  $C_1 = 3.0$ , the LRR-predictions and the APS-predictions (for  $C_R = 2/3$ ) are indistinguishable when applied to the relaxation of homogeneous turbulence to an isotropic state. However, these two closure strategies predict significantly different responses in non-inertial frames.

In this chapter, the APS-theory is applied to rotating homogeneous shear flows and the results provide a basis to compare the LRR-model and the APS-model (see Section 5.5). The standard k- $\epsilon$  transport equations are employed to determine the turbulent time scale (i.e.  $k/\epsilon$ ) for both the LRR- and APS-models. However, recent research (see Speziale et al., 1987) suggests that the scalar dissipation equation should also have an explicit Coriolis effect. Earlier DNS results for isotropic decay by Bardina et al. [1985] and by Speziale et al. [1987] seem to support this view. However, this fundamental question is not addressed in this dissertation. Instead, the explicit Coriolis effects in the operator  $\frac{A}{\epsilon}$  (see Eq. (4.2)) are evaluated and compared with the LRR-model.

#### 5.2 Pre-closure Theory

The turbulent pre-closure for rotating homogeneous shear is the same as that expressed by Eqs. (4.1), (4.2) and (4.7), with the exception that the velocity gradient in the inertial frame (cf. Eq. (4.2)) is replaced with the sum of the mean velocity gradient in the non-inertial frame and the rotation dyadic (see Section 4.1). Thus, the turbulent pre-closure for rotating homogeneous shear is

$$\underline{A}^{T} \cdot \langle \underline{u}'\underline{u}' \rangle \cdot \underline{A} = \frac{2\alpha}{3} \underline{I} + 2k\underline{H}, \qquad (5.8)$$

where

$$A = I + \tau_R \left( \nabla \langle \underline{u} \rangle + \underline{\Omega} \right) = I + N_R \left[ \left( 1 + \frac{\Omega}{S} \right) e e - \frac{\Omega}{S} e e \right].$$
(5.9)

The trace of Eq. (5.8) utilizing Eq. (5.9) yields the following expression for the isotropic portion of the pre-stress:

$$\frac{\alpha}{k} = 1 + 2N_R R_{yz} + \left(\frac{\Omega}{S}\right)^2 N_R^2 R_{zz} + \left(1 + \frac{\Omega}{S}\right)^2 N_R^2 R_{yy} . \tag{5.10}$$

Eqs. (5.8) along with (5.9) and (5.10) gives the following component equations for the pre-closure:

$$R_{xx} = \frac{1}{3} \frac{\alpha}{k} + H_{xx}, \tag{5.11}$$

$$R_{yy} = \frac{1}{3} \frac{\alpha}{k} + H_{yy} + 2 \frac{\Omega}{S} N_R R_{yz} - \left(\frac{\Omega}{S}\right)^2 N_R^2 R_{zz}, \qquad (5.12)$$

$$R_{zz} = \frac{1}{3} \frac{\alpha}{k} + H_{zz} - 2 \frac{\Omega}{S} N_R R_{yz} - 2 N_R R_{yz} - \left(1 + \frac{\Omega}{S}\right)^2 N_R^2 R_{yy}, \tag{5.13}$$

and

$$\left[-1 + \frac{\Omega}{S}\left(1 + \frac{\Omega}{S}\right)N_R^2\right](-R_{yz}) = H_{yz} + \frac{\Omega}{S}N_RR_{zz} - \left(1 + \frac{\Omega}{S}\right)N_RR_{yy}.$$
 (5.14)

Note that Eqs. (5.10)-(5.14) reduce to Eqs. (4.40) and (4.34)-(4.37) for  $\Omega = 0$ .

As was observed in Chapter 3, the isotropic portion of the pre-stress (Eq. (5.10)) serves to redistribute energy among the normal components of the Reynolds stress. Each of the last three terms on the right-hand-side of Eq. (5.10) is found in the normal component equations with equal magnitude, but opposite sign. In Chapter 3, it was noted

that the term  $2N_RR_{yz}$  shifts energy from  $R_{yy}$  and  $R_{xx}$  to the streamwise component  $R_{zz}$ . Conversely, the final two terms in Eq. (5.10) cause a redistribution due to coupling with the frame rotation to remove energy from  $R_{yy}$  and  $R_{zz}$ , which subsequently transfers it to the axis of rotation, i.e. to  $R_{xx}$ . The term  $2(\Omega/S)N_RR_{yz}$  also arises in the component equations for  $R_{yy}$  and  $R_{zz}$ , but with opposite sign. These relate directly to the source/sink terms for velocity fluctuations due to coupling with the rotation dyadic (see Eq. (1.30)). Because they are of opposite sign, energy transfers from  $R_{yy}$  to  $R_{zz}$  (or vice versa, depending on the direction of rotation).

The mathematical nature of the operator  $\underline{\underline{A}}$  is important in that, if its determinant were zero, then there would be no algebraic connection between the Reynolds stress and the statistical correlations responsible for the pre-stress (see Eq. (4.7)). For homogeneous shear flows, the determinant of  $\underline{\underline{A}}$  is

$$det(A) = 1 + N_R^2 \frac{\Omega}{S} \left( 1 + \frac{\Omega}{S} \right). \tag{5.15}$$

From Eq. (5.15), it is apparent that det(A) could only possibly be negative for  $-1 < \Omega/S < 0$ . In this range, it follows directly that  $N_R < 2$  is a sufficient condition for det(A) > 0. For the asymptotic state associated with a particular value of  $\Omega/S$ , it would be possible to verify a posteriori that det(A) > 0. However, for a transient calculation in the range  $-1 < \Omega/S < 0$ , there would exist some upper bound above which an initial condition for  $N_R$  could not be specified:

$$N_{R, max} = \left[ \left( -\frac{\Omega}{S} \right) \left( 1 + \frac{\Omega}{S} \right) \right]^{-1/2} \ge 2, \quad \text{for} \quad -1 < \Omega/S < 0.$$
 (5.16)

#### 5.3 Coriolis Redistribution of Turbulent Energy for Homogeneous Flows

In the absence of a mean shear, the pre-closure still predicts a frame dependence on the Reynolds stress due to rotation. With S = 0 and  $N_R = \tau_R S$ , Eq. (5.9) reduces to:

$$A = I + \tau_R \Omega = I + \tau_R \Omega \left[ e e_{-y-z} - e_{-z-y} \right] . \tag{5.17}$$

From Eq. (5.10), it follows directly that the isotropic portion of the pre-stress is given by

$$\frac{\alpha}{k} = 1 + (\tau_R \Omega)^2 (R_{yy} + R_{zz}). \tag{5.18}$$

For isotropic turbulence in an inertial frame,  $\underline{H} = \underline{0}$  and  $\alpha/k = 1$ , since  $\underline{A} = \underline{I}$ . As  $\Omega$  changes from zero (either positive or negative), the anisotropic pre-stress remains zero in the absence of any mean field deformation process. However, this isotropic part of the prestress changes according to Eq. (5.18) and the operator  $\underline{A}$  depends on the rotational rate  $\Omega$ . Therefore, with S = 0, Eqs. (5.8) and (5.17) lead to the following component equations for the pre-closure:

$$R_{xx} = \frac{1}{3}\alpha/k,\tag{5.19}$$

$$R_{yy} + (\tau_R \Omega)^2 R_{zz} = \frac{1}{3} \alpha / k,$$
 (5.20)

$$R_{zz} + (\tau_R \Omega)^2 R_{yy} = \frac{1}{3} \alpha / k,$$
 (5.21)

and

$$R_{\rm vz}=0. ag{5.22}$$

Eqs. (5.20) and (5.21) combine with Eq. (5.18) to give

$$R_{yy} = R_{zz} = \frac{1}{3 + (\tau_p \Omega)^2}.$$
 (5.23)

This implies that

$$R_{xx} = \frac{1 + (\tau_R \Omega)^2}{3 + (\tau_R \Omega)^2} , \qquad (5.24)$$

since  $R_{xx} + R_{yy} + R_{zz} = 1$ .

Thus, the noninertial pre-closure theory for the Reynolds stress predicts a redistribution of turbulent kinetic energy among the components of the fluctuating velocity in the absence of any mean field deformation. As the characteristic time scale for the turbulence becomes large compared to the time scale for rotation (i.e.  $|\tau_R \Omega| \gg 1$ ), the turbulence approaches a one-component state (cf. Figure 1.1), with the turbulent energy aligned along the axis of rotation. This redistribution process is symmetric about  $\tau_R \Omega = 0$  and is summarized in Figure 5.2. It is also noted that Eqs. (5.23) and (5.24) express a realizable turbulent state for all  $\tau_R \Omega \in [-\infty, \infty]$ .

The goal of this chapter is to apply the noninertial pre-closure theory to homogeneously sheared turbulence (see Issue (iv), Section 1.2). The asymptotic states for both the IPS- and APS- theories are examined along with the effect of rotation on the qualitative nature of the turbulence. The symmetry about  $\Omega = 0$  predicted by Eqs. (5.23) and (5.24) will be broken by the presence of S > 0.

### 5.4 Isotropic Pre-Stress Theory for Rotating Homogeneous Shear

Similar to the approach taken in Chapters 3 and 4, the consequences of the IPS-theory are considered prior to evaluating the APS-theory. Thus, for the following analysis in this

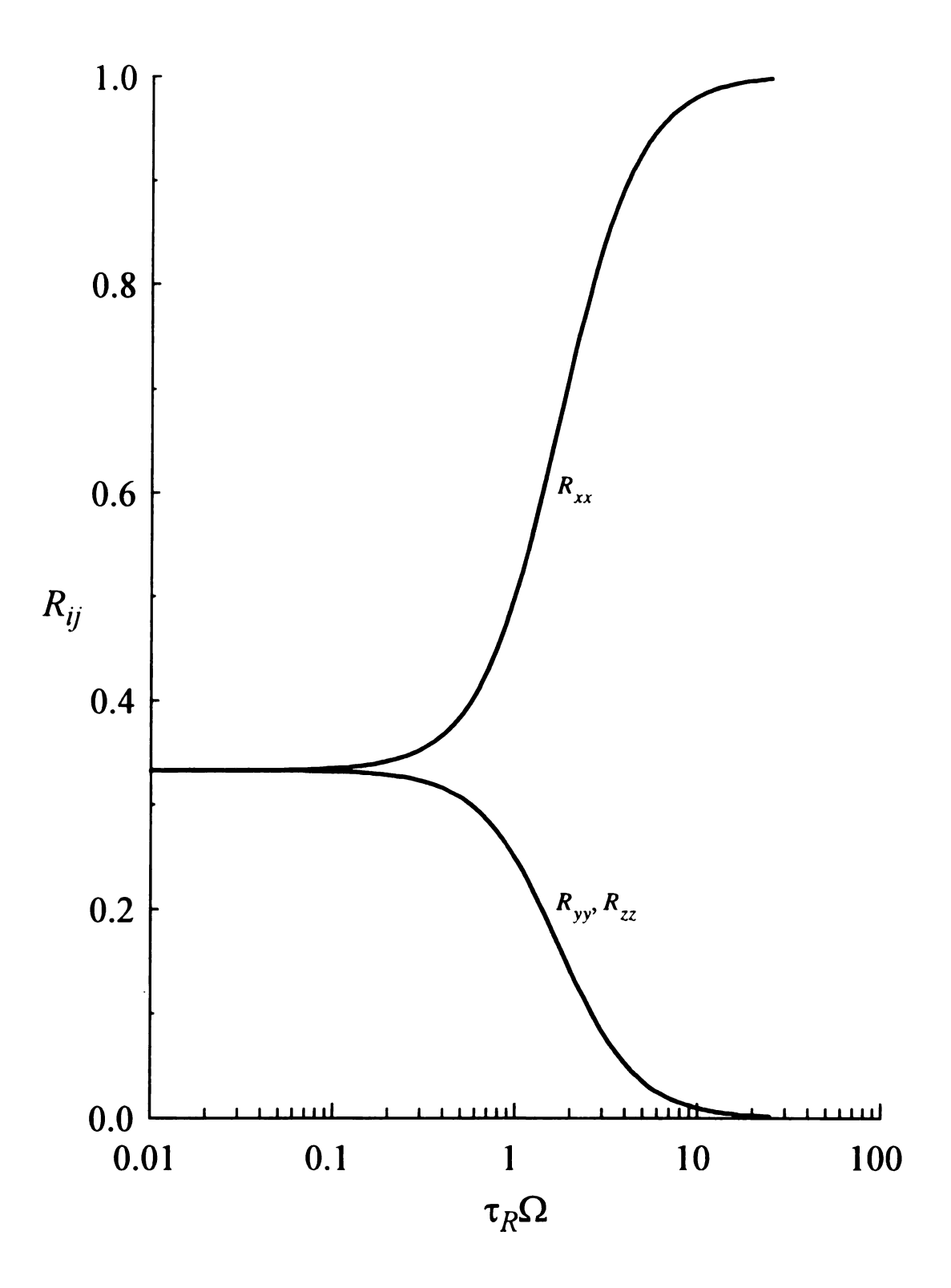


Figure 5.2 Coriolis Redistribution of Turbulent Kinetic Energy for Homogeneous Flows

section, H = 0. For the problem of rotating homogeneous shear, no new phenomenological parameters are introduced, so the results may be computed directly from the parameters outlined in Table 3.1.

The asymptotic states for the IPS-theory are determined by solving the initial value problem for the relaxation group  $N_R$  at a fixed value of  $\Omega/S$ . Since the evolution equation for  $N_R$  does not explicitly introduce frame-dependent effects, the governing equation is the same as Eq. (4.68):

$$\frac{dN_R}{d\xi} = 2N_R R_{yz} (C_P - 1) + C_R (C_D - 1) . ag{5.25}$$

If asymptotic states exist (i.e.  $dN_R/d\xi \to 0$ ), then it follows directly from Eq. (5.25) that  $N_R R_{\nu z}$  does not depend on  $\Omega/S$  inasmuch as:

$$\lim_{\xi \to \infty} (-N_R R_{yz}) = \frac{C_R (C_D - 1)}{2 (C_P - 1)} = 0.230 . \tag{5.26}$$

The above numerical result assumes that the IPS parameters listed in Table 3.1 are universal. With  $R_{xx} = 1 - R_{yy} - R_{zz}$  and H = 0, Eqs. (5.11)-(5.14) may be reduced to three coupled algebraic equations for  $R_{yy}$ ,  $R_{zz}$ , and  $R_{yz}$ . During the transient calculations, the coefficient matrix for equations relating these three components is inverted using a Gauss-Jordan elimination technique (Carnahan *et al.*, 1969). Although there is no explicit dependence on  $\Omega/S$  in the equation for  $N_R$ , the asymptotic state  $N_R^a$  does depend on  $\Omega/S$  due to the Reynolds stress components. The initial state used to compute the approach to the asymptotic states is the inertial frame asymptote:

$$N_{p}^{o} = 0.945. (5.27)$$

The initial value problem was solved using a fourth order Runge-Kutta integration scheme (Carnahan et al., 1969; see also Appendix H).

With  $\underline{H} = 0$ , Eqs. (5.12) and (5.13) may be expressed as follows:

$$\begin{pmatrix} C_{11} & C_{12} \\ C_{21} & C_{22} \end{pmatrix} \cdot \begin{pmatrix} R_{yy} \\ R_{zz} \end{pmatrix} = \begin{pmatrix} 1 \\ 1 \end{pmatrix} - 2N_R R_{yz} \begin{pmatrix} \Omega/S \\ 1 + \Omega/S \end{pmatrix},$$
(5.28)

where

$$C_{11} = C_{22} = 2, (5.29a)$$

$$C_{12} = 1 + N_R^2 \left(\frac{\Omega}{S}\right)^2,$$
 (5.29b)

and

$$C_{21} = 1 + N_R^2 \left( 1 + \frac{\Omega}{S} \right)^2.$$
 (5.29c)

For  $\xi \to \infty$ ,  $N_R R_{yz}$  approaches 0.230 as indicated above. Therefore, the determinant of the coefficient matrix in Eq. (5.28) must be non-zero:

$$\det(\underline{C}) = 4 - \left[1 + N_R^2 \left(\frac{\Omega}{S}\right)^2\right] \left[1 + N_R^2 \left(1 + \frac{\Omega}{S}\right)^2\right] \neq 0 .$$
 (5.30)

For a fixed value of  $\Omega/S$ , there exists an  $N_R^*$  such that the condition  $\det(\underline{C}) = 0$  is met; this identifies states for which asymptotic states do not exist. Thus, the limits on  $\Omega/S$  for which an asymptotic state cannot exist is determined by the intersection of  $N_R^*$  and  $N_R^a$ . Both  $N_R^*$  and  $N_R^a$  depend on  $\Omega/S$ . The solution to Eq. (5.30) for  $\det(\underline{C}) = 0$  is

$$(N_R^*)^2 = \frac{(1+\phi)}{2(1+\Omega/S)^2} \left[ -1 \pm \sqrt{1 + \frac{12\phi}{(1+\phi)^2}} \right],$$
 (5.31)

where

$$\phi \equiv \left[ \frac{(1 + \Omega/S)}{(\Omega/S)} \right]^2.$$

Note that only the positive root from Eq. (5.31) is considered, as  $N_R^*(\Omega/S)$  is a real-valued quantity.

Figure 5.3. presents the results of the IPS-asymptotic states for  $N_R^a$ . These results are qualitatively similar to other second-order closure models. The IPS-theory predicts unbounded growth of k and  $\epsilon$  over the range  $-1.26 < \Omega/S < 0.26$ . A similar behavior is predicted by the second-order closure of Launder *et al.* [1975] for  $-0.11 < \Omega/S < 0.39$ . Outside of this range, the flow changes character; both k and  $\epsilon$  become decaying functions and  $N_R \to \infty$  (see below). The minimum value of the relaxation group is  $N_{R, min}^a = 0.834$ , which occurs at  $\Omega/S = -0.5$ ; the maximum value of the relaxation group is  $N_{R, min}^a = 1.27$ , occurring at  $\Omega/S = 0.26$  and  $\Omega/S = -1.26$ .

Figures 5.4 and 5.5 complement Figure 5.3 in that they show the components of the asymptotic Reynolds stress as a function of  $\Omega/S$  and the corresponding behavior on the turbulent energy simplex. Figure 5.4 shows the redistribution effects due to the isotropic pre-stress and the rotation coupling outlined in Section 5.2. As  $|\Omega/S|$  increases, the terms  $(\Omega/S)^2 N_R^2 R_{zz}$  and  $(1 + \Omega/S)^2 N_R^2 R_{yy}$  grow, causing the isotropic pre-stress to transfer turbulent energy to the rotation axis. Similarly, the redistribution term arising due to rotation  $(-(\Omega/S) N_R R_{yz})$  causes a net transfer of energy to  $R_{zz}$  from  $R_{yy}$  when  $\Omega/S > 0$  and vice versa when  $\Omega/S < 0$ . Both figures indicate that the solution is symmetric about the point  $\Omega/S = -0.5$ . Specifically, the following properties are noted:

$$R_{xx}(\Omega/S) = R_{xx}(-\Omega/S - 1), \qquad (5.32)$$

$$R_{yy}(\Omega/S) = R_{zz}(-\Omega/S - 1), \qquad (5.33)$$

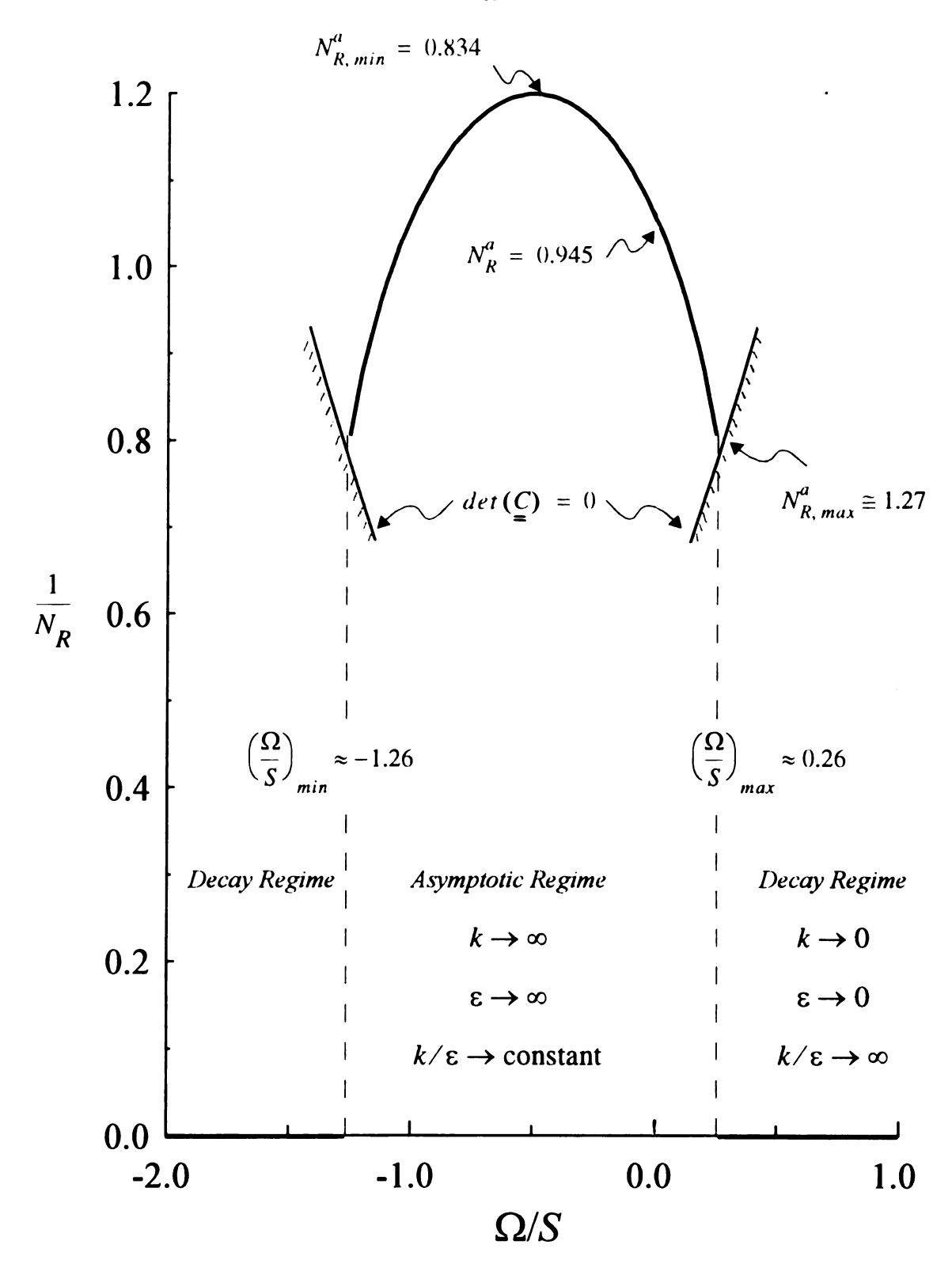


Figure 5.3 The Effect of Rotation on the Turbulent Relaxation Time  $(N_R \equiv \tau_R S)$  for Asymptotic Homogeneous Shear (IPS-Theory)

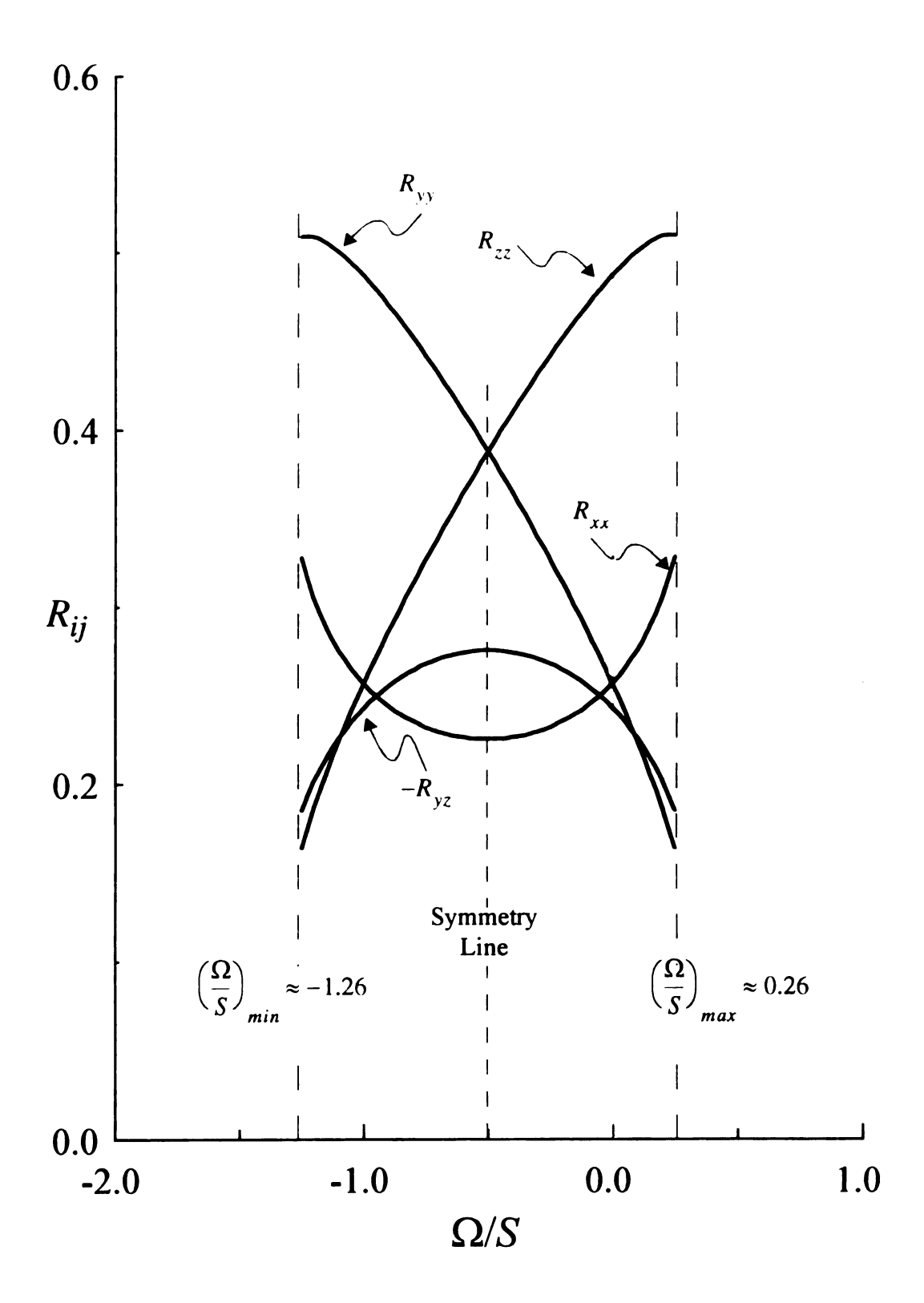


Figure 5.4 The Effect of Rotation on the Components of the Asymptotic Reynolds Stress for Homogeneous Shear (IPS-Theory)

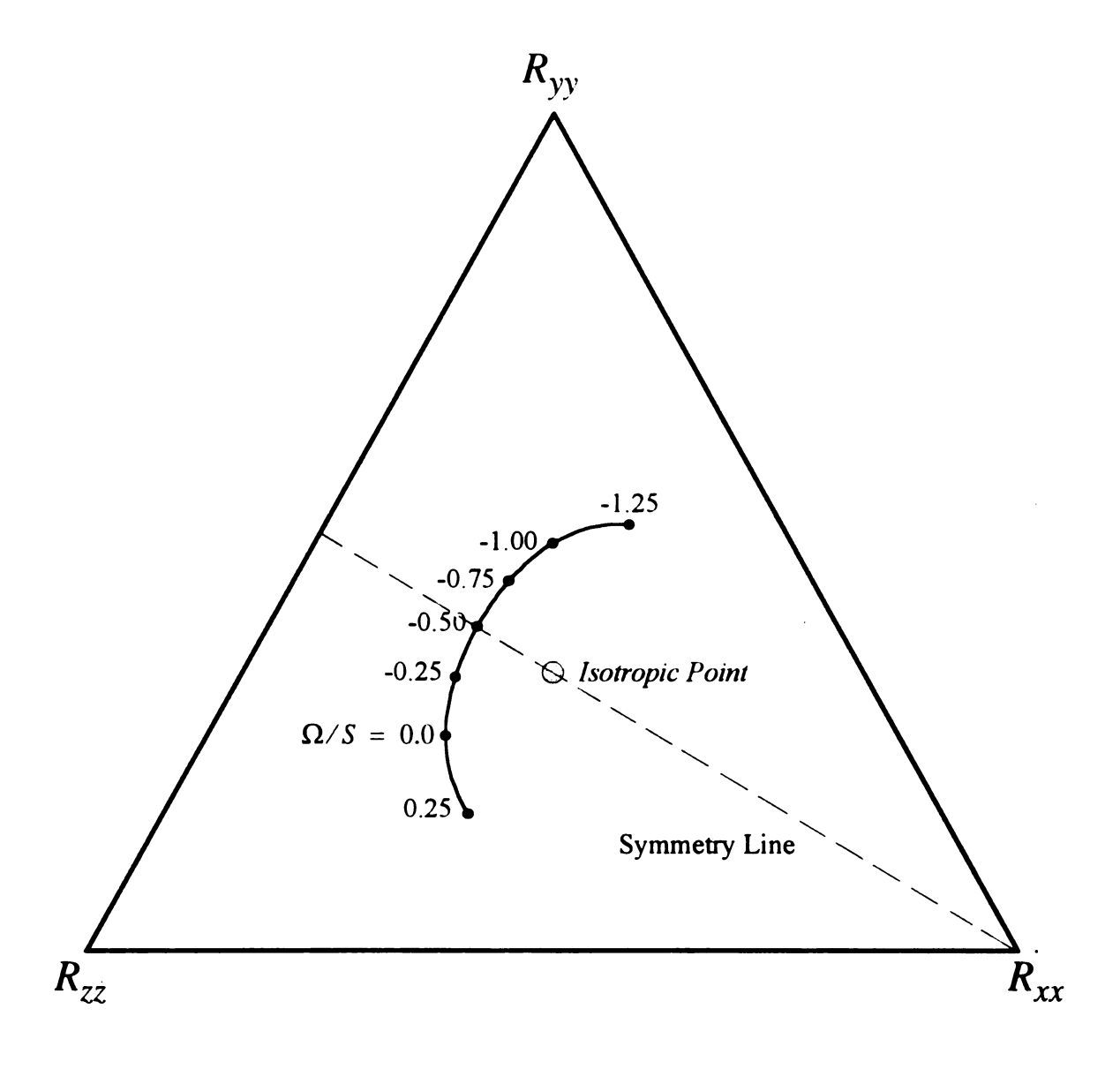


Figure 5.5 Distribution of the Energy Components for Homogeneously Sheared Turbulence in a Rotating Frame (IPS-Theory).

and

$$R_{yz}(\Omega/S) = R_{yz}(-\Omega/S - 1). \tag{5.34}$$

It follows directly from Eqs. (5.32)-(5.34) and the property  $R_{xx} + R_{yy} + R_{zz} = 1$  that the anisotropy invariants share the same symmetry property:

$$II(\Omega/S) = II(-\Omega/S - 1), \tag{5.35}$$

and

$$III(\Omega/S) = III(-\Omega/S - 1). \tag{5.36}$$

These results stem from the isotropic pre-stress assumption and the fact that

$$\underline{A}(\Omega/S) = \underline{A}^{T}(-\Omega/S - 1). \tag{5.37}$$

Eq. (5.37) notwithstanding, subsequent introduction of an *anisotropic* pre-stress will be seen to destroy the symmetry properties possessed by the IPS theory.

Figure 5.6 shows the transient behavior at infinite Reynolds numbers of  $N_R$  for three values of  $\Omega/S$ . The initial conditions correspond to  $N_R^o = 1$ . The results illustrate that two different flow regimes occur: an asymptotic regime (described by Eq. (5.4)) and a decay regime (described by Eq. (5.5)). For  $\Omega/S = -0.5$ ,  $N_R$  approaches a constant value in about ten dimensionless time units. For  $\Omega/S = 1.0$  and -2.0, however,  $N_R$  grows monotonically without bound.

The relative growth rates of the turbulent quantities k,  $\epsilon$ , and Re follow directly from Eqs. (3.2) and (3.3):

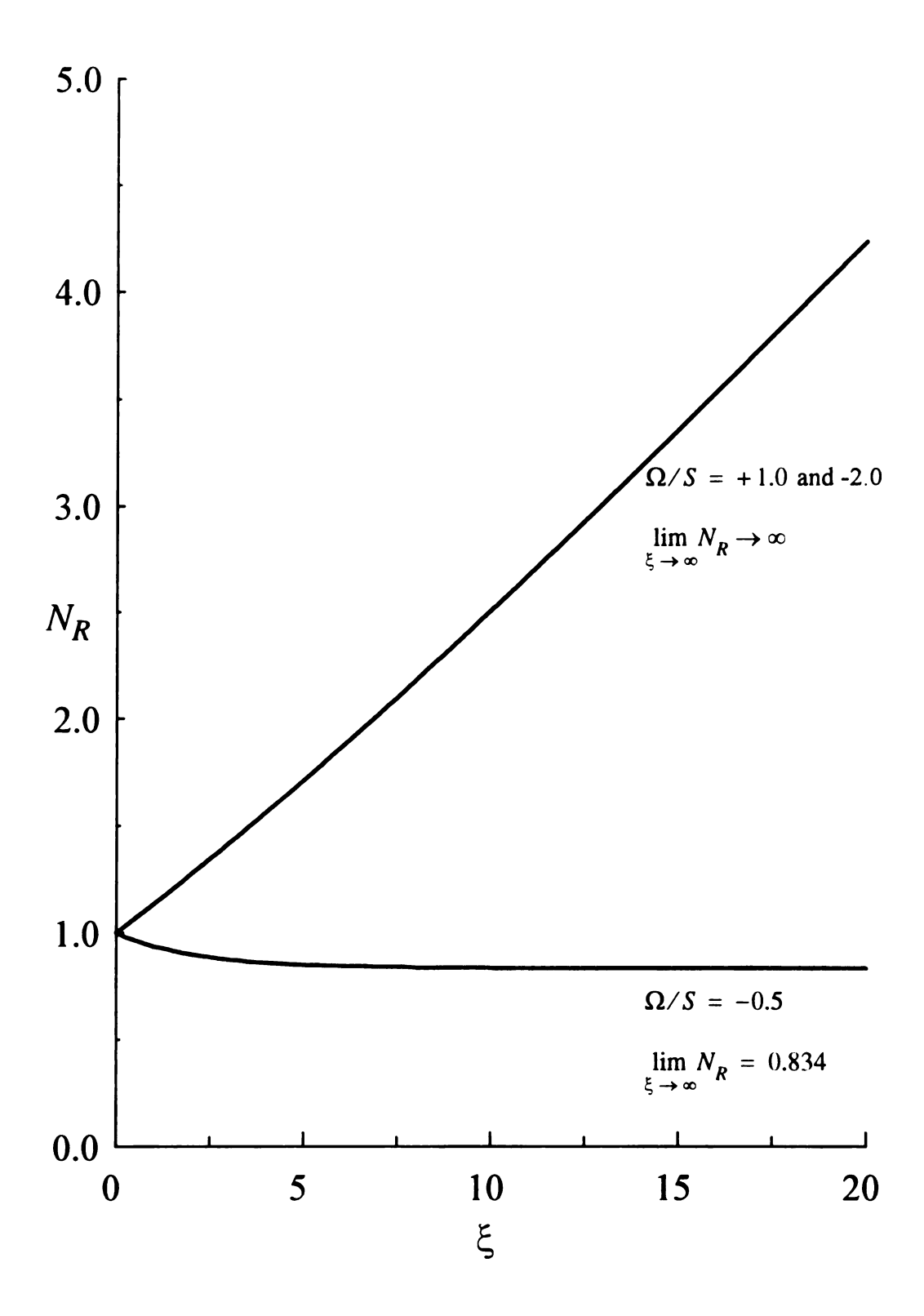


Figure 5.6 Transient Response of the Relaxation Group for Homogeneously Sheared Turbulence in a Rotating Frame (IPS-Theory).

$$\frac{\tau_D}{k}\frac{dk}{dt} = -\frac{2N_R R_{yz}}{C_R} - 1 \quad , \tag{5.38}$$

$$\frac{\tau_D}{\varepsilon} \frac{d\varepsilon}{dt} = -\frac{2C_P N_R R_{yz}}{C_R} - C_D, \qquad (5.39)$$

and

$$\frac{\tau_D}{Re} \frac{dRe}{dt} = -\frac{2(2 - C_P)N_R R_{yz}}{C_P} - (2 - C_D) \quad . \tag{5.40}$$

In the above equations,  $\tau_D = k/\epsilon$ . In the absence of turbulent production (i.e.  $N_R R_{yz} = 0$ ) Eqs. (5.38)-(5.40) describe the decay problem presented in Chapter 2. If an asymptotic state obtains (see Eq. (5.26)), then all three of the above parameters approach the same limit given by

$$\left(\frac{\tau_D}{k}\frac{dk}{dt}\right)_a = \left(\frac{\tau_D}{\varepsilon}\frac{d\varepsilon}{dt}\right)_a = \left(\frac{\tau_D}{Re}\frac{dRe}{dt}\right)_a = \frac{C_D - C_P}{C_P - 1}.$$
 (5.41)

For the IPS-parameters listed in Table 3.1, the dimensionless asymptotic growth rate is 1.024. The relative growth rates in the asymptotic regime are shown in Figure 5.7.

Figure 5.7 shows that, after approximately ten dimensionless time units, k,  $\epsilon$ , and Re achieve their limiting growth rates. Similarly, Figure 5.8 indicates that roughly the same amount of time is required for the Reynolds stress components to reach their asymptotic values. As expected,  $(N_R R_{yz})_a$  is reproduced exactly (see Eq. (5.26)). The initial values for the Reynolds stress components are determined by the isotropic portion of the prestress; a specification of values for  $N_R^o$  and  $\Omega/S$  causes an instantaneous reorganization of an isotropic turbulent state to an anisotropic turbulent state defined by Eqs. (5.10)-(5.14) with H = 0.

Figures 5.9 and 5.10 show the transient behavior of the turbulent time scales and the

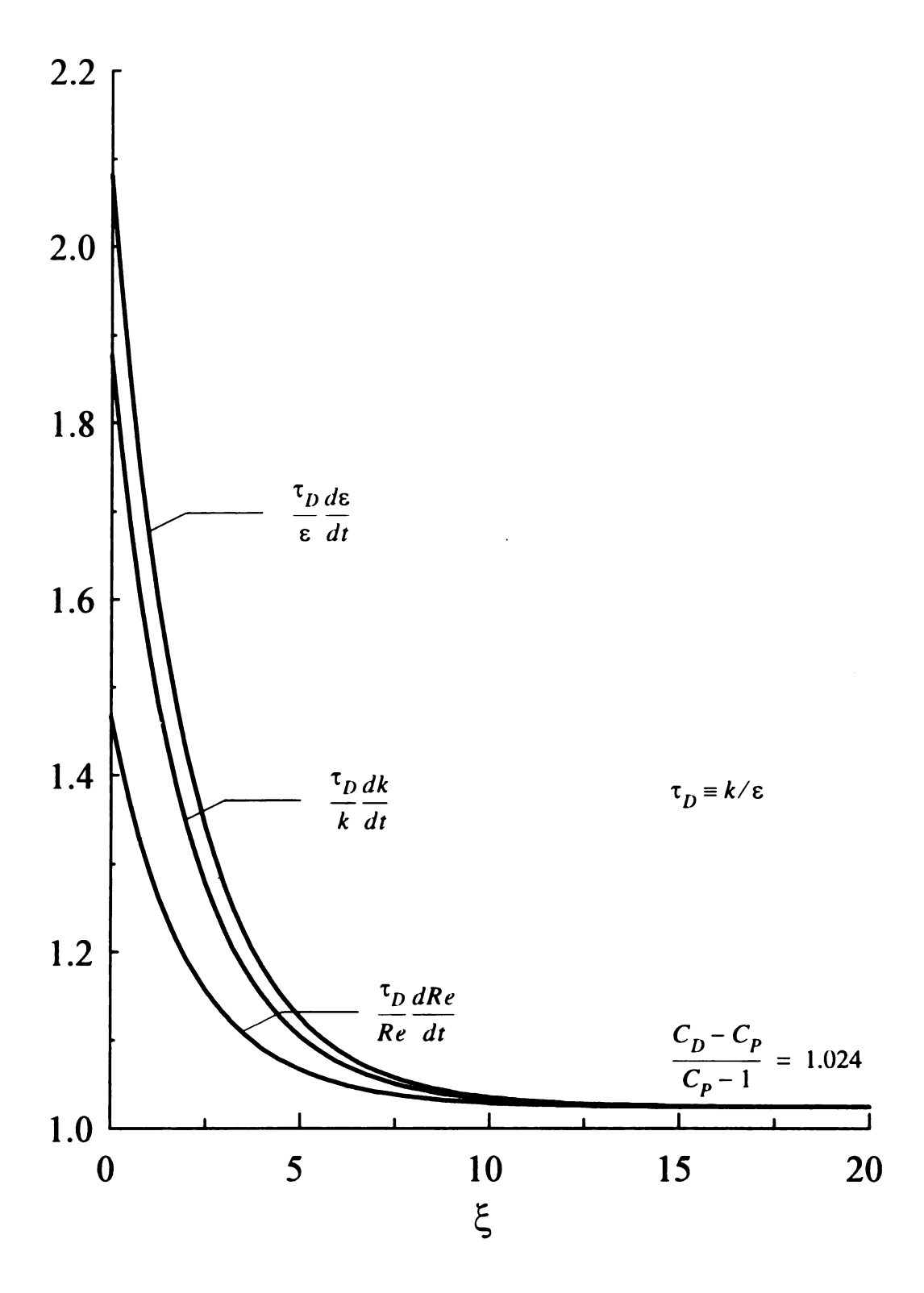


Figure 5.7 Relative Growth Rates of Turbulent Statistics in the Asymptotic Regime (IPS-Theory;  $N_R^o = 1.0$ ,  $\Omega/S = -0.5$ ).

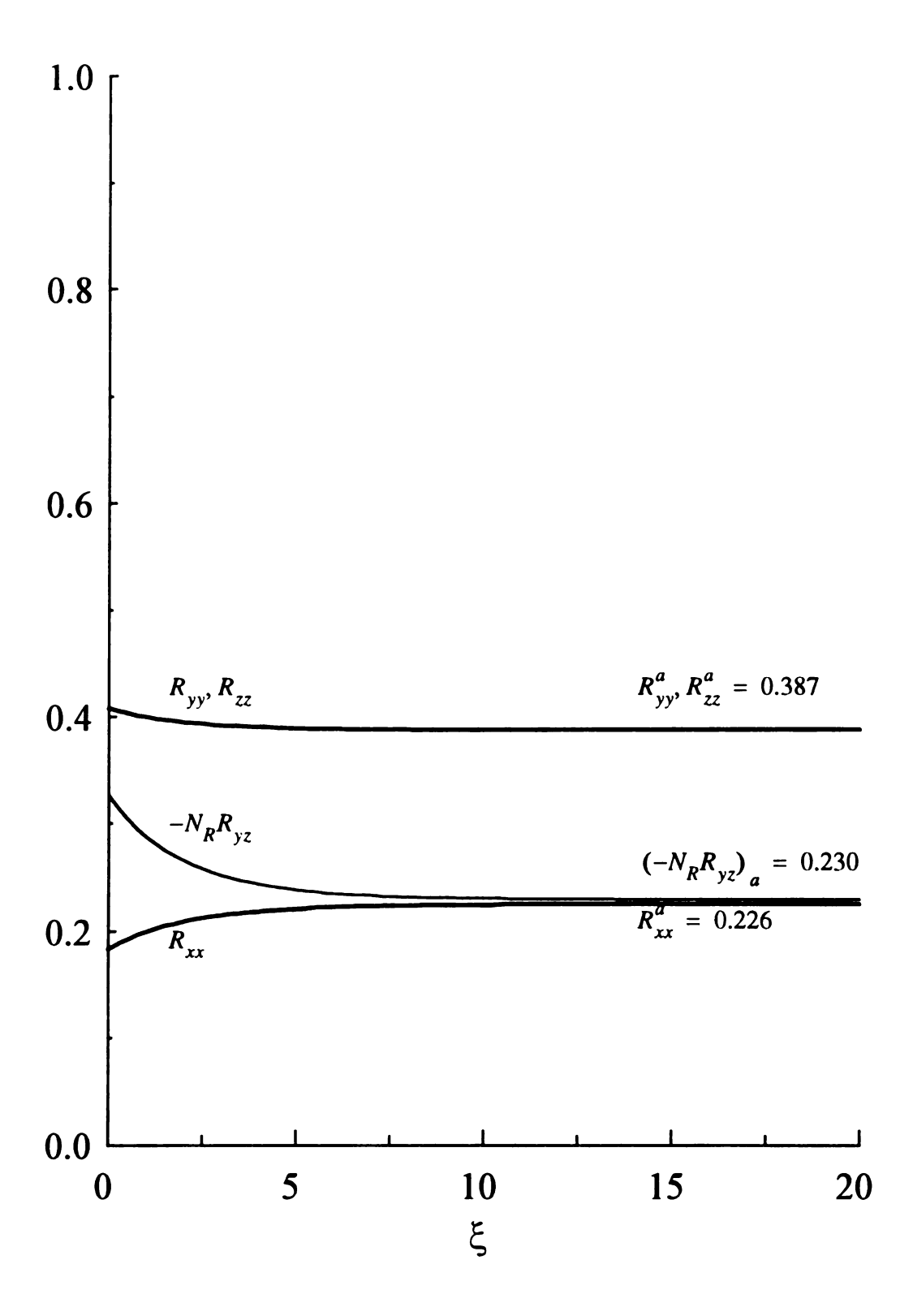


Figure 5.8 Relaxation of the Reynolds Stress Components in the Asymptotic Regime (IPS-Theory;  $N_R^o = 1.0$ ;  $\Omega/S = -0.5$ ;  $R_R^o = R(N_R^o, \Omega/S)$ , cf. Eqs. (5.10)-(5.14)).

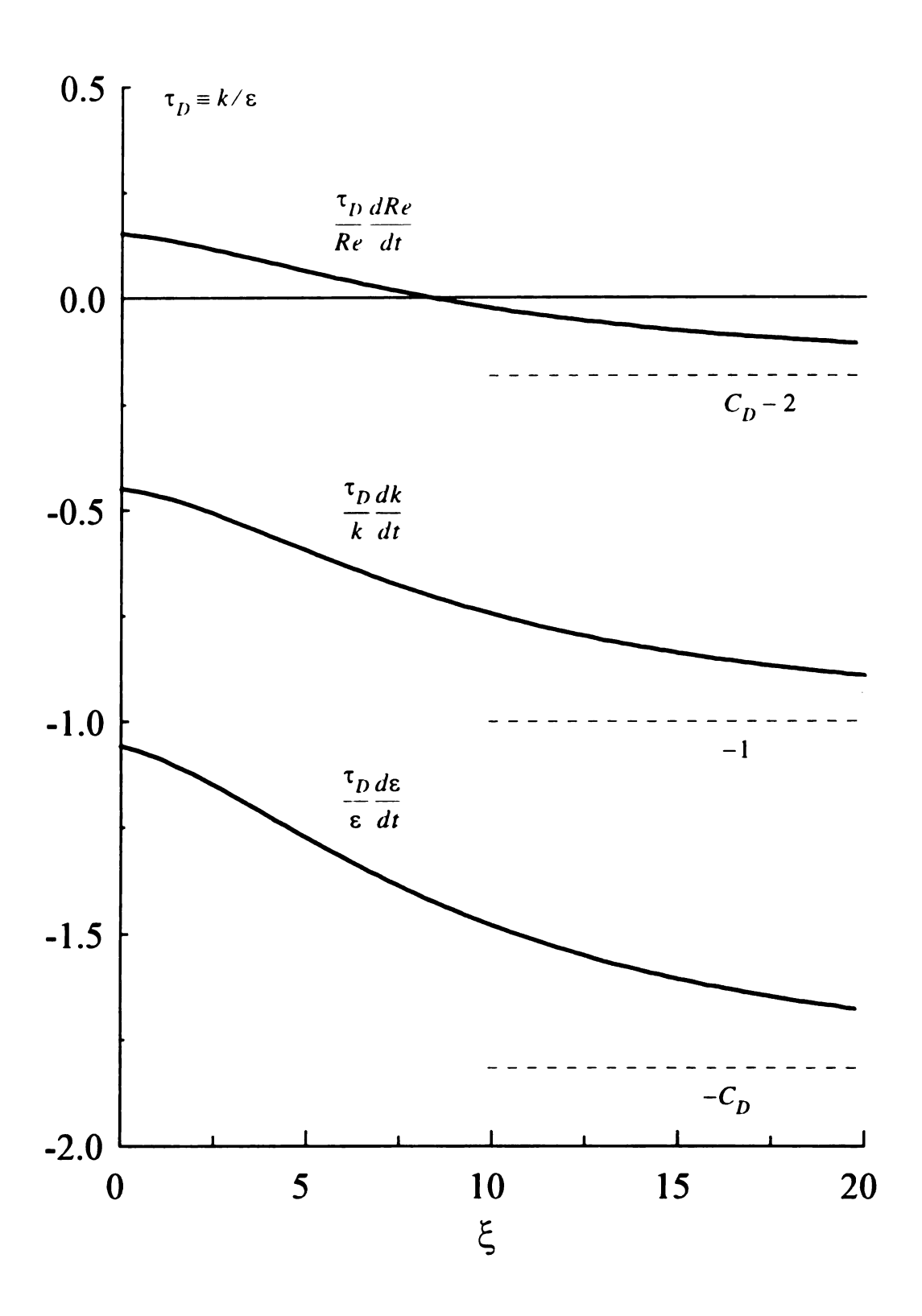


Figure 5.9 Relative Growth Rates of Turbulent Statistics in the Decay Regime (IPS-Theory;  $N_R^o = 1.0$ ;  $\Omega/S = +1.0$  and +2.0).

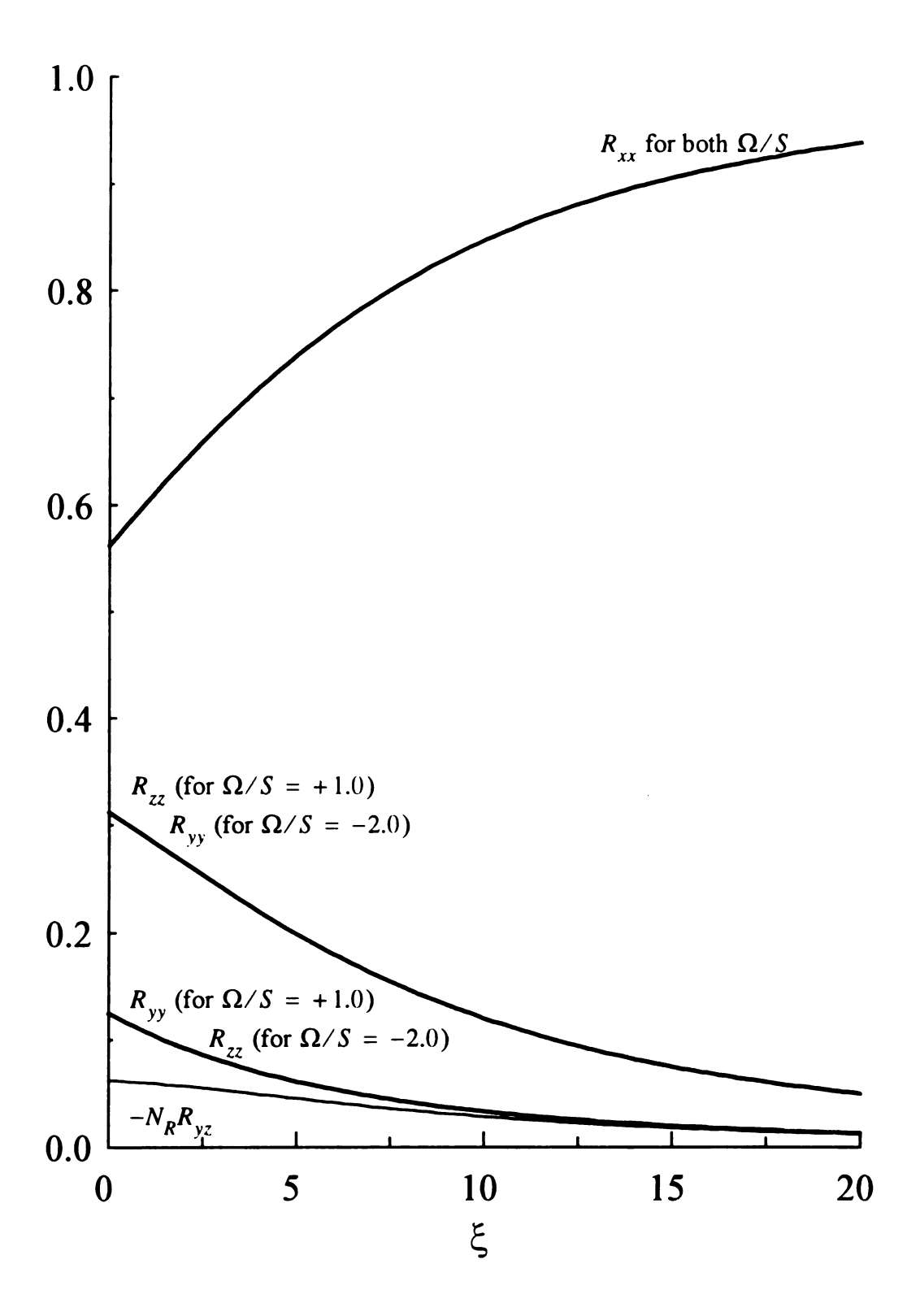


Figure 5.10 Relaxation of the Reynolds Stress Components in the Decay Regime (IPS-Theory;  $N_R^o = 1.0$ ;  $\Omega/S = +1.0$  and +2.0;  $\underline{R}^o = \underline{R} (N_R^o, \Omega/S)$ , cf. Eqs. (5.10)-(5.14)).

Reynolds stress in the decay regime  $(\Omega/S = +1.0, -2.0)$ . k,  $\epsilon$ , and Re ultimately decay with time (i.e. negative growth rates at large development times). This occurs because  $N_R R_{yz} \to 0$  in the decay regime (as seen in Figure 5.10). The asymptotic decay rates for k,  $\epsilon$ , and Re follow directly from Eqs. (5.38)-(5.40) by setting  $N_R R_{yz} = 0$  These asymptotes are indicated in Figure 5.9 by the dashed lines. Although  $N_R \to \infty$  in the decay regime,  $R_{yz}$  remains realizable and decays more rapidly than  $N_R$  grows, such that the product is also approaching zero. Additionally, it is seen that the effect of rotation in the decay regime is to asymptotically shift the turbulent energy into the energy component along the axis of frame rotation:

$$R_{yy} \rightarrow 1,$$
 (5.41)

$$R_{yy} \to 0, \tag{5.42}$$

and

$$R_{zz} \to 0. ag{5.43}$$

For an isotropic pre-stress, it follows directly from Eqs. (5.11) and (5.41) that

$$\frac{\alpha}{k} \to 3 \tag{5.44}$$

in the decay regime. Thus, Eq. (5.41) implies that  $\langle u'_x u'_x \rangle \to 2k \to 0$ . Eq. (5.12) with  $H_{xx} = 0$  and Eq. (5.44) together with the observation that  $N_R R_{yz} \to 0$  yield the following limiting behavior for  $R_{yy}$ ,

$$R_{yy} \to 1 - (\Omega/S)^2 N_R^2 R_{zz}.$$
 (5.45)

Since  $R_{yy} \to 0$ , the product  $N_R^2 R_{zz}$  must be approaching a constant in the decay regime in order to balance the first term on the right-hand-side of Eq. (5.45). Thus, in the decay regime for large values of  $N_R$ , Eq. (5.45) reduces to

$$R_{zz} \to \frac{1}{\left(\Omega/S\right)^2 N_R^2}. (5.46)$$

Similarly, Eqs. (5.13) and (5.44) combine to give

$$R_{zz} \to 1 - (1 + \Omega/S)^2 N_R^2 R_{yy}$$
 (5.47)

in the decay regime. Thus, for large values of  $N_R$ , Eq. (5.47) implies that

$$R_{yy} \to \frac{1}{(1 + \Omega/S)^2 N_R^2}$$
 (5.48)

It follows directly from Eq. (5.14) that  $R_{yz} = 0$  for the limiting behavior expressed by Eqs. (5.46) and (5.48). Thus, Schwarz's inequality is satisfied.

For decaying homogeneously sheared turbulence, Eqs. (5.46) and (5.48) provide a prediction for the distribution of turbulent energy in the plane of rotation:

$$\frac{R_{zz}}{R_{yy}} = \frac{(1 + \Omega/S)^2}{(\Omega/S)^2}.$$
 (5.49)

For the two relative rotation rates presented in the decay regime (i.e. +1.0, -2.0), the transient ratio of  $R_{zz}/R_{yy}$  approaches 4.0 and 0.25, respectively, which is in accord with Eq. (5.49).

Figures 5.11 and 5.12 address the issue of realizability of the IPS-theory for rotating homogeneous shear. Figure 5.11 shows all of the states within the asymptotic regime (i.e.

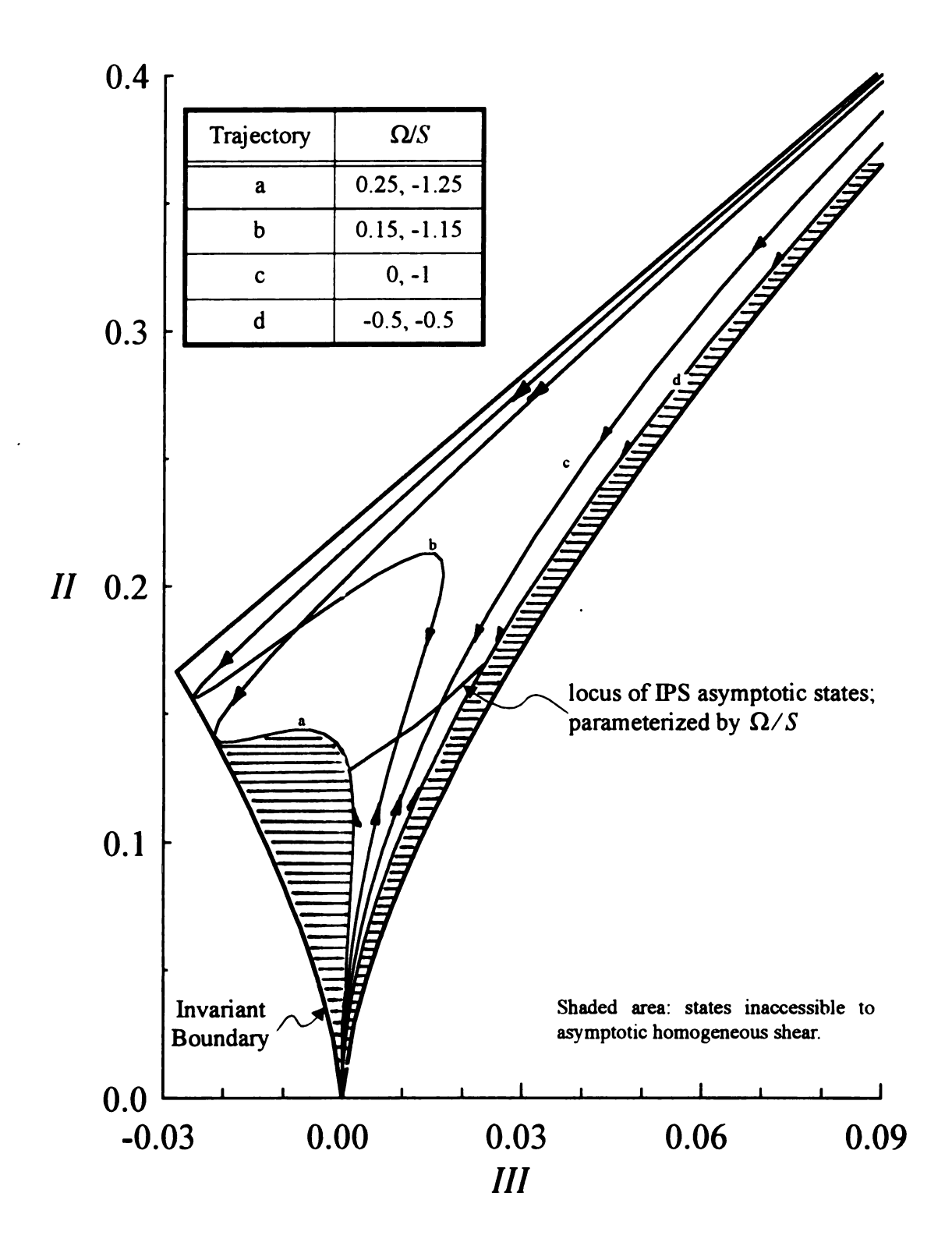


Figure 5.11 Anisotropy Invariants for the Asymptotic States of Homogeneously Sheared Turbulence in a Rotating Frame (IPS-Theory).

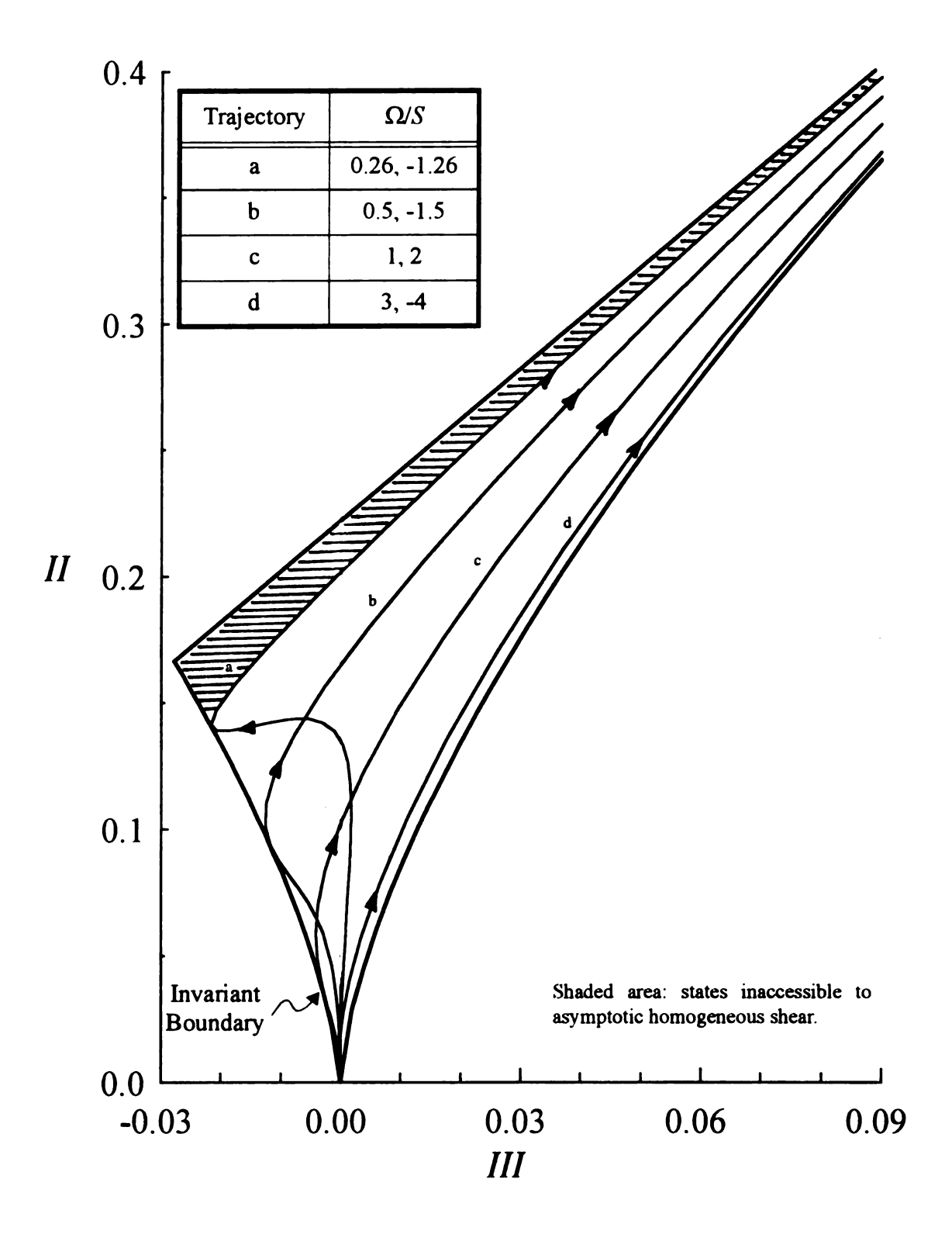


Figure 5.12 Anisotropy Invariants for the Decaying States of Homogeneously Sheared Turbulence in a Rotating Frame (IPS-Theory).

 $-1.26 < \Omega/S < 0.26$ ). Each point within the L-diagram is parameterized by at least one pair of  $(\Omega/S, N_R)$ , with the exception of the two shaded areas. These regions contain no IPS-trajectories which relax to an asymptotic state. Trajectories on the L-diagram represent lines of constant  $\Omega/S$ , along which the various points are parameterized by  $N_R$ . Due to the symmetry of the IPS-theory about  $\Omega/S = -0.5$  (see, esp., Eqs. (5.35) and (5.36)), each trajectory corresponds to two values of the relative rotation rate. The trajectories for  $\Omega/S$  and  $-\Omega/S - 1$  are identical. All trajectories are realizable and are attracted to the highlighted line in the figure, which represents the locus of asymptotic states for  $-1.26 < \Omega/S < 0.26$ . The arrows indicate the path that the anisotropy invariants take as they approach the asymptote.

Figure 5.12 is the analog of Figure 5.11 for the decaying homogeneous shear states  $(\Omega/S > 0.26$  and  $\Omega/S < -1.26)$ . For the decaying states, only one region of the L-diagram is inaccessible. As indicated in Figure 5.10, the decaying states all relax towards a one-component turbulence asymptote, with all of the turbulent energy aligned along the rotation axis. All states between the isotropic state and the one-component limit remain realizable.

From the preceding results, it is apparent that a rotation of frame coupled with a mean shear has two significant effects. First, for small absolute relative rotation rates in the asymptotic regime, rotation causes two redistribution effects among the normal components of the Reynolds stress via the isotropic pre-stress:  $R_{zz} \leftrightarrow R_{yy}$  and  $(R_{yy}, R_{zz}) \rightarrow R_{xx}$ . In this case, however, the flow retains the same qualitative character it had in the inertial frame: both k and  $\epsilon$  grow without bound, but at the same relative rates. However, at larger absolute relative rotation rates, the effect of frame rotation drastically affects the turbulent structure. Large rotation rates have the effect of completely cutting off turbulent production due to coupling of the mean shear and Reynolds stress (i.e.  $N_R R_{yz} \rightarrow 0$  rather than  $N_R R_{yz} \rightarrow \text{constant}$ ). This causes the turbulence to decay and, thereby, to transform into a one-component turbulence with  $R_{xx} \rightarrow 1$ . It is noteworthy that

either asymptotic or decay trajectories by the IPS-model remain within the L-diagram, although some of the L-states are only attainable in one of the two regimes. All states predicted by the IPS-theory are realizable.

## 5.5 Anisotropic Pre-Stress Theory for Rotating Homogeneous Shear

The extension of the model predictions for the APS-theory follows directly from the procedure outlined for the IPS-theory. The phenomenological model for the anisotropic pre-stress was developed in Chapter 4. Again, no additional unknown closure terms and/or phenomenological parameters arise in the rotating frame (relative to the inertial frame), so the parameters in Table 4.1 allow the complete description of the rotating homogeneous shear flow.

Eq. (5.25) for the evolution of the relaxation parameter applies as it did previously. However, the asymptotic invariant for the product  $N_R R_{\nu z}$  is now given by

$$(-N_R R_{yz})_a = \frac{C_R (C_D - 1)}{2 (C_P - 1)} = 0.186.$$
 (5.50)

The previous approach for determining the asymptotic states by solving the initial value problem remains valid; however, instead of having one differential equation for  $N_R$  coupled with a set of algebraic equations, additional differential equations are required to determine the anisotropic pre-stress  $\underline{H}$ . Since the model for  $\underline{H}$  is frame invariant, the governing equations have the same form as before (see Eqs. (4.42), (4.45)-(4.47), and (4.50)-(4.52)). Specifically, the four components of the anisotropic pre-stress are governed by the following set of ordinary differential equations:

$$De_{t}\frac{dH_{xx}}{d\xi} + (1+q)H_{xx} - \frac{2}{3}aDe_{t}H_{yz} = 0, \qquad (5.51)$$

# **NOTE TO USERS**

Page(s) were not included in the original manuscript and are unavailable from the author or university. The manuscript was microfilmed as received.

153

**UMI** 

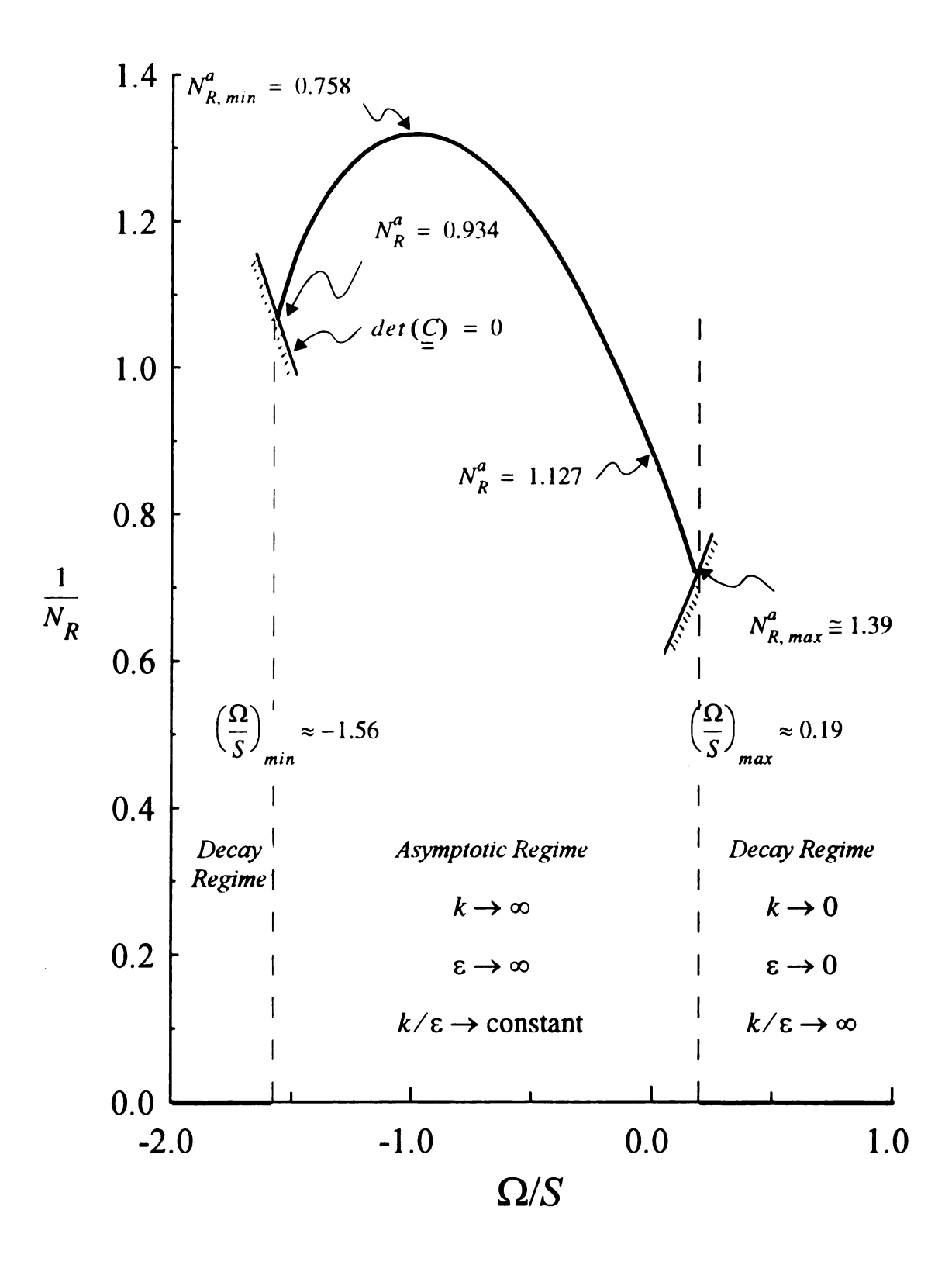


Figure 5.13 The Effect of Rotation on the Turbulent Relaxation Time  $(N_R \equiv \tau_R S)$  for Asymptotic Homogeneous Shear (APS-Theory)

group. The boundaries of the asymptotic regime are shifted  $(-1.56 < \Omega/S < 0.19)$  in the asymptotic regime), but, more significantly, the symmetry about  $\Omega/S = -0.5$  no longer occurs.

Figures 5.14 and 5.15 show how the components of the Reynolds stress and the anisotropic pre-stress are distributed in the asymptotic regime. Figure 5.15 indicates that, even though the phenomenological equation governing H is frame indifferent, the implicit dependence of H upon the frame due to the coupling with the relaxation group causes the pre-stress anisotropy to vary with  $\Omega/S$ . From Eqs. (5.11)-(5.14), it is seen that the anisotropic pre-stress serves to systematically increase the levels of  $R_{zz}$  and  $R_{yz}$ , while  $R_{xx}$  and  $R_{yy}$  are systematically decreased. These trends directly result in the destruction of the symmetry property that existed for the IPS-theory about the point  $\Omega/S = -0.5$ .

Figures 5.16 and 5.17 show the asymptotic states for the APS-theory on the energy simplex and the L-diagram. The locus of asymptotic states on the energy simplex further illustrates the asymmetry of the energy distribution illustrated by Figure 5.14. Qualitatively, the trend of redistributing the turbulent kinetic energy into the component of the Reynolds stress along the rotation axis is seen again at the boundaries of the asymptotic regime. The broken symmetry is less pronounced on the L-diagram, although it is seen slightly due to the fact that points along the locus of asymptotic states are no longer parameterized by two values of  $\Omega/S$ ; for the APS-theory, each point is characterized by a unique value of  $\Omega/S$ .

The trajectories for the APS-theory are not presented in the same detail as for the IPS-theory. The purpose of these calculations was to demonstrate the qualitative differences between the asymptotic and decay regimes. The transition between these two regimes is controlled by the behavior of the product  $N_R R_{yz}$  (see Eqs. (5.38)-(5.40)). Although the asymptotic growth rates of k,  $\epsilon$ , and Re have different numerical values for the two theories (a value of 0.374 vs. 1.024, see Eq. (5.41)), the qualitative features of the flow remain unchanged. Figure 5.18 shows the effect of rotation on the relaxation group  $N_R$  for

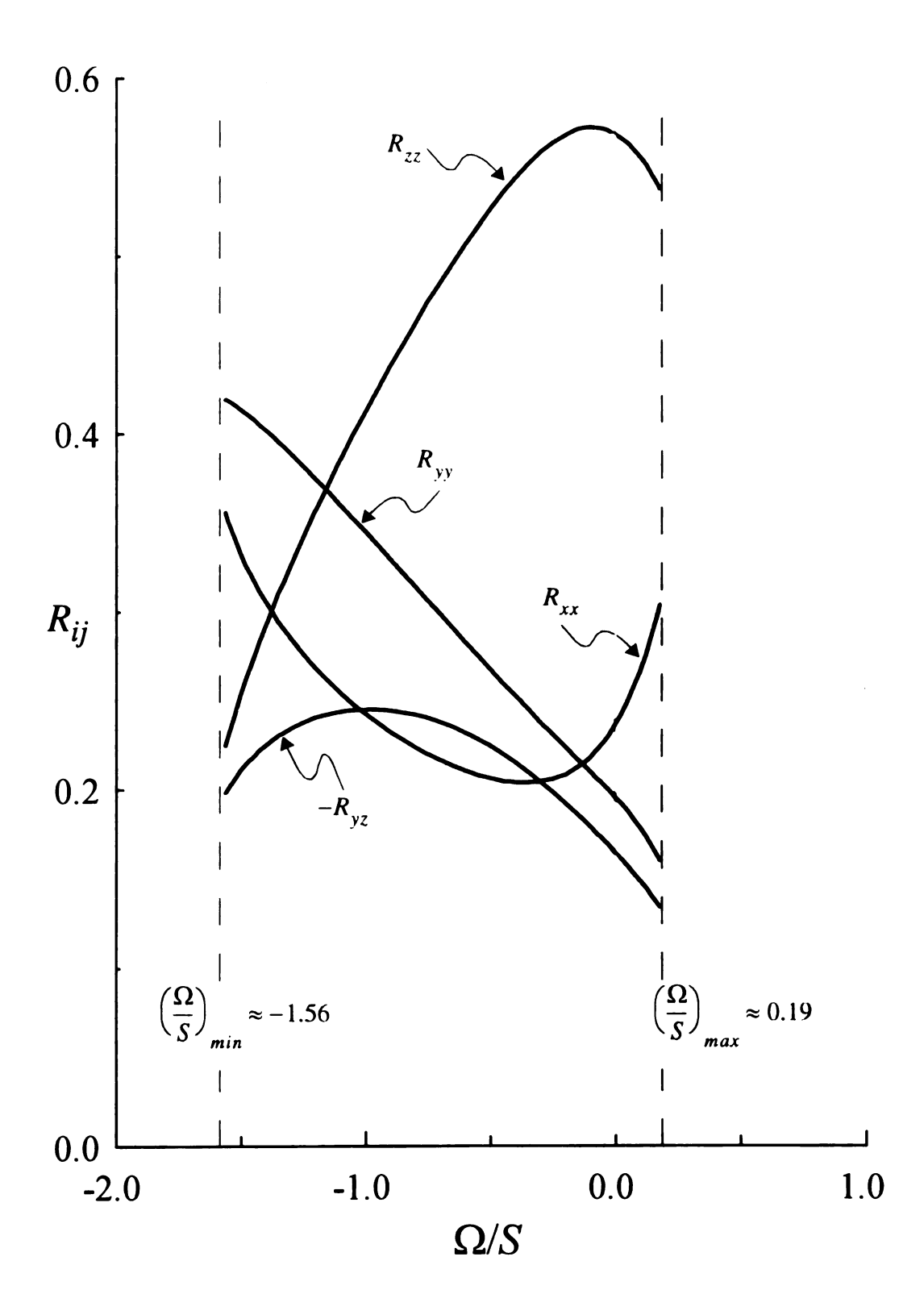


Figure 5.14 The Effect of Rotation on the Components of the Asymptotic Reynolds Stress for Homogeneous Shear (APS-Theory)

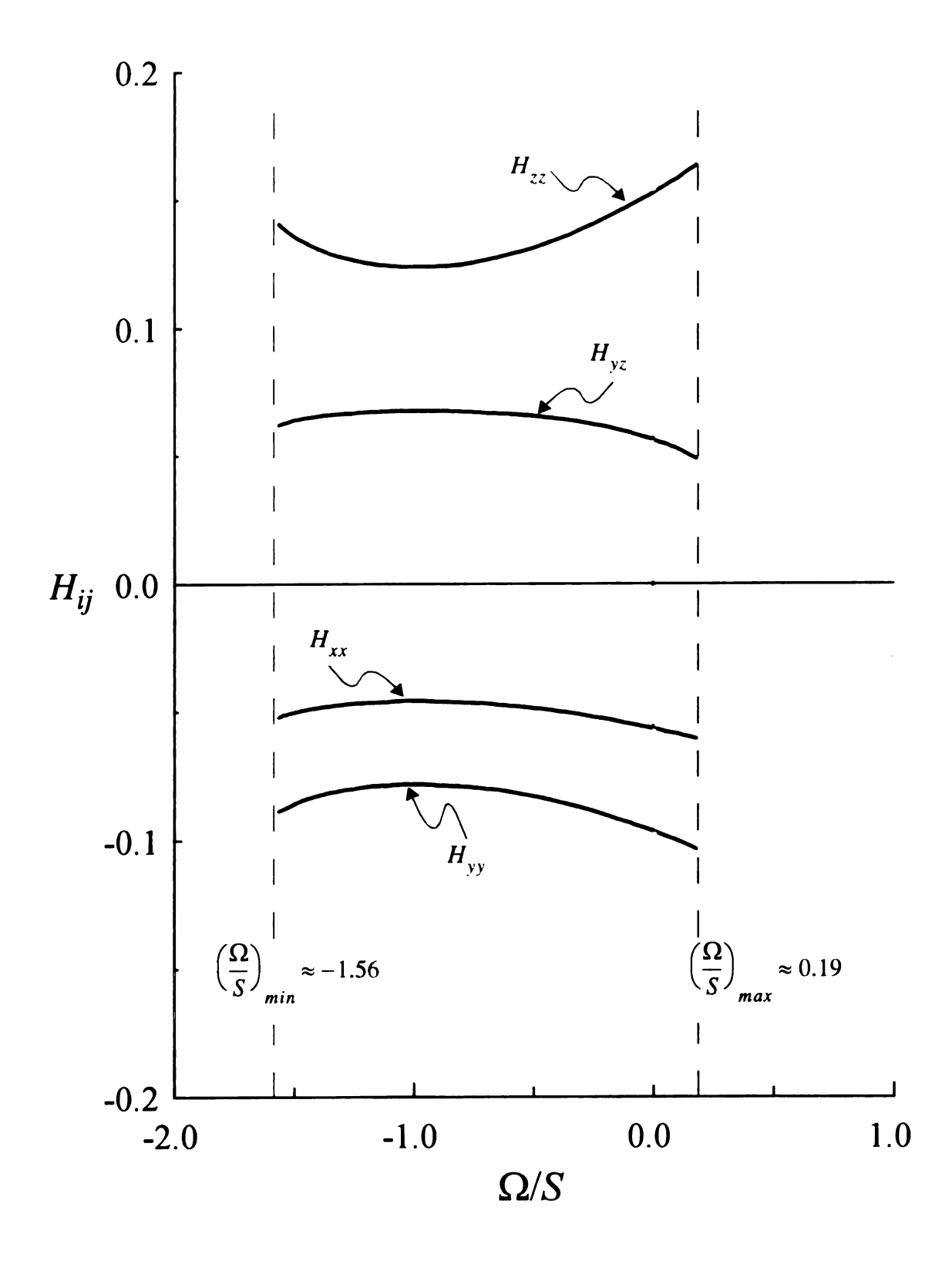


Figure 5.15 The Effect of Rotation on the Asymptotic Pre-Stress Anisotropy for Homogeneous Shear (APS-Theory)

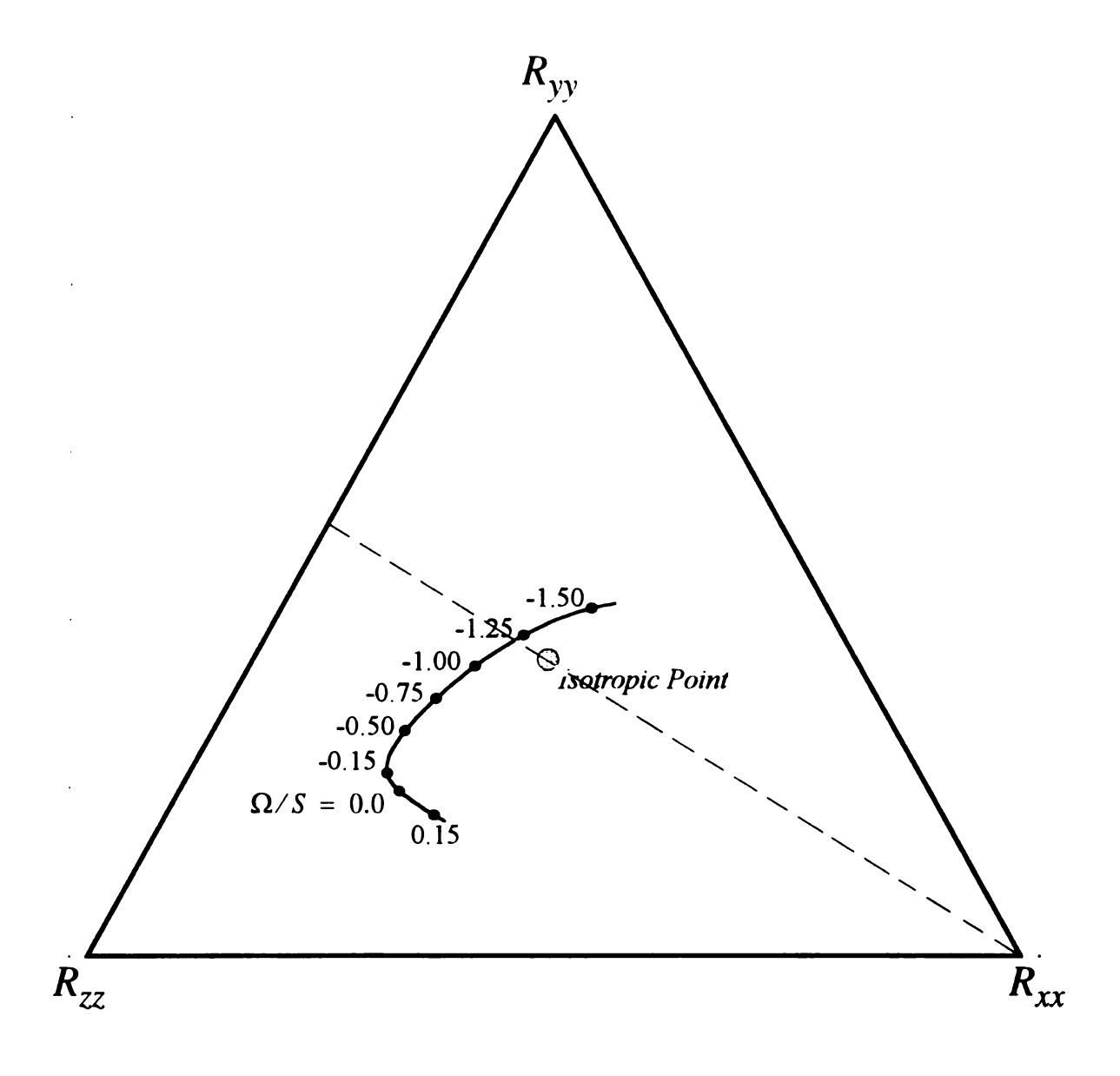


Figure 5.16 Distribution of the Energy Components for Homogeneously Sheared Turbulence in a Rotating Frame (APS-Theory).

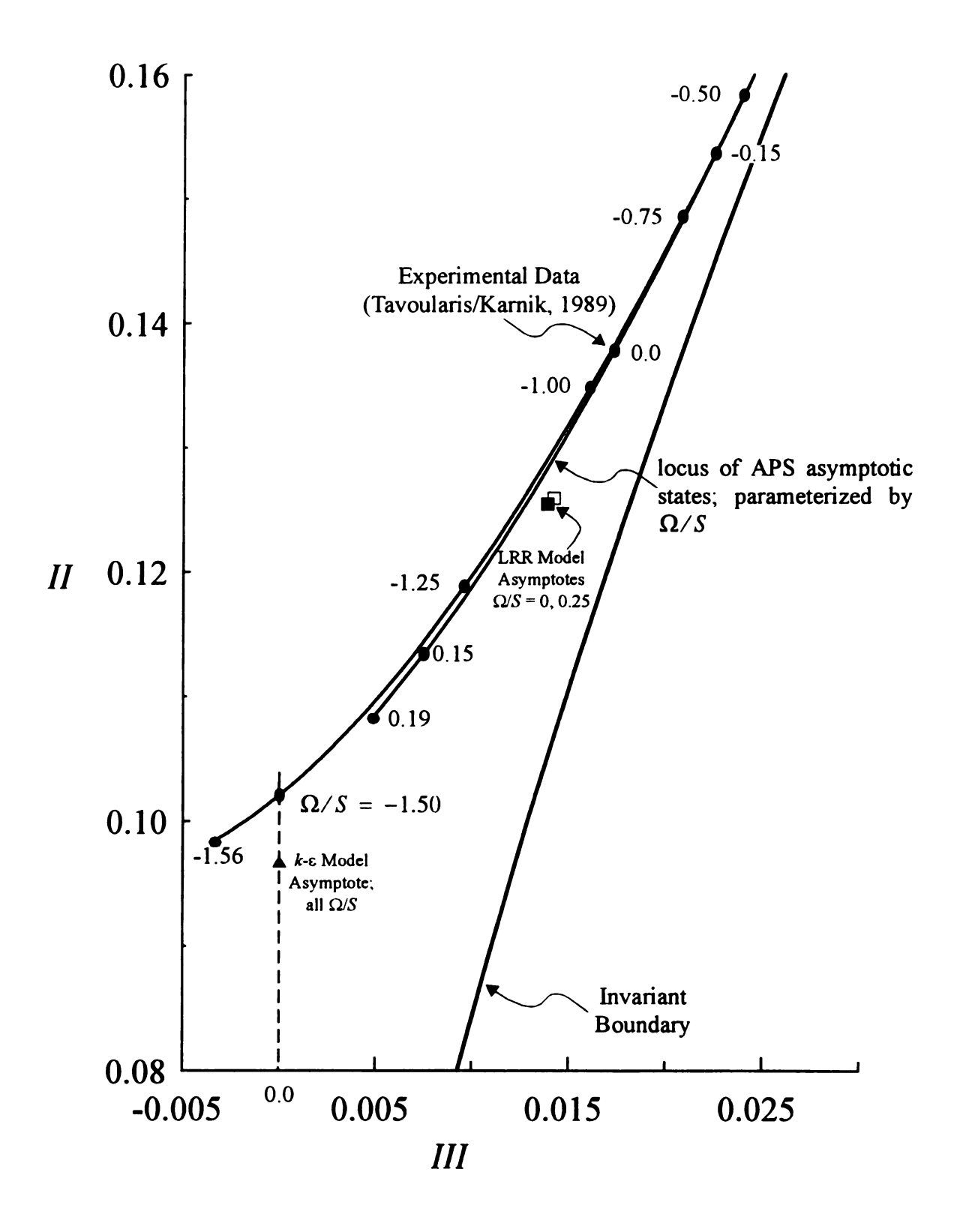


Figure 5.17 Asymptotic Anisotropy Invariants for Homogeneously Sheared Turbulence in a Rotating Frame (APS-Theory).

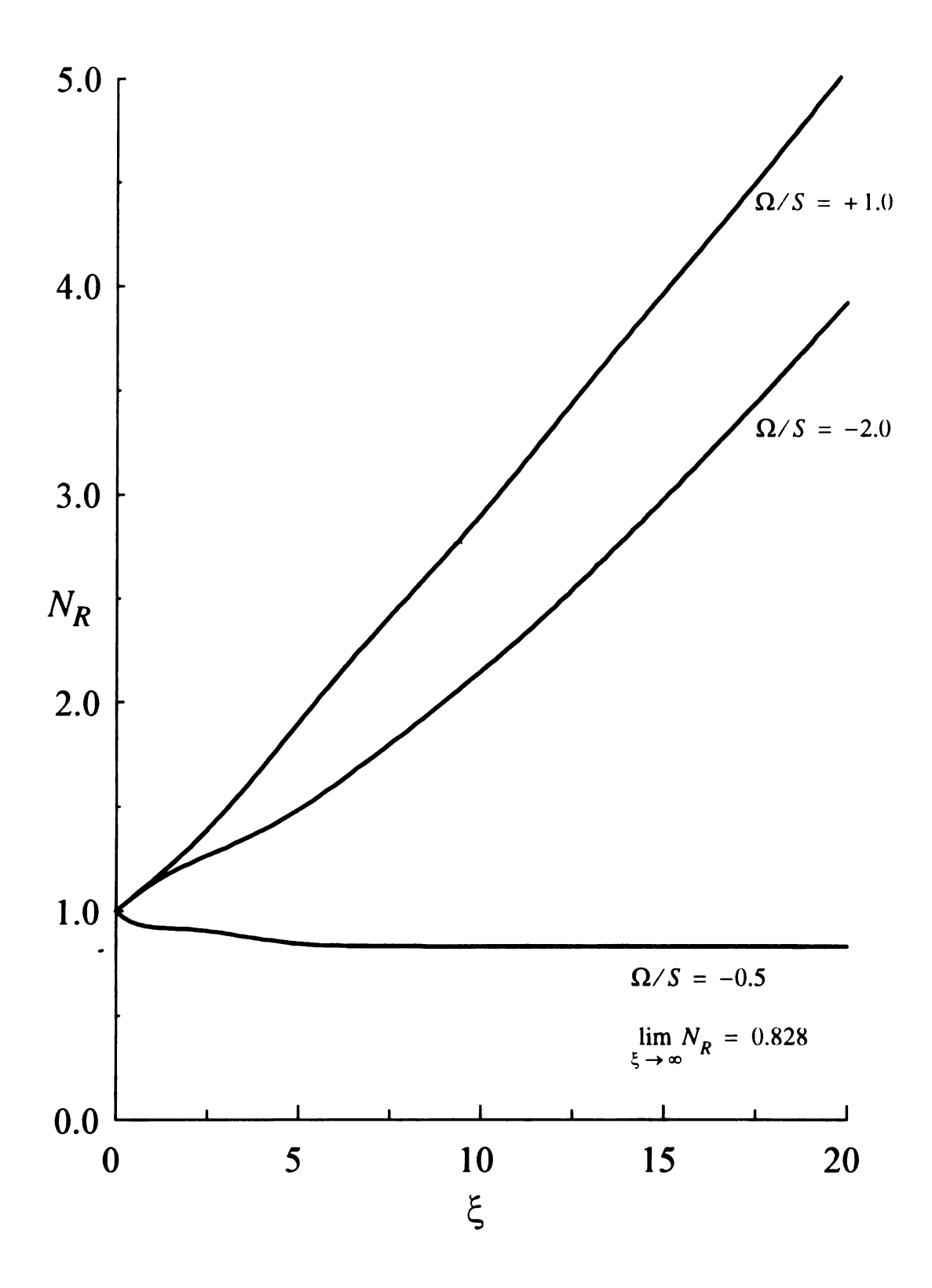


Figure 5.18 Transient Response of the Relaxation Group for Homogeneously Sheared Turbulence in a Rotating Frame (APS-Theory,  $N_R^o = 1.0$ ;  $\underline{\underline{H}}^o = 0$ ).

 $\Omega/S = -2.0$ , -0.5, 1.0. As before, the *stable* trajectory approaches its asymptote in roughly ten time units, while the two cases in the decay regime exhibit unbounded growth. The lack of symmetry is also evidenced in this plot by the different growth rates of  $N_R$  for the two cases  $\Omega/S = -2.0$  and +1.0.

## 5.6 Conclusions

Both the IPS- and APS-theories predict two distinct regimes for homogeneously sheared turbulence in a rotating frame of reference. In an intermediate range of relative rotation rates, i.e.  $(\Omega/S)_{min} < \Omega/S < (\Omega/S)_{max}$ , an asymptotic regime is observed in which both the turbulent kinetic energy and dissipation grow without bound, but at the same relative rates. In this regime, the isotropic portion of the pre-stress serves to redistribute the components of the Reynolds stress as a function of  $\Omega/S$  and  $N_R R_{yz}$  approaches a constant independent of  $\Omega/S$ .

For  $\Omega/S < (\Omega/S)_{min}$  and  $\Omega/S > (\Omega/S)_{max}$ , the two closure theories examined predict a qualitative change in the nature of the flow. The presence of large absolute relative rotation rates completely eliminates turbulent production (i.e.  $N_R R_{yz} \to 0$  for large development times, rather than  $N_R R_{yz} \to \text{constant}$ ). Thus, the turbulence becomes uniformly decaying, with all of the turbulent energy being aligned along the axis of rotation.

The nature of the pre-closure operator A combined with the isotropic pre-stress assumption yields a symmetry property for the asymptotic state about  $\Omega/S = -0.5$ . Subsequent introduction of an anisotropic pre-stress with non-zero normal stress differences breaks this symmetry property.

The IPS-theory is shown to predict only realizable states for  $-\infty < \Omega/S < \infty$  and is seen to span the entire L-diagram of anisotropic stress invariant pairs. Certain regions of

the L-diagram are only accessible to the asymptotic or decaying turbulent regimes. The asymptotic states of the APS-theory are verified a posteriori to be realizable.

#### **CHAPTER 6**

### **CONCLUSIONS**

The concept of realizability was addressed for each of the homogeneous flows studied herein. Specifically, it was desired to construct a turbulence model which would only predict realizable turbulent states. Where possible, this quality was verified a priori. When the nature of the governing equations did not permit such an analysis, the realizability of the turbulent states was verified a posteriori.

For the problem of isotropically decaying turbulence, the decay coefficient  $C_D$  in the dissipation equation was selected to generate a realizable decay process for  $0 < Re < \infty$ . Specifically, if  $1 < C_D(Re) < 2$ , both k and  $\varepsilon$  are decaying and non-negative. In the final form of the model,  $C_D(Re)$  ranges between 1.4 and 1.83, guaranteeing a realizable decay. Similarly, the algebraic nature of the pre-closure when applied with the isotropic pre-stress assumption yielded a Reynolds stress tensor which was realizable for all values of the relaxation group  $0 < N_R < \infty$ . This is due to the fact that the pre-closure has the property that, given non-negative eigenvalues for the pre-stress, the Reynolds stress will also have non-negative eigenvalues. Thus, since the eigenvalues for the IPS-theory are always positive, realizability is preserved for all turbulent states characterized by a given value of  $N_R$ . With the anisotropic pre-stress theory, however, the coupling of the ODEs for the anisotropic pre-stress H and the algebraic pre-closure equations for R did not present a priori evidence that the solutions are always realizable. However, it was found by computation that the transient and asymptotic states were always realizable for all

realizable initial conditions tested (i.e.  $0 < N_R^o < 10$ ).

A semi-theoretical treatment of the Kármán-Howarth equation for isotropic turbulence yielded a prediction of the dissipation destruction coefficient  $C_D(Re)$ . The predicted destruction coefficient utilizes two limiting values:  $C_D(0)=1.4$  based on the final decay data of Batchelor and Townsend (1948); and,  $C_D(\infty)=1.83$  based on the high Reynolds number data of Comte-Bellot and Corrsin (1971). Notable is the fact that the predicted form of the dissipation destruction coefficient does not exhibit a monotonic progression between the two limits, as is the case in other, empirical approaches to this problem (see Hanjalic and Launder, 1976; Lumley, 1978). This functional form was then applied to various experimental and direct simulation data sets and was found to be capable of quantitatively reproducing the decay process over a wide range of initial turbulent Reynolds numbers:  $7.5 < Re_o < 750$ .

The application of the isotropic pre-stress theory to the problem of homogeneously sheared turbulence was found to yield a significant improvement compared to Boussinesq-type turbulence models in that it predicts a non-zero primary normal stress difference as a direct result of the pre-closure theory. Specifically, the primary normal stress difference receives contributions from both the isotropic and anisotropic portions of the pre-stress (see Eq. (4.38)). Thus, even though  $\frac{H}{E} = \frac{0}{2}$  in this case, the isotropic prestress contribution  $(\alpha/k)$  provides a non-trivial primary normal stress difference. The development times required for the turbulence to approach its asymptotic state are in close agreement with those times found in experimental treatment of homogeneous shear, being on the order of 10 dimensionless developmental time units  $(zS/\langle u_z\rangle)$ . The prediction of a non-zero second normal stress difference was not possible without some contribution from the anisotropic portion of the pre-stress (see Eq. (4.39)).

In order to capture this second normal stress difference as well as to reproduce the relaxation effects seen in the return-to-isotropy experiments, the anisotropic portion of the pre-stress was modeled phenomenologically with an objective convected time derivative

which included both pre-stress relaxation and linear mean strain coupling effects. This allowed the exact reproduction of the experimentally observed asymptotic state, which was not possible with the isotropic pre-stress assumption. It was found that coupling of the relaxation and linear strain-coupling effects resulted in the fact that both were required in order to reproduce a non-zero second normal stress difference. Additionally, the combination of these two effects results in a transient approach to the asymptotic state which exhibits oscillatory behavior. These oscillations stem from the choice of the convected derivative parameter  $-\sqrt{3} < a < \sqrt{3}$ , which results in imaginary eigenvalues for the system of equations governing the decay process.

The expression of the pre-stress  $\tau_R^2 \langle f \underline{f} \rangle$  in terms of an isotropic portion  $(2\alpha/3)I$  and an anisotropic portion 2kH results in two qualitatively different responses to an external mean shear. The isotropic portion, which is determined algebraically and is derived from the pre-closure without any additional closure hypothesis, results in a "fast" response to an external mean shear. The decision to include the phenomenological effect of relaxation in the model for the anisotropic pre-stress, however, results in a "slow" response to a mean shear, causing the turbulence to evolve transiently through time.

The application of the pre-closure theory to homogeneously sheared turbulence in a rotating frame of reference was found to predict two qualitatively different asymptotic states as a function of the ratio of the frame rotation rate to the mean shear rate  $(\Omega/S)$ . For intermediate  $\Omega/S$  (i.e.  $-1.26 < \Omega/S < 0.26$  for the IPS-theory), the turbulence maintains the character it displays in the inertial frame: both k and  $\epsilon$  grow without bound and  $k/\epsilon \rightarrow$  constant. At large values of  $|\Omega/S|$  (i.e.  $\Omega/S > 0.26$  and  $\Omega/S < -1.26$  for the IPS-theory), however, the turbulence changes to a uniformly decaying process. This exchange is caused by a concentration of turbulent energy along the axis of rotation, which effectively eliminates turbulent production, leaving only turbulent destruction effects. Additionally, the IPS-theory is found to yield realizable predictions for all  $-\infty < \Omega/S < \infty$ , again owing to the character of the pre-closure which preserves the trait

of positive eigenvalues in the pre-stress.

The qualitative features mentioned above apply equally to both the isotropic and anisotropic formulations for the pre-stress. Small quantitative differences exist, such as the exact values of  $\Omega/S$  which delineate the boundaries between the asymptotic and decay regimes. For instance, the asymptotic regime for the APS-theory exists over the range  $-1.56 < \Omega/S < 0.19$ , which is similar to the range for the IPS-theory given above. The salient difference between the two theories lies in the symmetry property exhibited by IPS-theory about  $\Omega/S = -0.5$  which is not present in the APS-theory. This is due exclusively to the fact that the pre-stress is no longer isotropic (i.e.  $H \neq 0$ ) and its components provide contributions to the Reynolds stress components which are not all equal.

A major portion of this work has been dedicated to the development and evaluation of two closure hypotheses for the pre-closure theory developed in Chapter 3. The isotropic pre-stress (IPS-) theory was initially investigated because it introduced no additional closure hypotheses. This was then extended to an anisotropic pre-stress (APS-) theory in order to capture relaxation effects as well as a second normal stress difference for simple shear flows. In retrospect, however, each of the two closure theories has its own distinctive advantages and disadvantages.

For instance, the IPS-theory represents a significant improvement over the traditional Boussinesq approach; in a simple shear flow, the IPS-theory is uniformly realizable and predicts a non-zero primary normal stress difference. Relative to the APS-theory, the algebraic character of the IPS-theory may make it more attractive for use in practical applications. Although a 3x3 matrix inversion must be performed at each discrete point in a given domain, no additional differential equations beyond the four required for the continuity equation and the equation of motion are needed. This is a computational advantage compared to both the APS-theory as well as other traditional second-order Reynolds stress modeling approaches, which require the solution of an additional six

differential equations in the most general case. Additionally, the algebraic nature of the IPS-theory lends itself more readily to theoretical analysis. For instance, it is possible to demonstrate a priori that the IPS-theory predicts only realizable states for homogeneous shear flows and that the entire Lumley diagram is accessible to the theory, with each point therein being parameterized by one or more pairs of values for  $(N_R, \Omega/S)$ .

In contrast the APS-theory expands upon the predictive capabilities of the IPS-theory by providing additional degrees of freedom in terms of model parameters which allow it to capture more physical effects. For example, the phenomenological model for the anisotropic pre-stress is able to reproduce both the relaxation effect seen in return-to-isotropy as well as the second normal stress difference exhibited in homogeneous shear flows. As mentioned above, however, this improved predictive capabilities come at the cost of additional differential equations for each of the six anisotropic pre-stress components. Not only would this greatly increase the computational burden for more complex flow simulations, but, from a theoretical standpoint, also makes analysis and interpretation of results more complicated.

## **CHAPTER 7**

#### RECOMMENDATIONS

## 7.1 Further Study

The analysis of the Kármán-Howarth equation involved the semi-empirical expression of several integral properties of the double and triple longitudinal velocity correlations. While there is not the expectation that the absolute values of the integrals themselves are necessarily correct, the working hypothesis is that the integral ratios, as they appear in the analysis of the Kármán-Howarth equation, are reasonably well characterized. Either direct simulation or experimental measurements of isotropically decaying turbulence could be applied in order to estimate the extent to which these integral properties are adequately represented, provided that both the double  $(B_{LL})$  and triple  $(T_{LLL})$  longitudinal velocity correlations are accurately determined (cf. Eqs. (2.36)-(2.38)).

With this simulation and/or experimental data, the validity of the modeled ratios  $I_2/I_1$  (see Eq. (2.63)) and  $I_3/I_1$  (see Eq. (2.71)) which appear in the modeled form of the IKH-equation (Eq. (2.44)) may be verified directly, as the parameters Re, P, and B can all be derived from the velocity correlation data. The variation of the integral parameter  $I_1$  with the turbulent Reynolds number (or, equivalently, within the context of this theory, the destruction coefficient B) can be verified by integrating Eq. (2.69):

$$\ln(I_1/I_{1,o}) = -\frac{1}{2} \int_{\delta}^{\delta} \left[ 1 + (a-1) \sqrt{\frac{14}{10\delta}} \right] d\ln(\delta).$$
 (7.1)

Ultimately, the degree to which the integral approximations applied in the theory do or do not agree with experimental values will either lend support to this approach or suggest further avenues for research, in terms of the manner in which the integral ratios are modeled.

The process of return-to-isotropy could be further addressed, as it has been analyzed only for the case of a positive third invariant (the state observed for homogeneous shear in an inertial frame) and has been modeled as a universal constant. There exists a larger body of experimental data which may suggest that either: (1) the time constant for decay is a function of the local turbulent state such that  $C_{\lambda} = C_{\lambda}(II, III, Re)$ ; and/or, (2) the decay process should include both linear and non-linear relaxation effects (Sarkar and Speziale, 1990; Speziale, 1991).

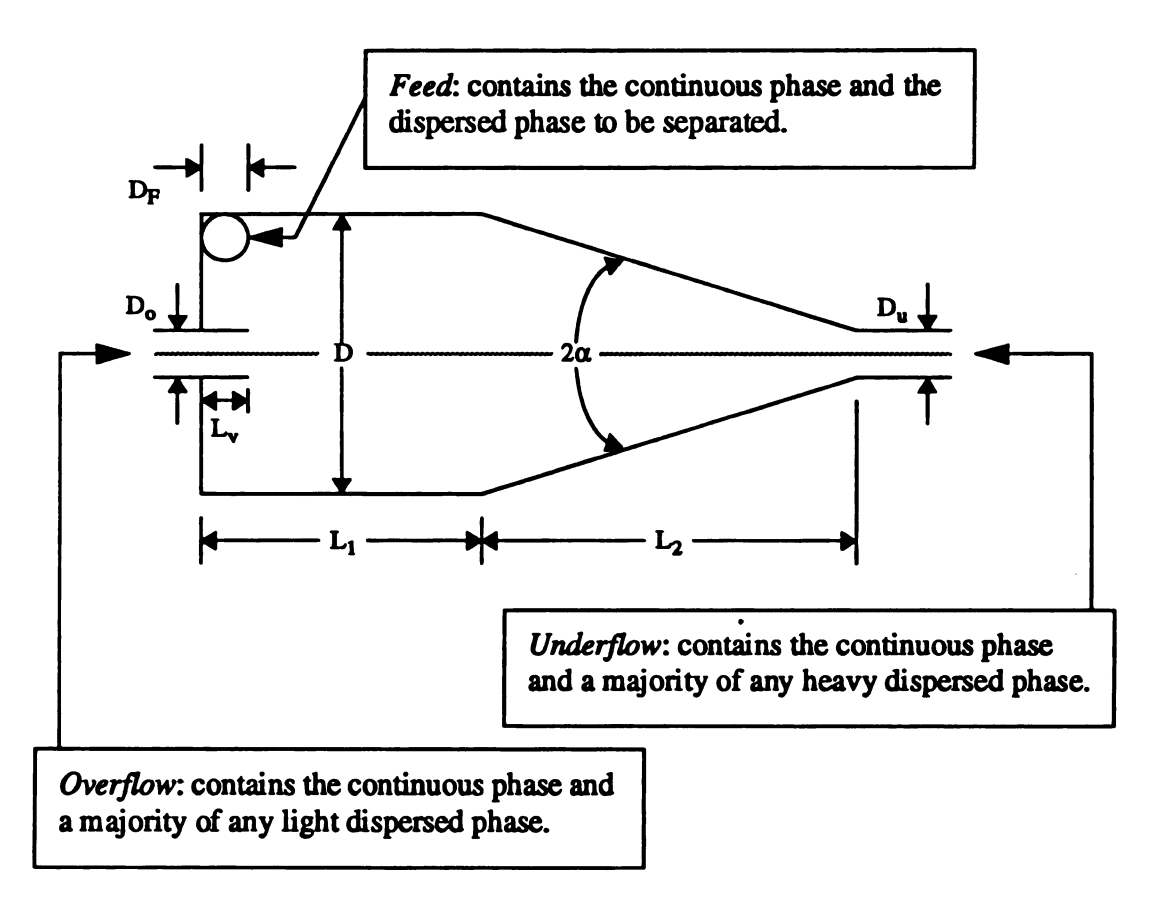
The dissipative time scale in the  $\varepsilon$ -equation has been modeled as  $\tau_D \propto k/\varepsilon$ . This formulation is not capable of explaining the effect of a slower rate of decay of an isotropic turbulence in a rotating frame of reference. Specifically, direct simulations of this flow (Bardina et al., 1985; Speziale et al., 1987) indicate that an increasing rate of frame rotation has a pronounced effect in that it reduces the turbulent dissipation  $\varepsilon$ , causing the turbulent kinetic energy k to persist over a longer period of time. This flow is governed by a system of two ordinary differential equations, one each for k and  $\varepsilon$ . The equation governing the turbulent energy (see Eq. (2.2)), however, is exact and has no explicitly frame-dependent terms. Therefore, this increased persistence of turbulent energy must be localized to the modeled equation for the turbulent dissipation (see Eq. (2.4)). It is thus suggested that the  $\varepsilon$ -equation be revisited and the characteristic time scale  $\tau_D$  be modified to include frame-dependent effects.

## 7.2 Further Application

The work contained herein was primarily aimed towards achieving Objectives (i)-(iv) in Section 1.2. That is, theoretical problems were selected such that each of these four issues could be isolated or built upon based on previous results within the dissertation. For example, the flows of isotropic decay and return-to-isotropy allow the determination of the model parameters  $C_D$  and  $C_\lambda$ , respectively, independent of all other model parameters. With this basis, the application of the APS-theory to homogeneous shear flow then allows the final calibration of model parameters to achieve the goal of accurately representing both the primary and secondary normal stress differences.

Objective (v), i.e. universality, however, is not addressed directly in this work. This question can be answered through the further application of the APS-theory to other test flows with a subsequent comparison of the predictions with known results. Of course, the extent to which the mean field and turbulent quantities agree with experimental values is important. However, other questions also arise. For example, for a given flow, what restrictions, if any, are required to ensure realizability or to ensure that the pre-closure operator  $\underline{\underline{A}}$  (see Eq. (4.1)) is invertible. Of course, an additional test of universality is the application of the theory to a practical application of engineering significance. Since this study was, in part, motivated by the poor performance of the Boussinesq theory in flows with streamline curvature, a cyclone would be an ideal case for testing the developed model.

The cyclone as a centrifugal separator has a wide variety of separation and classification functions. A generic cyclone with its relevant dimensions is shown in Figure 7.1. A classical application for a cyclone is the separation of particulate solids from a gas or liquid medium. Another example is the use of a hydrocyclone for liquid/liquid separations. For this application, there generally exists a relatively small centrifugal



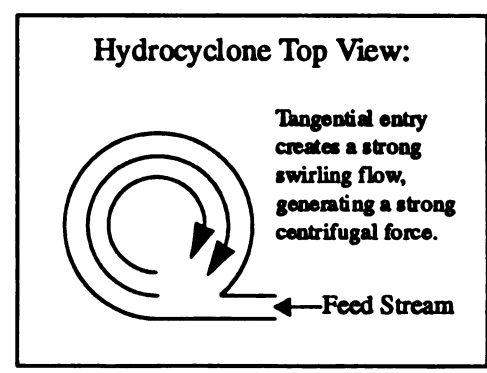


Figure 7.1 Qualitative Sketch of a Hydrocyclone Centrifugal Separator

driving force due to the small density difference between the two liquid phases (typically ~ 0.2 g/ml). While it is generally true that the ability to accurately predict the interior flow patterns may aid in cyclone design, this capability is more important in the liquid/liquid separator. The large density difference in a solid/fluid cyclone can yield acceptable separation efficiencies for a wide range of operating parameters. Because this density difference is so small for the liquid/liquid application, however, it is important to be able to characterize the interior flow within the hydrocyclone in order to potentially maximize the separation driving force provided by the interior flow.

There are several characteristics common to cyclone flows. In general, they are all high Reynolds number flows with a significant swirl component. This swirl flow is a Rankine-type vortex with a forced vortex structure along the cyclone core and a free-like vortex structure in the outer region. Although the flow may be adequately characterized as axisymmetric, an undulating axial velocity profile combined with toroidal recirculation zones makes for a fully three-component flow field.

Despite the challenges that swirling flows present towards modeling, there exists a need for a practical engineering model which can accurately predict not only mean field quantities, but also turbulence quantities. An accurate turbulence model is instrumental in providing much of the information required to predict hydrocyclone separation efficiencies. Specifically, a converged solution to a turbulent flow problem provides both information concerning the mean field velocities and pressure as well as the six components of the Reynolds stress. The role of these terms becomes apparent when one examines the equation governing the acceleration of a dispersed phase particle (in a Lagrangian frame: Brodkey, 1967):

$$m_{d} \frac{dv}{dt} = 3\pi\mu d(v - u) - \frac{m_c}{\rho_c} \nabla p + \frac{m_c}{2} \left[ \frac{dv}{dt} - \frac{\partial u}{\partial t} - v \cdot \nabla u \right]. \tag{7.2}$$

In the above equation,  $\underline{v}$  is the dispersed phase velocity and  $\underline{u}$  the continuous phase

velocity. Similarly,  $m_d = (\pi d^3 \rho_d)/6$  and  $m_c = (\pi d^3 \rho_c)/6$  represent, respectively, the mass of a spherical volume of diameter d for the dispersed and continuous phase.

Eq. (7.2) relates the acceleration of the dispersed phase particle acceleration to the Stokes' drag force, the fluid pressure gradient, and the added mass effects. Eq. (7.2) does not include the Basset term, nor does it account for particle-particle interactions or drop coalescence/break-up/deformation. The application of Eq. (7.2) allows one to compute dispersed phase trajectories as a function of particle size which further permits the prediction of separation efficiencies given an inlet feed size distribution.

Eq. (7.2) is written for the instantaneous particle and continuous phase velocities, but a turbulence model yields mean field quantities. There are two ways to proceed from this starting point. Integration of the particle trajectory equations several times for a given initial position and particle size would allow the formation of an ensemble mean collection probability. In this case, the instantaneous fluid velocity at a given location for a given component is computed in an *ad hoc* manner as the mean plus a random fluctuation proportional to the *rms* value of the fluctuations. This is the approach of Boysan, *et al.* (1982) and Hargreaves and Silvester (1990). An alternate method entails the Reynolds averaging of Eq. (7.2) in order to form the equation for the mean particle acceleration. In this case, there arises the following term which is not a result of the turbulence model predictions and must therefore be further modeled:

$$\langle \underline{v} \cdot \nabla \underline{u} \rangle = \langle \underline{v} \rangle \cdot \nabla \langle \underline{u} \rangle + \langle \underline{v}' \cdot \nabla \underline{u}' \rangle. \tag{7.3}$$

From Eq. (7.2), the role of the individual mean velocity components upon the separation is evident. Among the three mean velocity components, a good quantitative prediction of the tangential velocity  $\langle u_{\theta} \rangle$  is key, as the separation force is proportional to the swirl velocity, squared. The axial velocity  $\langle u_{z} \rangle$  is also influential in that it largely determines the residence time of a dispersed phase particle in the cyclone which correlates

with the time available for separation. The radial velocity  $\langle u_r \rangle$  is important in that it is the reference velocity against which the drift velocity is computed and can also have an effect on recirculation flows that can either work for or against the separation. With accurate computations of the complete mean velocity field, one can estimate dispersed phase trajectories as a function of particle size in order to evaluate a cyclone's performance given a dispersed phase of a specified density and size distribution. Determination of the mean pressure distribution in the cyclone facilitates the computation of the power requirement for pumping the fluid through the unit operation.



# Appendix A: Navier-Stokes Equations in a Rotating Frame of Reference

The governing equations which are applied in turbulent flow situations stem directly from the instantaneous continuity equation and the Navier-Stokes equations. These are based on a mass and a momentum balance on an infinitesimal fluid element, respectively (Bird, et al., 1960). In a rotating frame of reference, the terms representing the centrifugal and Coriolis forces which arise may be referenced from Greenspan (1968):

$$\nabla \cdot \boldsymbol{u} = 0 \tag{A.1}$$

and

$$\frac{D\underline{u}}{Dt} + 2\underline{\Omega} \times \underline{u} = -\nabla P_r + \nu \nabla^2 \underline{u}. \tag{A.2}$$

In Eq. (A.2), the substantial derivative is the instantaneous substantial derivative, i.e.  $D/Dt \equiv \partial/\partial t + \underline{u} \cdot \nabla$ . In the Navier-Stokes equation (Eq. (A.2)), it is important to note that body forces (such as gravity) are not shown. Secondly, a homogeneous density is assumed, such that  $P_r$  is actually the kinematic reduced pressure, defined by

$$P_{r} = \left(\frac{p_{r}}{\rho}\right) = \left(\frac{p}{\rho}\right) - \frac{1}{2}\left(\underline{\Omega} \times \underline{r}\right) \cdot \left(\underline{\Omega} \times \underline{r}\right). \tag{A.3}$$

Eqs. (A.1) and (A.2) can be written in terms of mean field quantities by introducing the Reynolds decomposition. Explicitly, for the pressure and velocity, this decomposition is

$$\underline{u} = \langle \underline{u} \rangle + \underline{u}' \tag{A.4}$$

and

$$p = \langle p \rangle + p'. \tag{A.5}$$

These expressions may be subsequently inserted into the instantaneous equations and then averaged as per Hinze (1975). This results in the final governing equations: the mean continuity equation

$$\nabla \cdot \langle u \rangle = 0, \tag{A.6}$$

and the Reynolds-averaged equation of motion

$$\frac{D\langle \underline{u} \rangle}{Dt} + 2\underline{\Omega} \times \langle \underline{u} \rangle = -\nabla \langle P_r \rangle + \nu \nabla^2 \langle \underline{u} \rangle - \nabla \cdot \langle \underline{u}' \underline{u}' \rangle. \tag{A.7}$$

In Eq. (A.7), the term D/Dt now represents the substantial time derivative associated with the mean velocity field:  $D/Dt \equiv \partial/\partial t + \langle u \rangle \cdot \nabla$ . The last term in Eq. (A.7) is the Reynolds stress. These equations represent a system of four scalar equations for ten unknowns: mean velocity (3), mean pressure (1), and the symmetric Reynolds stress tensor (6). It is this unclosed nature of the governing equations which necessitates turbulence modeling. That is, given a phenomenological or theoretical expression for the Reynolds stress in terms of mean field quantities, Eqs. (A.6) and (A.7) would be closed.

In this example, a transport equation has been developed for the mean velocity, but contains unspecified second-order moments. In general, were an equation for an arbitrary  $n^{\text{th}}$ -order moment to be developed, it would contain unknown moments of order (n+1). The derivation for the transport equation for second-order moments is given in Appendix B.

# Appendix B:Reynolds Stress Equations in a Rotating Frame of Reference

The derivation for the equation governing the Reynolds stress  $(\langle \underline{u}'\underline{u}'\rangle)$  begins with the equation for the fluctuating velocity  $(\underline{u}')$ . This equation is formed by subtracting the Reynolds-averaged equation from the instantaneous (i.e. Navier-Stokes) equation:

$$\frac{D\underline{u}'}{Dt} + 2\underline{\Omega} \times \underline{u}' = -\nabla \frac{\underline{p}'}{\rho} + \nu \nabla^2 \underline{u}' + \nabla \cdot \langle \underline{u}'\underline{u}' \rangle - \underline{u}' \cdot \nabla \underline{u}' - \underline{u}' \cdot \nabla \langle \underline{u} \rangle. \tag{B.1}$$

The fluctuating velocity equation may then be rearranged with all of its terms on one side and written in general operator form:

$$\mathcal{L}(u') = 0. ag{B.2}$$

The equation in this form is the source of both the equations for the Reynolds stress as well as the turbulent kinetic energy and the turbulent dissipation (see Appendix C for the dissipation). The second order transport equation is formed by taking the following moment:

$$\langle \underline{u}' \underline{l} (\underline{u}') + \underline{l} (\underline{u}') \underline{u}' \rangle = \underline{0}. \tag{B.3}$$

The resulting equation is

$$\frac{D\langle \underline{u}'\underline{u}'\rangle}{Dt} + 2\underline{\Omega} \times \langle \underline{u}'\underline{u}'\rangle + 2\left(\underline{\Omega} \times \langle \underline{u}'\underline{u}'\rangle\right)^{T} = -\left[\langle \underline{u}'\underline{u}'\rangle \cdot \nabla \langle \underline{u}\rangle + (\langle \underline{u}'\underline{u}'\rangle \cdot \nabla \langle \underline{u}\rangle)^{T}\right]$$

$$+\langle p'(\nabla \underline{u}' + \nabla \underline{u}'^T)\rangle - \underline{\varepsilon} - \nabla \cdot (\langle \underline{u}'\underline{u}'\underline{u}'\rangle + \langle p'\underline{u}'I\rangle + \langle p'\underline{u}'I\rangle^T) + \nu \nabla^2 \langle u'\underline{u}'\rangle. (B.4)$$

The second term on the LHS of Eq. (B.4) represents a redistribution effect due to the

Coriolis terms in the equation for the velocity. On the RHS of Eq. (B.4), the terms are, respectively: (1) turbulent production due to coupling with the mean shear; (2) pressure-strain redistribution; (3) viscous dissipation; (4) turbulent transport; and, (5) molecular diffusion.

While this research does not apply the Reynolds stress transport equation directly, it does serve as the basis for the k-equation. The turbulent kinetic energy is defined as

$$2k \equiv \langle u' \cdot u' \rangle. \tag{B.5}$$

Thus, the contraction of the Eq. (B.4) yields the k-equation.

$$\frac{Dk}{Dt} = -\langle \underline{u}'\underline{u}' \rangle : \nabla \langle \underline{u} \rangle - \varepsilon - \nabla \cdot (\frac{1}{2} \langle (\underline{u}' \cdot \underline{u}') \underline{u}' \rangle + \langle p'\underline{u}' \rangle) + \nu \nabla^2 k.$$
 (B.6)

Each of the terms on the RHS of Eq. (B.6) are the scalar analogs of the terms in Eq. (B.4). An advantage of the k-equation is that the pressure-strain term, which is the focus of most second order modeling approaches, is identically equal to zero due to incompressibility. The only term which is unclosed is the diffusion term, being generally modeled with some form of gradient hypothesis (Hanjalic and Launder, 1972). It is also important to note that, although the Reynolds stress equation is frame dependent, there is no explicit appearance of the frame rotation rate in the kinetic energy equation. This is important, as it implies that rotation only serves to redistribute turbulent energy rather than to create or destroy it.

# Appendix C:Turbulent Dissipation Equation in a Rotating Frame of Reference

The second variable required as a turbulent scale-determining parameter is the scalar dissipation rate. Similar to the Reynolds stress equation, the dissipation equation is based on the equation for the fluctuating velocity. In this case, however, an alternate moment is formed (Speziale, 1991):

$$2v\langle \nabla u^{T}: \nabla \mathcal{L}(u^{\prime}) \rangle = 0. \tag{C.1}$$

This yields the following equation for the scalar dissipation rate:

$$\frac{D\varepsilon}{Dt} = P_{\varepsilon} - \Phi_{\varepsilon} + D_{\varepsilon} + \nu \nabla^{2} \varepsilon . \tag{C.2}$$

In Eq. (C.2), the fourth term on the RHS is the molecular transport term, while  $P_{\epsilon}$ ,  $\Phi_{\epsilon}$ , and  $D_{\epsilon}$  represent production, destruction, and turbulent diffusion of dissipation. Their exact expressions are

$$P_{\varepsilon} = -2v\langle\nabla\underline{u}^{T}\cdot\nabla\underline{u}^{T}\cdot\nabla\underline{u}^{T}\cdot\nabla\underline{u}^{T}\cdot\nabla\underline{u}^{T}\rangle:\nabla\langle\underline{u}\rangle-2vtr\Big[\langle\underline{u}^{T}\nabla\underline{u}^{T}\rangle:(\nabla\nabla\underline{u}^{T})^{T}\Big]$$
$$-2v\langle\Big[\nabla\underline{u}^{T}:(\nabla\underline{u}^{T}\cdot\nabla\underline{u}^{T})^{T}\Big]\rangle, (C.3)$$

$$\Phi_{F} = 2v^{2}tr\langle\nabla\nabla\underline{u}':(\nabla\nabla\underline{u}')^{T}\rangle, \qquad (C.4)$$

$$D_{p} = -\nu \nabla \cdot \langle \underline{u}' (\nabla \underline{u}' \cdot \nabla \underline{u}'^{T}) \rangle - 2\nu \nabla \cdot \langle \nabla p' \cdot \nabla \underline{u}' \rangle. \tag{C.5}$$

In the dissipation equation, there is no explicit frame dependance, providing that the dissipation is isotropic. In contrast to the Reynolds stress and k-equations, virtually all of the terms in the dissipation equation must be modeled. Typically, what is done is to

assume that each of the given processes in the dissipation equation are analogous to their k-equation counterpart, scaled by an empirical coefficient and a characteristic turbulent time scale (Hanjalic and Launder, 1972).

# Appendix D:Objectivity of Convected Time Derivatives

The generalized convected derivative is (Denn, 1990; Joseph, 1990):

$$\frac{\delta_a}{\delta t}(\underline{A}) = \frac{\partial A}{\partial t} + \langle \underline{u} \rangle \cdot \nabla \underline{A} - \langle \underline{W} \rangle^T \cdot \underline{A} - \underline{A} \cdot \langle \underline{W} \rangle - a \left[ \langle \underline{S} \rangle \cdot \underline{A} + \underline{A} \cdot \langle \underline{S} \rangle \right], \tag{D.1}$$

where a assumes any value within in the range  $-\infty < a < \infty$  and A is any objective operator:

$$\underline{A}^{\bullet} = \underline{Q} \cdot \underline{A} \cdot \underline{Q}^{T}. \tag{D.2}$$

 $\langle \underline{\underline{S}} \rangle$  is the symmetric, objective portion of the velocity gradient and  $\langle \underline{\underline{W}} \rangle$  is the antisymmetric, frame-dependent portion of the velocity gradient (Bird, et al., 1977):

$$\langle \underline{S} \rangle^{\bullet} = \underline{Q} \cdot \langle \underline{S} \rangle \cdot \underline{Q}^{T} \text{ and}$$
 (D.3)

$$\left\langle \underline{\underline{W}} \right\rangle^{\bullet} = \underline{\underline{Q}} \cdot \left\langle \underline{\underline{W}} \right\rangle \cdot \underline{\underline{Q}}^{T} + \underline{\underline{Q}} \cdot \underline{\underline{Q}}^{T}, \tag{D.4}$$

where  $\underline{Q}$  is a time dependent, proper orthogonal (i.e.  $det(\underline{Q}) = +1$ ) coordinate transformation tensor and  $\underline{\dot{Q}}$  its time derivative:

$$\underline{Q} \cdot \underline{Q}^T = I. \tag{D.5}$$

Eq. (D.1) in a rotating frame of reference is written as

$$\frac{\delta_{a}}{\delta t} \left( \underline{A}^{*} \right) = \frac{\partial}{\partial t} \left( \underline{A}^{*} \right) + \langle \underline{u} \rangle^{*} \cdot \nabla^{*} \underline{A}^{*},$$

$$-\langle \underline{W} \rangle^{*T} \cdot \underline{A}^{*} - \underline{A}^{*} \cdot \langle \underline{W} \rangle^{*} - a \left[ \langle \underline{S} \rangle^{*} \cdot \underline{A}^{*} + \underline{A}^{*} \cdot \langle \underline{S} \rangle^{*} \right]. \quad (D.6)$$

Each of the four terms on the RHS of Eq. (A.6) are summarized below:

I: 
$$\frac{\partial}{\partial t} (\underline{Q} \cdot \underline{A} \cdot \underline{Q}^T) = \underline{Q} \cdot \left[ \frac{\partial}{\partial t} (\underline{A}) \right] \cdot \underline{Q}^T + \underline{\dot{Q}} \cdot \underline{A} \cdot \underline{Q}^T + \underline{\dot{Q}} \cdot \underline{A} \cdot \underline{\dot{Q}}^T,$$
 (D.7)

II: 
$$(\underline{Q} \cdot \langle \underline{u} \rangle \cdot \underline{Q} \cdot \nabla) \cdot (\underline{Q} \cdot \underline{A} \cdot \underline{Q}^T) = (\langle \underline{u} \rangle \cdot \underline{Q}^T \cdot \underline{Q} \cdot \nabla) \cdot (\underline{Q} \cdot \underline{A} \cdot \underline{Q}^T) = \underline{Q} \cdot [\langle \underline{u} \rangle \cdot \nabla \underline{A}] \cdot \underline{Q}^T$$
, (D.8)

III: 
$$(\underline{Q} \cdot \langle \underline{W} \rangle \cdot \underline{Q}^T + \underline{Q} \cdot \underline{Q}^T) \cdot (\underline{Q} \cdot \underline{A} \cdot \underline{Q}^T) - (\underline{Q} \cdot \underline{A} \cdot \underline{Q}^T) \cdot (\underline{Q} \cdot \langle \underline{W} \rangle \cdot \underline{Q}^T + \underline{Q} \cdot \underline{Q}^T) = \underline{Q} \cdot [\langle \underline{W} \rangle \cdot \underline{A} - \underline{A} \cdot \langle \underline{W} \rangle] \cdot \underline{Q}^T - (\underline{Q} \cdot \underline{A} \cdot \underline{Q}^T) - (\underline{Q} \cdot \underline{A} \cdot \underline{Q}^T) \cdot (\underline{D}.9)$$

$$\begin{aligned} \text{IV: } a \Big[ \underline{Q} \cdot \langle \underline{S} \rangle \cdot \underline{Q}^T \cdot \underline{Q} \cdot \underline{A} \cdot \underline{Q}^T + \underline{Q} \cdot \underline{A} \cdot \underline{Q}^T \cdot \underline{Q} \cdot \langle \underline{S} \rangle \cdot \underline{Q}^T \Big] &= \\ a \Big[ \underline{Q} \cdot (\langle \underline{S} \rangle \cdot \underline{A} + \underline{A} \cdot \langle \underline{S} \rangle) \cdot \underline{Q}^T \Big]. \end{aligned} \tag{D.10}$$

Combining Eqs. (D.6) - (D.10) yields

$$\frac{\delta_a^*}{\delta_t} (\underline{A}^*) = \underline{Q} \cdot \left[ \frac{\delta_a}{\delta_t} (\underline{A}) \right] \cdot \underline{Q}^T, \tag{D.11}$$

and the convected time derivative  $\delta_a/\delta t$  is thus objective for any choice of the parameter  $-\infty < a < \infty$ .

Appendix E:

Tables of Referenced Data

Table E.1: Summary of Isotropic Decay Data; Batchelor and Townsend [1948]; M=0.635cm (grid mesh)

U=1	50 cm/s	U = 6	43cm/s	U = 12	U = 1286cm/s		
x/M	k/U²	x/M	k∕U²	x/M	k∕U²		
20	8.81 x 10 <sup>-4</sup>	20	4.85 x 10 <sup>-3</sup>	60	1.84 x 10 <sup>-4</sup>		
40	3.15 x 10 <sup>-4</sup>	40	5.86 x 10 <sup>-4</sup>	80	1.46 x 10 <sup>-4</sup>		
60	2.12 x 10 <sup>-4</sup>	60	3.01 x 10 <sup>-4</sup>	100	1.19 x 10 <sup>-4</sup>		
80	1.49 x 10 <sup>-4</sup>	80	1.99 x 10 <sup>-4</sup>	120	1.00 x 10 <sup>-4</sup>		
100	1.17 x 10 <sup>-4</sup>	100	1.50 x 10 <sup>-4</sup>	140	8.56 x 10 <sup>-5</sup>		
120	9.41 x 10 <sup>-5</sup>	120	1.23 x 10 <sup>-4</sup>	160	7.33 x 10 <sup>-5</sup>		
140	7.44 x 10 <sup>-5</sup>	140	9.76 x 10 <sup>-5</sup>	180	6.39 x 10 <sup>-5</sup>		
160	6.11 x 10 <sup>-5</sup>	160	8.21 x 10 <sup>-5</sup>	200	5.58 x 10 <sup>-5</sup>		
180	5.27 x 10 <sup>-5</sup>	180	7.06 x 10 <sup>-5</sup>	220	4.81 x 10 <sup>-5</sup>		
200	4.68 x 10 <sup>-5</sup>	200	5.96 x 10 <sup>-5</sup>	240	4.24 x 10 <sup>-5</sup>		
220	4.01 x 10 <sup>-5</sup>	220	4.96 x 10 <sup>-5</sup>	260	3.72 x 10 <sup>-5</sup>		
		240	4.55 x 10 <sup>-5</sup>				
		260	4.36 x 10 <sup>-5</sup>				

Table E.2: Summary of Isotropic Decay Data; Comte-Bellot and Corrsin [1971];  $U_o=10m/s$ 

M(cm)	U₀t/M	u <sub>rms</sub> (cm/s)	$\varepsilon(cm^2/s^3)$	$Re_{\lambda}$	Re <sup>†</sup>
5.08	42	22.2	4740	71.6	769
	98	12.8	633	65.3	640
	171	8.95	174	60.7	553
2.54	45	20.5	7540	48.6	354
	120	10.6	731	41.1	253
	240	6.75	145	38.1	218
	385	5.03	48.5	36.6	201

<sup>†:</sup> This column has been appended to the original Table 4 of Comte-Bellot and Corrsin [1971] using the isotropic relation  $(3/20) Re_{\lambda}^2 = Re$ .

Table E.3: Summary of Isotropic Decay Data; Sirivat and Warhaft [1983]; M=2.5cm (grid mesh)

U = 340  cm/s			U = 630cm/s						
ε	ε(	$cm^2/s^3$	)	$k(cm^2/s^2)$	x/M		$\varepsilon (cm^2/s^3)$	)	$k (cm^2/s^2)$
		389			40		2670		
		224			50		1670		
		165			60		1090		
		125			70		796		
		88.8		1.53	80		615		
		74.1			90		473		
		56.4		28.0	100	)	381	T	103
		49.4			110	)	285		
		33.2			125		192		

Table E.4: Summary of Isotropic Decay Data of Speziale et al. [1987];  $Re_0 = 35.1$ 

$\tau (= \varepsilon_o/k_o)$	k/k <sub>o</sub>
0.000	1.000
0.083	0.919
0.167	0.842
0.250	0.774
0.333	0.716
0.417	0.665
0.500	0.625
0.667	0.545
0.833	0.435
1.000	0.435
1.167	0.393
1.333	0.356
1.500	0.323
1.667	0.293
1.833	0.266
2.000	0.242
2.167	0.221
2.333	0.203

Table E.5: Summary of Isotropic Decay Data Bardina et al. [1985];  $Re_o = 45.4$ 

$\tau (=   _o/k_o)$	k/k <sub>o</sub>
0.000	1.000
0.050	0.951
0.100	0.906
0.200	0.821
0.300	0.747
0.400	0.680
0.500	0.620
0.600	0.567
0.800	0.477
1.000	0.405
1.250	0.335
1.500	0.281
1.750	0.240
2.000	0.208
2.500	0.163
3.000	0.134
3.500	0.115
4.000	0.100

Table E.6: Homogeneous Shear Flow Data (Tavoularis and Karnik "A", 1989)

τ	τ <sub>ref</sub>	R <sub>xx</sub>	R <sub>yy</sub>	Rzz	R <sub>yz</sub>	Sk∕e	$N_R^{\dagger}$
8.0	0.0	0.276	0.223	0.501	-0.168	4.09	0.792
10.0	2.0	0.273	0.220	0.506	-0.167	4.10	
12.0	4.0	0.270	0.218	0.512	-0.167	4.12	
14.0	6.0	0.268	0.215	0.517	-0.167	4.13	
16.0	8.0	0.265	0.213	0.523	-0.167	4.14	
18.0	10.0	0.262	0.210	0.528	-0.166	4.15	
20.0	12.0	0.259	0.208	0.533	-0.166	4.16	
22.0	14.0	0.256	0.205	0.539	-0.166	4.17	
24.0	16.0	0.253	0.203	0.544	-0.165	4.18	
26.0	18.0	0.250	0.200	0.550	-0.165	4.19	

 $<sup>\</sup>underline{M}$ : 25.4 mm  $\overline{U}_c$ : 13 m/s S: 84 s<sup>-1</sup>

 $<sup>^{\</sup>dagger}$ : Initial  $N_R$  selected by minimizing the error in the initial state for the Reynolds stress components.

Table E.7: Homogeneous Shear Flow Data (Tavoularis and Karnik "D", 1989)

τ	Tref	R <sub>xx</sub>	R <sub>yy</sub>	R <sub>zz</sub>	R <sub>yz</sub>	Sk/E	$N_R^{\dagger}$
1.0	0.0	0.274	0.295	0.431	-0.188	4.12	0.675
3.0	2.0	0.273	0.267	0.460	-0.183	4.29	
5.0	4.0	0.272	0.241	0.488	-0.178	4.48	
7.0	6.0	0.271	0.214	0.516	-0.173	4.69	
8.0	7.0	0.270	0.200	0.530	-0.170	4.81	

 $\underline{M}$ : 25.4 mm  $\overline{U}_c$ : 13 m/s S: 38.4 s<sup>-1</sup>

 $<sup>^{\</sup>dagger}$ : Initial  $N_R$  selected by minimizing the error in the initial state for the Reynolds stress components.

Table E.8: Homogeneous Shear Flow Data (Tavoularis and Karnik "G", 1989)

τ	Tref	R <sub>xx</sub>	R <sub>yy</sub>	Rzz	R <sub>yz</sub>	Sk/E	$N_R^{\dagger}$
2.0	0.0	0.301	0.268	0.451	-0.167		0.645
4.0	2.0	0.323	0.256	0.461	-0.162		
6.0	4.0	0.345	0.244	0.471	-0.158		
8.0	6.0	0.367	0.232	0.480	-0.153		
10.0	8.0	0.389	0.220	0.490	-0.148		

 $\underline{M}$ : 25.4 mm  $\overline{U}_c$ : 13 m/s S: 39.9 s<sup>-1</sup>

 $<sup>^{\</sup>dagger}$ : Initial  $N_R$  selected by minimizing the error in the initial state for the Reynolds stress components.

Table E.9: Homogeneous Shear Flow Data (Tavoularis and Karnik "TC", 1989)

τ	Tref	R <sub>xx</sub>	R <sub>yy</sub>	R <sub>zz</sub>	R <sub>yz</sub>	Sk/E	$N_R^{\dagger}$
5.0	0.0	0.290	0.206	0.504	-0.146	5.88	0.735
7.0	2.0	0.287	0.202	0.511	-0.145	5.99	
9.0	4.0	0.285	0.197	0.518	-0.143	6.10	
11.0	6.0	0.282	0.194	0.524	-0.141	6.22	
12.8	7.8	0.280	0.190	0.530	-0.140	6.33	

 $\underline{M}$ : 30.5 mm  $\overline{U}_c$ : 12.4 m/s S: 46.8 s<sup>-1</sup>

 $<sup>^{\</sup>dagger}$ : Initial  $N_R$  selected by minimizing the error in the initial state for the Reynolds stress components.

Table E.10: Homogeneous Shear Flow Data (Tavoularis and Karnik "L", 1989)

τ	Tref	R <sub>xx</sub>	R <sub>yy</sub>	R <sub>zz</sub>	R <sub>yz</sub>	Sk/e	$N_R^{\dagger}$
2.0	0.0	0.297	0.265	0.438	-0.161	3.02	0.615
4.0	2.0	0.285	0.250	0.464	-0.159	3.06	
6.0	4.0	0.273	0.236	0.491	-0.158	3.09	
8.0	6.0	0.261	0.222	0.517	-0.155	3.13	
8.25	6.25	0.260	0.220	0.520	-0.155	3.14	

 $\underline{M}$ : 25.4 mm  $\overline{U}_c$ : 13 m/s S: 29 s<sup>-1</sup>

 $<sup>^{\</sup>dagger}$ : Initial  $N_R$  selected by minimizing the error in the initial state for the Reynolds stress components.

Table E.11: Return to Isotropy Data: Choi and Lumley [1984] (Plane Distortion)

$2k/U^2 \times 10^3$	b <sub>22</sub>	b <sub>33</sub>	$b_{23}^{\dagger}$	II
1.76	0.151	-0.139		0.0422
1.51	0.131	-0.119		0.0315
1.33	0.126	-0.108		0.0279
1.19	0.116	-0.095		0.0229
1.07	0.107	-0.086		0.0193
0.966	0.100	-0.077		0.0165
0.884	0.097	-0.068		0.0148
0.784	0.090	-0.067		0.0130
0.704	0.094	-0.069		0.0142
0.636	0.090	-0.062		0.0128
0.580	0.086	-0.054		0.0114

<sup>&</sup>lt;sup>†</sup> Data not available; only normal components were measured.

Table E.12: Return to Isotropy Data: Choi and Lumley [1984] (Axisymmetric Expansion)

$2k/U^2 \times 10^3$	b <sub>22</sub>	b <sub>33</sub>	b <sub>23</sub> †	II
0.665	0.196	-0.117		0.0585
0.613	0.189	-0.112		0.0541
0.575	0.185	-0.110		0.0521
0.541	0.175	-0.103		0.0463
0.510	0.177	-0.101		0.0471
0.483	0.171	-0.099		0.0446
0.457	0.163	-0.091		0.0401
0.427	0.163	-0.093		0.0401
0.400	0.163	-0.094		0.0404
0.376	0.160	-0.093		0.0388
0.356	0.154	-0.091		0.0361
0.339	0.150	-0.091		0.0343
0.324	0.146	-0.083		0.0322

<sup>†</sup> Data not available; only normal components were measured.

Table E.13: Return to Isotropy Data: LePenven et al. [1985] (Positive Third Invariant)

$2k/U^2 \times 10^3$	b <sub>22</sub>	<i>b</i> <sub>33</sub>	$b_{23}^{\dagger}$	II
0.238	0.183	-0.045		0.0548
0.229	0.181	-0.046		0.0532
0.216	0.179	-0.049		0.0516
0.207	0.174	-0.050		0.0480
0.193	0.167	-0.053		0.0439
0.182	0.164	-0.049		0.0426
0.167	0.159	-0.052		0.0396
0.159	0.158	-0.054		0.0387
0.148	0.154	-0.052		0.0369
0.139	0.154	-0.055		0.0364
0.134	0.150	-0.053		0.0349

<sup>&</sup>lt;sup>†</sup> Data not available; only normal components were measured.

# Appendix F: Relation of Homogeneous, Isotropic Turbulent Production to the Velocity Derivative Skewness

Eq. (2.31) presents a relationship between the velocity derivative skewness and the Taylor microscale, along with properties of the double and triple velocity correlations. The velocity derivative skewness is

$$-S_{k} = \langle \left(\frac{\partial u'}{\partial x}\right)^{3} \rangle / \left[ \langle \left(\frac{\partial u'}{\partial x}\right)^{2} \rangle \right]^{3/2}. \tag{F.1}$$

The mean of the velocity derivative squared can be related to the second derivative of the double velocity correlation (see p.145, Monin and Yaglom, 1965):

$$\left\langle \left(\frac{\partial u'}{\partial x}\right)^2 \right\rangle = -\left(\frac{\partial^2 \tilde{B}_{LL}}{\partial r^2}\right)_{r=0}.$$
 (F.2)

Eqs. (2.23) and (F.2) can be combined further to yield the following result, namely,

$$\left\langle \left(\frac{\partial u'}{\partial x}\right)^2 \right\rangle = \frac{\tilde{B}_{LL}(0)}{\lambda^2}. \tag{F.3}$$

Similarly, the mean of the velocity derivative cubed is related to the third derivative of the triple longitudinal velocity correlation (see p.145 Monin and Yaglom, 1965):

$$\left\langle \left(\frac{\partial u'}{\partial x}\right)^3 \right\rangle = \left(\frac{\partial^3 \tilde{T}_{LLL}}{\partial r^3}\right)_{r=0}.$$
 (F.4)

It follows directly from Eqs. (F.1), (F.3), and (F.4) that

$$\frac{\lambda^{3}}{\left(\tilde{B}_{II}(0)\right)^{3/2}} \left(\frac{\partial^{3} \tilde{T}_{LLL}}{\partial r^{3}}\right)_{r=0} = \left\langle \left(\frac{\partial u}{\partial x}\right)^{3} \right\rangle / \left[\left\langle \left(\frac{\partial u}{\partial x}\right)^{2} \right\rangle\right]^{3/2} \equiv -S_{k}, \tag{F.5}$$

which is the result expressed by Eq. (2.31). Furthermore, the combination of Eqs. (F.5) and (2.28) yield the relationship between turbulent production in homogeneous, isotropic turbulence and the velocity derivative skewness (cf. Eq. (2.13)):

$$P = \frac{7}{3\sqrt{15}} S_k \sqrt{Re}. \tag{F.6}$$

## Appendix G:Asymptotic State for Homogeneous Shear

This appendix details the algebra required to express the asymptotic values of the anisotropic pre-stress components for homogeneously sheared turbulence (as given in Eqs. (4.54)-(4.57)). The asymptotic values for the normal components of the anisotropic pre-stress follow directly from Eqs. (4.45)-(4.47) by setting the derivatives with respect to  $\xi$  equal to zero:

$$(1+q^a)H_{xx}^a - \frac{2}{3}aDe_t^aH_{yz}^a = 0, (G.1)$$

$$(1+q^a)H_{yy}^a + \left(\frac{a}{3}+1\right)De_t^a H_{yz}^a = 0, (G.2)$$

and

$$(1+q^a)H_{zz}^a + \left(\frac{a}{3} - 1\right)De_t^a H_{yz}^a = 0. {(G.3)}$$

Rearranging Eqs. (G.1)-(G.3) yields the relations given in Eqs. (4.54)-(4.56):

$$H_{xx}^{a} = \frac{2a}{3} \frac{De_{t}^{a} H_{yz}^{a}}{1 + q^{a}},$$
 (G.4)

$$H_{yy}^{a} = -\left(1 + \frac{a}{3}\right) \frac{De_{t}^{a} H_{yz}^{a}}{1 + q^{a}},$$
 (G.5)

and

$$H_{zz}^{a} = \left(1 - \frac{a}{3}\right) \frac{De_{t}^{a} H_{yz}^{a}}{1 + a^{a}}.$$
 (G.6)

Similarly, Eq. (4.72) combines with Eqs. (G.5) and (G.6) to give the expression for the asymptotic value of the shear component of the anisotropic pre-stress:

$$0 = \frac{1}{2} \frac{C_{\beta}}{C_{\lambda}} - \frac{(1+q^a)}{De_t^a} H_{yz}^a - \frac{De_t^a}{(1+q^a)} H_{yz}^a + \frac{a^2}{3} \frac{De_t^a}{(1+q^a)} H_{yz}^a, \tag{G.7}$$

whence, upon rearrangement, becomes

$$H_{yz}^{a} = \frac{C_{\beta}}{2C_{\lambda}} \frac{(1+q^{a})De_{t}^{a}}{(1+q^{a})^{2} + (De_{t}^{a})^{2} (1-a^{2}/3)},$$
 (G.8)

which is identical to the asymptotic result given in Eq. (4.57).

## Appendix H:Computer Program Listings

### H.1 Program TRANS.BAS

The program TRANS.BAS is written Microsoft QuickBasic<sup>TM</sup>. Its function is to integrate the initial value problem posed for the case of homogeneous shear flow. For the IPS-theory, the differential equation for  $N_R$  is solved, as are the algebraic pre-closure equations for R. With the extension of the model to include an anisotropic pre-stress, four additional differential equations are solved for the components of H. Initial conditions as well as program control parameters are read as input through the file HOMG\_SHE.INI. Transient output data is directed to a user-specified file and the final time step is output to the file SUMMARY.TXT.

#### Variable Listing

a convected derivative parameter a

ak  $\alpha/k$ 

B holding matrix for Gauss-Jordan inversion

 $Cd, Cp \qquad C_D, C_P$ 

cr,cb,cl  $C_R$ ,  $C_\beta$ ,  $C_\lambda$ 

De relaxation group  $N_R$ 

Deb, Del  $(C_{\beta}/2C_R)N_R$ ;  $(C_{\lambda}/C_R)N_R$ 

Det  $dN_R/d\xi$ 

dt, fdt Δξ, variable step size parameter

g  $\Omega/S$ 

H, Hold anisotropic pre-stress  $\underline{H}$ , holding variable for old values

Ht  $dH/d\xi$ 

q, qq parameter q (see Eq. (4.43));  $(1+q)/De_t$ 

```
R normalized Reynolds stress R
```

ske  $Sk/\epsilon$ 

t, told dimensionless time ξ, holding variable for old time

#### Program Listing

```
REM full relaxation model with H + lambda*DH/Dt = beta*<S> (D/Dt: Mixed Objective Derivative)
REM full inversion of coefficient matrix to solve R given H and N_R
REM transient calculation
' Variables
DIM R(3, 3) AS DOUBLE
DIM B(3, 4) AS DOUBLE
DIM H(3, 3) AS DOUBLE
                                   'reynolds stress
                                    'transformation tensor to be inverted
                                    'anisotropic pre-stress
DIM Hold (3, 3) AS DOUBLE
                                    'anisotropic pre-stress
DIM dt, t, told, fdt AS DOUBLE 'time variables
DIM De, Deb, Del AS DOUBLE 'Deborah numbers
DIM Deold AS DOUBLE
                                    'Deborah numbers
DIM ak AS DOUBLE
                                    'alpha/k
DIM ske AS DOUBLE
                                    'Sk/eps
                                    'Omega/S (relative rotation rate)
DIM g AS DOUBLE
' Time derivatives of variables
DIM Ht (3, 3, 4) AS DOUBLE
                                   'anisotropic pre-stress time derivative
DIM Det(4) AS DOUBLE
                                    'Deborah number time derivative
DIM cr, cb, cl AS DOUBLE
DIM Cd, Cp AS DOUBLE
                                    'rr model constants
                                    'eps-egn constants
DIM q, qq AS DOUBLE
DIM a AS DOUBLE
                                    'conv. derivative parameter
DIM i, j, k, 1 AS INTEGER
DIM m, n AS LONG
DIM buff AS STRING
                                    'identifier for IPS/APS model
DIM model AS STRING
' Read initial values for H. De:
  OPEN "d:\data\msu\homg_she\homg_she.ini" FOR INPUT AS #1
   'read model type (IPS/APS)
    LINE INPUT #1, buff$: model$ = UCASE$(LEFT$(buff$, 3))
    LINE INPUT #1, buff$
    FOR i = 1 TO 3
      INPUT #1, H(i, 1): INPUT #1, H(i, 2): INPUT #1, H(i, 3)
    NEXT i
   'read other parameters
LINE INPUT #1, buff$: INPUT #1, De
    LINE INPUT #1, buff$: INPUT #1, g
    LINE INPUT #1, buff$: INPUT #1, dt, fdt, tmax
    LINE INPUT #1, buff$: INPUT #1, nprint
    LINE INPUT #1, buff$: INPUT #1, outfile$
  CLOSE #1
' Specify model parameters
  SELECT CASE model$
    CASE 'IPS'
      cr = .227#
      cb = 0#
      cl = 0#
      Cd = 1.83#
      Cp = 1.41#
```

```
a = 0#
          CASE 'APS'
               cr = .2706#
               cb = .1742
               cl = .666666666666666
               Cd = 1.83#
               Cp = 1.604#
               a = -.6788999999999999
          CASE ELSE
              PRINT "No valid model specified; program aborted": END
    END SELECT
' Open data file for output
    OPEN "d:\data\msu\homg_she\" + (outfile$) FOR OUTPUT AS $1
    PRINT #1, USING *##.###, *; q
' Begin time integration
    CLS
    t = 0#
    n = 0
  'determine initial Reynolds stress
    IF (model$ = "IPS") THEN
         H(1, 1) = 00: H(1, 2) = 00: H(1, 3) = 00: H(2, 1) = 00: H(2, 2) = 00: H(2, 3) = 00: 
         H(3, 1) = 00: H(3, 2) = 00: H(3, 3) = 00
    GOSUB 1000
  '4th order RK loop
    DO
       'output
         IF ((n / nprint) = INT(n / nprint)) THEN
              PRINT t; De; R(2, 2); R(2, 3)
PRINT #1, USING *###.###, *; t;
              PRINT 01, USING "000.0000, "; L;
PRINT 01, USING "00.00000, "; Do;
PRINT 01, USING "0.00000, "; R(1, 1); R(2, 2); R(3, 3); R(2, 3);
PRINT 01, USING "0.00000, "; H(1, 1); H(2, 2); H(3, 3); H(2, 3)
         END IF
       'save old values
         Deold = De
          Hold(1, 1) = H(1, 1)
          Hold(2, 2) = H(2, 2)
          Hold(3, 3) = H(3, 3)
         Hold(2, 3) = H(2, 3)
         told = t
       '1st integration step
         IF (model$ = "APS") THEN
              Del = (cl / cr) * De

q = Del * (-2# * R(2, 3) - cr / De)
               qq = (1# + q) / Del
              Ht(2, 3, 1) = -qq + H(2, 3) + (cb / cl / 20) + .50 + H(3, 3) + (-10 - a) + .50 + H(2, 2) + (10 - a)
             H(1, 1) = Hold(1, 1) + .50 * dt * Ht(1, 1, 1)
H(2, 2) = Hold(2, 2) + .50 * dt * Ht(2, 2, 1)
H(3, 3) = Hold(3, 3) + .50 * dt * Ht(3, 3, 1)
H(2, 3) = Hold(2, 3) + .50 * dt * Ht(2, 3, 1)
              H(3, 2) = H(2, 3)
          END IF
       'determine Reynolds stress for step 1
         GOSUB 1000
       '2nd integration step
```

```
IF (model$ = "APS") THEN
   Del = (cl / cr) * De
q = Del * (-2# * R(2, 3) - cr / De)
   qq = (1# + q) / Del
   Ht(2, 3, 2) = -qq * H(2, 3) + (cb / cl / 20) + .50 * H(3, 3) * (-10 - a) + .50 * H(2, 2) * (10 - a)
   H(1, 1) = Hold(1, 1) + .50 + dt + Ht(1, 1, 2)

H(2, 2) = Hold(2, 2) + .50 + dt + Ht(2, 2, 2)

H(3, 3) = Hold(3, 3) + .50 + dt + Ht(3, 3, 2)

H(2, 3) = Hold(2, 3) + .50 + dt + Ht(2, 3, 2)
   H(3, 2) = H(2, 3)
 FIND IF
'determine Reynolds stress for step 2
 GOSUB 1000
'3rd integration step
 Det(3) = (2 * De * R(2, 3) * (Cp - 1 *)) + (cr * (Cd - 1 *))
 De = Deold + dt * Det(3)
 IF (model$ = "APS") THEN
Del = (cl / cr) * De
   q = De1 * (-2* * R(2, 3) - cr / De)
   qq = (1# + q) / Del
   Ht(1, 1, 3) = -qq + H(1, 1) + (2# + a / 3#) + H(2, 3)
   Ht(2, 2, 3) = -qq + H(2, 2) - H(2, 3) + (a / 30 + 10)
Ht(3, 3, 3) = -qq + H(3, 3) - H(2, 3) + (a / 30 - 10)
   Ht(2, 3, 3) = -qq + H(2, 3) + (cb / cl / 20) + .50 + H(3, 3) + (-10 - a) + .50 + H(2, 2) + (10 - a)
   H(1, 1) = Hold(1, 1) + dt * Ht(1, 1, 3)
   H(2, 2) = Hold(2, 2) + dt * Ht(2, 2, 3)
   H(3, 3) = Hold(3, 3) + dt + Ht(3, 3, 3)
   H(2, 3) = Hold(2, 3) + dt + Ht(2, 3, 3)
   H(3, 2) = H(2, 3)
 END IF
'determine Reynolds stress for step 3
COSTUR 1000
'4th integration step
 Det(4) = (20 * De * R(2, 3) * (Cp - 10)) + (cr * (Cd - 10))
 IF (model$ = "APS") THEN
  Del = (cl / cr) * De
q = Del * (-2* * R(2, 3) - cr / De)
   qq = (1# + q) / Del
   Ht (1, 1, 4) = -qq + H(1, 1) + (2 + a / 3) + H(2, 3)
   Ht (2, 2, 4) = -qq + H(2, 2) - H(2, 3) + (a / 30 + 10)
Ht (3, 3, 4) = -qq + H(3, 3) - H(2, 3) + (a / 30 - 10)
  Ht(2, 3, 4) = -qq + H(2, 3) + (cb / cl / 20) + .50 + H(3, 3) + (-10 - a) + .50 + H(2, 2) + (10 - a)
 END IF
'4th-order RK-step
n = n + 1
 t = t + dt
 De = Deold + (dt / 60) * (Det(1) + 20 * Det(2) + 20 * Det(3) + Det(4)) IF (model$ = "APS") THEN
  H(1, 1) = Hold(1, 1) + (dt / 68) * (Ht(1, 1, 1) + 28 * Ht(1, 1, 2) + 28 * Ht(1, 1, 3) + Ht(1, 1, 4))

H(2, 2) = Hold(2, 2) + (dt / 68) * (Ht(2, 2, 1) + 28 * Ht(2, 2, 2) + 28 * Ht(2, 2, 3) + Ht(2, 2, 4))
  H(3, 3) = Hold(3, 3) + (dt / 60) * (Ht(3, 3, 1) + 20 * Ht(3, 3, 2) + 20 * Ht(3, 3, 3) + Ht(3, 3, 4))
  H(2, 3) = Hold(2, 3) + (dc / 60) + (Hc(2, 3, 1) + 20 + Hc(2, 3, 2) + 20 + Hc(2, 3, 3) + Hc(2, 3, 4))
  H(3, 2) = H(2, 3)
 END IF
'determine Reynolds stress for step 4
GOSUB 1000
 dt = dt * fdt
 traceH = H(1, 1) + H(2, 2) + H(3, 3)
```

```
IF (ABS(traceH) > .000001) THEN
        PRINT "H not traceless: "; traceH
        EXIT DO
     END IF
  LOOP UNTIL (t > tmax)
' final output
  PRINT t; De; R(2, 2); R(2, 3)
PRINT #1, USING *###.# (1, 1); PRINT #1, USING *###.# (1, 1); PRINT #1, USING *###.# (1, 1); R(2, 2); R(3, 3); R(2, 3);
PRINT #1, USING *#.#####.# (1, 1); R(2, 2); R(3, 3); R(2, 3);
PRINT #1, USING *#.######.# (1, 1); H(2, 2); H(3, 3); H(2, 3)
  CLOSE #1
' Write asymptotic results to a summary file
  OPEN *d:\data\msu\homg_she\summary.txt* FOR APPEND AS $1
     PRINT #1, USING *##.###, *; g;
PRINT #1, USING *###.###, *; t;
     CLOSE #1
END
1000 ' compute R from H
' Compute initial B (coefficient matrix)
  B(1, 1) = 3# - ((1# + g) * De) ^ 2#
  B(1, 2) = 2\theta + (g + De) ^ 2\theta

B(1, 3) = -(6\theta + g + 2\theta) + De
  B(2, 1) = 2\theta * ((1\theta + g) * De) ^ 2\theta 
 B(2, 2) = 3\theta - (g * De) ^ 2\theta 
 B(2, 3) = (6\theta * g + 4\theta) * De
  B(3, 1) = (1 + g) + De
  B(3, 2) = -g * De
B(3, 3) = 1# - g * (1# + g) * De ^ 2#
' Compute initial B (known vector)
  B(1, 4) = 10 + 30 + H(2, 2)
B(2, 4) = 10 + 30 + H(3, 3)
B(3, 4) = H(2, 3)
' Gauss-Jordan Elimination
  FOR k = 1 TO 3
     FOR j = 4 TO k STEP -1
       B(k, j) = B(k, j) / B(k, k)
     NEXT j
     FOR 1 = 1 TO 3
        IF (i \Leftrightarrow k) THEN

FOR j = 4 TO k STEP -1
            B(i, j) = B(i, j) - (B(i, k) * B(k, j))
          NEXT j
       END IF
     NEXT i
  NEXT k
' Note: post-inversion, 1st three columns are identity matrix,
           and the 4th column is the solution vector.
  R(2, 2) = B(1, 4)
  R(3, 3) = B(2, 4)

R(3, 1) = 16 - R(2, 2) - R(3, 3)

R(2, 3) = B(3, 4)
' Verify realizability of R:
  IF (R(2, 3) ^2 > R(2, 2) * R(3, 3)) THEN
     PRINT "Schwarz inequaltiy not satisfied.": END
   END IF
  IF (R(1, 1) < 0) THEN
PRINT "Rxx negative": END
  END IF
  IF (R(2, 2) < 0) THEN
    PRINT "Ryy negative": END
  END IF
  IF (R(3, 3) < 0) THEN
PRINT "Rzz negative": END
```

```
END IF

R(3, 2) = R(2, 3)

RETURN
```

#### H.2 Program IPS\_ROT.BAS

The program IPS\_ROT.BAS is written in Microsoft QuickBasic<sup>TM</sup>. It solves the algebraic pre-closure equations for  $\underline{R}$  given values for  $N_R$  and  $\Omega/S$ . Program control parameters are read as input through the file IPS\_STAT.INI. Output data is directed to a user-specified file.

#### Variable Listing

The variables used are the same as listed in Section H.1.

#### Program Listing

```
REM IPS-model calculations for turbulent states as a function of Cmega/S
REM full inversion of coefficient matrix to solve R given H and N_R
' Variables
DIM R(3, 3) AS DOUBLE 'reynolds stress
DIM B(3, 4) AS DOUBLE
                       'transformation tensor to be inverted
DIM H(3, 3) AS DOUBLE 'anisotropic pre-stress
DIM De AS DOUBLE
                      'Relaxation Group
DIM De1, De2 AS DOUBLE 'Relaxation Group, initial/final
DIM DeDel AS DOUBLE 'delta Relaxation Group
                      'Omega/S (relative rotation rate)
DIM g AS DOUBLE
DIM cr, cb, cl AS DOUBLE 'rr model constants
DIM Cd, Cp AS DOUBLE
                           'eps-eqn constants
DIM i, j, k, 1 AS INTEGER
DIM m, n AS LONG
DIM buff AS STRING
DIM natep AS INTEGER
DIM model AS STRING
                          'identifier for IPS/APS model
' Read initial values for gamma:
 OPEN "d:\data\msu\homg_she\ips_stat.ini" FOR INPUT AS #1
   'read other parameters
   LINE INPUT #1, buff$: INPUT #1, g
   LINE INPUT #1, buff$: INPUT #1, De1, De2, DeDe1, fDe
```

```
LINE INPUT #1, buff$: INPUT #1, outfile$
  CLOSE #1
' Specify model parameters
  ' CASE 'IPS'
     cr = .227#
      cb = 0#
      cl = 0#
      Cd = 1.83#
      Cp = 1.41#
      a = 0#
      H(1, 1) = 0: H(1, 2) = 0: H(1, 3) = 0
      H(2, 1) = 00: H(2, 2) = 00: H(2, 3) = 00
      H(3, 1) = 00: H(3, 2) = 00: H(3, 3) = 00
' Open data file for output
  OPEN "d:\data\msu\homg_she\" + (outfile$) FOR OUTPUT AS #1
  PRINT #1, USING *##.###, *; g
  De - De1
  DO
    GOSUB 1000
    PRINT De; R(2, 2); R(2, 3)
    PRINT #1, USING *##.###, *; De;
    PRINT #1, USING *#.#####, *; R(1, 1); R(2, 2); R(3, 3); R(2, 3)
   De = De + DeDel
   DeDel = DeDel * fDe
  LOOP UNTIL (De > De2)
  CLOSE #1
END
1000 ' compute R from H
' Compute initial B (coefficient matrix)
 B(1, 1) = 3# - ((1# + g) * De) ^ 2#
 B(1, 2) = 2# * (g * De) ^ 2#
 B(1, 3) = -(60 * g + 20) * De
  B(2, 1) = 2# * ((1# + g) * De) ^ 2#
  B(2, 2) = 3# - (g * De) ^ 2#
  B(2, 3) = (6# * g + 4#) * De
 B(3, 1) = (1# + g) * De
 B(3, 2) = -g * De
 B(3, 3) = 1\% - g * (1\% + g) * De ^ 2\%
' Compute initial B (known vector)
 B(1, 4) = 1# + 3# + H(2, 2)
 B(2, 4) = 10 + 30 + H(3, 3)
 B(3, 4) = H(2, 3)
' Gauss-Jordan Elimination
  FOR k = 1 TO 3
   FOR j = 4 TO k STEP -1
    B(k, j) = B(k, j) / B(k, k)
   NEXT j
   FOR 1 = 1 TO 3
     IF (i <> k) THEN
       FOR j = 4 TO k STEP -1
         B(i, j) = B(i, j) - (B(i, k) * B(k, j))
       NEXT j
     END IF
   NEXT i
 NEXT k
' Note: post-inversion, 1st three columns are identity matrix,
       and the 4th column is the solution vector.
```

```
R(2, 2) = B(1, 4)

R(3, 3) = B(2, 4)
 R(1, 1) = 10 - R(2, 2) - R(3, 3)

R(2, 3) = B(3, 4)
' Verify realizability of R:
 IF (R(2, 3) ^2 > R(2, 2) * R(3, 3)) THEN
   PRINT *Schwarz inequaltiy not satisfied. *: END
 END IF
 IF (R(1, 1) < 0) THEN
  PRINT "Rox negative": END
 END IF
 IF (R(2, 2) < 0) THEN
  PRINT "Ryy negative": END
 END IF
 IF (R(3, 3) < 0) THEN
  PRINT "Rzz negative": END
 END IF
 R(3, 2) = R(2, 3)
```

RETURN

# Appendix I: Properties of the Eigenvalues of the Reynolds Stress

As mentioned in Chapter 1, the Reynolds stress  $\langle u'u' \rangle$  has the following properties:

$$\langle u' \cdot u' \rangle = 2k, \tag{I.1}$$

and

$$\underline{z} \cdot \langle \underline{u}'\underline{u}' \rangle \cdot \underline{z} \ge 0. \tag{I.2}$$

More specifically, the trace of the Reynolds stress is twice the turbulent kinetic energy and the Reynolds stress is positive semi-definite. Since the normalized Reynolds stress is defined as

$$R = \frac{\langle \underline{u}'\underline{u}' \rangle}{2k}, \tag{I.3}$$

Eq. (I.1) implies that the trace of the normalized Reynolds stress is unity:

$$tr\left(\underset{=}{R}\right) = 1. \tag{I.4}$$

However, the trace of a tensor operator is also an invariant property of that operator which equals the sum of the eigenvalues:

$$tr(R) = 1 = \lambda_{R,1} + \lambda_{R,2} + \lambda_{R,3},$$
 (I.5)

where  $\lambda_{R,i}$  is the  $i^{th}$  eigenvalue of the operator R. The positive, semi-definite nature of the Reynolds stress expressed by Eq. (I.2) implies that each of the eigenvalues of the Reynolds stress  $\langle \underline{u}'\underline{u}' \rangle$  is non-negative. This character yields the following condition upon the values  $\lambda_{R,i}$ :

$$0 \le \lambda_{R, i} \le 1, \tag{I.6}$$

since each of the eigenvalues is non-negative and the sum of the eigenvalues is one.

The condition given by Eq. (I.6) yields information concerning the eigenvalues of the anisotropy tensor  $\underline{b}$ , defined as

$$\frac{b}{z} = \frac{R}{z} - \frac{1}{3}I. \tag{I.7}$$

It follows directly from Eq. (I.7) that

$$\lambda_{b,i} = \lambda_{R,i} - \frac{1}{3},\tag{L8}$$

where  $\lambda_{b,i}$  is the  $i^{th}$  eigenvalue of the operator  $\frac{b}{z}$ . Combination of Eqs. (I.6) and (I.8) yields the result stated in Chapter 1:

$$-\frac{1}{3} \le \lambda_{b, i} \le \frac{2}{3}. \tag{L9}$$

#### LIST OF REFERENCES

- J. Bardina, J. Ferziger, and R. Rogallo, 1985, "Effect of rotation on isotropic turbulence: computation and modeling," J. Fluid Mech., 154, 321.
- G. Batchelor and A. Townsend, 1948, "Decay of turbulence in the initial period," *Proc. Roy. Soc.*, A194, 538.
- G. Batchelor and A. Townsend, 1948, "Decay of turbulence in the final period," *Proc. Roy. Soc.*, A196, 527.
- J. Bennett, and S. Corrsin, 1978, "Small Reynolds number nearly isotropic turbulence in a straight duct and a contraction," *Phys. Fluids*, 21(12), 2129.
- R. Bird, A. Armstrong, O. Hassager, 1977, The Dynamics of Polymeric Fluids, volume II, McGraw Hill.
- R. Bird, A. Armstrong, O. Hassager, 1987, *The Dynamics of Polymeric Fluids*, volume I, McGraw Hill.
- F. Boysan, W. Ayers, J. Swithenbank, 1982, "A fundamental mathematical modeling approach to cyclone design," *Trans IChemE*, 60, 222.
- R. Brodkey, 1967, The Phenomena of Fluid Motion, Addison Wesley.
- B. Carnahan, H. Luther and J. Wilkes, 1969, Applied Numerical Methods, John Wiley and Sons.
- K. Choi, 1983, "A study of the return to isotropy of homogeneous turbulence", Ph.D. Dissertation, Cornell University.
- K. Choi and J. Lumley, 1984, "Return to isotropy of homogeneous turbulence revisited," in *Turbulence and Chaotic Phenomena in Fluids*, ed. T. Tatsumi, New York: North Holland.
- G. Comte-Bellot and S. Corrsin, 1971, "Simple Eulerian time correlation of full- and narrow-band velocity signals in grid generated, isotropic turbulence," J. Fluid Mech., 48, 273.
- M. Denn, 1990, "Issues in viscoelastic fluid mechanics," Ann. Rev. Fluid Mech., 22, 13.

- M. Gibson and V. Kanellopoulos, 1987, "Turbulence measurements in a nearly homogeneous shear flow," Conference on Transport Phenomena in Turbulent Flows: Theory, Experiment, and Numerical Simulation.
- H. Greenspan, 1968, The Theory of Rotating Fluids, Breukelen Press.
- K. Hanjalic and B. Launder, 1972, "A Reynolds stress model of turbulence and its application to thin shear flows," J. Fluid Mech., 52(4), 609.
- K. Hanjalic and B. Launder, 1976, "Contribution towards a Reynolds stress closure for low Reynolds number turbulence," J. Fluid Mech., 74(4), 593.
- K. Hanjalic, 1994, "Advanced turbulence closure models," Int. J. Heat and Fluid Flow, 15(3), 178.
- J. Hargreaves and R. Silvester, 1990, "Computational fluid dynamics applied to the analysis of de-oiling hydrocyclone performance," *Trans IChemE*, 68(A), 365.
- J. Hill and C. Petty, 1996, "Turbulent transport of a passive scalar field," Chem. Eng. Commun., 152-153, 413.
- J. Hinze, 1959, Turbulence, McGraw-Hill.
- M. Huang and A. Leonard, 1994, "Power-law decay of homogeneous turbulence at low Reynolds numbers," *Phys. Fluids*, 6(11), 3765.
- D. Joseph, 1990, Fluid Dynamics of Viscoelastic Fluids, Springer Verlag.
- T. von Kármán and L. Howarth, 1938, "On the statistical theory of isotropic turbulence," *Proc. Roy. Soc.*, A164, 192.
- O. Kitoh, 1991, "Experimental study of turbulent swirling flow in a straight pipe," J. Fluid Mech., 205, 445.
- J. Kim, P. Moin, and R. Moser, 1987, "Turbulent statistics in fully developed channel flow at low Reynolds numbers," J. Fluid Mech., 177, 133.
- B. Launder, D. Spalding, 1974, "The numerical computation of turbulent flows," Comp. Meth. Appl. Mech. and Eng., 3, 269.
- B. Launder, G. Reece, and W. Rodi, 1975, "Progress in the development of a Reynolds stress closure," J. Fluid Mech., 68(3), 537.
- L. LePenven, J. Gence, and G Comte-Bellot, 1985, "On the approach to isotropy of homogeneous turbulence: effect of the partition of kinetic energy among velocity components," in *Frontiers in Fluid Mechanics*, ed. S. Davis and J. Lumley, Berlin: Springer Verlag.

- J. Lumley, 1978, "Computational modeling of turbulent flows," Adv. App. Mech., 18, 123.
- N. Mansour and A. Wray, 1994, "Decay of isotropic turbulence at low Reynolds numbers," *Phys. Fluids*, 6(2), 808.
- G. Mase and G. Mase, 1992, Continuum Mechanics for Engineers, CRC Press.
- A. Monin and A. Yaglom, 1965, Statistical Fluid Mechanics: Mechanics of Turbulence, volumes 1 and 2, MIT Press.
- P. Morse and H. Feshbach, 1953, Methods of Theoretical Physics, part I, McGraw-Hill.
- S. Parks, K. Weispfennig, and C. Petty, 1997, "An Algebraic Pre-Closure Theory for the Reynolds Stress", submitted to *Phys. Fluids*.
- V. Patel, W. Rodi, and G Scheuerer, 1997, "Turbulence models for near-wall and low Reynolds number turbulence", AIAA J., 23(9), 1308.
- C. Petty, 1975, "A statistical theory for mass transfer near interfaces," Chem. Eng. Sci., 30, 413.
- W. Reynolds, 1989, "Towards a structure-based turbulence model", Studies in Turbulence; editors T. Gatski, S. Sarkar, and C. Speziale; p.76, Springer Verlag.
- J. Rohr, E. Itsweire, K. Helland and C. Van Atta, 1988, "An investigation of the growth of turbulence in a uniform mean shear flow," J. Fluid Mech., 187, 1.
- S. Sarkar and C. Speziale, 1990, "A simple nonlinear model for the return to isotropy in turbulence," *Phys. Fluids A*, 2(1), 84.
- U. Schumann, 1977, "Realizability of Reynolds stress turbulence models," *Phys. Fluids*, 20(5), 721.
- A. Sirivat and Z. Warhaft, 1983, "The effect of a passive cross-stream temperature gradient on the evolution of temperature variance and heat flux in grid turbulence," J. Fluid Mech., 128, 323.
- C. Speziale, 1987, "On nonlinear k-l and k-ε models of turbulence," J. Fluid Mech., 178, 459.
- C. Speziale, N. Mansour, and R. Rogallo, 1987, "The decay of isotropic turbulence in a rapidly rotating frame," Center for Turbulence Research, Proceedings of the 1987 Summer Program, (Stanford U.P., Stanford, CA, 1987) 205.
- C. Speziale and N. Mac Giolla Mhuiris, 1989, "On the prediction of equilibrium states in homogeneous turbulence," J. Fluid Mech., 209, 591.
- C. Speziale, 1991, "Analytical methods for the development of Reynolds-stress closures

- in turbulence," Ann. Rev. Fluid Mech., 25, 107.
- C. Speziale, R. Raj, and T. Gatski, "Modeling the dissipation rate in rotating turbulent flows," *Studies in Turbulence*; editors T. Gatski, S. Sarkar, and C. Speziale; p.129, Springer Verlag.
- D. Taulbee, 1989, "Engineering turbulence models", Advances in Turbulence; editors W. George and R. Arndt; p.75, Hemisphere.
- S. Tavoularis, J. Bennett, and S. Corrsin, 1978, "Velocity derivative skewness in small Reynolds number, nearly isotropic turbulence," J. Fluid Mech., 88(1), 63.
- S. Tavoularis and S. Corrsin, 1981, "Experiments in a nearly homogeneous turbulent shear flow with a uniform mean temperature gradient," J. Fluid Mech., 104, 311.
- S. Tavoularis and U. Karnik, 1989, "Further experiments on the evolution of turbulent stresses and scales in uniformly sheared turbulence," J. Fluid Mech., 204, 457.
- H. Tennekes and J. Lumley, 1972, A First Course in Turbulence, MIT Press.
- K. Weispfennig, 1997, "Relaxation/retardation model for fully developed turbulent channel flow", Ph.D. Dissertation, Michigan State University.

